

THÈSE

Présentée en vue de l'obtention du grade de

DOCTEUR DE L'UNIVERSITÉ LOUIS PASTEUR

Sciences de la Terre et de l'Univers

Physique, Chimie et Biologie de l'Environnement

par

Julia Berger

**Hydratation des argiles gonflantes et influence des bactéries
Etude expérimentale de réaction in situ**

*Hydration of swelling clay and bacteria interaction
An experimental in situ reaction study*

soutenue publiquement le 31 janvier 2008

Mme Faïza Bergaya
Mme Françoise Elsass
Mme Marie-Claire Lett
Mr Frédéric Villieras
Mr Laurence N. Warr

DR CNRS, Orléans
IR INRA, Versailles
Professeur, ULP Strasbourg
DR, CNRS, Nancy
Professeur, Greifswald

Rapporteur Externe
Examineur
Rapporteur Interne
Rapporteur Externe
Directeur de thèse

*Von der Mehrzahl der Werke bleiben nur die Zitate übrig,
warum nicht also von Anfang an nur die Zitate aufschreiben...?
(Stanislaw Jerzy Lec)*

Acknowledgements

This work was financed by a three years grant of the french ministry of research.

I'd like to thank my supervisor Laurence Warr, who brought me to Strasbourg and proposed me to work on this fascinating project. His ideas were always creative and he transmitted especially this creative scientific approach to me. Thank you for all support especially at initial stages of the PhD project. I would like as well to thank Norbert Clauer who helped enormously when I did the application for this grant. I would like to thank François Gauthier-Lafaye for the welcome in the CGS and François Chabaux as director of the ecole doctorale. Thanks as well to Daniel Tessier for the welcome in Versailles at the TEM facility. A special Thank to Marie-Claire Lett and her team for having me invited to use the facilities of the microbiology institute. Whenever I had questions or I needed other support I felt welcomed. Here a special thank to Sandrine who was very patient with the "non-frenchspeaking non-microbiologist".

I'd like to thank all members of the Jury Faïza Bergaya, Françoise Elsass, Marie-Claire-Lett and Frédéric Villieras for having accepted to judge the thesis, for compliments and for constructive criticism.

A very special thanks to the Geoparticles Group that received me warmly and although at the beginning my French was limited to "Bonjour" the communication was not disturbed and increasing understanding followed. Here a special thank to Jean-Luc who was extremely patient and who never got tired talking to me and later with me as soon as the language improved (Collioure...). Thanks to everybody of the X-ray lab, Jean-Luc, Fabienne and Amelie for the good working atmosphere and for having accepted the new ideas and methods I tested. Introducing microbiological methods, introduced as well microbiological smell (the finest Munster) and here a special thanks for your patience. Thanks as well to Gilles who was doing the ESEM and SEM with me and who was willing to search a long time until we had the first "Shewanella-smectite family" pictures. Thanks to Nico and Françoise who helped me with the TEM-EDX in Versailles; their help contributed significantly to main results of this thesis and working together was both effective and fun. Thanks to Joelle who was always willing to help concerning both scientific and language questions. Thanks to Mickaël and Valérie who share the experience of working at the interface of biology, geology and chemistry and who helped with staining and imaging bacteria. Thanks to all (Ex)-members of this dynamic and international group: Karim (Funkenmariechen from Morocco) who has always a sunshine effect on everybody, Christian the Québécois, who reintroduced the "coffebreak group feeling", Pavlina from Czech Republic who is attracting somehow the everyday-catastrophes more than me and became, not only because of that, a precious friend to me. Mohammed from Algeria who always distributed optimism and who was the main source of "dattes" for this group. Thanks to Rabia and Raja from Tunesia, Tania (adding Italian temperament), Emna and Malika. Special thanks to the new group leader Jean-Louis Crovisier who supported me and my project and was always willing to help.

Special thanks to Françoise who partly overtook scientific supervision and helped me especially during the writing phase: working with her was relaxed and at the same time extremely effective and I felt encouraged to defend my ideas. Thank you very much, you were the right person at the right time. Here as well special thanks to Nico who was an important discussion partner and who managed to criticize and to encourage at the same time. Both his scientific and personal support was of prime importance for me and without him I could not have finished the thesis.

Thanks as well to the Heidelbergers, especially to Margot and Christian who always gave a warm welcome. Their help with analytics contributed significantly to main results of the thesis

and working with them was always a pleasure. Thanks as well to all the other (Ex)-Heidelbergers, especially Bernd for still celebrating the walk to “Botanik”, Anja, the half American who periodically became French and especially shared the initial stages of my Strasbourg PhD experience, Heiko who never lost contact, whose Thesis was extremely helpful for me and who supported me during the defence day. A big hello to Axel, Christian, Seppl and Mirjam.

Thanks to all people of the CGS, especially Pavlina, Jérémie, Anne-Laure, Julien, Delphine, Momo. A hello to the Czech connection especially Honza, Prokop, Pavla, Andrej, Suzanna, Monica and Vladia and to the French connection Laurence, Michel, Majdi and all other doctorate students. Thanks for the everyday help to Yves, Cathie, les Danielles, Betty, Joëlle and thanks to Valérie and Erika for having partially or entirely read and corrected the manuscript.

On a personal note, I want to thank those who give my life meaning: my husband, best friend and scientific accomplice Nico, my family, especially my mother Regine and my sisters Nicole, Jenny, Ilana and Janna who never understood what I’m doing but who were always optimistic that it will lead to something and thanks to Marianne for continuous support. Thanks to my father and my grandmother who did not survive the end of the thesis but strongly supported me from their cloud.

RESUME

Cette étude traite du comportement physico-chimique des argiles dioctaédriques gonflantes (smectites) et de leurs interactions avec la solution aqueuse en présence et en l'absence de la bactérie *Shewanella putrefaciens*. Les résultats expérimentaux sont présentés pour des argiles compactées, hydratées en conditions de volume confiné, en utilisant un nouveau type de cellule réactionnelle (la "wet-cell" décrite dans Warr & Hoffman, 2004) conçue afin de réaliser des mesures de diffraction des rayons X (DRX) *in-situ*. En combinant des mesures de suivi dans le temps de DRX *in-situ* avec les mesures gravimétriques et les spectres de diffraction calculés à l'aide du logiciel CALCMIX (Plançon & Drits, 1999), la dynamique d'incorporation et de stockage de l'eau a pu être quantifiée avec succès. Cette méthode analytique, combinée aux données publiées d'adsorption de la vapeur d'eau a permis de déterminer l'abondance des couches d'eau structurales développées dans l'espace interfoliaire ainsi que la quantité d'eau contenue dans les différents sites de stockage (interfoliaires, surfaces et porosité). Par ailleurs, une information qualitative sur les surfaces et l'organisation texturale des échantillons a été obtenue sur la base de calculs des modifications de l'épaisseur moyenne des particules et de l'organisation des couches d'eau (ordering). En complément, d'autres expériences ont été réalisées avec des suspensions de smectites contenant des bactéries.

Les expériences d'hydratation de smectites en conditions abiotiques réalisées sur une large gamme de bentonites naturelles et industrielles (SWy-2, IBECO, MX80, TIXOTON) ont permis de définir le rôle des cations interfoliaires, des densités de compaction variables et de la force ionique sur la solution infiltrée. Le taux d'hydratation des smectites, comme attendu, a été défini comme fortement dépendant du type de cation interfoliaire (augmenté en présence de Ca^{2+} , contrairement à Na^+) et de la force ionique de la solution (taux d'incorporations augmentés en présence de solutions salines, particulièrement lors de l'infiltration de smectites sodiques). Une variété de modifications dynamiques de l'état microstructural a également été mise en évidence, apparaissant comme une fonction de la densité de compaction. Ces modifications expliquent un grand nombre des différences de comportement observées lors de l'hydratation des smectites calciques et sodiques. Les mécanismes d'hydratation des smectites, observés en volume confiné, sont inclus dans un modèle schématique prenant en compte différentes échelles, de l'angström pour les feuillettes, à la structure argileuse globale. Alors que la nature des cations interfoliaires affecte l'hydratation à toutes les échelles, la force ionique de la solution infiltrée affecte principalement la structure globale.

En parallèle, l'impact d'une sélection de smectites (SWy-2, MX80 et nontronite) sur le développement des cultures de *S. putrefaciens* a été étudié lors d'expérimentations en solution "batch" sous agitation, combinées avec des comptages de cellules. La survie prolongée des bactéries dans les suspensions de smectites, comparée à leur développement en milieu de culture, est attribué à : un apport continu et durable de nutriments cationiques et de carbone organique (C_{org}), à la capacité tampon de la smectite et aussi, à la grande surface des argiles qui favorise l'accumulation de nutriments, sert de sites de fixation et permet la sorption des déchets toxiques produits.

Le taux d'altération/dissolution des smectites induit par les bactéries a été étudié dans les suspensions par ICP-OES et microscopie (confocale, MEB environnemental et MET couplé à un système de microanalyse en EDS). Un appauvrissement en cations majeurs apparaît dans la solution extraite de la nontronite, qui est attribué à la capture (binding) de cations par *S. putrefaciens*, et est probablement lié à la production de chélateurs. L'appauvrissement constant en Ca^{2+} est très probablement dû à son stockage dans le biofilm abondant produit (substance exo polymérique, EPS). L'importante libération de cations dans le cas de la

nontronite, dans les expériences à long-terme, a été particulièrement mise en évidence en ce qui concerne Fe^{3+} et Al^{3+} , correspondant à plus de 10% de dissolution partielle. A l'inverse, la smectite sodique pauvre en fer n'a pas semblé affectée de la même manière par l'activité bactérienne : l'augmentation de la libération d'Al lors de lessivage acide correspond à un maximum de 1,4% de dissolution partielle de la smectite. La présence de *S. putrefaciens* a causé de nombreux changements texturaux observés en microscopie (confocale, MEB environnemental) associés à la formation d'agrégats smectitiques et de biofilms. En conditions de volume confiné, la présence de bactéries dans un milieu de smectite sodique a montré l'augmentation, à la fois de l'incorporation d'eau en position interfoliaire, et de la quantité d'eau stockée en position externe (pores et surfaces). Dans ce type de smectite compactée, l'augmentation de l'épaisseur totale des couches d'eau apparaît due à l'augmentation, induite par les bactéries, de la porosité de l'échantillon. Ceci a été confirmé par les observations issues de la combinaison des mesures de DRX et la modélisation avec CALCMIX. Dans le cas de la nontronite, de l'eau additionnelle a été stockée en position externe, indiquant une augmentation similaire de la porosité, mais, dans ce cas, le flux d'eau entrant dans la cellule réactionnelle diminue, très certainement dû au colmatage de la porosité par le biofilm.

En termes d'utilisation des bentonites comme matériel de confinement des déchets, cette étude montre que l'activité bactérienne peut modifier les propriétés chimiques et physiques des smectites. Même si les bactéries ne sont pas susceptibles de survivre longtemps dans un milieu smectitique hydraté et hermétique, leurs effets semblent actifs à long terme, spécialement dus aux substances produites par les bactéries, notamment les chélateurs et les EPS.

SUMMARY

This study reports on the physical-chemical behaviour of swelling dioctahedral clays (smectites) and their interaction with aqueous solutions and bacteria (*Shewanella putrefaciens*). Experimental results are presented for compacted clays, hydrated under confined volume conditions, using a new type of reaction-cell (the “wet-cell” of Warr & Hoffman, 2004) that was designed for in situ X-ray diffraction (XRD) measurement. For comparison, dispersed clay systems were studied using standard batch solutions subjected to varying degrees of agitation. The combination of time-dependent in situ XRD measurements with gravimetric measurements and calculated diffraction patterns using the CALCMIX software (Plançon & Drits, 1999) allowed to successful quantification of the dynamics of water uptake and storage. This analytical procedure combined with published water vapour adsorption data enabled determination of the abundance of structured water layers, developed in the interlayer space, and the amount of water contained in different storage sites (interlayers, surfaces and pore spaces). Qualitative information on surface area and textural organization was also estimated based on calculated changes in the average particle thickness and the organization of water layer structures (ordering).

Abiotic smectite hydration experiments, using a range of natural and industrial bentonites (SWy-2, IBECO, MX80, TIXOTON), focused on defining the role of the interlayer cation, variable clay packing densities and the ionic strength of the infiltrating solution. The rate of smectite hydration, as expected, was seen to be highly dependent on the type of interlayer cation (enhanced for Ca as opposed to Na) and the ionic strength of solution (enhanced uptake rates with saline solutions, particularly as they infiltrate Na-smectite). A range of dynamic changes in microtextural state occurred as a function of packing density. These changes explain the differences in hydration behaviour observed between Na- and Ca-smectite. The hydration mechanisms of compacted smectite occurring within a confined volume system are presented in a schematic model involving different scales, ranging from the Å-scale of lattice layers to the bulk clay structure. Whereas the nature of interlayer cation affects hydration on all scales, the ionic strength of the infiltrating solution primarily affects the bulk texture.

The impact of selected smectites (SWy-2, MX80 and nontronite) on the growth of *S. putrefaciens* was studied using agitated batch solution experiments combined with viable cell counts. The prolonged survival of bacteria in smectite suspensions compared to growth in culture medium is attributed to i) a continuous and sustainable supply of cationic nutrients and C_{org} , ii) the buffering capacity of the smectite clay and iii) the large clay surface areas, which accumulate nutrients, serve as attachment sites and sorb toxic waste products. The rate of bacterially induced smectite alteration/dissolution in batch solutions, as monitored by ICP-OES and microscopy (confocal, ESEM and TEM coupled to EDX), shows depletion of the main cations in the nontronite extracted solution. This is attributed to the initial consumption and/or binding of cations by *S. putrefaciens*, which is probably related to the production of chelating agents. The constantly depleted Ca is most likely stored in the abundant EPS (exopolymeric substance). Enhanced cation release in the case of nontronite in long-term experiments was especially evident for Fe and Al that corresponds to more than 10% partial dissolution. In contrast, the Fe-poor, Na-smectite was not seen to be affected by bacterial activity in this way and the increased release of Al by acid leaching corresponds to only 1.4% partial smectite dissolution. The presence of *S. putrefaciens* induced abundant textural changes as observed by microscopic investigations (confocal microscopy, ESEM), associated with the formation of smectite-aggregates and biofilms. In confined volume conditions, the presence of bacteria in Na-smectite clay was seen to enhance both the uptake of interlayer water and the amount of externally stored surface and pore water. In this type of compacted smectite, an increase in the total thickness of water layer structures occurs due to bacterial

enhancement of sample porosity as seen by combined X-ray diffraction study and CALCMIX profile calculations. In the case of nontronite, additional water was stored as external water indicating a similar enhancement of porosity, but here, the rate of water inflow into the reaction cell decreased, most likely due to clogging of the pores by biofilm.

With respect to the application of bentonites as a suitable backfill material in underground waste disposal sites, this study demonstrates that bacterial activity can modify both chemically and physically the properties of the smectite. Even if bacteria are not likely to survive in a hydrated bentonite seal, their effects are considered to be long-term, especially due to bacterially produced substances such as EPS and organic ligands.

CONTENTS

ACKNOWLEDGEMENTS i
RÉSUMÉ i
SUMMARY iii
CONTENTS v
FIGURES LIST xi
TABLES LIST xix
ABBREVIATIONS LIST xxii

CHAPITRE 1 INTRODUCTION1

1.1. Argiles gonflantes et vie microbienne..... 2
1.2. Argiles gonflantes dans l'industrie..... 3
1.3. Utilisation des argiles gonflantes dans le stockage des déchets nucléaires..... 4
1.4. Objectifs de l'étude..... 7
1.5. Plan de la thèse 7

CHAPTER 1 INTRODUCTION.....9

1.1. Swelling clays and microbial life..... 10
1.2. Swelling clays in industry 11
1.3. Swelling clays in nuclear waste disposal 12
1.4. Objectives of the study 14
1.5. Outline of the study 15

CHAPTER 2 STRUCTURE AND PROPERTIES OF SMECTITES AND OF RELATED BACTERIA	17
2.1. Smectites.....	18
2.1.1. Layer charge and cation exchange capacity (CEC).....	19
2.1.2. Edge charges	20
2.1.3. Interlayer hydration properties and analytical approaches to study hydration.....	21
2.1.4. The diffuse double layer, DLVO theory, and implications for smectite swelling ...	23
2.1.5. Hydration of non-interlayer sites: Surface and pore water	25
2.1.6. Smectite swelling in a confined volume system	26
2.2. The role of bacteria	27
2.2.1. Structure, properties and requirements of bacteria.....	27
2.2.2. The bacterial cell wall	28
2.2.3. Requirements for bacterial growth	29
2.2.4. <i>Shewanella putrefaciens</i>	31
2.2.5. Impact of bacteria on their environment	31
2.3. Conclusion an approach of this study	32
CHAPTER 3 MATERIALS AND ANALYTICAL METHODS.....	35
3.1. Sample materials	36
3.1.1. Bentonite samples: MX80, IBECO, TIXOTON	36
3.1.2. Nontronite and montmorillonite separates	38
3.1.3. Solutions: ground water, sea water and experimentally mixed saline solutions.....	39
3.1.4. Bacteria.....	40
3.2. Analytical Methods	41
3.2.1. X-ray diffraction study	41
3.2.1.1. Concept of a laboratory analogue: reaction-cell X-ray diffractometry	44
3.2.2. Monitoring hydration	46
3.2.2.1. Quantification of interlayer hydration using CALCMIX	46
3.2.2.2. Quantification of non-interlayer hydration.....	47

3.2.3. XRD characterization of clay minerals	47
3.2.4. Microscopy	48
3.2.4.1. Confocal microscopy	48
3.2.4.2. Electron microscopy	48
3.3. Bacteria preparation and analyses	50
3.3.1. Aseptic techniques.....	50
3.3.2. Culture preparation.....	51
3.3.3. Viable cell counts	51
3.4. Solution chemistry	52
CHAPTER 4 ABIOTIC INFLUENCE ON SMECTITE HYDRATION	55
Abstract	56
4.1. Introduction	57
4.2. Analytical procedure.....	59
4.3. Hydration results of compacted smectite clay under confined volume.....	60
4.3.1. Total water uptake as a function of interlayer cation, solution chemistry and clay packing density.....	60
4.3.2. Influence of solution chemistry on the hydration mechanisms of Wyoming montmorillonite (SWy-2).....	64
4.3.2.1. Dynamics of water layer development in SWy-2.....	64
4.3.2.2. Organization of interlayer water (ordering) in SWy-2.....	67
4.3.2.3. Particle thickness and theoretical surface area in SWy-2.....	69
4.3.3. Influence of initial packing density and water content on the hydration behaviour of MX80 bentonite.....	71
4.3.3.1. Dynamics of water layer development in MX80	71
4.3.3.2. Organization of interlayer water (ordering) in MX80.....	74
4.3.3.3. Water uptake into different storage sites in MX80	76
4.3.3.4. Particle thickness and theoretical surface area in MX80.....	78
4.3.4. Hydration behaviour of bentonite in natural solution	80
4.3.4.1. Dynamics of water layer development in IBECO and TIXOTON	80
4.3.4.2. Water uptake into different storage sites in IBECO and TIXOTON	82

4.3.4.3. Particle thickness and surface area estimates in IBECO and TIXOTON	84
4.4. Discussion	86
4.4.1. The influence of the type of smectite and solution chemistry	86
4.4.2. Progressive hydration in solution under confined volume conditions	88
4.4.3. The influence of initial conditions	93
4.4.4. Implications of confined volume laboratory analogue for understanding natural systems.....	94
CHAPTER 5 BACTERIAL INFLUENCE ON SMECTITE HYDRATION	97
Abstract	98
5.1. Introduction	100
5.2. Analytical procedure	102
5.2.1. Agitated batch experiments.....	102
5.2.2. Confined volume experiments using reaction-cell XRD	103
5.2.3. Analyses of reaction products	104
5.3. Results	105
5.3.1. Bacterial growth in a clay suspension	105
5.3.2. Effects of bacterial action on smectite solution chemistry.....	110
5.3.2.1. pH variations	110
5.3.2.2. Nontronite cation release into solution.....	114
5.3.2.3. Montmorillonite cation release into solution.....	117
5.3.3. Microscopic Analysis.....	120
5.3.3.1. The role of biofilm: Confocal microscopy and ESEM.....	120
5.3.3.2. Microscale interaction and microchemistry investigated by TEM	122
5.4. Bacteria - compacted clay interaction under confined volume conditions	126
5.4.1. In situ monitoring of smectite hydration by reaction-cell X-ray diffraction.....	126
5.4.1.1. Bacterial effects on total water uptake	126
5.4.1.2. Bacterial effect on interlayer water uptake.....	127
5.4.1.3. Bacterial effects on the storage of water	132
5.4.2. Characterization of reaction products	135
5.4.2.1. Powder XRD	135

5.4.2.2. XRD-texture characterization of samples	138
5.4.2.3. Chemistry of solution extractions.....	145
5.4.2.4. The role of Fe-reduction under confined volume conditions	149
5.4.2.5. Microscopical observations of long-term experiments	151
5.5. Discussion.....	153
5.5.1. The influence of smectite on bacterial activity	153
5.5.2. Physical and chemical influence of bacteria on smectite clay	157
5.5.2.1. Complexation and binding of potential nutrients and effects on smectite	157
5.5.2.2. Effects of bacterial respiration on smectite	159
5.5.2.3. Bacterially induced dissolution of nontronite.....	160
5.5.2.4. Textural alteration	162
5.5.3. Concluding remarks	163
CHAPTER 6 IMPLICATIONS ON SMECTITE HYDRATION IN ABIOTIC AND BIOTIC ENVIRONMENTS	165
6.1. Environmental processes and the importance of laboratory analogue experiments ...	166
6.2. Application of confined volume experiments: constraints for backfill hydration ..	169
6.2.1. Predicting the rates of clay barrier saturation	170
6.2.2. Diffusion and transport capacity for radionuclides	173
6.3. Limitations of the study: challenges for further research	173
GENERAL CONCLUSIONS	175
LITERATURE	179
APPENDIX	193

FIGURES LIST

Chapter 1

Fig. 1.1. Schematic sketch of an underground repository for the storage of nuclear waste. The multi-barrier concept includes the bedrock as a natural barrier as well as the backfill and waste containers as engineered barriers. 12

Chapter 2

Fig. 2.1. Schematic representation of the crystal structure of smectite. The alternating succession of tetrahedral (T) and octahedral (O) units makes up the sheet-like structure. The interlayer space (IL) contains cations and separates the TOT sheets. The resulting lattice thickness of the structure (d-value) is 9.6Å (modified after Grim, 1962). 19

Fig. 2.2. Schematic representation of the pH dependent edge charges (modified after Lagaly, 1993). 21

Fig. 2.3. a) Schematic representation of the diffuse double layer of a smectite particle in suspension. b) Formation of tactoid particles due to osmotic swelling (modified after Lagaly, 1993). 24

Fig. 2.4. a) With increasing ionic strength the dimension of the diffuse double layer is decreased. b) The curves for interaction energy show decreasing electrostatic repulsion and increasing influence of Van-der-Waals attractive forces. c) Coagulation of particles forming stair-step-card house structures (Hofmann, 2003; modified after Lagaly et al. 1997). 25

Fig. 2.5. Internal structure of a prokaryotic cell (modified after Madigan et al. 2003). 28

Fig. 2.6. Schematic representation of the gram-negative and the gram-positive cell wall (Cleassens, 2006; modified after Willey et al. 1996). 29

Chapter 3

Fig. 3.1. Schematic representation of cation sites in the dioctahedral smectite structure (non-stoichiometric). Abbreviations are as follows: IL- interlayer, T- tetrahedral sites and O- octahedral sites (after Velde 1992). 38

*Fig. 3.2. TEM image of *S. putrefaciens* cultivated in minimal medium showing the presence of a flagellum. 41*

Fig. 3.3. Photograph through the window of the D-5000 Bruker-Siemens diffractometer showing the X-ray tube, the goniometer and the sample holder. 42

Fig. 3.4. Two dimensional schematic sketch of X-ray diffraction and the Bragg's law. The incident X-ray beam with the wavelength λ interacts with the atoms arranged in a periodic manner (grey dots) forming different sets of planes in the crystal (dotted lines). Bragg's law

gives the condition for the occurrence of constructive interference and the position of the diffraction peak. 42

Fig. 3.5. Increase of *d*-values due to intercalation of water layers. 43

Fig. 3.6. a) Schematic representation of the reaction-cell sealed by Capton foil. b) Closed reaction-cell with Teflon bottles, c) reaction-cell mounted on the sample holder of the diffractometer. 45

Fig. 3.7. a) SEM image of a nontronite aggregate. b) ESEM image of swelling nontronite... 50

Fig. 3.8. Example of a serial dilution conducted prior to viable cell counts. 0.1ml of the initial sample are introduced into 0.9ml sterile water and mixed. 0.1ml of this dilution is then introduced to another tube that contains as well 0.9ml water and so on. Each step leads to a 10 fold dilution. 0.1ml of the final dilution is then spread on an agar plate. In the example presented there are too many colonies on the first two plates (10^{-1} and 10^{-2}) but the third dilution gives good results with 125 colonies on the plate yielding a count of $1.25 \cdot 10^5$ cfu/ml (after Madigan et al. 2003). 52

Chapter 4

Fig. 4.3.1. Solution uptake into pressed smectite powders in ml/g. Ca-smectite (TIXOTON, NAu-1) reaches steady state earlier than Na-smectite (IBECO, MX80 and SWy-2) and generally incorporates higher amounts of solution. *I*=ionic strength. 61

Fig. 4.3.2. Influence of ionic strength on solution uptake into pressed smectite powders. Correction of weight due to higher ionic strength is indicated as dotted line. a) SWy-2 purified montmorillonite infiltrated by 1M NaCl solution and purified water (packing density 1.36 and 1.37 g/cm³). B) IBECO Na-montmorillonite infiltrated by sea water and ground water (packing density 1.14 and 1.15 g/cm³). c) TIXOTON Ca-montmorillonite infiltrated by sea water and ground water (packing density 0.94 g/cm³). *I*=ionic strength..... 62

Fig. 4.3.3. Correlation between packing density and total water uptake for various samples. Materials containing predominantly Ca in smectite interlayers take more water in than the Na varieties. Interpolating the plots to zero water uptake (dotted lines) yields for both varieties the same values for packing density (2.1 g/cm³) that corresponds to mineral density. 63

Fig. 4.3.4. Development of water layers in Na-exchanged purified montmorillonite (SWy-2). a) During infiltration of purified water and b) during infiltration of 1M NaCl. c) Storage sites for solution when infiltrated by purified water and d) by 1M NaCl. Values for weight of NaCl corrected..... 65

Fig. 4.3.5. Schematic representation of the formation of new external surfaces associated with decreasing particle thicknesses. *N*=number of layers per particle (stack). 66

Fig. 4.3.6. Ordering of mixed water layer structures (grey bars) expressed as probabilities (*p*) and the corresponding water layer abundance (empty bars) for SWy-2 a) infiltrated by water b) infiltrated by NaCl. c) Stacking probability plotted for SWy-2 expressed as the deviation

from the random stacking state ($R=0$) when infiltrated by purified water and d) for SWy-2 infiltrated by NaCl solution..... 69

Fig. 4.3.7. Plot showing the change in the number of layers per stack and the corresponding increase of surface area with time a) for SWy-2 infiltrated by purified water and b) by 1M NaCl. c) Shows the distribution of stored water and the estimated amount of surface adsorbed water for the saturated stable state (indicated as a horizontal dotted line) assuming a concentration of 4mmol/g. The distance between the surface absorbed water line and the external water curves (marked by a vertical arrow) represents the amount of bulk pore water at the end of the hydration experiment..... 70

Fig. 4.3.8. Development of water layer structures in montmorillonite during hydration of MX80 bentonite. a) Dehydrated sample with a packing density of 1.35g/cm^3 . b) Dehydrated sample with elevated packing density (1.43g/cm^3). c) Initially hydrated sample with a packing density of 1.60g/cm^3 . The number in brackets corresponds to the dry packing density. 73

Fig. 4.3.9. Ordering of mixed water layer structures (grey bars) expressed as probabilities (p) and the corresponding water layer abundance (black empty bars). a) Initial stages of the experiment and b) the final stages. Expressed as the deviation from the random stacking state ($R=0$). c) Initial stages and d) final stages..... 75

Fig. 4.3.10. Water uptake into the different storage sites of MX80 bentonite. a) Dehydrated sample with an intermediate packing density (1.35g/cm^3). b) Dehydrated sample with an elevated packing density (1.43g/cm^3). c) Initially hydrated sample. Note the packing density is higher when including the initial water content (1.60g/cm^3) compared to that of the dry state (1.31g/cm^3). 77

Fig. 4.3.11. Plot showing the change in the number of layers per stack and the corresponding increase of surface area with time for dehydrated and compacted MX80 powder. a) Dehydrated and compacted MX80 powder (1.35g/cm^3). b) Dehydrated and highly compacted MX80 powder (1.43g/cm^3). Estimation of surface adsorbed water according to increased smectite surface area for c) dehydrated and compacted MX80 powder (1.35g/cm^3) and d) dehydrated and highly compacted MX80 powder (1.43g/cm^3). Dotted lines indicate the calculated amount of water corresponding to the stable saturated state assuming 4 or 2.5mmol/g required to cover the external surface area. TW-total water, ILW-interlayer water, EW-external water (combined surface and pore water). 79

Fig. 4.3.12. Water layer development in smectite contained in bentonite powders. a) IBECO infiltrated by ground water. b) IBECO infiltrated by sea water. c) TIXOTON infiltrated by ground water. d) TIXOTON infiltrated by sea water. Ionic strength for ground and sea water is 0.0013 and 0.64M, respectively. Modified after Warr & Berger (2007). 81

Fig. 4.3.13. Partitioning of water storage sites in bentonites infiltrated by natural solutions. The weight of sea water was corrected for the amount of dissolved ions. Modified after Warr & Berger (2007). 83

Fig. 4.3.14. Changes in the number of layers per stack and the corresponding surface areas of montmorillonite contained in bentonite (a-d). 85

Fig. 4.4.1. Different hydration sites in a smectite powder as a function of scale. a) Interlayer, b) surface of particles composed of several layers, c) aggregates composed of several particles and d) arrangements of aggregates. The aggregate model shown in c is modified after Suzuki et al. (2005). Hydration sites are marked with arrows..... 86

Fig. 4.4.2. Schematic sketch of water uptake and hydration of smectite in confined volume conditions (bulk textural scale). a+b) Initial stages of hydration dominated by pore water intake. c+d) Pore water serves as a reservoir for interlayer expansion leading to the formation of hydration aggregates. e+f) Interlayer hydration and local particle separation leads to the expansion of aggregates and pore closure. In the case of Na-smectite (e) the formation of gels fill remaining pore spaces and voids associated with mineral impurities (inserted image). 92

Chapter 5

Fig. 5.2.1. a) Schematic representation of the reaction-cell device (without upper sealing plate). b) Set up for flow-through experiments with solution bottles attached. At any stage of the hydration experiment, the reaction-cell in a) can be placed in the X-ray diffractometer for measurement. 104

Fig. 5.3.1. a) Growth curves of *S. putrefaciens* in culture media (solid black lines, LB indicates Luria Bertrani medium and MM the minimal medium defined by Myers & Nealson (1988)) and smectite suspensions of two different mineral concentrations. The light grey background indicates the population span for the nontronite (NAu-1) culture and the dark grey background for the two montmorillonite rich samples MX80 and SWy-2. Bacterial populations are measured as colony forming units per ml of suspension (cfu/ml) plotted against reaction time (days). b) Schematic representation of the growth curves showing the main differences in the duration of recognized phases (numbers in italics). 106

Fig. 5.3.2. Changes in pH over time for the different smectite suspensions (density 0.01g/ml). Montmorillonite suspensions are highlighted with a dark background, nontronite suspension with a light grey one. Filled symbols indicate the presence of bacteria, empty ones present sterile controls..... 110

Fig. 5.3.3. Changes in pH over time for a-b) montmorillonite suspensions (aerobic), c) the nontronite (NAu-1) suspension (aerobic) and d) the montmorillonite (MX80) suspension (anaerobic). Filled symbols with solid lines indicate the evolution of pH values for samples containing bacteria; the empty symbols with dotted lines represent sterile controls. The corresponding growth curves are presented as dashed lines, and the recognized phases marked with vertical arrows: A-lag, B-exponential, C- stationary and D-death. 111

Fig. 5.3.4. Relative difference in the pH of bacteria containing smectite suspensions from the abiotic control expressed as a %. The phases of growth (A-D) are indicated as shown in Fig 5.3.2. Abbreviations for the growth phases: A-lag, B-exponential, C- stationary and D-death.. 113

Fig. 5.3.5. a) The concentration of cations released from nontronite into purified water. Light grey columns indicate cation release into the solution after 2h of dispersion, dark grey columns after 264h. Columns in dotted lines correspond to 2% theoretical stoichiometrical cation release. b) Mineral formula and a schematic representation of cation sites in layered

smectite structure (non-stoichiometric). Abbreviations: IL- interlayer, T- tetrahedral sites and O- octahedral sites. 114

Fig. 5.3.6. The concentration of cations in solution derived from the bacteria containing nontronite suspension after 2h (filled light grey columns) and 264h (filled dark grey columns). Empty columns indicate the amount of depletion compared to the cation concentration of the sterile control. 116

Fig. 5.3.7. The concentration of cations released from Wyoming montmorillonite (SWy-2) into purified water after 2h (light grey columns) and 264h (dark grey columns). Columns in dotted lines represent stoichiometrical cation release. b) Mineral formula and a schematic representation of cation sites in the smectite structure (non-stoichiometric). Abbreviation: IL- interlayer, T- tetrahedral sites and O- octahedral sites..... 117

Fig. 5.3.8. a) The concentration of cations released from montmorillonite (contained in MX80) into purified water after 2h and 264h. Columns in dotted lines correspond to 3% theoretical stoichiometrical cation release. b) Mineral formula and a schematic representation of cation sites in the smectite structure (non-stoichiometric). Abbreviation: IL- interlayer, T- tetrahedral sites and O- octahedral sites..... 118

Fig. 5.3.9. The concentration of cations in solution derived from bacteria containing MX80 suspension. Empty columns indicate the amount of depletion compared to the cation concentration of the sterile control. In the case of Ca, Fe and K less cations are dissolved in solution when bacteria are present. Na and Si in contrast are slightly enhanced..... 119

Fig. 5.3.10. The concentration of cations in solution derived from bacteria containing SWy-2 suspension. Empty columns indicate the amount of depletion compared to the cation concentration of the sterile control. Virtually all cations in solution are present in higher concentrations when bacteria are present. 119

Fig. 5.3.11. Confocal transmitted light microscopy image of smectite incubated with S. putrefaciens. a) MX80 and b) nontronite. Biofilm appears within aggregates as diffuse structure. 120

Fig. 5.3.12. a) ESEM image of a two day old S. putrefaciens culture forming biofilm around precipitates from the medium. b) Bacteria incorporated in biofilm attached to a phosphate needle that precipitated from the medium. c) ESEM image of a two week old culture after the majority of cells have died. The biofilm is still visible. d) ESEM picture of biofilm forming on mineral particles. 121

Fig. 5.3.13. a) TEM microphotograph of S. putrefaciens cultivated in minimal medium. b) EDX microanalysis of part of the cell marked by an arrow. The analysis shows high amounts of Na, P, S and Ca, as well as a Cu peak from the sample grid..... 122

Fig. 5.3.14. a) TEM microphotograph of S. putrefaciens cultivated in Fe-rich minimal medium. b) EDX microanalysis of the coated grid. c) EDX microanalysis of the cell showing the bacterium to containing elements of the medium. The dark areas of the cell are Fe-rich (the Cu-peak is from the sample grid)..... 123

Fig. 5.3.15. TEM microphotograph and corresponding EDX spectra of nontronite particles. Microanalysis shows typically high amounts of iron (12.1 wt% Fe_{tot}). Quantification was done without correcting for C content derived from the sample coating. The Cu-peak comes from the sample grid. 123

Fig. 5.3.16. a) TEM microphotograph of nontronite incubated with bacteria for 10 days. b-c) Corresponding EDX spectra showing typical nontronite composition in darker regions and a Si-rich gel-like structure surrounding the grains. The Cu-peak comes from the sample grid. d) TEM microphotograph of nontronite covering a bacterial cell (position marked with arrow)... .. 124

Fig. 5.3.17. a) TEM microphotograph of montmorillonite (MX80) showing relicts of a bacterial cell. The corresponding EXD spectrum shows typical values for montmorillonite. b) TEM microphotograph of bacteria cultivated in the presence of MX80 bentonite. The image shows a bacterial cell with montmorillonite wrapped around it. c) EDX spectrum of the cell. d) EDX spectrum of the montmorillonite. 125

Fig. 5.4.1. Total water uptake into smectite powder determined by weight. 127

Fig. 5.4.2. a-b) Abundance of water layers for nontronite (NAu-1) and montmorillonite (MX80) without and with *S. putrefaciens*, expressed in percent (%) vs. the reaction time (in hours). Encircled symbols indicate the number of water layers within the hydrating interlayer. The dashed lines show the normalized total water uptake determined by weight. 129

Fig. 5.4.3. Ordering of mixed water layer structures expressed as a deviation from the R0 (random) stacking state for a) nontronite without bacteria, b) nontronite with bacteria, c) montmorillonite (MX80) without bacteria, and d) montmorillonite (MX80) with bacteria... 131

Fig. 5.4.4. a-d. Storage of water in interlayer and non-interlayer sites from nontronite (NAu-1) and montmorillonite (MX80) without and with *S. putrefaciens*. 132

Fig. 5.4.5. a) XRD patterns of initial (black) and final (grey) bacteria containing nontronite powders extracted from the reaction-cell experiments. Basal reflections of hydrated nontronite (Ntr) and the internal standard kaolinite (Kln) are indicated with corresponding d-values in Å. Additionally both samples contain goethite (Gt), tridymite (Trd), biotite (Bt) and precipitations of the Al-sulphate basaluminite (Bal). Mirabilite (Mir) and vivianite (Viv) are only contained in the final reaction products (bold). b) XRD patterns of the initial sterile nontronite (black) and the final measurements made at the end of the experiment (grey). The final reaction products show enhanced basaluminite precipitation (bold)... .. 135

Fig. 5.4.6. a) Selected XRD patterns of sterile MX80 measured in situ during the reaction-cell experiment. The initial measurement is shown in black and the last measurement (after 9600 h) in light grey. The d-values for montmorillonite (Mnt) present mostly a mixture of 2- and 3-WL hydrates. All samples contain illite (Ill), quartz (Qtz) and feldspar (Fsp). Non-silicates are present as bassanite (Bas), rhodochrosite (Rds), and in some measurements, calcite (Cal) is visible. b) The amount of green rust is observed to increase and decreases during the period of the experiment, suggestive of precipitation and subsequent dissolution. All d-values are given in Å..... 136

Fig. 5.4.7. a) Selected XRD patterns of bacteria containing MX80 measured in situ during the reaction-cell experiment. The initial measurement is shown in black and the last measurement (after 3150 h) in light grey. The *d*-values for montmorillonite (Mnt) present mostly a mixture of 2- and 3-WL hydrates. All samples contain illite (Ill), quartz (Qtz) and feldspar (Fsp). Non-silicates are bassanite (Bas), rhodochrosite (Rds) and in some measurements calcite (Cal). Reflections indicating dissolution/precipitation are shown in the magnified images: b) increase of green rust c) increase of lepidocrocite (Lpc) and d) decrease of calcite (Cal). The 2.42 Å peak of pyrite (Py) is perhaps present in c). All *d*-values are given in Å. 138

Fig. 5.4.8. a) XRD patterns of air dried (AD) and glycolated (EG) texture preparations of the original nontronite sample (upper sketch, light grey), of the sample extracted from the sterile reaction-cell (middle dark grey) and the sample extracted from the *S. putrefaciens* containing reaction-cell (black). b) Enlarged image of the (001) reflection with *d*-values. The numbers in italics indicate the relative air humidity (RH) for air dried samples at the time of measurement..... 139

Fig. 5.4.9. XRD patterns of Mg-exchanged and glycerol-saturated texture preparations extracted from sterile (S) and bacteria containing (B) reaction-cell experiments. The enlarged image shows the position of 001 reflections and their corresponding *d*-values. The light grey pattern represents the Mg-exchanged and glycerol- saturated original sample (O) that was taken as a reference..... 141

Fig. 5.4.10. XRD patterns of nontronite reaction-cell experiments with and without bacteria. a) Air dried, b) heated to 80°C, c) heated to 120°C and d) heated to 160°C. 143

Fig. 5.4.11. a) XRD patterns of montmorillonite (MX80 sample) measured as air dried texture slides prepared from the sterile (grey) and bacteria containing (black) reaction-cells. The numbers in brackets indicate the order of diffracting basal planes (00*l* series of montmorillonite) and their corresponding *d*-values in Å. b) Enlarged image of the (001) reflection. The numbers in italics indicate the relative air humidity (RH) during measurement. 144

Fig. 5.4.12. a) XRD patterns of montmorillonite (MX80) measured as air dried texture slides prepared from the sterile (S, grey, RH 45%) and bacteria containing (B, black, RH 42%) reaction-cells. b) XRD patterns of the collapsed interlayer structure after heat treatment (24h 80°C). 145

Fig. 5.4.13. Concentration of cations leached into solution of samples taken from nontronite reaction-cell experiments (with and without bacteria). a) Absolute concentrations, b) normalized to 10% of stoichiometric cation release (zero line). 146

Fig. 5.4.14. A comparison between the concentrations of cations extracted from nontronite using water (solid lines) and HCl (dashed lines). The results show higher cationic content for HCl leaching especially for Fe. Generally bacteria containing samples (grey columns) release more cations into solution than bacteria free (white columns). 147

Fig. 5.4.15. Concentration of cations leached into solution of samples taken from the MX80 montmorillonite reaction-cell experiments (with and without bacteria). a) Absolute values obtained from ICP-OES analyses. b) Normalized to 3% stoichiometric cation release (zero line). 148

Fig. 5.4.16. Comparison between the concentrations of cations extracted from montmorillonite using water (solid lines) and HCl (dashed lines). The results show higher cationic content for HCl leaching analysis of bacteria containing montmorillonite samples. Without bacteria (white columns) the values are comparable to the water extracts. 149

Fig. 5.4.17. Measured Fe(II) values for reaction-cell extractions (solid lines) with and without bacteria. Dotted columns represent values taken from the literature, which show initial Fe(II) concentration (empty column) and that after clay-bacteria interaction in batch experiments (Kim et al. 2004, striped column). 150

Fig. 5.4.18. Relative differences in Fe(II) content for the bacteria-containing reaction-cell experiments in % (dark grey column) when normalized to the sterile control. Anaerobic batch cultures (light grey column) and aerobic batch cultures (empty column). The numbers in brackets represent the absolute differences in mmol/g. 151

Fig. 5.4.19. a) TEM microphotograph of nontronite and *S. putrefaciens* taken from reaction-cell experiment. The size of the bacterium does not exceed 0.7 μ m in length and is partly damaged. b) EDX microanalysis of the nontronite grain shown in a) contains Si, Al, Fe, Ca and K. c) EDX microanalysis of the bacterial cell showing the same cations along with additional S and Cl due to the presence of bacteria. The Cu is derived from the sample grid. 152

Fig. 5.5.1. The behavior of smectite and bacteria in solutions. a) With monovalent cations the electrostatic repulsion keeps clay and bacteria in suspension. b) The presence of divalent cations serve as bridges and allow the formation of aggregates. 155

Fig. 5.5.2. Schematic sketch showing the interaction of nontronite and *S. putrefaciens* at the lattice layer scale. a) Octahedrally coordinated Fe(III) is mobilized at unstable edge sites and the Ca from interlayer sites is released into solution. Bacterially produced ligands (here catecholate) form siderophore complexes with Fe(III) as the central cation (modified after Konhauser, 2007). b) Calcium acts as a bridge between clay and bacteria. The complex is transported to the cell, the Fe(III) is dismantled and reduced or is involved in the formation of Fe(III)-coatings at the cell surface. As the complexation leads to continuous dissolution, Si is released and precipitated as amorphous silica, which is presumably associated with EPS. 161

Fig. 5.5.3. Bacteria in confined volume conditions. a) Directly after closing the reaction cell the bacteria occupy open pores between mineral grains and aggregates. b) Pores are closed due to increased swelling during smectite hydration. Exudates of bacteria cause aggregation in their vicinity. c) After death and lyses of bacteria newly formed porosity becomes available for additional swelling. 163

Chapter 6

Fig. 6.1. Schematic sketch of the time required to saturate a 1m thick bentonite barrier as a function of initial packing density and the difference types of solutions infiltrated. 171

TABLES LIST

Chapter 2

Table 2.1. *Compilation of layer charge and idealized formula of some representative 1:1 and 2:1 phyllosilicates modified from Bergaya & Lagaly (2006).* 19

Table 2.2. *Compilation of bacterial nutrients (Madigan et al., 2003; Todar, 2006).*..... 30

Chapter 3

Table 3.1. *List of samples and their important mineralogical characteristics. Data taken from (Hofmann et al., 2004)¹⁾, (Sauzeat et al., 2001)²⁾, (Mermut & Cano, 2001)³⁾, (Keeling et al., 2000)⁴⁾ and (Chipera & Bish, 2001)⁵⁾. *Own data.* 37

Table 3.2. *Chemical composition of the used materials. Data taken from (Hofmann et al., 2004)¹⁾, (Sauzeat et al., 2001)²⁾, (Mermut & Cano, 2001)³⁾, (Keeling et al., 2000)⁴⁾.* 39

Table 3.3. *Cationic compositions of the natural solutions used in this study determined by atomic adsorption spectroscopy (Warr & Berger, 2007).* 40

Table 3.4. *Cation composition of the Luria Bertrani medium (LB) and a list of the major compounds in the minimal medium (MM) as defined by Myers and Nealson (1988). The electron acceptor was only added to adapt bacteria to Fe(III)-respiration and for incubation under anaerobic conditions.*..... 40

Chapter 4

Table 4.1.1. *Summary of the key properties of the studied materials after sample preparation and a list of the experimental conditions used in the hydration experiments.* 59

Table 4.3.1. *Total water uptake for confined volume experiments infiltrated by solutions. *Uptake after correcting the weight of concentrated solutions.*..... 61

Table 4.3.2. *Water uptake into different storage sites of SWy-2montmorillonite. *Weight of NaCl corrected.* 66

Table 4.3.3. *Average number of layers per stack and the corresponding theoretical surface area. *Calculated assuming 4mmol/g. The dry BET surface area is 27.64m²/g.* 71

Table 4.3.4. *Water layer abundance (%) and the difference in mean lattice layer thickness in Å between the initial and final state of hydration.* 74

Table 4.3.5. *Experimental results used to calculate the rates of water uptake into the various storage sites of MX80 montmorillonite as a function of different packing densities and initial hydration states.* 77

Table 4.3.6. Results used to estimate the amount of surface water based on decreasing layers per stack. *Assuming a mean of 19 layers per stack at dry state..... 78

Table 4.3.7. Water layer abundance (%) and the difference in mean lattice layer thickness in Å between the initial and final state of hydration for bentonites infiltrated by natural solution. 82

Table 4.3.8. Experimental results used to calculate the rates of water uptake into the various storage sites of Na- and Ca-bentonites. The weight of sea water was corrected for salt content. 84

Table 4.4.1. Calculated rates of water uptake into the interlayer sites. *Na- smectite, ⁺Ca-smectite..... 87

Table 4.4.2. Calculated saturation velocities for the different clays powders used in this study. The time to saturate 1m of compacted smectite is calculated based on the distance across the reaction cell (24mm) and the time required to reach the fully hydrated state..... 95

Chapter 5

Table 5.3.1. Starting densities of bacteria expressed as colony forming units per ml clay suspension (cfu/ml)..... 105

Table 5.3.2. Data used to calculate the time to double during the exponential growth phase expressed as generation time (g) in hours. Initial and final cell numbers correspond to the beginning (68h) and end (164h, see Fig. 5.3.1.b) of the exponential phase and were used to calculate the slope..... 107

Table 5.3.3. Theoretical cationic nutrients available in g/l for the different smectites if particles were dissolved to 100%..... 109

Table.5.4.1. Ionic strength of solutions and bacterial densities. 127

Table 5.4.2. Water layer abundances (%) and corresponding basal lattice d-values for sterile and *Shewanella*-bearing nontronite and MX80 bentonite clays 130

Table 5.4.3. Values for interlayer and non-interlayer water uptake for nontronite and montmorillonite (contained in MX80) with and without bacteria. 133

Table 5.4.4. Mean number of layers per stack and corresponding theoretical surface area for MX80 montmorillonite with and without bacteria. *Assuming 19 layers per stack for the “dry” state and *4 and **2.5 mmol H₂O/g for the amount of adsorbed surface water..... 134

Table 5.4.5. XRD peak characteristics (001 reflection) of nontronite materials after various chemical and physical treatments. *FWHM= full width at half maximum. 141

Table 5.4.6. XRD peak characteristics for montmorillonite (contained in MX80)..... 145

*Table 5.4.7. Composition of minimal medium (MM) and the salt solution that were used in experiments with their contribution to cationic content of leaching solutions. *Based on 2.2E-02 l MM in 1 l leaching solution. 146*

*Table 5.4.8. Theoretical iron content in nontronite as described by Keeling et al. 2000, *Andrade et al. 2002; Kim et al. 2004 and **O'Reilly et al. 2005..... 150*

Chapter 6

Table 6.1. A summary of the effects clay minerals have on bacterial growth in batch experiments (solution dominated system) and compacted confined volume experiments (mineral-dominated). TEA = Terminal electron acceptor. 168

Table 6.2. Compilation of bentonite clay backfill properties and possible abiotic and biotic effects as a function of scale. IL = Interlayer water WL = Water layer HC = Hydraulic conductivity. 169

ABBREVIATIONS LIST

<i>BET</i>	<i>Brunauer-Emmet-Teller</i>
<i>CEC</i>	<i>Cation exchange capacity</i>
<i>cfu</i>	<i>Colony forming unit</i>
<i>C_{org}</i>	<i>Organic carbon</i>
<i>EDX</i>	<i>Energy dispersive spectroscopy</i>
<i>EPS</i>	<i>Exopolymeric substance</i>
<i>ESEM</i>	<i>Environmental scanning electron microscopy</i>
<i>EW</i>	<i>External water</i>
<i>FEBEX</i>	<i>Full-scale engineered barrier experiment</i>
<i>HC</i>	<i>Hydraulic conductivity</i>
<i>IL</i>	<i>Interlayer</i>
<i>ILW</i>	<i>Interlayer water</i>
<i>LBM</i>	<i>Luria Bertrani medium</i>
<i>MM</i>	<i>Minimal medium</i>
<i>SSA</i>	<i>Specific surface area</i>
<i>TEA</i>	<i>Terminal electron acceptor</i>
<i>TEM</i>	<i>Transmission electron microscopy</i>
<i>TW</i>	<i>Total water</i>
<i>WL</i>	<i>Water layer</i>
<i>WLs</i>	<i>Water layers</i>
<i>XRD</i>	<i>X-ray diffraction</i>

CHAPITRE 1

-

INTRODUCTION

1. INTRODUCTION

1.1. Argiles gonflantes et vie microbienne

L'ubiquité et la réactivité des bactéries et des minéraux sur Terre offrent un potentiel énorme pour une grande variété d'interactions dans les environnements hydriques. Les premiers travaux liant les domaines de la géologie et de la microbiologie ont été publiés au début du siècle dernier, traitant notamment de l'implication de microorganismes dans la formation de sulfure d'hydrogène et de carbonates de calcium (Nadson, 1903; in Ivanov & Karavaiko, 2004). Depuis, l'étude des interactions microbe-minéral est devenu un sujet de première importance dans la thématique des sciences de l'environnement et de la vie. Il a été montré que les bactéries ont des effets prononcés sur la croissance cristalline (Gorshkov et al., 1992; Kohler et al., 1994; Ehrlich, 1999; Kawano & Tomita, 2001) et la dissolution des minéraux (Bennett et al., 1996; Liermann et al., 2000b; Rosenberg & Maurice, 2003; Aouad et al., 2006; O'Reilly et al., 2006). L'association de minéraux avec des bactéries et/ou des exsudats bactériens provoque souvent une augmentation des taux d'altération à l'interface minéral/bactérie et une variété de mécanismes possibles ont été suggérés afin d'expliquer cet effet (Marshall et al., 1971; Van Loosdrecht et al., 1990; Maurice & Warren, 2006). Il a été, par ailleurs, observé que les interactions minéral-bactéries peuvent modifier la composition chimique de l'eau environnante, notamment son pH et son état d'oxydo-réduction. De plus, il est maintenant admis que la connaissance détaillée de ces interactions est essentielle afin de mieux comprendre la chimie de l'hydrosphère et de la lithosphère (Ehrlich, 1996; Liermann et al., 2000a; Haas, 2004).

L'interaction entre activité bactérienne et smectite a en particulier été abordée dans des études pionnières publiées par Stotzky (1966a; 1966b) et Stotzky & Rem (1966; 1967). L'implication des caractéristiques de la montmorillonite (p. ex. la capacité d'échange cationique et la surface spécifique) sur l'activité et l'écologie des microorganismes du sol a été spécialement étudiée en ce qui concerne les changements qu'elle induit sur les habitats microbiens. Du fait de la haute teneur en eau des smectites et de leur abondance dans les sols et sédiments, la nature de l'interaction entre les bactéries et les minéraux argileux gonflants est d'un intérêt particulier. Les smectites sont des minéraux possédant des propriétés physiques et chimiques uniques : elles présentent une faible charge de feuillets facilitant leur écartement et

l'adsorption ou absorption de grandes quantités d'eau (ou autres substances polaires) et d'une grande variété de cations au sein de leur structure. Récemment, une attention particulière a été donnée aux modifications induites par les bactéries des propriétés de la charge des feuillets de smectite riche en fer (nontronite) induites par les bactéries. Il est aujourd'hui admis qu'une réduction (anaérobie), chimique ou biologique, du Fe(III) dans la structure de la smectite provoque une augmentation de la charge de surface. Il a également été montré que de telles modifications diminuent la capacité d'hydratation de la smectite riche en fer (Stucki et al., 1987; Wu et al., 1988; Lovley, 1991; Kostka et al., 1996; Kostka et al., 1999; Kim et al., 2004; Kim et al., 2005; Lee et al., 2006; Stucki & Kostka, 2006). Dans une expérience réalisée en conditions anaérobiques par Kim et al. (2004), il a même été reporté que l'activité de *Shewanella oneidensis* induisait la transformation de la smectite en illite par la fixation de K dans l'espace interfoliaire. Comme dans cette expérience la réaction avait eu lieu à 25°C et sur une période de seulement 2 semaines, les auteurs suggèrent que l'interaction "smectite riche en fer – bactéries" peut jouer un rôle clé en tant qu'initiateur des réactions argilo-minérales dans les environnements anaérobiques. Bien que de nombreuses études portent aujourd'hui sur cette thématique de recherche, l'amélioration de la connaissance des interactions microbe-minéral reste un défi de premier plan, spécialement en ce qui concerne la nature complexe des réactions prenant place dans le système bactéries-smectites.

1.2. Argiles gonflantes dans l'industrie

Les minéraux argileux gonflants (smectites) sont les principaux composants de la bentonite, qui, du fait de son fort pouvoir ad-absorbant et de sa capacité d'imperméabilisation, en fait un des composés argileux industriellement utilisés les plus importants (Murray, 1977; Elzea & Murray, 1990). Le terme de bentonite a été pour la première fois introduit en 1898, il faisait alors référence à une roche trouvée dans une "Benton-Shale" au Wyoming, mais ce terme désigne de nos jours un matériau contenant essentiellement de la smectite (O'Driscoll, 1988; 1989). Ses applications les plus importantes sont en tant que liant pour l'extraction des minerais de fer, en tant que moule de fonderie ou comme constituant des boues de forages pétroliers (Harvey & Lagaly, 2006). Sous forme de dispersions, la bentonite est utilisée en contexte d'ingénierie civile, comme agent épaississant (p. ex. dans les peintures), comme adsorbant chimique (p. ex. pour les protéines) ainsi que pour la stabilisation de la bière et du vin (Sarmiento et al., 2000). Du fait de leur importante capacité d'adsorption, de leur grande

surface spécifique et de leur propriété d'imperméabilisation quand elles sont hydratées, les smectites sont également utilisées comme des barrières ouvragées dans les sites d'enfouissement et de stockage de déchets. En raison de l'augmentation actuelle en besoins énergétiques et du développement concomitant de l'énergie nucléaire, de nouveaux défis ont vu le jour concernant le stockage sûr des déchets nucléaires. Dans cette optique, les argiles gonflantes (bentonites) sont considérées comme un bon matériau pour constituer les barrières ouvragées inhérentes au futur stockage en profondeur des déchets. Cette application est décrite plus en détails dans le paragraphe suivant.

1.3. Utilisation des argiles gonflantes dans le stockage des déchets nucléaires

Les déchets radioactifs sont des matériaux extrêmement dangereux et leur isolation de la biosphère est essentielle (Pusch, 2006b). Ces déchets proviennent de toutes les phases du cycle de production de l'énergie nucléaire et de l'utilisation de produits radioactifs dans l'industrie ainsi que pour des applications médicales. Le type de déchet le plus dangereux est le type des déchets "de haute activité et à vie longue" (HAVL), qui sont dérivés du résidu non-recyclable de la combustion nucléaire. De tels déchets doivent être confinés pendant approximativement un million d'années avant que leur niveau de radioactivité approche le niveau de l'environnement naturel (ANDRA, 2005).

La majorité des pays producteurs de déchets radioactifs envisagent leur stockage en profondeur au cœur de formations géologiques profondes de manière à avoir une barrière épaisse et naturelle entre les déchets et la biosphère. Différents types de formations rocheuses sont actuellement étudiées pour servir d'encaissant, par exemple du granite en Suède et Finlande, des dômes de sel en Allemagne, des tufs pyroclastiques aux Etats-Unis et des roches argileuses en Suisse, Belgique et France (OECD, 1999; ANDRA, 2005; OECD, 2006). En dépit de ces différences dans les types d'encaissant considérés, tous les projets de stockage impliquent le concept de multi-barrière. Celui-ci consiste en un container d'acier contenant les déchets radioactifs vitrifiés, éventuellement entouré de béton, un matériau de remplissage smectitique étant alors introduit entre le container d'acier et la roche encaissante. Finalement, le tunnel d'accès sera remblayé afin de sceller le site (Fig. 1.1.).

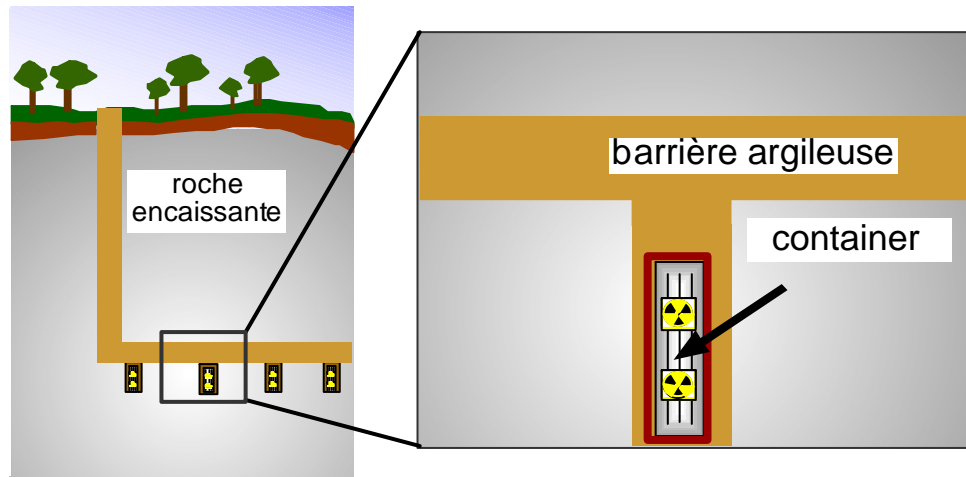


Fig. 1.1. Représentation schématique du dispositif d'enfouissement des déchets nucléaires. Le concept "multi-barrière" inclut la roche encaissante en tant que barrière naturelle, ainsi la barrière ouvragée argileuse dans laquelle repose les containers en acier remplis de déchets vitrifiés.

Le remplissage est supposé réduire les infiltrations d'eaux souterraines susceptibles de corroder les containers et de transporter des produits toxiques vers la biosphère (Karnland, 2003). Les bentonites sont considérées comme étant le matériau le plus adapté à un tel remplissage du fait de leur faible conductivité hydraulique, de leur capacité de colmatage (self-sealing) et de leur forte capacité de rétention des radionucléides (Herbert & Moog, 1999; Hermann-Stengele & Plötze, 2000; Komine & Ogata, 2004; Pusch, 2006b). Dans ce cas, le flux d'eau devrait être drastiquement réduit et la diffusion est supposée représenter le processus de transport dominant. D'éventuelles fissures dans la barrière sont supposées être colmatées par l'augmentation du gonflement (self sealing) et les fortes capacités d'échange cationique et de sorption des argiles devraient restreindre le transport de radionucléides toxiques dans l'éventualité d'une fuite de solutions contaminées (Müller-Vonmoos & Kohler, 1993; Molera et al., 2003; Montes-Hernandez et al., 2005c).

Bien que les smectites soient très stables dans leur environnement naturel d'origine, tout changement de leurs propriétés en contexte de stockage souterrain est susceptible de diminuer les performances de la barrière. Comme une solution aqueuse de composition variable est susceptible d'infiltrer le site de stockage, des réactions à long terme peuvent être attendues sous l'effet des modifications des conditions géochimiques (Karnland & Sandén, 2000; Karnland, 2003). A titre d'exemple, une altération minérale (des minéraux accessoires aussi bien que de la smectite) peut être induite par le contact avec la solution infiltrée ; ce processus étant fortement dépendant des caractéristiques chimiques de la solution (pH, force ionique). De telles réactions peuvent prendre place lorsque des solutions salines entrent dans la zone de

remplissage, ce qui est un scénario possible lors du confinement au cœur de formations salines (Hofman, 2003). Par ailleurs, des infiltrations d'eau de mer sont possibles dans le cas de sites de confinements proches de zones côtières (projet japonais) si le niveau de la mer augmente du fait du réchauffement climatique (Gustafsson, 2004).

De nombreuses approches ont été adoptées afin d'étudier les réactions dans le matériau smectitique et l'encaissant rocheux adjacent. Ces approches ont inclus des études sur analogues naturels (Montes-Hernandez et al., 2003a), des tests en laboratoires souterrains (Marcos, 2002; Delay et al., 2007; Garavito et al., 2007; Rothfuchs et al., 2007), des expérimentations in situ à large échelle (Martin & Barcala, 2005; ENRESA, 2007) et le développement de modèles numériques (Haycox et al., 2006; Rotenberg et al., 2007). Toutes ces études se sont focalisées sur le comportement supposé des argiles de la barrière avec le temps. Un aspect important réside dans la caractérisation des changements dynamiques ayant lieu pendant l'hydratation de la smectite en conditions de volume confiné, équivalentes aux conditions de stockage souterrain. Dans ce cas, la connaissance des mécanismes et de la quantité d'eau admise dans le système est un facteur prédominant pour la compréhension et la prédiction de la capacité de colmatage et d'imperméabilisation du matériau smectitique ainsi que son efficacité à adsorber ou transporter les radionucléides. Un des aspects clés d'une telle étude est de quantifier la quantité d'eau présente dans les sites interfoliaires en opposition à l'eau moins stable adsorbée à la surface des particules et remplissant l'espace poral disponible. Bien que peu d'études aient été réalisées sur le sujet, ces aspects sont considérés comme essentiels au regard de l'évaluation des performances des barrières ouvragées.

Le rôle des bactéries présentes dans les stockages souterrains est également sujet à débat. En effet, diverses études ont portées sur la possibilité d'une rétention des radionucléides par les bactéries et les biofilms associés (Stroes-Gascoyne & Sargent, 1998; Jolley, 2002) et sur la corrosion des containers induite par les bactéries (Stroes-Gascoyne & West, 1994; King et al., 1999; King et al., 2004). Cependant, jusqu'à présent, peu d'études ont été réalisées afin de déterminer comment les bactéries peuvent influencer les propriétés d'hydratation des bentonites et des smectites riches en fer. Ceci reflète probablement le manque de méthodes analytiques permettant le suivi in situ de l'hydratation de la smectite en solution en volume confiné, avec et sans bactéries. De manière à combler ce manque, la présente étude utilise un nouveau type de cellule réactionnelle, adaptable à un diffractomètre de rayons X afin de réaliser des mesures in situ de l'état d'hydratation d'argiles compactées. Accroître les connaissances concernant les taux et mécanismes d'hydratation de la smectite en conditions stériles et en présence de bactéries est de première importance au regard des applications

industrielles actuelles. De plus, une telle connaissance contribuerait à augmenter notre compréhension des réactions de subsurface ayant lieu dans les environnements argileux compactés.

1.4. Objectifs de l'étude

Les principaux buts que nous nous sommes fixés dans le cadre de cette thèse étaient :

- de développer un ensemble de techniques analytiques permettant d'étudier in situ l'hydratation de la smectite pendant l'infiltration des solutions aqueuses, en conditions de volume confiné, avec et sans présence de bactéries
- de déterminer la nature des interactions smectite-bactéries en solution et comparer avec des systèmes en volume confiné
- et enfin d'explorer les implications des résultats obtenus à partir du large panel d'expériences en laboratoires présentées et d'évaluer leur importance dans le contexte de l'enfouissement des déchets nucléaires.

1.5. Plan de la thèse

Le chapitre 2 fournit une description de la structure des smectites, de leurs propriétés physico-chimiques ainsi que de réactions d'altération correspondantes. Il introduit brièvement les approches analytiques couramment utilisées pour étudier l'hydratation des smectites. Il contient par ailleurs, par ailleurs, une brève présentation des bactéries, de leur structure et de leurs besoins nutritionnels, ainsi qu'un résumé des interactions connues dans les environnements de surface et plus particulièrement dans les milieux argileux.

Dans le chapitre 3, les matériaux smectitiques utilisés dans cette étude (smectite purifiée, poudre de bentonite) sont décrits et les caractéristiques de l'espèce bactérienne utilisée (*Shewanella putrefaciens*) sont présentées. Les méthodes analytiques utilisées sont décrites, et le principe de fonctionnement de la cellule réactionnelle ("wet-cell", Warr & Hoffman, 2004) utilisée pour étudier l'hydratation des argiles gonflantes en volume confiné est expliqué en détail, notamment son emploi en tant qu'analogie au laboratoire des conditions d'enfouissement souterrain.

Dans le chapitre 4, les résultats obtenus sur l'hydratation des smectites en conditions abiotiques et en volume confiné sont discutés en fonction du type de cation interfoliaire, de la densité de compaction et de la composition de la solution infiltrée. L'hydratation de la smectite est caractérisée par la combinaison de mesures de diffraction in situ des rayons X et le traitement des spectres de diffraction ainsi obtenus. Ceci permettant de quantifier l'eau interfoliaire. Combinés avec des mesures gravimétriques, ces résultats ont également été utilisés afin de calculer le volume d'eau incorporé à la fois dans les sites interfoliaires et non-interfoliaires (surface et porosité). Les valeurs de surfaces spécifiques et l'organisation texturale de ces argiles, calculées de manière qualitative à partir des changements d'épaisseur des particules et l'organisation des couches d'eau (ordering) sont également présentées.

Le chapitre 5 présente les résultats des expériences mettant en interaction la smectite et *S. putrefaciens*, pour une sélection de smectites. La première partie est basée sur des expériences en batch, d'argiles en suspension réalisées afin de quantifier l'impact de différents types de smectites (nontronite et MX80) sur la croissance microbienne de *S. putrefaciens*, en utilisant des méthodes de comptage de cellules viables. En parallèle, l'impact des bactéries sur la composition et les propriétés des smectites a été déterminé par ICP-OES, microscopie confocale et électronique (MEB environnemental et MET couplé à un système EDX). Dans la seconde partie, les résultats montrant l'impact des bactéries sur le comportement d'hydratation in situ des smectites en volume confiné sont présentés. L'ensemble de ces résultats est, par la suite, discuté afin de définir la nature de l'altération chimique et texturale induite par les bactéries.

Dans le chapitre 6 les résultats présentés dans les chapitres 4 et 5 sont résumés et discutés au regard de l'application des matériaux smectitiques dans le contexte du stockage de déchets, avec un intérêt particulier sur le rôle des bactéries. Finalement, une dernière partie présente les conclusions majeures et originales de ce travail de thèse.

CHAPTER 1

-

INTRODUCTION

1. INTRODUCTION

1.1. Swelling clays and microbial life

The reactive nature of both bacteria and fine-grained minerals on Earth provide an enormous potential for various types of interaction in hydrous environments. First publications linking the fields of geology and microbiology appeared at the beginning of the last century when the involvement of microorganisms in the formation of hydrogen sulfide and calcium carbonates was reported (Nadson, 1903; in Ivanov & Karavaiko, 2004). Since this time, microbe - mineral interaction has become a topic of central importance in environmental and life sciences. Bacteria have been shown to have pronounced effects on both mineral growth (Gorshkov et al., 1992; Kohler et al., 1994; Ehrlich, 1999; Kawano & Tomita, 2001) and mineral dissolution (Bennett et al., 1996; Liermann et al., 2000b; Rosenberg & Maurice, 2003; Aouad et al., 2006; O'Reilly et al., 2006). Additionally, minerals coated with bacteria and/or bacterial exudates often exhibit increased rates of alteration at the interface (Marshall et al., 1971; Van Loosdrecht et al., 1990; Maurice & Warren, 2006). As bacteria-mineral interactions are also observed to alter the chemical composition of resident water, including the pH and redox state, it is now accepted that detailed knowledge of these reactions is essential for understanding the chemistry of the hydrosphere and lithosphere (Ehrlich, 1996; Liermann et al., 2000a; Haas, 2004).

The interaction between bacterial activity and smectite was also addressed in pioneering papers by Stotzky (1966a; 1966b) and Stotzky and Rem (1966; 1967). Especially, the implication of montmorillonite characteristics (e.g. cation exchange capacity and specific surface area) on the activity and ecology of microorganisms in soils was studied with regard to changes on microbial habitats. Because of the high water content of smectites and their abundance in soils and sediments, the nature of interplay between bacteria and the swelling clay minerals is of special interest. Smectites are minerals with unique physical and chemical properties: they exhibit a weak permanent layer charge and can therefore sorb into their structure large quantities of water (or other polar substances) and various cations. In recent years, particular attention has been given to the bacterially induced changes in the layer charge properties of Fe-smectite (nontronite). It is now accepted that a chemical or biologically driven (anaerobic) reduction of Fe(III) in the smectite structure leads to an

increase in the surface layer charge. Such changes have also been shown to diminish the hydration capacity of the Fe-smectite (Stucki et al., 1987; Wu et al., 1988; Lovley, 1991; Kostka et al., 1996; Kostka et al., 1999; Kim et al., 2004; Kim et al., 2005; Lee et al., 2006; Stucki & Kostka, 2006). In the anaerobic experiment of Kim et al. (2004), the activity of *Shewanella oneidensis* was even reported to induce the smectite to illite (10Å-phase) transformation by fixation of K into the interlayer space. As this reaction occurred at 25°C, and over the time period of just 2 weeks, it was suggested that Fe-smectite-bacterial interaction can play a key role in driving clay mineral reactions in anaerobic environments. Despite these numerous studies now conducted in this field of research, it remains a great challenge to advance the understanding of the relationship between microbes and minerals and, especially, to elucidate the complex nature of reactions occurring between bacteria and the smectite clays.

1.2. Swelling clays in industry

Swelling clay minerals form the main component of bentonite, which, because of their high sorbent properties and sealing capacity, constitute one of most important industrially applied clay mineral materials (Murray, 1977; Elzea & Murray, 1990). The name bentonite was first introduced in the year 1898 and it refers to a rock found in the « Benton-Shale », Wyoming. Nowadays, it is used for materials that essentially contain smectite (O'Driscoll, 1988; 1989). The most important applications include its use as a binding agent in the pelletization of iron ores, as foundry mouldings or as oil well drilling fluids (Harvey & Lagaly, 2006). Bentonite dispersions are also used in civil engineering, as a thickening agent (e.g. in paints), as chemical sorbants (e.g. for proteins) and in the stabilization of beer and wine (Sarmiento et al., 2000). Because of their extensive adsorption capacity, high surface area and the impermeable nature when hydrated, the smectite minerals are also applied as sealant barriers in waste disposal sites. With today's increasing need for energy, and the development of nuclear power, new challenges have arisen concerning the safe storage of the generated nuclear waste. Here the swelling clays (bentonites) are considered for construction of the engineered backfill barrier in many planned underground waste repositories, as described in more detail in the following section.

1.3. The use of swelling clays in nuclear waste disposal

Radioactive waste is an extremely hazardous material and its isolation from the biosphere is essential (Pusch, 2006b). It is derived from all phases of the nuclear fuel cycle and from the use of radioactive materials in industry as well as from medicinal applications. The most hazardous type of waste is the so-called "high-level and long-lived intermediate-level waste", derived from spent fuel cells. Such waste must be confined for up to one million years before its level of radioactivity approaches levels such as those found in the natural environment (ANDRA, 2005).

The majority of nuclear waste producing countries are considering disposal in underground repositories placed within deep geological formations in order to provide a thick, natural barrier between the waste and the biosphere. Different types of host rock formations are currently being studied, for example granite in Sweden and Finland, salt domes in Germany, pyroclastic tuffs in the USA and clay rocks in Switzerland, Belgium and France (OECD, 1999; ANDRA, 2005; OECD, 2006). Despite the differences in host rock, all planned repository sites involve the multi-barrier concept with additional engineered barriers. The engineered barriers consist of steel containers that hold the glassed radioactive waste, possibly surrounded by concrete, and then a backfill material introduced between the steel containers and the geological host rock. Finally, the access tunnel system will be backfilled to seal the site (Fig. 1.1.).

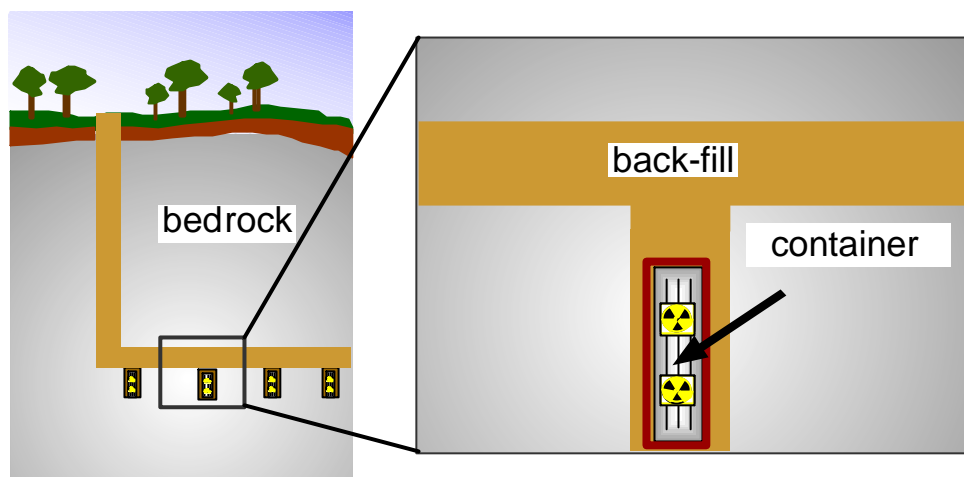


Fig. 1.1. Schematic sketch of an underground repository for the storage of nuclear waste. The multi-barrier concept includes the bedrock as a natural barrier as well as the backfill and waste containers as engineered barriers.

The main function of the backfill is to reduce ground water inflow that could corrode containers and transport hazardous compounds to the biosphere (Karland, 2003). Bentonites are considered to be the most suitable backfill material because of the low hydraulic conductivity, the so-called self sealing capacity and the high retention capacity for radionuclides (Herbert & Moog, 1999; Hermann-Stengele & Plötze, 2000; Komine & Ogata, 2004; Pusch, 2006b). Here, the flow of water is expected to be drastically reduced that diffusion is the dominating transport process. Cracks in the barrier are expected to be closed during enhanced swelling (self sealing) and the high cation exchange and sorption capacity of the clay should restrict the transport of hazardous radionuclides in the case of leakage of contaminated solutions (Müller-Vonmoos & Kohler, 1993; Molera et al., 2003; Montes-Hernandez et al., 2005c).

Although smectites are very stable in their original natural environment, any changes in the minerals properties within the underground repository could decrease the performance of the backfill barrier. As aqueous solution of varying composition may infiltrate the site, long term reactions can be expected under the changing geochemical conditions (Karland & Sandén, 2000; Karland, 2003). Depending on the solution chemistry (pH, ionic strength) both accessory minerals and smectite can be altered. For example concentrated saline solutions may enter the backfill zone when storing waste in salt formations (Hofman, 2003). As well the infiltration of sea water is possible if repositories are close to coastal areas (planned in Japan) and the sea level rises due to global warming (Gustafsson, 2004).

A wide range of approaches has been adopted in order to study reactions within the smectitic backfill material and its adjacent wall rock. These have included natural analogue studies (Montes-Hernandez et al., 2003a), testing within underground laboratories (Marcos, 2002; Delay et al., 2007; Garavito et al., 2007; Rothfuchs et al., 2007), large scale in situ experiments (Martin & Barcala, 2005; ENRESA, 2007) and the development of numerical models (Haycox et al., 2006; Rotenberg et al., 2007). All these studies addressed the expected behaviour of the clay barrier with time. One important aspect is the characterization of the dynamic changes that occur during the hydration of the smectite within confined volume conditions, equivalent to the underground repository. Here, knowledge of the mechanisms and amount of water intake and retention is critical for understanding and predicting the sealing capability of the smectite material and its effectiveness in the adsorption or transport of radionuclides. A key aspect of such a study is, to quantify the amount of structured (bound) water stored in the interlayer sites, as opposed to more loosely held water adsorbed on particle

surfaces and in pore space. Although few studies have been conducted on this topic, these aspects are considered to be essential when evaluating the performance of clay barriers.

The role of bacteria present in underground repositories is also a theme of current debate. Studies here have focused on the possibility of radionuclide retention by bacteria and associated biofilms (Stroes-Gascoyne & Sargent, 1998; Jolley, 2002) and the microbially induced corrosion (MIC) of the steel containers (Stroes-Gascoyne & West, 1994; King et al., 1999; King et al., 2004). However, little research has been undertaken to determine how bacteria can influence the hydration properties in bentonite and Fe-smectites. This probably reflects the lack of an analytical approach that allows in situ monitoring of smectite hydration in solution, with and without bacteria in a confined volume system. To fill this niche, this study employed a new type of flow-through reaction cell that can be mounted onto an X-ray diffractometer for in situ measurements of the state of compacted clay hydration. Gaining knowledge on the rates and mechanisms of smectite hydration in sterile and bacterial-containing samples is considered to be of major importance with respect to current industrial applications and furthers our general understanding of subsurface reactions in compacted clay environments.

1.4. Objectives of the study

Therefore the objectives of this study were set as follows:

- To develop a set of analytical techniques to study in situ smectite hydration during the infiltration of aqueous solution under confined volume conditions with and without bacteria.
- To determine the nature of smectite - bacteria interaction in batch solution experiments and to compare it with compacted clay systems.
- To explore the implications of the results obtained from the broad range of laboratory experiments presented and to discuss their importance within the context of nuclear waste disposal in underground repositories.

1.5. Outline of the thesis

Chapter 2 provides an overview of smectite structure, their physical-chemical properties and relevant alteration reactions. A short introduction is given on the common analytical approaches used to study smectite hydration. Additionally, a brief introduction is provided on bacteria, their structure and nutritional requirements for growth, as well as a summary of known interactions in surface environments and more specifically within clay mineral substrates.

In Chapter 3, the smectite based materials studied (purified smectite and bulk rock bentonite powder) are described as well as the characteristics of the bacteria used in this study (*Shewanella putrefaciens*) are presented. The analytical methods are outlined, and the reaction-cell (“wet-cell”, Warr & Hoffman 2004) applied to study the hydration of swelling clay under confined volume condition is described. This device is used as a laboratory analogue for underground repository conditions.

In Chapter 4, the results of abiotic smectite hydration under confined volume conditions are presented and discussed as a function of the type of interlayer cation, packing density and the ionic strength of infiltrated solution. Smectite hydration is characterized by combining in situ X-ray diffraction and the calculation of diffraction patterns, which allows quantification of the amount of structured water layers occurring in hydrated interlayers. Combined with gravimetric measurement, these results are also used to calculate the volume of water incorporated into both interlayer and non-interlayer (surface and pore) sites. Qualitative information on surface area and textural organization is also presented based on calculated changes in particle thickness and the structural organization of water layer structures (degree of ordering).

In Chapter 5, the experimental results of smectite – *S. putrefaciens* interaction are presented for selected smectite minerals. The first part is based on batch experiments conducted to quantify the impact of smectite (nontronite and MX80) on the growth of *S. putrefaciens* by using viable cell counts. The impact on smectite composition and mineral properties was determined by ICP-OES, confocal and electron microscopy (ESEM and TEM coupled to EDX). In the second part, results showing the impact of bacteria on the in situ hydration behaviour of smectite under confined volume conditions are presented. These results are then discussed in order to define the nature of bacterially induced chemical and textural alteration.

In Chapter 6, the results presented in Chapters 4 and 5 are summarized and discussed with regard to the application of smectite based buffer materials in an underground waste repository, with special focus on the role of bacteria. The thesis finishes with a list of general conclusions.

CHAPTER 2

-

STRUCTURE AND PROPERTIES OF SMECTITES AND OF RELATED BACTERIA

CHAPTER 2 – STRUCTURE AND PROPERTIES OF SMECTITES AND OF RELATED BACTERIA

2.1. Smectites

Swelling clay minerals belong to the hydrated phyllosilicates subclass (Table 2.1) and are rather unique in the Earth's environment because they have the ability to adsorb quantities of water, and other polar substances by the ordered expansion of their crystal lattices (Hofman & Bilke, 1936; Mooney et al., 1952; Norrish, 1954; MacEwan & Wilson, 1980; Sposito & Prost, 1982; Sato et al., 1992; Bergaya & Lagaly, 2006; Brigatti et al., 2006). Smectites are 2:1 phyllosilicates that are built up by a succession of tetrahedral-octahedral tetrahedral sheets (TOT). Two successive TOT are separated by an interlayer space (Fig. 2.1). The tetrahedron is composed of a central Si^{4+} atom (substitutions with Al^{3+} and/or Fe^{3+}) surrounded by four oxygen atoms that are linked via the corners in a sheet-like manner to form the so-called tetrahedral sheet (Bailey, 1980; Brigatti et al., 2006). In the case of the octahedron the central cation is usually Al^{3+} , Mg^{2+} , Fe^{2+} or Fe^{3+} that is surrounded by six oxygen atoms. The sharing of neighboring oxygens results in an edge-linked, octahedral sheet structure (Velde, 1992). In the case of dioctahedral smectites (e.g. montmorillonite, beidellite, nontronite) the octahedral sheet is predominantly occupied by trivalent cations whereas the octahedral sheet of trioctahedral smectites (e.g. hectorite and saponite) is dominated by divalent cations (Bailey, 1980; Brigatti et al., 2006). In this study, montmorillonite and an Fe-smectite, nontronite, were selected for detailed experimental investigation as these clays are considered to be particularly important for understanding bentonite back fill systems and their predicted alteration productions (Chapter 3).

Charge per formula unit (PFU)	Di octahedral species	Tri octahedral species
<i>Serpentin-kaolin group</i>		
~0	Kaolinite (Si ₂) ^{IV} (Al ₂) ^{VI} O ₅ (OH) ₄	Serpentine (Si ₂) ^{IV} (Mg ₃) ^{VI} O ₅ (OH) ₄
<i>Talk-Pyrophyllite group</i>		
~0	Pyrophyllite (Si ₄) ^{IV} (Al ₂) ^{VI} O ₁₀ (OH) ₂	Talc (Si ₄) ^{IV} (Mg ₃) ^{VI} O ₁₀ (OH) ₂
<i>Smectite group</i>		
~0.2-0.6	Montmorillonite (M _y ⁺ *nH ₂ O)(Al ³⁺ ₂₋₃ Mg ²⁺ _y) Si ⁴⁺ ₄ O ₁₀ (OH) ₂	Hectorite (M _y ⁺ * nH ₂ O)(Mg ²⁺ _{3-y} Li ⁺ _y) Si ⁴⁺ ₄ O ₁₀ (OH) ₂
	Beidellite (M _x ⁺ *nH ₂ O)Al ³⁺ ₂ (Si ⁴⁺ ₄ Al ³⁺ _x)O ₁₀ (OH) ₂	Saponite (M _x ⁺ * nH ₂ O)Mg ²⁺ ₃ (Si ⁴⁺ _{4-x} Al ³⁺ _x)O ₁₀ (OH) ₂
	Nontronite (M _x ⁺ * nH ₂ O)Fe ³⁺ ₂ (Si ⁴⁺ _{4-x} Al ³⁺ _x)O ₁₀ (OH) ₂	
<i>Vermiculite group</i>		
~0.6-0.9	(Si _{4-x} Al _x) ^{IV} (Fe _{2-y} Mg _y) ^{VI} O ₁₀ (OH) ₂ (x+y)M ⁺	(Si _{4-x} Al _x) ^{IV} (Mg _{3-y} M _y ³⁺) ^{VI} O ₁₀ (OH) ₂ (x-y)/2Mg ²⁺
<i>Illite</i>		
~0.9	(Si _{4-x} Al _x) ^{IV} (Al _{2-y} Mg _y) ^{VI} O ₁₀ (OH) ₂ (x+y)K ⁺	
<i>True mica group</i>		
~0.9-1	Muscovite (Si ₃ Al) ^{IV} (Al ₂) ^{VI} O ₁₀ (OH) ₂ K ⁺	Phlogopite (Si ₃ Al) ^{IV} (Mg ₃) ^{VI} O ₁₀ (OH) ₂ K ⁺

Table 2.1. Compilation of layer charge and idealized formula of some representative 1:1 and 2:1 phyllosilicates modified from Bergaya & Lagaly (2006).

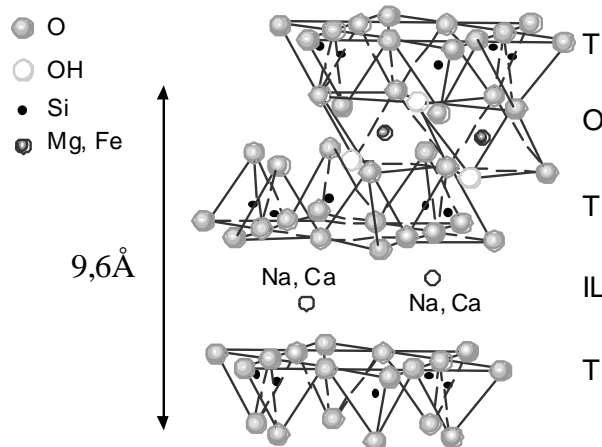


Fig. 2.1. Schematic representation of the crystal structure of smectite. The alternating succession of tetrahedral (T) and octahedral (O) units makes up the sheet-like structure. The interlayer space (IL) contains cations and separates the TOT sheets. The resulting lattice thickness of the structure (d-value) is 9.6Å (modified after Grim, 1962).

2.1.1. Layer charge and cation exchange capacity (CEC)

Besides the above described structural characteristics, smectite minerals can be additionally characterized by the density and location of layer charge (Brigatti et al., 2006).

The layer charge of smectite, derived from substitutions in either tetrahedral or octahedral sheets, leads to an excess negative charge (ξ). For smectites this charge typically ranges between -0.2 and -0.6 per formula unit (PFU, table 2.1), whereas for vermiculites, this charge is higher and lies between -0.6 and -0.9 PFU (MacEwan & Wilson, 1980). The layer charge may result from predominantly octahedral substitutions as in the case of montmorillonite where trivalent Al^{3+} is substituted by divalent cations, or from tetrahedral substitutions, as described for nontronite, where Si^{4+} is partly substituted by trivalent Al^{3+} (Velde, 1992). The ability to exchange cations is expressed by the so-called cation exchange capacity (CEC) which is highest in the case of smectites and linked to a particular range of layer charge values. As the layer charge property controls many important characteristics, such as hydration, swelling, clay fabric, and surface reactivity (Stucki, 1988) the electrostatic balance of charge is a key parameter affecting the transfer and retention of water and elements that serve as nutrients (e.g. in a soil) or pollutants in natural and anthropogenic environments. However, with increasing layer charge the mineral loses the ability to exchange cations because the interlayer cations become increasingly bound (such as K^+ fixation in illite).

2.1.2. Edge charges

Another type of charge located at the edges of smectite particles makes up more than 20% of the CEC (Lagaly, 1993; , 2006). The sign and density of this charge is, unlike the permanent interlayer charge, dependent on the pH of the surrounding solution and therefore referred to as the variable charge. In an acidic solution, the excess protons lead to the formation of positive edge charges whose density decreases with increasing pH (Fig. 2.2.). Alkaline solutions in contrast provoke the dissociation of silanol and aluminol groups leading to negative edge charges that are compensated with cations. Uncharged edge sites are only found in solutions of slightly acidic pH (5-6) but here ligand exchange occurs where OH groups are exchanged, for example, by sulfate or phosphate groups (Lagaly, 1993). The edge charge is seen to play an important role in buffering and sorption reactions within solution. For example a higher proportion of edge sites was shown to enhance the overall retention of pollutants such as UO_2^{2+} (Zachara & McKinley, 1993).

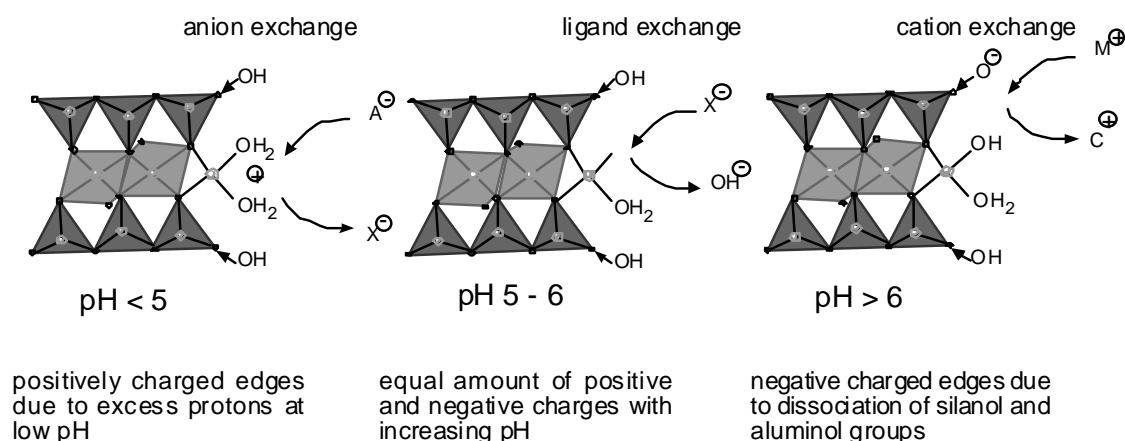


Fig. 2.2. Schematic representation of the pH dependent edge charges (modified after Lagaly, 1993).

2.1.3. Interlayer hydration properties and analytical approaches to study hydration

The low negative layer charge of smectite (table 2.1) enables water molecules to coexist with the interlayer cations and to hydrate them as a function of water activity (Norrish & Quirk, 1954; Prost, 1975; Sposito & Prost, 1982). This process is generally known as intracrystalline swelling and corresponds to the intercalation of H_2O molecules in the interlayer space as it expands (Nagelschmidt, 1936; Norrish, 1954; Norrish & Quirk, 1954; Grim, 1962; Watanabe & Sato, 1988; Sato et al., 1992; Tamura et al., 2000; Suzuki et al., 2005). This intercalation is governed by the size and charge of the saturating cation and as well by the magnitude and localization of layer charge (MacEwan & Wilson, 1980).

At ambient conditions, monovalent interlayer cations preferentially form a one water layer structure, which if homogeneously distributed along all interlayers, results in a d-value of $\sim 12.3\text{\AA}$. Divalent cations are normally surrounded by two water layers and yield an ideal d-value of $\sim 15.2\text{\AA}$. In the case of Ca^{2+} , this spacing is stabilized by the formation of octahedrally co-ordinated hexahydrate groups with the composition $[\text{Ca}(\text{H}_2\text{O})_6]^{2+}$ (Méring, 1946). However it is very rare that smectites are strictly homoionic and the presence of more than one type of cations (typically mixtures of Na^+ , Ca^{2+} , K^+ or Mg^{2+}) in the interlayer space is common with variations of the hydrated interlayer spacings accordingly (MacEwan & Wilson, 1980).

The amount of water intercalated in the interlayer space increases with humidity and can form up to 4 layers of structured water (Bradley et al., 1937). As the mobility of the interlayer

cation successively increases with hydration state (Lagaly, 1993) the name “quasi-crystalline” was proposed to describe the thicker water layer structures (Hofmann et al., 1957). If smectite expands more than 20Å the quasi-crystalline structure is lost and the interlayer cations build diffuse double layers. Experimental studies of interlayer expansion under conditions of elevated relative humidity have also shown transformations to take place in a step-wise manner with the occurrence of discrete hydration states (Mooney et al., 1952; Norrish, 1954; MacEwan & Wilson, 1980). The early observation of continuous swelling by Nagelschmidt (1936) and Hofman and Bilke (1936) is considered to represent random interstratifications of different hydrates (MacEwan & Wilson, 1980).

The state of interlayer hydration can be determined from X-ray diffraction patterns by quantifying the position and shape of the basal lattice layer reflections (Chapter 3). In analogy with mixed layered clay minerals, that are formed of two or more kinds of intergrown layers (e.g. illite-smectite), the diffraction properties of smectite containing a mixture of different water layer structures can be treated according to Méring’s principle (Méring, 1949). The basal X-ray diffraction peaks of mixed layered clays occur between the nominal positions of both members and their precise position is fixed by the relative proportions of the interstratified phases (Moore & Reynolds 1997; Chapter 3).

Smectite interstratifications are generally considered to be random ($R=0$) or ordered (e.g. $R=1$) although the precise nature of ordering at the lattice scale is still a topic of debate. Moore and Hower (1986) described the regular (non-random) stacking of 1 and 2 water layer hydrates resulting in varying basal spacing (d_{001}) that formed as a function of the relative humidity. The ordered arrangement was suggested to be more stable, resulting from the electrostatic interaction of the interlayer cation with the hydroxyl ions. When the two water layer thicknesses were present in equal abundance (e.g. 50% 1WL and 50% 2WL) with regular interstratification, the formation of a superstructure was observed by X-ray diffraction and confirmed by peak calculations.

The types of ordering present in mixed layered minerals are best studied by matching measured XRD patterns with calculated profiles. The best known program for simulating one-dimensional diffraction patterns is NEWMOD (Reynolds, 1985), but there are limitations to the number of mixed-layered phases that can be mixed simultaneously. Recent simulations of smectite swelling under elevated air humidity consider that complex diffraction patterns are best reproduced by calculating mixtures of both pure and mixed layered structures to be necessary to account for observed heterogeneities (Ferrage et al., 2005a; Ferrage et al., 2005b). However, in this study the observed XRD patterns were most satisfactorily fitted

assuming only mixed layered structures, as long as enough components were included. Preliminary tests using non mixed layered components yielded poorer results.

Molecular simulations have also been applied to model the hydration structure of smectites when experimental constraints are absent. Based on such studies, the chemical properties, reaction mechanisms, thermodynamics, and kinetics of the hydration mechanism were identified (Monsalvo et al., 2006). Simulations using the Monte-Carlo algorithm are most common. In this approach the energy of a randomly chosen compound in a system (with defined coordinations) is calculated by varying randomly its position or rotation until a minimum energy is obtained. Here, the change from an old to the new state is based on the assumption of certain probabilities and energetic minimums. The calculated molecular structures serve as a basis for calculating various crystal-chemical parameters such as the thickness of the hydrated interlayer (Meleshyn, 2005). Simulations of Na-montmorillonite confirmed the presence of four stable hydration states (at 9.7, 12.0, 15.5, and 18.3Å, respectively), the thicknesses of which are in good agreement with experimental data (Karaborni et al., 1996). Based on such studies, the combination of experimental results and computer simulations is seen to be an essential part of understanding complex molecular reactions such those involved in smectite hydration.

2.1.4. The diffuse double layer, DLVO theory, and implications for smectite swelling

The double layer model (Gouy-Chapman-Model) is used to describe the ionic environment in the vicinity of a charged particle and explains how electrical repulsive forces occur. A negatively charged particle causes firmly attached positive ions to concentrate at the surface of the clay particle (known as counter-ions) to form the so-called “Stern layer” (represented as one layer of positive charges in Fig. 2.3). The diffuse layer results as a consequence of positive ions being attracted by the negative charged surface but simultaneously repelled by the “Stern layer” and other positive ions trying to approach the particle (Shaw, 1992). The concentration of positively charge ions decreases with increasing distance from the particle surface until equilibrium with the solution is attained. The Stern- and the diffuse-layer together are called the “diffuse double layer” (Fig. 2.3.a). The DLVO theory (independently proposed by Derjaguin and Landau in 1941 and by Verwey and Overbeek in (1948) provides a quantitative description of interaction of negatively charged

particles and includes the basic concept of mutual repulsion of overlapping diffuse double layers and the attraction of particles due to the London-van der Waals forces.

The behaviour of smectite particles in solution can be well understood by applying the diffuse double layer model. The thickness at which swelling occurs is driven by the forces of the charged surfaces and the transition to osmotic swelling, which is controlled by concentration gradients. This transition usually corresponds to layer separations $>30\text{\AA}$ as indicated by small angle scattering techniques (Tchoubar & Cohaut (2006). This contrasts to the proposed 20\AA limit of Hofmann et al. (1957). At this point the interlayer becomes detached and the exposed cations build a diffuse double layer between the layers that repulse each other as the coherence between particles is lost (Fig. 2.3.b). This so-called osmotic swelling transforms interlayers into free surfaces and create very thin independent particles which do not overlap (Lagaly, 1993; Likos, 2004; Lagaly, 2006).

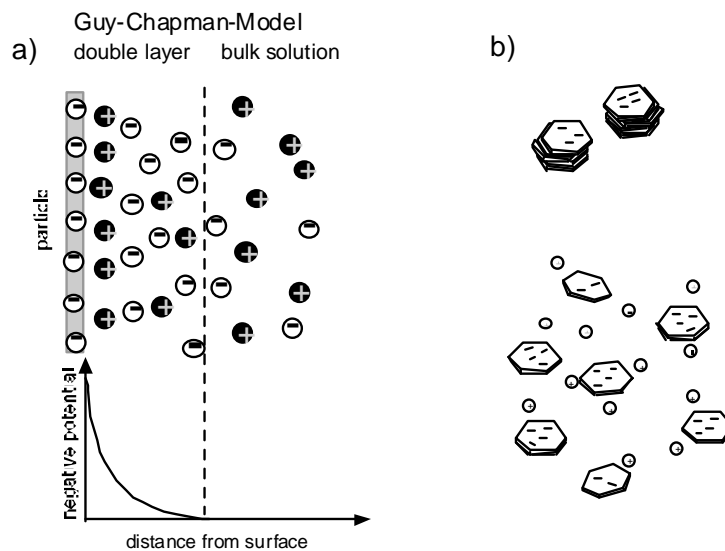


Fig. 2.3. a) Schematic representation of the diffuse double layer of a smectite sheet-silicate particle in suspension. b) Formation of tactoid particles due to osmotic swelling (modified after Lagaly, 1993).

With increasing concentration of the electrolyte (Fig. 2.4.a) the diffuse double layer is suppressed and particles are able to approach each other (McNeil, 1970; Lagaly, 1993; , 2006). When particles approach a distance of $\sim 10\text{\AA}$ the Van-der-Waals attractive forces overcome the electrostatic repulsion forces and the particles coagulate to form aggregates (Fig. 2.4c, Lagaly 1993). A typical value for the critical coagulation concentration of Wyoming montmorillonite is 3.5 mmol/l NaCl ($\sim 0.2\text{g/l}$) for a maximal of 18g/l dispersed clay (Lagaly, 2006). In addition to dissolved salts, numerous other components can lead to

coagulation (see Lagaly 2006) including organic macromolecules. Here, important mechanisms are charge neutralization (the molecule and the clay surface having opposite charge) and the molecular bridging of adjacent particles.

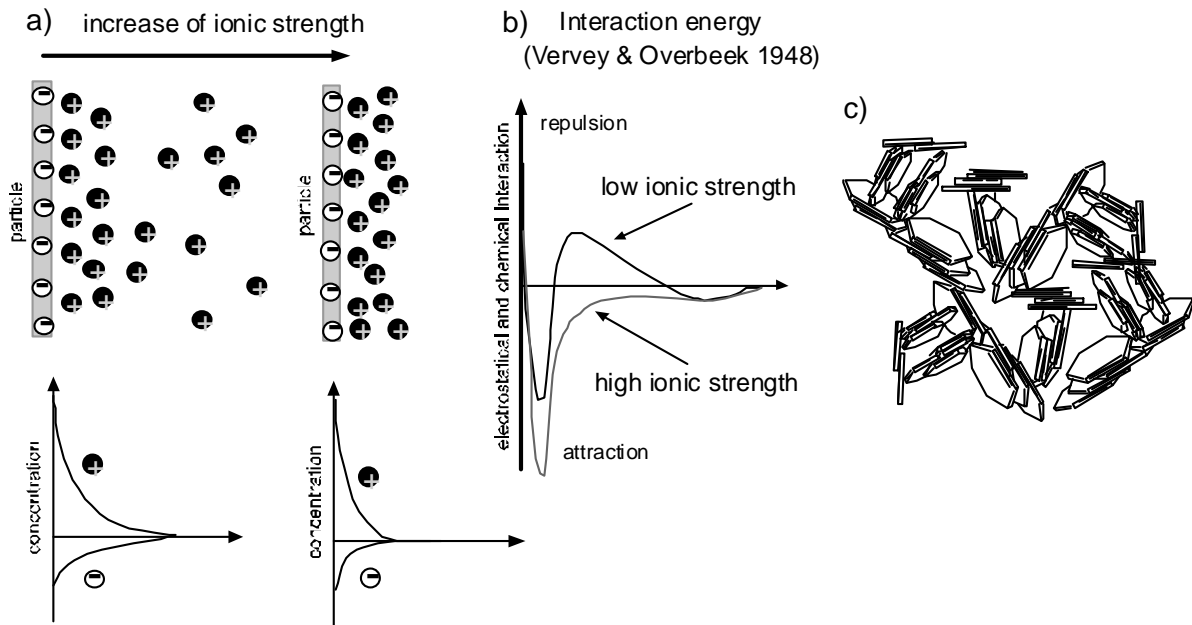


Fig. 2.4. a) With increasing ionic strength the dimension of the diffuse double layer is decreased. b) The curves for interaction energy show decreasing electrostatic repulsion and increasing influence of Van-der-Waals attractive forces. c) Coagulation of particles forming stair-step-card house structures (Hofmann, 2000; modified after Lagaly et al. 1997).

2.1.5. Hydration of non-interlayer sites: surface and pore water

In smectite-rich clay such as bentonite, water is not only stored within interlayers but is also located outside the crystal structure, namely as adsorbed water on external particle surfaces or as free pore water stored between adjacent grains or minerals aggregates (Prost, 1975; Sposito & Prost, 1982). In the case of smectite the enormous specific surface area (SSA) is one of the most important properties controlling surface phenomena including the uptake of organic and inorganic molecules (Michot & Villieras, 2006). The amount of available surface area is highly dependent on the state of particle swelling. Maximal values for external surfaces range up to 850 m²/g; a surface which is theoretically available for water adsorption (Schramm & Kwak, 1982; Michot & Villieras, 2006). In addition to this immense surface area, smectites commonly have relatively high porosities due to their microtextural arrangement. A

typical porosity of a smectite-rich soil for example ranges between 58% and 51% (Horgan, 1999), corresponding to a bulk density of 1.1 and 1.3 g/cm³, respectively. Such porosities provide a natural capacity to store water in micropores as infiltrating aqueous solution replaces air. In the hydrated state these pores are however frequently not connected and in such conditions the smectites have characteristically low hydraulic conductivities (depending on the packing density, ranging between 1E-11 and 1E-14 m/s, Pusch 1994; 2006).

Water adsorption on the siloxane surface of smectite particles, which is the basal plane of a tetrahedral sheet, is mostly depending on the local charge distribution (Sposito & Prost, 1982). For montmorillonite the isomorphic substitution occurs in the octahedral sheet and the resulting excess negative charge allows the surface to form adsorption complexes with cations and water molecules by weak hydrogen bonds (Sposito & Prost, 1982; Sposito et al., 1999). This effect is even more enhanced in nontronite where substitution occurs mostly in the tetrahedral sheet. The resulting excess negative charge localized closer to the siloxane surface leads to stronger adsorption complexes and the formation of stronger hydrogen bonds is possible (Sposito et al., 1999).

2.1.6. Smectite swelling in a confined volume system

Although a restricted reaction volume is the common situation in many natural and engineered systems, the hydration behaviour in such conditions is not well studied experimentally. The uptake of water in a confined volume and the associated expansion depending on the packing density can generate swelling pressures ranging from 0.06 to 12 MPa (Pusch, 2006a; 2006b). The latter value is typical for pressures at more than 10km crustal depth. Therefore swelling under such conditions is different from that observed in free swelling. The elevated solid to liquid ratio in engineered clay systems and the effect of bulk characteristics such as the pore water chemistry has been addressed in various models (Muurinen & Lehtikoinen, 1999; Bradbury & Baeyens, 2003; Wersin et al., 2004). In such studies the main reactions could be identified depending on the system parameters, such as the degree of equilibrium attained in the bulk mineral assemblage, Na⁺-Ca²⁺ exchange reactions and deprotonation of functional surface groups. However it is generally considered that many uncertainties remain with regard to the effects of smectite swelling and the chemical properties of the interstitial water (Wersin, 2003).

The different water storage sites, namely the interlayer, surface and pore spaces are most likely to influence the mechanisms of sealing, sorption and transport in fundamentally different ways. A quantification of the distribution of water between these sites is therefore considered as important for predicting of the behaviour of hydrated smectite clays in both natural and anthropogenic environments.

2.2. The role of bacteria

Another aspect of importance is the role bacteria play in influencing clay mineral reactions in low temperature aqueous environments. Bacteria are abundant in near surface conditions and have been shown to be present in deep geological formations (Fredrickson & Onstott, 1996) and in naturally occurring bentonite (Pedersen, 2000, Fukunaga et al. 2005). The impact they have in affecting mineral reactions is strongly dependent on the type of clay and bacteria present, but in a number of cases they have been shown to enhance mineral dissolution (Banfield & Welch, 2000). Dissimilatory reduction of Fe-smectites under anaerobic conditions by *Shewanella* species was shown to increase layer charge and decreased particle swelling (Gates et al 1993, Kostka et al 1999, Kim et al. 2003; 2004) and was accompanied by partial mineral dissolution (Stucki et al. 1987, Wu et al. 1988, Gates et al, 1993, Kostka et al. 1999, Kim et al 2003, 2004, Kostka et al. 2003b).

2.2.1. Structure, properties and requirements of bacteria

Bacteria are abundant in soils and sediments in both terrestrial and marine environments. They flourish in the extreme conditions of hot springs (Corliss et al., 1979), deep in the Earth's crust (Fredrickson & Onstott, 1996) and have even been reported in nuclear waste material (Fredrickson et al., 2004; Nazina et al., 2004). The biochemical functions they perform in system Earth are numerous and of critical importance in the ecological environment, serving as decomposers, gas fixators and agents of fermentation. They also play an important role in bioremediation by degrading and transforming hazardous contaminants such as toxic metals and radionuclides (Willey et al., 1996; Banfield & Welch, 2000; Lloyd, 2003; Madigan et al., 2003; Konhauser, 2007; Muller et al., 2007). Members of the genus *Shewanella* were among the first organisms shown to grow by dissimilatory metal and

radionuclide reduction and they have been intensively studied with regard to biogeochemical cycling and bioremediation (Haas et al., 2001; Marshall et al., 2006; Payne & DiChristina, 2006).

Bacteria are a group of single-cell microorganisms with prokaryotic cellular configuration (Fox et al., 1977; Woese & Fox, 1977; Woese, 1987; Madigan et al., 2003). Typically, a few μm in length, individual bacterial shapes range from spheres to rods and spirals. In contrast to animals or plants, a bacterial cell can carry out the key life functions such as growth, energy generation and reproduction independently without the need of other cells. A prokaryotic cell (bacteria and Archaea) is compared to the eukaryotic cell more simple in structure, lacking a membrane-bound nucleus and instead of having chromosomal DNA, their genetic information is contained in a circular loop called a nucleoid (Fig. 2.5).

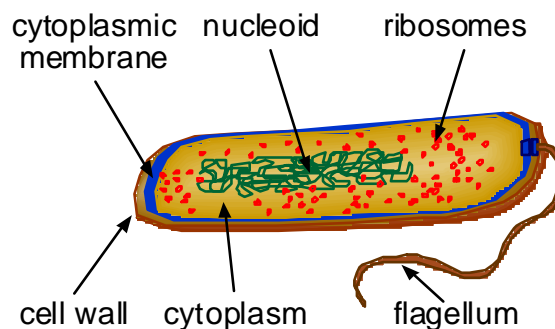


Fig. 2.5. Internal structure of a prokaryotic cell (modified after Madigan et al. 2003)

2.2.2. The bacterial cell wall

Two major groups of bacteria are recognizable based on their cell wall structure: the gram negative and the gram positive (based on the cells response to the so-called gram stain). Gram-positive cell walls consist primarily of one type of molecule, the peptidoglycan, which provides strength to the wall by forming a relatively thick layer (Fig. 2.7). In contrast, the cell wall of gram-negative bacteria is made up of a complex multilayered structure that contains besides the peptidoglycan layer an additional layer made of lipopolysaccharide. The lipopolysaccharides form the outer membrane of the cell walls of gram-negative bacteria and contain macromolecules with carboxylate, phosphate and amino groups (e.g., Beveridge and Murray, 1980; Plette et al., 1995). Generally bacteria cells are negatively charged in most environmental conditions (Haas, 2004; Kronhauser, 2007) but the cell walls can be protonated

or deprotonated, depending on the pH of the outside solution. This is basically due to the macromolecules of the cell wall that contain exposed ionizable functional groups. Additionally, buffering reactions can be linked to the bacterial metabolism such as the active transport of protons (proton pump) and the subsequent release of exudates (Banfield & Hamers, 1997; Barker et al., 1997; Banfield & Welch, 2000; Haas, 2004).

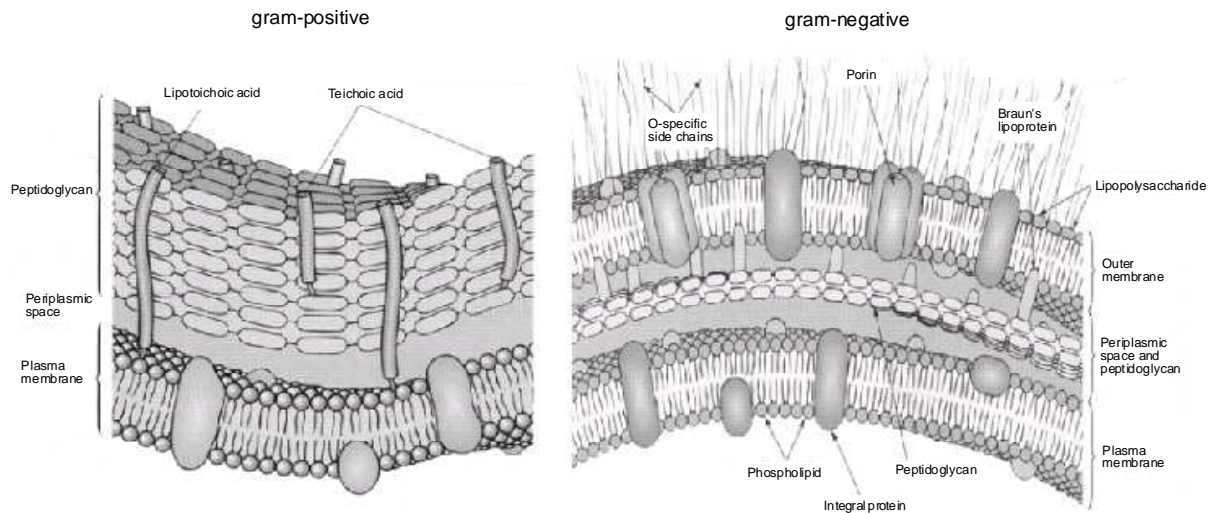


Fig. 2.6. Schematic representation of the gram-negative and the gram-positive cell wall (Cleassens, 2006; modified after Willey et al. 1996).

2.2.3. Requirements for bacterial growth

Bacteria are relatively small with a common size of about 0.5-1 μm in diameter and upto ~4 μm in length. As a consequence, they have a large specific surface area compared to their volume (e.g. 55m²/g for *Shewanella putrefaciens*, Haas 2004). As the surface area controls the rate of nutrient transport into a cell as well as the rate of waste products excreted, bacterial size fundamentally affects both the cells metabolism and growth rate. For successful growth in nature or in the laboratory bacteria require water, an energy source, carbon and a range of other nutrients (table 2.2).

Carbon is the major constituent of all cellular materials and in the case of bacteria it makes up around 50% of its dry weight. It is therefore the main nutrient desired by all bacteria (Madigan et al., 2003; Konhauser, 2007). After carbon, the second most abundant element in a cell is nitrogen with around 12% dry weight. This element is a major constituent of amino acids, nucleic acids nucleotides, and coenzymes (table 2.1). Phosphorous is required primarily

as a constituent of nucleic acids and phospholipids, whereas sulphur is a constituent of amino acids (cysteine, methionine) and several co-enzymes. Potassium is the main inorganic cation and acts as a cofactor for certain enzymes. Other inorganic cellular cations are magnesium and calcium that are cofactors for enzymatic reactions. Iron is the key component of cytochromes and thus plays a major role in cellular respiration. A summary of the main elements required as nutrients and some of their functions are compiled in table 2.2.

Element	% of dry weight	Source	Function
Carbon (C)	~50	organic compounds or CO ₂	Main constituent of cellular material
Nitrogen (N)	~12	NH ₃ , NO ₃ , organic compounds, N ₂	Constituent of amino acids, nucleic acids nucleotides, and coenzymes
Phosphorous (P)	~3	inorganic phosphates (PO ₄)	Constituent of nucleic acids, nucleotides, phospholipids, LPS, teichoic acids
Sulphur (S)	~1	SO ₄ , H ₂ S, S ⁰ , organic sulphur compounds	Constituent of cysteine, methionine, glutathione, several coenzymes
Potassium (K)	~1	Potassium salts	Main cellular inorganic cation and cofactor for certain enzymes
Magnesium (Mg)	~0.5	Magnesium salts	Inorganic cellular cation, cofactor for certain enzymatic reactions
Sodium (Na)	~0.5	Sodium salts	Mostly required by marine bacteria
Calcium (Ca)	~0.5	Calcium salts	Inorganic cellular cation, cofactor for certain enzymes
Iron (Fe)	~0.2	Iron salts	Component of cytochromes and certain nonheme iron-proteins and a cofactor for some enzymatic reactions

Table 2.2. Compilation of bacterial nutrients, including their source and function (Madigan et al., 2003; Todar, 2006).

In order to drive cellular biosynthesis and function, the bacteria require energy. This energy can either come from the conversion of radiant energy (light) into chemical energy via the process of photosynthesis (phototroph) or from oxidation-reduction reactions involving inorganic or organic molecules (autotroph and heterotroph).

Additionally, a suitable range of physical conditions, especially temperature, and optimal pH conditions are required. This is however highly depending on the bacterial species. Hyperthermophilic bacteria, for example, prefer temperatures around the boiling point of water as identified in samples from deep sea hydrothermal vents (Huber et al., 1989) whereas other bacteria have been reported to be actively growing in the Siberian permafrost at temperatures as low as -20°C (Rivkina et al., 2000). Acidophiles can live at pH values below 2 and are for example found in acid mine drainage whereas alkaliphiles grow at pH values up to 11 and are often associated with soda lakes and carbonate rich soils (Konhauser, 2007).

2.2.4. *Shewanella putrefaciens*

The gram negative *S. putrefaciens* are heterotroph and therefore require organic carbon (C_{org}) to couple its oxidation with the reduction of an oxidized compound, the terminal electron acceptor (TEA). As facultative anaerobes, they can switch between aerobic and anaerobic types of metabolism. Under anaerobic conditions (no O_2) *S. putrefaciens* can gain energy by reducing various metals in particular Fe (Lovley, 1991; Lovley et al., 2004; Stucki & Kostka, 2006) and Mn (Myers & Nealson, 1988; , 1990) whereas in the presence of O_2 they switch to aerobic respiration. According to their natural habitats optimal conditions of temperature, salinity, and pH are that of typical marine and freshwater environments (Venkateswaran et al., 1999). The strain used in this study (*S. putrefaciens* DMS 6067) grows at optimal temperatures around 30°C and a near neutral pH (7).

2.2.5. Impact of bacteria on their environment

Within limits, bacteria can react and even evolve to changes in their environment and thus readily adapt to a particular situation (Roszak & Colwell, 1987; Todar, 2006). Mineral surfaces are preferred sites for metabolically active bacteria because nutrients are often accumulated (Brown et al., 1977; Ellwood et al., 1982; Bright & Fletcher, 1983). In order to attach to surfaces the majority of microorganisms in aquatic systems form biofilms and assemble themselves in microcolonies (Flemming, 1995; Konhauser, 2007). Such a biofilm consists mainly of highly hydrated exopolymeric substances (EPS) that are secreted by the bacteria who are embedded within it. Biofilms trap nutrients for the growth of the microbial population and help prevent cells from desiccating (Van Loosdrecht et al., 1989; , 1990; Madigan et al., 2003).

Additionally, bacteria can produce compounds to acquire nutrients or other compounds. It was for example shown that *Shewanella oneidensis* was shown to produce reductase proteins that specifically interact with the mineral surface after the potential as a TEA was recognized (Lower et al., 2001). As well the production of electron-shuttling compounds for electron transfer was reported to be involved (Lovley et al., 2004). Another mechanism is the

excretion of low molecular weight ligands that are especially produced to sequester essential elements. Fe(III)-specific ligands are called siderophores (Neilands, 1989) that form coordinative positions around the central Fe(III) cation. This complexation keeps iron in a soluble form making it more easily accessible for bacteria (Birkel et al., 2002). It was described that some bacteria (e.g. *Pseudomonas mendocina*) are able to adapt the siderophore production to the availability of Fe(III) and so actively adapt to their environment (Hersman et al., 1995; Hersman et al., 2000).

2.3. Conclusion an approach of this study

Smectites are unique minerals with very special properties such as their permanent and variable layer charge, cation exchange capacity and large surface areas. The way that smectites interact with the environment is directly linked to these properties and the behaviour of the diffuse double layer in aqueous solution. Approaches to studying smectite hydration are traditionally based on X-ray diffraction analyses under conditions of elevated air humidity in combination with calculated diffraction patterns and more recently Monte-Carlo simulations.

Despite the wealth of knowledge on the hydration behaviour of bentonite clay in solution, less work has been conducted to determine the mechanism and rate of hydration during the infiltration of solution into pressed bentonite powders within a confined reaction volume. In Chapter 4 this topic is addressed by using confined volume reaction-cells (“wet-cells”) that are used to study hydration in situ as potential analogues for the infiltration of solutions into a backfill section of a waste disposal site. Time-dependent results on the mechanism of hydration in relation to the total influx of water into compacted bentonite are obtained and the partitioning of solution into different water storage sites is quantified.

Bacteria are extremely diverse and inhabit almost every near surface environment in and on the planet. Requirements for growth are highly dependent on the type of bacteria but all require a source of carbon, a range of nutrients, energy, water and a favourable pH and temperature range. Many species of bacteria not only appear to interact with their environment but actively react with the solid interfaces of minerals. The bacteria chosen for this study belongs to the phylogenetically diverse genus *Shewanella* that have been isolated from a wide range of freshwater and marine environments as well as from terrestrial environments including soils (Bowman, 2005). This broad occurrence in nature in

combination with their broad versatility with regard to anaerobic respiration make them a “model” organism for studying environmental processes.

Being aware that the diversity of microbial life and the complexity of environmentally relevant processes in natural systems imply an enormous challenge to resolve, this work is based on a defined system of only one type of mineral (smectite) and one type of bacteria (*Shewanella putrefaciens*). The materials and methods used to study the interactions of this clay and bacteria are presented in the following chapter (Chapter 3).

CHAPTER 3

-

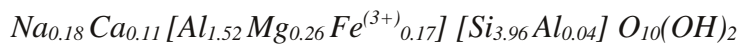
MATERIALS AND ANALYTICAL METHODS

CHAPTER 3 MATERIALS AND ANALYTICAL METHODS

3.1. Sample materials

3.1.1. Bentonite samples: MX80, IBECO, TIXOTON

Three different industrially available bentonites were selected for experimentation: “MX80”, “IBECO SEAL-80” und “TIXOTON TE”. For reasons of simplicity, the latter two will be referred to as IBECO and TIXOTON in the following text. MX80 is a commercial bentonite that is sold by « CETCO France » (17 Avenue Général De Gaulle, 94220 Le Plessis Trevisé, France) and was chosen for this study as an example of a possible future back fill material in the context of nuclear waste disposal (ANDRA, 2005). For experimental investigation, it was used without further purifying treatment and, therefore, the interlayers of the montmorillonite are heteroionically occupied by Na^+ and Ca^{2+} according to the formula (Sauzeat et al., 2001):



Montmorillonite makes up around 76% of the raw material and the remaining fraction consists of mica, feldspar, quartz, calcite and pyrite (table 3.1).

The other two industrial bentonites are considered to be “activated”, which means that the interlayer cations of the montmorillonite minerals have been exchanged to enhance desired properties (Lagaly, 1993). IBECO is activated with Na^+ and can be obtained as a powder from “IBECO Bentonit-Technologie GmbH” (Ruhrorter Strasse 72, 68219 Mannheim, Germany). TIXOTON is a mixture of different bentonites from south German bentonite deposits. The Ca^{2+} activated powder is available from “Süd-Chemie AG” (Steinbockstrasse 12, 85368 Moosburg, Germany). These bentonites contain more than 80% montmorillonite and accessory minerals such as mica, feldspar, quartz, and calcite (table 3.1).

Because of their low layer charge (ranging between 0.28 and 0.33 equivalents per half unit $[\text{eq}/(\text{Si,Al})_4 \text{O}_{10}]$) and high cation exchange capacities (CEC, ranging between 70 and 82 milliequivalents (meq) per 100g), they are considered to be suitable for industrial applications, in particular, as back fill materials (Hermann-Stengele & Plötze, 2000; Sauzeat

et al., 2001; Hofmann et al., 2004; Pusch, 2006b). In addition, their high surface area (BET surface area ranging from ~30 to over 100m²/g) provides numerous sites suitable for the adsorption of toxic substances.

Sample name	IBECO seal 80 ¹⁾	TIXOTON-TE ¹⁾	MX80 (BF100) ²⁾	SWy-2 ^{3,5)}	NAu-1 ^{4,5)}
Material	Na-activated bentonite	Ca-activated bentonite	bentonite	bentonite	Pure nontronite
Lokality	South Germany	South Germany	Wyoming, USA	Wyoming, USA	Uley Mine, Australia
Source	IBECO Bentonit-technologie GmbH, Germany	Süd-Chemie AG, Germany	CETCO, France	CMS source clay collection	CMS source clay collection
Smectite					
Amount [%]	> 80%	> 80%	> 80%	>95%	>93%
	montmorillonite	montmorillonite	montmorillonite	montmorillonite	nontronite
Interlayer cation	Na	Ca	Na, Ca	Na	Ca
CEC [meq/100g]	82	72	69.6	76.4	71
Surface area [m ² /g]*	55.33	103.01	30.03	27.64	83.98
Layer charge [eq/(Si,Al) ₄ O ₁₀]	0.33	0.29	0.28	0.32	0.52
Grain size	Not separated	Not separated	14% silt + sand, 86% <2µm	<1 µm	<0.5 µm
Accessory minerals [%]					
Mica	<3	1-2	2.8-3.8	<1	-
Kaolinite	-	-	-	-	4
Biotite*	-	-	-	-	trace
Chlorite	-	-	-	>1	-
Feldspar	<3	5-6	4.5	1	-
Quartz	-	8-9	5-6	4	<1
Goethite	-	-	-	-	3
Calcite	8-12	1	0.3-1.4	-	-
Gypsum	-	-	-	1	-
Pyrite	-	-	0.5	-	-

Table 3.1. List of samples and their important mineralogical characteristics. Data taken from (Hofmann et al., 2004)¹⁾, (Sauzeat et al., 2001)²⁾, (Mermut & Cano, 2001)³⁾, (Keeling et al., 2000)⁴⁾ and (Chipera & Bish, 2001)⁵⁾. *Own data.

3.1.2. Nontronite and montmorillonite purification

Pure smectite fractions were prepared from samples obtained from the clay minerals society (CMS) source clay collection (Source Clay Minerals Repository, 1150 LILY Hall, Purdue University West Lafayette, IN 47907-1150). Nontronite NAu-1 is a dioctahedral smectite that contains a high proportion of structural Fe(III) in the octahedral sites (~ 34 wt.% Fe₂O₃, table 3.2) and basically divalent Ca²⁺ ions at interlayer sites. Substitutions occurring both at tetrahedral (Al³⁺ for Si⁴⁺) and octahedral sites (Fe²⁺ for Fe³⁺, see Fig. 3.1) result in a negative layer charge of around 0.52 equivalents per half unit (Keeling et al., 2000; Gates et al., 2002). According to Keeling and co-workers (2000) the structural formula is best expressed as:



Because the raw powder samples obtained from the source clays collection contain impurities such as kaolinite, quartz, biotite and goethite, they were washed and a reality pure < 0.5µm nontronite fraction separated by centrifugation (for remaining impurities, see table. 3.1). The nontronite was chosen as a representative Fe-rich smectite, which is predicted to form as an alteration product of montmorillonite when in contact with the Fe-containers of a repository site (Wilson et al., 2006).

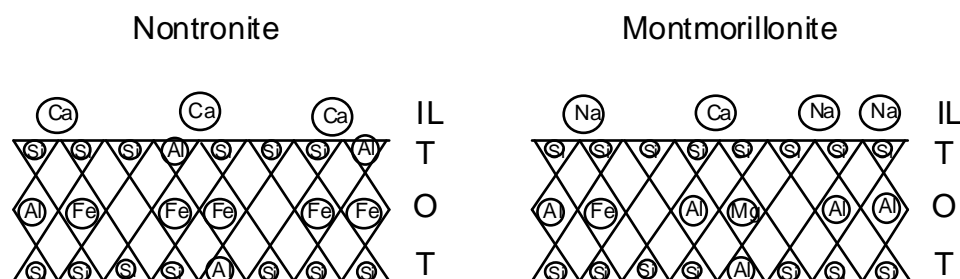
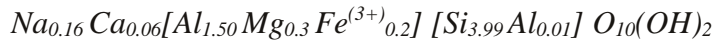


Fig.3.1. Schematic representation of cation sites in the dioctahedral smectite structure (non-stoichiometric). Abbreviations are as follows: IL- interlayer, T- tetrahedral sites and O-octahedral sites (after Velde 1992).

SWy-2 is the sample name of the Wyoming bentonite standard from the clay minerals society (CMS). The raw material contains around 80 % montmorillonite with Na as the principle interlayer cation. The layer charge of around 0.28 equivalents per half unit results

mainly from the octahedral substitution of Mg^{2+} for Al^{3+} (cp Fig. 3.1). The generalized formula after Mermut & Cano (2001) and Mermut & Lagaly (2001) is:



In order to obtain a monocationic sample the (<1 μ m fraction) was saturated with Na^+ and was used in experiments as a standard reference for pure Na-montmorillonite.

Element [% oxide]	IBECO seal - 80 ¹⁾	TIXOTON-TE ¹⁾	MX80 (BF100) ²⁾	SWy-2 Montmorillonite ³⁾	NAu-1 Nontronite ⁴⁾
SiO ₂	52.9	53.8	57.5	62.9	53.33
Al ₂ O ₃	16.6	17.5	18.66	19.6	10.22
TiO ₂	0.8	0.3	0.14	0.09	-
Fe ₂ O ₃	4.6	5.1	4.16	3.35	34.19
FeO	-	-	1.65	0.32	-
MnO	0.1	0.1	-	0.006	-
MgO	3.9	3.0	2.17	3.05	0.27
CaO	6.1	3.7	1.42	1.68	3.47
Na ₂ O	2.6	2.2	2.18	1.53	0.08
K ₂ O	0.5	1.3	0.64	0.53	0.03
P ₂ O ₅	0.1	0.1	0.25	0.049	0
S	-	-	0.27	0.05	-

Table 3.2. Chemical composition of the used materials. Data taken from Hofmann et al. (2004)¹⁾, Sauzeat et al. (2001)²⁾, Mermut & Cano (2001)³⁾ and Keeling et al. (2000)⁴⁾.

3.1.3. Solutions: ground water, sea water and experimentally mixed saline solutions

In this study, two natural solutions were used (table 3.3). A granitic ground water obtained from a surface source in Heidelberg, Germany, and an Atlantic sea water that was sampled from the Cornwall coastline, UK. The latter has been diluted by terrestrial waters and exhibits a lower salinity than the average sea water composition. The samples were filtrated (<0.45 μ m) and stored in a cool place until used for experiments. Additionally, a simplified salt solution containing KCl (0.28 g/l) and CaCl₂ (0.05 g/l) was mixed. All solutions were sterilized by filtration or autoclave prior to experimentation.

Cation	Atlantic sea-water [mg/l]	Granitic ground-water [mg/l]
Na	11300	8.13
K	468	4.76
Mg	1410	3.79
Ca	428	23.8
Li	0.27	<0.01
Fe	<0.01	0.213
Mn	<0.01	<0.01
Al	<0.01	<0.01
Total dissolved cations	~13606	~41
pH	8.2	7

Table 3.3. Cationic compositions of the natural solutions used in this study determined by atomic adsorption spectroscopy (Warr & Berger, 2007).

3.1.4. Bacteria

The bacterial growth media are special types of experimental solution (table 3.4). The Luria Bertrani (LB) medium was used for incubation of cultures prior to experimentation, whereas a chemically defined minimal medium (MM; Myers & Nealson (1988)) was used both as an incubation medium and experimental solution. Preparations were done under sterile conditions or the solutions were sterilized after preparation by filtration and/or autoclaving.

Luria Bertrani Medium (LB)		Minimal Medium (MM)	
Cation	[mg/l]	Compound	unit
			[mM]
Si	1.9	(NH ₄) ₂ SO ₄	9.0
Al	0.09	K ₂ HPO ₄	5.7
Mg	2.02	KH ₂ PO ₄	3.3
Ca	2.56	NaHCO ₃	2.0
Fe	0.35	MgSO ₄	1.0
Mn	0.008	CaCl ₂	0.5
Ti	0.022	Amino acids [mg/l]	
Na	n.d. (~10000)	Arginine	20
K	306	Glutamate	20
P	130	Serine	20
		Electron donor [mM]	
		Formate	20
		Electron acceptor [mM]	
		Fe(III) citrate	80

Table 3.4. Cation composition of the Luria Bertrani medium (LB) and a list of the major compounds in the minimal medium (MM) as defined by Myers and Nealson (1988). The electron acceptor was only added to adapt bacteria to Fe(III)-respiration and for incubation under anaerobic conditions.

Shewanella putrefaciens are motile rods that vary in size between 0.5 and 5 μm (Fig. 3.2.), depending on their growth state and environmental conditions (Chapter 2). These gram negative heterotrophic bacteria have been detected in a variety of aquatic and subsurface environments (Venkateswaran et al., 1999) as well as been isolated from some oil fields (Westlake et al., 1966). As facultative anaerobes, they are able to use oxygen as terminal electron acceptor (TEA) but under anaerobic conditions they can also utilize nitrate, fumarate, sulphite, chromate and U(V), Fe(III) and Mn(IV) (Obuekwe & Westlake, 1982; DiChristina et al., 1988; Lovley et al., 1991).

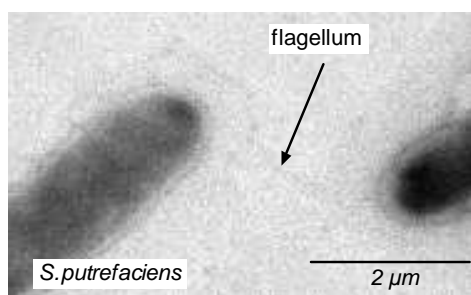


Fig. 3.2. TEM image of *S. putrefaciens* cultivated in minimal medium showing the presence of a flagellum.

The *S. putrefaciens* strain used in this study was obtained from the “Deutsche Sammlung von Mikroorganismen und Zellkulturen (DSMZ) as freeze dried pellets. The DMS specification (DMS 6067) is identical with the American Type Culture Collection specification ATCC 8071. This strain had been formerly called *Alteromonas putrefaciens* (Lee et al., 1977; MacDonell & Colwell, 1985) but was later re-classified (Gauthier et al., 1995). In pre-1977 literature, the names *Pseudomonas putrefaciens* or *Achromobacter putrefaciens* were used.

3.2. Analytical Methods

3.2.1. X-ray diffraction study

X-ray diffraction (XRD) is the main method used in this study for monitoring time dependent changes in crystal chemistry. This is a well-established technique commonly used for identification and characterization of smectites as it can routinely detect changes in lattice

structure at the angstrom scale (Brown & Brindley, 1984; Moore & Reynolds, 1997). As established by Max von Laue in 1914, X-rays diffract on the periodically arranged atoms of crystalline substances, allowing its structure and chemistry to be determined. X-rays are generated within an X-ray tube and focused onto powdered samples at varying angles within a controlled goniometer circle (Fig. 3.3).

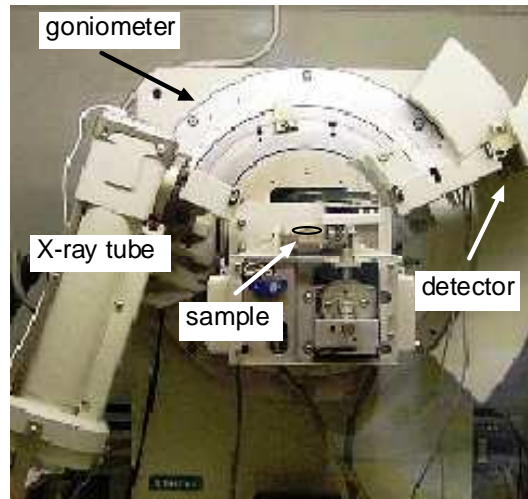


Fig. 3.3. Photograph through the window of the D-5000 Bruker-Siemens diffractometer showing the X-ray tube, the goniometer and the sample holder.

The X-ray photons from the incident beam collide with electrons in the crystalline sample causing some photons to be deflected away from their original direction (scattered X-rays). Constructive and destructive interference of diffracted waves with the crystal lattice allow interference maxima (peaks) to be recorded by the detector. Conditions for diffraction are given by the well known Bragg's law (Fig. 3.4).

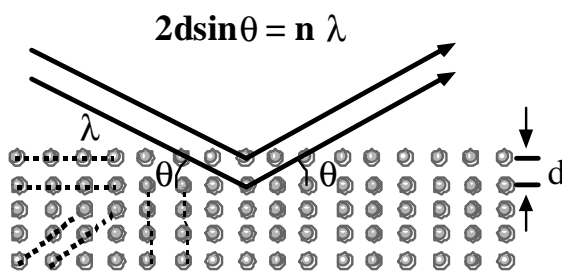


Fig. 3.4. Two dimensional schematic sketch of X-ray diffraction and the Bragg's law. The incident X-ray beam with the wavelength λ interacts with the atoms arranged in a periodic manner (grey dots) forming different sets of planes in the crystal (dotted lines). Bragg's law gives the condition for the occurrence of constructive interference and the position of the diffraction peak.

λ = wavelength of the X-ray

θ = scattering angle

n = integer representing the order of the diffraction peak.

d = lattice distance

The arrangement of atoms in a lattice are characteristic of each mineral phase and their X-ray scattering effects can be used for resolving structure, qualitative mineral identification and quantitative measurement of mineral abundance. Particularly important in the study of smectites is the determination of the thickness of the interlayer space which can be resolved from d-value of the 001 X-ray peak (Hofman & Bilke, 1936; Bradley et al., 1937; MacEwan & Wilson, 1980). This dimension varies dependant on the structure of adsorbed water and the type of hydrated interlayer cations (Fig. 3.5).

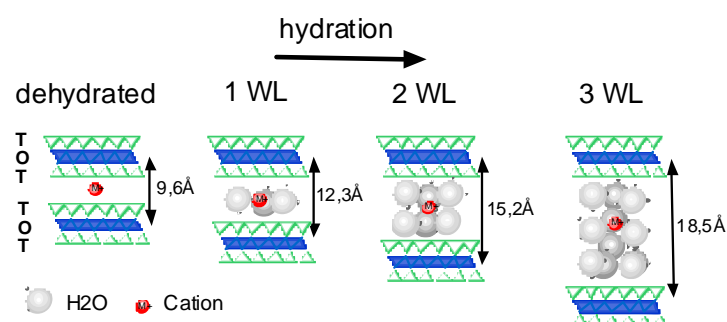


Fig. 3.5. Increase of d-values due to intercalation of water layers.
WL=water layers.

In addition to the position of X-ray diffraction peaks, the shape of the basal reflections holds important structural information of the material, in particular, the thickness of the coherent scattering domains (commonly referred to as particle size) and the abundance of mixed layered structures. A simple measurement of the shape of a reflection is the full-width-at-half-maximum (FWHM) parameter (peak-width). A small increment of peak broadening is caused by machine effects, such as defocusing or scattering of the beam (Klug & Alexander, 1954; Moore & Reynolds, 1997). However, installing a monochromator and narrowing the slits minimizes this effect. In the case of clay minerals, most of the peak broadening is due to small particle size and (in case of smectites) due to complex mixtures of mixed-layered hydration states (Reynolds, 1980). In the case of pure phase reflections (no mixed layers), the thickness of particles can be estimated by the Scherrer equation or from modifications of this empirical formula (see Klug & Alexander (1954), Drits et al. (1997) and Moore & Reynolds (1997) for details).

Although most natural smectites produce basal XRD reflections that are broadened by the effects of small particle thickness (typically <10 nm) and mixed hydration states, comparison with calculated XRD patterns, such as NEWMOD and CALCMIX, do allow

these parameters to be resolved. Mathematically, in contrast to the irrational distribution of mixed-layered broadened peaks (2 theta dependent), particle size broadening is rationally distributed over the XRD patterns and therefore not 2 theta dependent (Eberl et al., 1998).

The intensity of a given X-ray reflection is dependent on a number of factors such as phase abundance, density, mass adsorption coefficient and orientation (texture) of the clay mineral platelets (Lagaly, 1993; Moore & Reynolds, 1997). For perfectly oriented crystallites only the (00l) intervals are visible because diffraction is restricted to the crystallographic c-direction. Texture preparations, in contrast to powder preparations, approach this ideal because, during sedimentation, their particles orientate parallel to the sample holder (glass slide). Therefore, texture preparations were used in this study to characterize clay samples extracted from the experiments

Analyses were made using a theta-theta Bruker Siemens D5000 diffractometer with $\text{CuK}\alpha$ radiation, operated under a potential of 40kV and a beam current of 30mA with 1° divergent aperture diaphragms and a 0.15° detector diaphragm. Scanning parameters were set at 0.02 step width and a count time of 10 seconds. The measurement range was selected to suite certain samples and ranged between 2 and $15-70^\circ 2\theta$. Intensity variations between measurements caused by textural changes in the sample were calibrated by normalizing the height of the (001) kaolinite reflection at 7.14\AA .

3.2.1.1. Concept of a laboratory analogue: reaction-cell X-ray diffractometry

The reaction-cell device ("wet-cell" of Warr & Hofmann 2003) is a small flow-through reaction chamber made of a Teflon compound that can be routinely mounted onto the X-ray diffractometer. It allows in situ measurement of hydration reactions during the infiltration of a solution into fine-grained smectite powders. The sample chamber of the cell is disc shaped (Fig. 3.6 a) with a diameter of 24mm and a depth of 8mm (volume of 3.9cm^3), into which the sample is densely packed using a metal brass rod that gives a rough texture parallel to the upper surface of the sample holder.

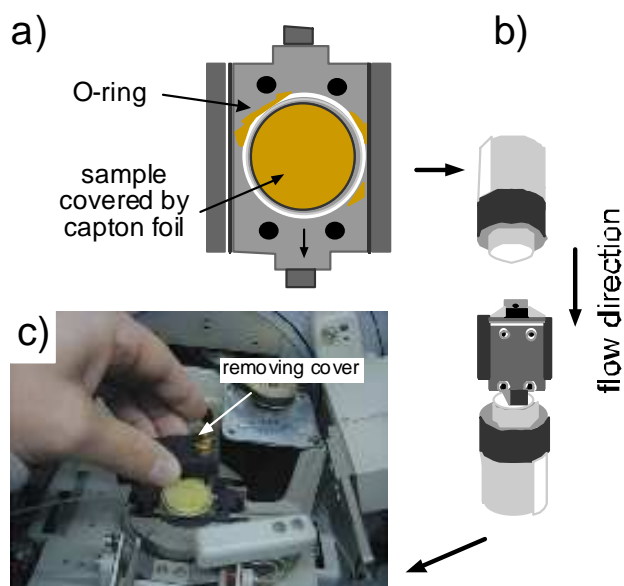


Fig. 3.6. a) Schematic representation of the reaction-cell sealed by Capton foil. b) Closed reaction-cell with Teflon bottles. c) Reaction-cell mounted on the sample holder of the diffractometer.

Bacteria containing samples were prepared by mixing the clay with the bacteria prior to loading it into the cell. Depending on the type of material and its initial hydration state, the amount of clay powder loaded into the cells varied between 3 and 5g. The reaction-cell was then sealed by a thin X-ray transparent Capton© foil and held in place with a sealing Teflon© O-ring. Around 200ml of solution was placed in 8cm tall Teflon© bottles which were screwed directly onto the cell to allow inflow (Fig. 3.6b). Before entering the reaction-cell and the sample powder, the solution passes a horizontal 0.8mm hole, 5mm in length. Once into contact with the powder, a radial zone of hydration moves across the reaction-cell chamber. Filters at the entrance of the cell ($<0.45\mu\text{m}$) prevent contaminations with unwanted microbes which are especially important when working with bacterial media. Additional filters at the end of the reaction-cell also prevent the powder from leaving the chamber.

In order to maintain constant reaction volume during the experiment, a pressure cap was screwed to the top of the cell and only removed for XRD study (Fig. 3.6.c). Subsequent measurements were made at selected intervals throughout the experiment, enabling sequential XRD patterns to be plotted against time. The frequency of measurements was adjusted according to the observed rate of reaction. For bacteria containing samples, the measurement frequency was kept low in order to minimize radiation damage and disturbance of the experimental setup.

3.2.2. Monitoring hydration

3.2.2.1. Quantification of interlayer hydration using CALCMIX

The hydration structure of smectite interlayers was quantified by comparison with calculated patterns. In this study, the CALCMIX software provided by Plançon & Drits (1999) was used because it could be easily modified and can deal with three phase systems simultaneously. This software calculates the theoretical diffraction patterns of mixed-layer minerals based on Méring's principle (Méring, 1949). In order to calculate different mixtures of different water layer structures, the standard mineral data base was modified for smectites containing 0, 1, 2, 3 and 4 water layers. The relevant chemical composition and structure of the minerals used was entered in the minerals database of the program.

In the CALCMIX program, the mean defect free domain can be selected and the particle thickness distribution calculated assuming lognormal distributions (Drits et al., 1997; Drits et al., 1998). This type of distribution reproduces well the broadened tails observed in clay mineral XRD 00 l reflections and is considered to be the common size distribution observed in clays and many other minerals (Drits et al., 1997). In the smectites studied, the mean defect free domain varied between 14 and 19 layers per stack for relatively dehydrated samples and between 3 and 8 units for hydrated samples. The degree of ordering for mixed-layered water-layer structures (the Reichweite) was selected manually. Initial values of R1 ordering were first tested which appeared to best match the shape of measured XRD reflections, followed by refinements made in the stacking probabilities to improve the correspondence between calculated and measured profiles. Based on these calculations, the abundance and ordering of water layer structures as well as the mean defect free domain thickness (particle thickness) were obtained. Further details on using the CALCMIX program can be found in the handbook of Plançon & Drits (1999).

The relative abundance of water layers obtained from CALCMIX-calculations were used to estimate the amount of interlayer water using data obtained from isotherm absorption experiments of montmorillonites (Bérend et al., 1995; Cases et al., 1997). The amount of water in nontronite interlayer's was calculated using data by Jähnchen et al. (2006) and Milliken & Mustard (2007). As 3 and 4 water layers have not been observed in relative humidity experiments, these values are extrapolated from the isotherm curves (see appendix for details).

3.2.2.2. Quantification of non-interlayer hydration

The total water uptake into clay samples during hydration was determined by monitoring gravimetrically the relative weight change of the reaction-cell apparatus throughout experimental runs. Subtraction of the calculated interlayer water from the measured total water content yields the volume of surface- and pore-water in the samples (i.e. non-interlayer water). Based on the decrease in numbers of layers per particle (n), the relative increase of surfaces and a theoretical corresponding surface area were obtained. These results were then used to estimate the amount of adsorbed water on particle surfaces (appendix for an example of this calculation).

3.2.3. XRD characterization of clay minerals

Experimentally induced changes in smectite composition and structure can be detected by simple chemical treatments in the laboratory combined with XRD analyses. Here, tests related to the oxidation state of Fe and its influence on layer charge properties are of particular importance. As octahedral Fe is reduced, the weak negative charge of the smectite (~ 0.3 - 0.5 per formula unit - PFU) increases and approaches that of vermiculite (~ 0.6 PFU, Bailey (1980)). As the permanent layer charge increases (>0.6 PFU), K can fix to interlayer sites to form a 10\AA illite phase (MacEwan & Wilson, 1980; Cuadros & Altaner, 1998; Meunier et al., 2000). Low layer-charged smectite can be distinguished from the higher charged vermiculite by Mg- exchange and glycerol solvation because vermiculite only accepts one plane of glycerol molecules (d-spacing 14.5\AA). Smectite, in contrast, swells to a basal spacing of 18\AA and intermediate spacings are suggestive of an intermediate layer charge. Illite clays, or mixed layered illite-smectite phases, produce basal reflections between 10 - 15\AA in the untreated air dried state. These type of minerals are best characterized by ethylene glycol solvation and heat treatments (Moore & Reynolds, 1997).

3.2.4. Microscopy

3.2.4.1. Confocal microscopy

Optical microscopy (epifluorescence) was used to study the formation of biofilm in clay bacteria mixtures. For this purpose, diluted bacteria containing and sterile smectite suspensions were directly pipetted onto a glass slide and studied in the wet state. In the case of optical epifluorescent microscopy, the biofilm was coloured with calcofluor and the bacteria with ethidium bromide (see details of procedure in appendix).

3.2.4.2. Electron microscopy

As powder XRD is a bulk analytical approach and does not provide vision information concerning reaction textures and fabrics, it is important to accompany such studies with electron microscopic investigations of the sample material. The electron microscope operates on the same basic principles as a light microscope but the focused electrons allow significantly higher resolutions to be obtained. A cathode at the top of the microscope emits electrons that are accelerated through the vacuum column of the microscope and focused by magnetic lenses to produce a very narrow beam. Energy dispersive X-ray analyses (EDX) allows multi-element analyses by detection of X-rays of specific energy that are characteristic individual elements. Because the electron beam can be reduced to a sub-micron diameter, microchemical information can be obtained from distinct clay particles and bacteria cells. The two different types of electron microscopes used in this study are briefly outlined as follows.

Transmission electron microscopy (TEM)

At the base of the TEM microscope, un-scattered electrons hit a fluorescent screen to produce a shadow image of the specimen with its different parts displayed in varied grey scales according to material thickness and density. The image can be studied directly by the operator or photographed with a camera. The highest resolution possible is, dependent on microscopic settings, in the order of a few angstroms (10^{-10} m). This is ideal for imaging bacteria and clay structure at the nanometric and micrometric size (Elsass, 2006). Coupled with an EDX analyzer, microchemical data on specific particles and bacteria can be routinely obtained. As it was shown by (Perdrial, 2007), it is not necessary to stain bacterial cells prior to imaging (as required for optical microscopy) and an acceleration voltage of 120 kV incurs minimal damage to the bacterial cells in transmission mode.

Because of the low resistance to irradiation of bacteria and swelling clays, the counting time for analyses was reduced to 30s and analyses were done with the sample in strictly eucentric position at an angle of +20° to the detector. Microchemical analyses (C-N-O-Na-Mg-Al-Si-P-S-Cl-K-Ca-Mn-Fe-Cu-Zn) were carried out in transmission mode with the same acceleration voltage and with the fluo-X signals being recorded between 0 and 20 keV with a Si/Li detector and an atmospheric thin window (ATW). The C coating of the copper grids (Formwar ©) always contains enrichment in Si, this is to be taken into account concerning all EDX microanalyses. The TEM/EDX was carried out at the Laboratory of Users of Electron Microscopes (LUME) of INRA, Center Versailles-Grignon. The TEM microscope, a Philips STEM 420 is equipped with an Oxford INCA EDX system and a SIS Megaview II CCD camera.

Environmental scanning electron microscopy (ESEM)

As both bacteria and smectite are very sensitive to drying, environmental scanning electron microscopy (ESEM) was used to investigate this sample material. This technique does not require desiccation or coating and, instead of completely evacuating the specimen chamber as in conventional SEM, water vapour is introduced into the chamber via a valve that controls the pressure (range 0-10torr or 0 - 0.013bar, respectively). The microscope used was a Philips XL30 ESEM equipped with a peltier cooled specimen stage that controls the temperature (range of -5°C to +60°C). In conjunction with chamber pressure, the resulting condensation keeps the sample wet. Relative humidity values, between 55-75%, were obtained by applying a pressure range between 5.9 and 6 torr and corresponding temperatures, ranging from 8°C to 22°C.

Electrons are emitted from a LaB6 cathode and, in order to achieve the best resolution in ESEM mode, the accelerating voltage was set to 25 keV. The signal to noise ratio and resolution were decreased and the resulting magnification limited to about 20 000 times due to the skirting effect: an electron scattering of the primary beam caused by the residual pressure between the objective lens and the scanned surface. Secondary electrons emitted from the surface of the sample encounter water vapour molecules, which amplifies the signal. A specific detector converts directly the electrical signal into images. In this study, the ESEM was used to monitor changes in the morphology and size of smectite particles, and to observe biofilm formation and structures under hydrated conditions. In Fig. 3.7 a) an example of a nontronite aggregate imaged by conventional SEM is shown with no swelling as opposed to the same material imaged in environmental mode (Fig. 3.7.b).

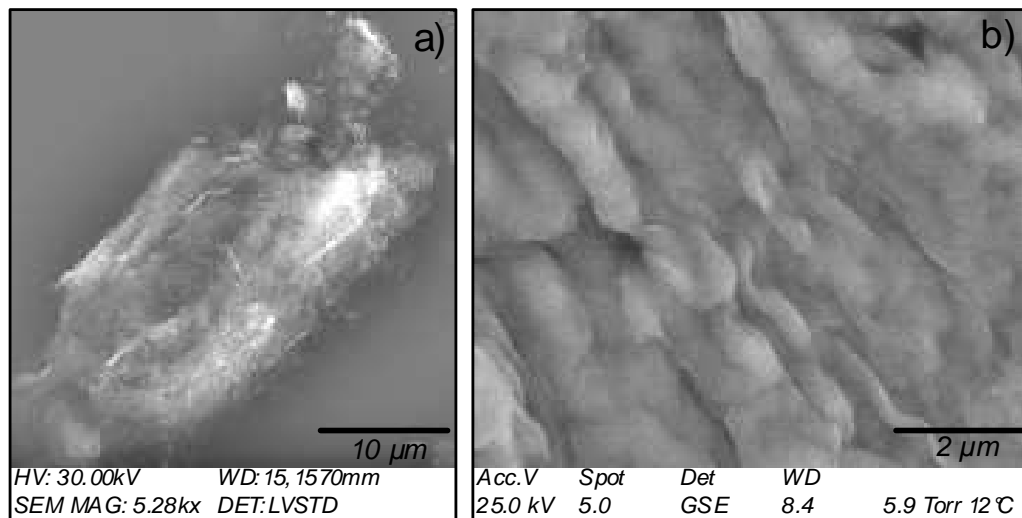


Fig. 3.7.a) SEM image of a nontronite aggregate b) ESEM image of swelling nontronite.

3.3. Bacteria preparation and analyses

3.3.1. Aseptic techniques

Working with pure cultures requires techniques that avoid contamination with unwanted microorganisms. Most of the laboratory items used, such as test tubes, were sterilized by heat treatment (normally at $>121^{\circ}\text{C}$) or by a combination of heat and elevated pressure treatment using an autoclave that normally operates at 1.03bar. The nutrient media were also sterilized by autoclave to remove living organisms and viruses. In the case of some components that cannot resist heat (e.g. amino acids), solutions were sterilized by filtration ($<0.2\mu\text{m}$ pore size).

As many contaminants are airborne it is essential to prevent contaminated air from entering the sterile materials. Therefore, the opening of containers or the transfer of a culture was usually done close to the flame of a Bunsen burner. The heated air is convecting and provides a sterile environment within a $\sim 20\text{-}30\text{cm}$ radius around the heat source (Madigan et al., 2003). Inoculating loops or needles were also sterilized by burning in the flame.

3.3.2. Culture preparation

The bacterial sample of *S. putrefaciens*, which was obtained as a dried pellet from the DSMZ, was first dissolved in LB medium and then cultured for 72h at 30°C. Secondly the culture was grown on LB-agar plates to control its purity and was then again introduced and grown in liquid LB for 72 hours. For storage in the freezer (-80°C), this culture was washed by centrifugation (4000rpm/10min) and then supplied with 20% of glycerol to prevent damage during freezing. This frozen culture served as a source for all subsequent experiments. Before usage, a small amount of the frozen culture was taken, re-grown in LB medium for 72 hours and washed. Experiments that were conducted under anaerobic conditions required a culture adapted to metal respiration (Fe(III)-respiration). For this purpose the stock culture was washed and grown in a defined minimal medium (Myers & Neelson, 1988) for 72h at 25°C (table 3.4). The culture was supplemented with 20mM formate, as an electron donor, and 80mM Fe(III) citrate, as TEA, before being stored anaerobically by using the CO₂ generating system of BioMerieux©. The Fe-citrate was applied to slowly adapt the bacteria's metabolism to respire Fe(III) instead of oxygen. Bacterial cultures for aerobic experimentations were not adapted.

3.3.3. Viable cell counts

The growth of a bacterial population can be measured by monitoring changes in the total numbers of cells (total cell counts) or by counting only those cells that are alive and are able to form colonies on an Agar plate (viable cell counts). This latter method was routinely applied in order to control the density of a bacterial culture both prior to experimentation and during bacterial growth within smectite samples. However, with this technique it is not possible to know if one colony has been formed by more than one bacterial cell and, therefore, the population growth is expressed as increase in “colony forming units” (cfu) per ml. For effective counting of single colony units, all samples were diluted using serial dilutions before being tested on agar plates. If the number of bacteria in a sample was too high, no single colonies could be observed as they merge to form bacterial mats. However, if this number is too low, the statistical error increases.

Prior to dilution, solid samples were dissolved and dispersed in sterile water. Several serial 10-fold dilutions were prepared for each sample by mixing 0.1ml of the initial solution

with 0.9ml diluent. Further dilutions were prepared by repeating the procedure by extracting 0.1ml of this dilution and introducing it to another 0.9ml of water (Fig. 3.8.). In the case of pure culture counts, the samples were diluted up to 7 times (10^{-7}) whereas for samples containing bacteria and smectite 3 dilutions (10^{-3}) were usually adequate. Colonies were grown by spreading 0.1ml of sample-suspension onto an agar plate (glass-pearls were used to obtain an even distribution), incubated (25°C for 72h) and after a few days of growth counted. To increase the reliability, preparations of each sample were repeated twice.

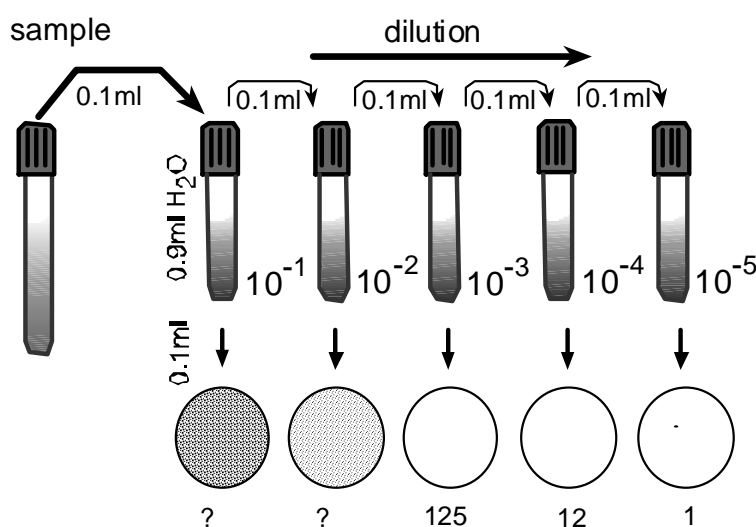


Fig. 3.8. Example of a serial dilution conducted prior to viable cell counts. 0.1 ml of the initial sample are introduced into 0.9 ml sterile water and mixed. 0.1 ml of this dilution is then introduced to another tube that contains as well 0.9 ml water and so on. Each step leads to a 10 fold dilution. 0.1 ml of the final dilution is then spread on an agar plate. In the example presented there are too many colonies on the first two plates (10^{-1} and 10^{-2}) but the third dilution gives good results with 125 colonies on the plate yielding a count of $1.25 \cdot 10^5$ cfu/ml (after Madigan et al. 2003).

3.4. Solution chemistry

Precise elemental concentrations of elute solutions were readily obtained using ICP-OES (Inductively-Coupled-Plasma Optical-Emission-Spectroscopy). Here, analyses were made using the „Plasma 400“ ICP-OES of Perkin-Elmer. Excited atoms and ions emit electromagnetic radiation characteristic of each particular element. An induction coil fed by a high frequency generator, releases an oscillating magnetic field at the plasma torch. Since it is easily ionified, argon is used as a plasma gas. With the induction of the coil, the high frequency generator supplies the energy for ionization in the plasma in which the sample is introduced. The intensities of emission are detected by a photosensitive detector and digitally

processed before calculation of the dissolved elemental concentrations by calibrating against standards.

This method is particularly suitable for metals, metalloids and some non-metals. In this study, the elemental concentrations of Al, Si, Mg, Na, K, Fe and Ca were measured. As the detection limit is in the order of ppm most of the samples required a dilution of 1:5 (minimum of 4ml) for accurate measurements.

CHAPTER 4

-

ABIOTIC INFLUENCE ON SMECTITE HYDRATION

CHAPTER 4 ABIOTIC INFLUENCE ON SMECTITE HYDRATION

Abstract

This chapter presents the study of smectite hydration in confined volume conditions in situ by using small-scaled reaction-cells (“wet-cells”, Warr & Hoffman, 2004) mounted on an X-ray diffractometer and applied to simulate conditions of an underground repository. The rate of smectite hydration was seen to be highly dependant on the type of interlayer cation (enhanced for Ca^{2+} as opposed to Na^+) and on the ionic strength of solution (enhanced uptake rate in the case of Na-smectite). Differences between Na and Ca-smectite were observed to occur due to microtextural variations and to decrease as a function of packing density. The combination of X-ray diffraction and the calculations of diffraction patterns by using the CALCMIX software (Plançon & Drits, 1999) revealed aggregate formation of particles with the same water layer thicknesses. Additionally, changes in particle thicknesses were used to calculate corresponding theoretical surface area increase. Results indicate the partial transformation of internal surfaces into external ones upon hydration that are partly available as sorption sites. Quantifications of water storage sites by using published data of water vapour absorption experiments (Cases et al., 1992; Bérend et al., 1995; Cases et al., 1997) revealed that in Na-smectite external water (surface- and pore water) is taken up and serves as a reservoir for interlayer hydration. Higher initial packing density decreased the thickness of water layers and led to enhanced external water uptake. The influence of solutions of higher ionic strength was seen to be most pronounced in the case of Na-smectites and was attributed to the formation of aggregates that enhance the porosity. The observed mechanisms of smectite hydration in confined volume is presented in a schematic model involving different scales: ranging from the Å-scale (layers) to the bulk structure, including particles, aggregates (arrangement of closed particles) and arrangements of aggregates. Effects on all scales were due to the nature of interlayer cation, whereas the ionic strength basically affected the bulk texture. Quantification of water storage sites as a function of solution chemistry, packing density, and the obtained uptake rates provide important constraints for predicting smectite hydration in terms of conductivity, sealing capacity and sorption and/or transport of radionuclides. Additional constraints for computer based models are provided by estimations of changes and availability of surface area during hydration.

4.1. Introduction

The majority of nuclear power producing countries are today considering disposal of radioactive waste in underground repositories using a system of clay-based natural and engineered barriers (OECD, 1999; ANDRA, 2005; OECD, 2006). In order to prevent or severely reduce the eventual release of radioactivity, the engineered barrier is of major importance with regard to physical and chemical containment. Swelling clays (smectite) are the primary constituent of the engineered back fill material which during hydration expands and self-seals, thus restricting the movement of aqueous fluids (Karnland & Sandén, 2000; Montes-Hernandez et al., 2005b; Pusch, 2006b). The sorbent properties of clays are also of interest because of the potential retention of toxic elements (Hermann-Stengele & Plötze, 2000; Karnland & Sandén, 2000; Karnland et al., 2000).

The sealing capacity of smectite is based on its ability to intercalate water molecules into the interlayer space that solvates the exchangeable interlayer cations (Farmer & Russel, 1971; Prost, 1975). During intercalation, the molecules order themselves in an arrangement of well-defined layers and successive intercalation leads to increasing expansion (Sposito & Prost, 1982; Karaborni et al., 1996). Water that is not stored in the interlayer space is found in external regions in inter-particles and aggregates, like external surfaces or micropores (Prost, 1975; Sposito & Prost, 1982). Experimental quantification of the mechanisms and rates of water incorporation is of major importance because the different storage sites of water influence the mechanisms of sealing, sorption and transport in notably different ways. The amount of water that is incorporated in interlayer spaces has already been successfully quantified based on water vapour adsorption-desorption isotherms (Cases et al., 1992; Bérend et al., 1995; Cases et al., 1997).

In a fully dispersed Na-bentonite solution of low ionic concentration, the proportion of external pore space increases dramatically as osmotic pressure transforms interlayers (internal surfaces) into free (external) surfaces by separating particles (Lagaly, 1993; , 2006). Such newly formed external surfaces might then be available as sorption sites. In bentonite powders, the quantity of additional water uptake on particle surfaces has been calculated on the basis of the Brunauer-Emmet-Teller (BET) method (Bérend et al., 1995; Cuadros & Altaner, 1998). Additionally, the size distribution of pore spaces was assessed by the Hg-injection technique (Olson, 1985).

In order to monitor the interlayer expansion, a common approach is to study the smectite hydration states by varying the conditions of relative humidity in combination with X-ray diffraction measurements (XRD) (Mooney et al., 1952; Collins et al., 1992; Kühnel & van der Gaast, 1993; Chipera et al., 1997; Ferrage et al., 2005b) or via bulk volume measurements (Likos, 2004). In contrast to experiments in elevated air humidity, a number of studies investigated swelling in aqueous and electrolyte solutions by using experimental systems where particles expanded freely (Norrish, 1954; Norrish & Quirk, 1954; Schramm & Kwak, 1982; Laird et al., 1995; Wilson et al., 2004). More recently, the influence of varying salt concentration on the total bulk expansion of montmorillonite particles in solution was quantified by in situ laser scanning microscopy (Suzuki et al., 2005) so the contributions of interlayer expansion and osmotically-driven swelling could be directly observed.

Hydration under repository conditions is, however, most likely to be highly influenced by the confined volume and therefore not comparable to free swelling in solution. In order to record essential parameters like heating, wetting rate and development of swelling pressure, large scale in situ experiments such as Mock-up in Sweden and Spain or the FEBEX (Full-scale Engineered Barriers EXperiment) were performed (Lloret & Villar, 2007; Pusch et al., 2007; Villar & Lloret, 2007). This approach is essential for evaluating the performance of a bentonite buffer in an almost full scale system (ENRESA, 2007).

Large scale analogues are, however, extremely costly, and require intensive preparation and once started, it is not possible to adapt or change the set up. Laboratory analogues are significantly cheaper and serve to simulate repository conditions, thus providing more easily won constraints for larger scale tests. At the same time, laboratory experiments allow specific problems to be investigated by using different set ups and materials that provide quantitative data for modelling reaction and transport processes. The experiments conducted in this study were therefore designed to monitor and quantify the hydration of different materials (purified smectite and bulk powdered bentonite) with regard to different initial conditions, such as packing density and initial hydration state, subjected to a range of infiltrating solutions (Table. 4.1.1).

	IBECO seal 80		TIXOTON-TE		MX80 (BF100)			SWy-2		Nau-1
Material	Na-activated bentonite		Ca-activated bentonite		bentonite			Purified montmorillonite	Purified nontronite	
Pre-treatment										
Grain size separation	-	-	-	-	-	-	-	1 μ m	1 μ m	0.5 μ m
Cation exchange	-	-	-	-	-	-	-	Na	Na	-
Hydration or dehydration	60° for 24h, re-equilibrated at 25-30 % RH				110°C 2 weeks	110°C 1 week	Hydrated (0.23 ml/g)	110°C for 2 weeks		110°C 1 week
Initial parameters										
packing density [g/cm ³]	1.15	1.14	0.94	0.94	1.43	1.35	1.60 (dry 1.31)	1.37	1.36	1.08
Temperature [°C]	25	25	25	25	25	25	25	25	25	25
Experimental parameters										
Experimental solution	Ground water	Sea water	Ground water	Sea water	Purified water	Salt solution	Salt solution	Purified water	NaCl	Purified water
Ionic strength [mol/l]	0.0013	0.639	0.0013	0.639	~0.001	0.011	0.011	~0.001	1	~0.001
Static fluid pressure [kPa]	0.7-05	0.7-05	0.7-05	0.7-05	0.7-05	0.7-05	0.7-05	0.7-05	0.7-05	0.7-05
Inflow rate [ml/g/h]	2.7E-04	1.1E-03	4.3E-03	3.8E-03	8E-05	1.7E-04	1.7E-04	1.9E-04	2.1E-04	1.2E-03

Table 4.1.1. Summary of the key properties of the studied materials after sample preparation and a list of the experimental conditions used in the hydration experiments.

4.2. Analytical procedure

In situ monitoring of smectite hydration by XRD was achieved by using a flow-through reaction-cell known as “wet-cell” (Warr & Hofmann, 2003). This small-scale reaction-cell provides a laboratory analogue for quantifying the dynamics of hydration in compacted smectite under confined volume conditions. Time dependent XRD measurements were acquired routinely during experimentation with minimal disturbance of the sample set up. The total water uptake was measured throughout experimental runs by monitoring the relative weight change of the cell. The relative proportion of WL structures obtained from the CALCMIX data were used to calculate the theoretical amount of water (mmol/g H₂O) in the interlayer space of Na-montmorillonite and Ca-montmorillonite based on the absorption isotherm experiments of Bérend (1995) and Cases et al. (1997). Subtracting the calculated interlayer water from the measured total water content yielded the combined volume of

surface- and pore-water, here referred to as external water. The specific surface area (BET) was used to estimate the contribution of surface adsorbed water to the external water in combination with changes in particle thickness. All calculations assumed a log normal size distribution commonly described for clay minerals (Drits et al., 1998; Eberl et al., 1998). As fitting was done manually by adjusting a range of variables, results are considered to represent best approximations to the measured patterns rather than perfectly fitted profiles.

4.3. Hydration results of compacted smectite clay under confined volume

4.3.1. Total water uptake as a function of interlayer cation, solution chemistry and clay packing density

As shown in Fig. 4.3.1, the total water uptake and saturation time vary as a function of the type of interlayer cation. Materials that contain predominantly Na as the interlayer cation (montmorillonite of IBECO- and MX80-bentonite and the purified Wyoming-montmorillonite, SWy-2) show continuous and relatively slow water intake. Uptake into the purified SWy-2 montmorillonite powder reaches stable state conditions after 2314h with a total uptake of 0.44ml/g at a relatively constant rate of $1.9\text{E-}04\text{ml/g/h}$ (table 4.3.1). The IBECO-bentonite powder hydrates over a 1368h duration and 0.37ml/g enter the clay (hydration rate of $2.7\text{E-}04\text{ml/g/h}$). Although some Ca^{2+} are contained in the interlayer space of this sample (0.11 Ca^{2+} and 0.18 Na^+ PFU, chapter 3), water uptake into MX80-bentonite is similar to other Na-montmorillonite, which is continuous and slow. Here, the steady state of water saturation develops over 5040h with a total uptake of 0.40ml/g at a rate of $8\text{E-}05\text{ml/g/h}$. This is the lowest water uptake rate observed in all hydration experiments (table 4.3.1, data not in plot).

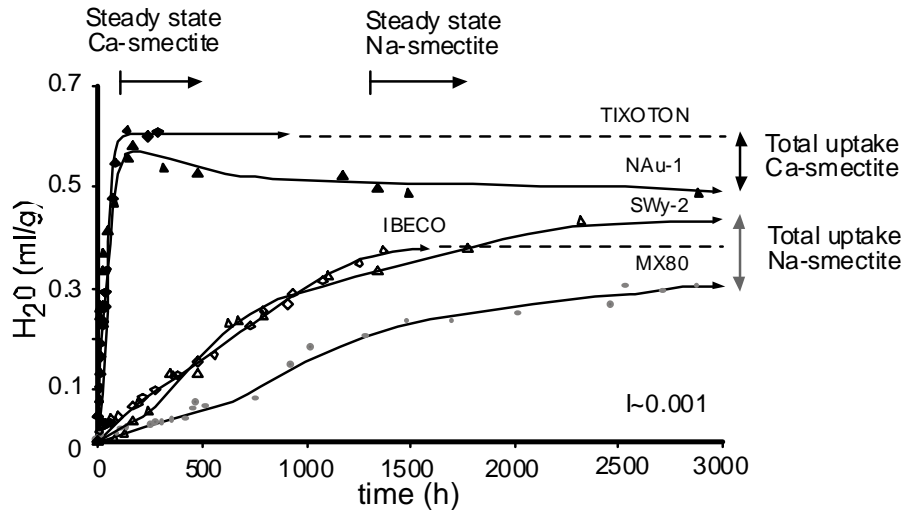


Fig. 4.3.1. Solution uptake into pressed smectite powders in ml/g. Ca-smectite (TIXOTON, NAu-1) reaches steady state earlier than Na-smectite (IBECO, MX80 and SWy-2) and generally incorporates higher amounts of solution. I= ionic strength.

Smectite with predominantly Ca²⁺ as the interlayer cation shows a different behaviour with more rapid and nonlinear water uptake. The Ca-activated TIXOTON-bentonite incorporates a total of 0.61ml/g at an average rate of 4.3E-03ml/g/h over the first ~ 142h of inflow. This is 10 times more rapid than observed for the IBECO and around 15 times more rapid compared to the SWy-2 sample. Notably less water enters the Ca-nontronite powder compared to the Ca-montmorillonite (TIXOTON) while, compared to Na-smectite, there is still 14-26% more water taken in. A total of 0.50ml/g is contained at the stable state that is reached after only 290h (rate 1.2E-03ml/g/h). The observed difference in water uptake for Na- and Ca-smectites can be attributed to the significant differences in hydration energy (enthalpy of hydration) of the Na and Ca cations positioned in the interlayer sites ($\Delta H_{\text{hyd}}\text{Na} = -405\text{kJ/mol}$ as opposed to $\Delta H_{\text{hyd}}\text{Ca} = -1592\text{kJ/mol}$, values from Huheey (1993)). The higher hydration energy of Ca explains both the more rapid water inflow and the larger amount of total water uptake.

Experimental solution	IBECO (Na)		TIXOTON (Ca)			MX80	SWy-2		Nau-1		
	Ground water	Sea water	Ground water	Sea water	Purified water		Purified water	NaCl			
Total solution uptake [ml/g]	0.37	0.45	0.43*	0.61	0.69	0.66*	0.40	0.44	0.45	0.43*	0.50
Saturation time [h]	1368	384	142	167.6	5040	2314	1994	290			
Uptake rate [ml/g/h]	2.7E-04	1.1E-03	4.3E-03	3.9E-03	8E-05	1.9E-04	2.1E-04	1.2E-03			

Table 4.3.1. Total water uptake for confined volume experiments infiltrated by solutions. *Uptake after correcting the weight of saline solutions to account for dissolved salt.

The effect of ionic strength (I) on water uptake is shown in Fig. 4.3.2 for samples of similar packing density. Each sample presented shows the water uptake behaviour for relatively lower (empty circles) and higher ionic solution strengths (filled circles). The Na^+ -exchanged and purified SWy-2 montmorillonite was infiltrated with purified water ($I = <0.001\text{mol/L}$) and concentrated 1M NaCl solution (Fig. 4.3.2.a). The total uptake of the 1M NaCl solution seems relative to the purified water enhanced by 0.45ml/g. But correcting the weight of the solution (dotted line), it is shown that the additional weight is due to the higher ionic strength (1M NaCl accounts for 0.058g/ml). A temporal plateau is visible between 340 and $\sim 820\text{h}$ after which water intake continues and reaches a stable state after $\sim 1994\text{h}$ with a total of 0.43ml/g leading to an uptake rate of $2.1\text{E}-04$. Here, the higher ionic strength leads to an increased rate of water intake but not to an increased amount.

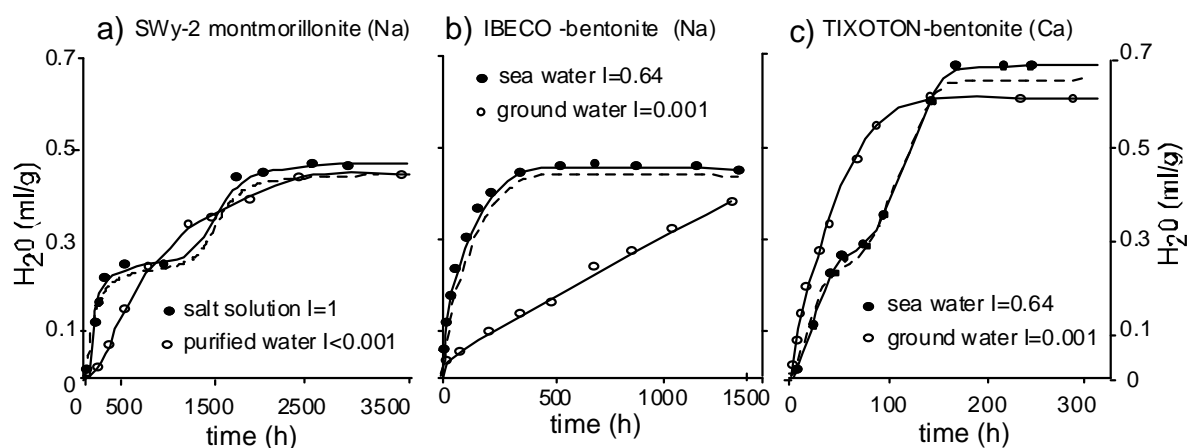


Fig. 4.3.2. Influence of ionic strength on solution uptake into pressed smectite powders. Correction of weight due to higher ionic strength is indicated as dotted line. a) SWy-2 purified montmorillonite infiltrated by 1M NaCl solution and purified water (packing density 1.36 and 1.37 g/cm^3). b) IBECO Na-montmorillonite infiltrated by sea water and ground water (packing density 1.14 and 1.15 g/cm^3). c) TIXOTON Ca-montmorillonite infiltrated by sea water and ground water (packing density 0.94 g/cm^3). I =ionic strength.

In contrast, for the bentonite sample infiltrated by both dilute ground water ($I = 0.0013\text{mol/L}$) and sea water ($I = 0.639\text{mol/L}$), more water enters the sample subjected to the more saline solution. Here, the difference in weight between ground and sea water is slightly less significant with 0.037g. In the case of the Na-montmorillonite containing IBECO-bentonite (Fig. 4.3.2b), there is accordingly $\sim 13\%$ more water intake (total = 0.43ml/g) over a more rapid time period (384h) with sea water compared to that of dilute ground water (1368h). This represents a four fold increase in the rate of inflow to $1.1\text{E}-03\text{ml/g/h}$ compared to $2.7\text{E}-04\text{ml/g/h}$. The Ca-bentonite (TIXOTON, Fig. 4.3.2c) hydrated in sea water incorporated a

total of 0.66ml/g, which represents ~7.5% more solution compared to the ground water sample (0.61ml/g) and, in contrast to the Na-bentonite, this occurred over a longer period of time (~ 168h compared to 142h). The resulting rate of 3.9E-03ml/g/h is similar to the rate obtained for the ground water-infiltrated sample (table 4.3.1).

The difference between Na- and Ca-smectite is also evident when plotting the total water uptake for the range of packing densities tested (Fig. 4.3.3, table 4.1.1.). Linear relationships are observed for both types of material over packing density range of 1.05 and 1.6g/cm³. Slopes of the linear trends are similar for both Na- and the Ca-smectite and are independent of the ionic strength of the solution used. Extrapolating the plots to 0ml water uptake leads to a packing density of 2.1g/cm³ for both types of interlayer cations, which is in good agreement with the range of published smectite mineral densities (between 1.8 and 2.3 g/cm³), as published by Dud'a et al. (1992).

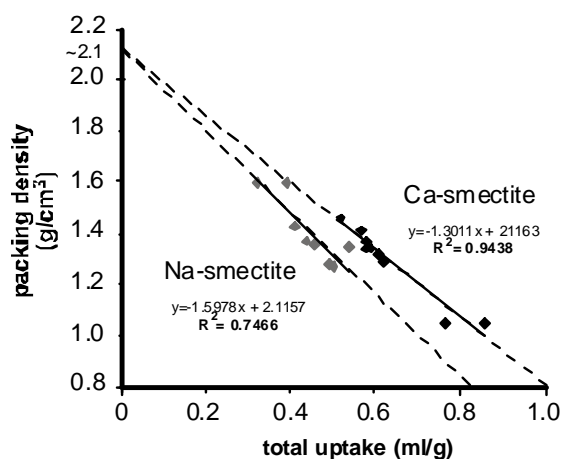


Fig. 4.3.3. Correlation between packing density and total water uptake for various samples. Materials containing predominantly Ca in smectite interlayers take more water in than the Na varieties. Interpolating the plots to zero water uptake (dotted lines) yields for both varieties the same values for packing density (2.1 g/cm³) that corresponds to mineral density.

As expected, less water is taken in when the material is packed more densely and therefore has a lower porosity. Also Ca-smectite generally incorporates more water than the Na-variety for equivalent packing densities, in accordance with the results presented in Figure 4.3.2. The higher packing density decreases the available pore space for accommodating pore water and the expansion of swelling smectite particles. The fact that the fitted slopes for packing density versus total water intake for mono- and divalent cations are similar indicates that the restriction of pore space in all packed swelling clay powders is controlled by the same physical parameter, namely the volume of the reaction-cell. Additionally, it is noted that the difference in water uptake for the different cations decreases with increasing packing density.

This indicates that initial microtextural differences occur that become negligible when particles are forced more closely together (Pusch, 2006a).

4.3.2. Influence of solution chemistry on the hydration mechanisms of Wyoming montmorillonite (SWy-2)

4.3.2.1. Dynamics of water layer development in SWy-2

The hydration of Na-montmorillonite (SWy-2) was monitored during the infiltration of purified water and 1M NaCl solution in order to constrain the effect of higher ionic strength on hydration behaviour. In order to exclude cation exchange effects, the sample powder was first Na-exchanged using a 1 M NaCl solution, washed, re-dried and powdered before loading into the reaction-cells. Similar packing densities were used in order to exclude porosity differences. The consistency of packing was achieved with 1.37g/cm^3 for the water-hydrated sample and 1.36g/cm^3 for the salt solution infiltrated powder.

Although the material was dehydrated in the oven for 2 weeks (at 110°C) around 5% of the SWy-2 powder remained hydrated with a 1 water layer (WL) structure (Fig. 4.3.4a+b). During infiltration with purified water, the collapsed layers (initially 95%) hydrated to form 1- and 2-WL structures. After only 480h all 0-WLs are replaced by hydrated structures (Fig. 4.3.4a). At this time the 1-WL structure is most abundant at 47% and from this point its proportion decreases successively to reach a stable state at 12%. The replacing 2-WL structure appears to be slowly replaced by 3-WL but continues to remain the most dominant structure with a steady state abundance of 63%. The thickest hydrated structure is the 3-WL structure that is steadily increasing in abundance during the experiment and stabilizes at 25% under saturated conditions. The normalized uptake curve, shown as a dashed line, matches most closely the formation of the 1- and later 2-WL structures.

The sample infiltrated with 1M NaCl solution has a similar initial hydration state to the pure water sample with 96% of completely collapsed layers and 4% abundance of the 1-WL structure (Fig. 4.3.4b). After 814h, the dehydrated structure (0-WL) is completely replaced by the growth of 1- and 2-WL structures. As in the pure water experiment, the 1-WL structure forms a maximum at 44% followed by a rapid decrease down to 21%. This decrease in the 1M NaCl solution occurs more rapidly than in the pure water system. The 2-WL increases during hydration and forms the dominant structure (64% abundance) whereas the 3-WL

structure forms only 15%, and does not exceed the number of 1-WL. Generally, the sample in salt solution shows a more rapid development of 2-WL structures but forms slightly less hydrated structures than the pure water one. This difference is best seen in the abundance of 1- and 3-WLs in the saturated steady state condition. Regarding the pure water system, the 3-WL is more abundant than the 1-WL structure, whereas with 1M NaCl solution it is just the opposite: here, the 1-WL is dominant over the 3-WL. The temporal plateau visible for the normalized water uptake curve (between ~500 and 1500h) might indicate either a hydration step (this would correspond to a sudden formation of the 3-WL structures) or a temporally blocked inflow induced by salt precipitations from the solution.

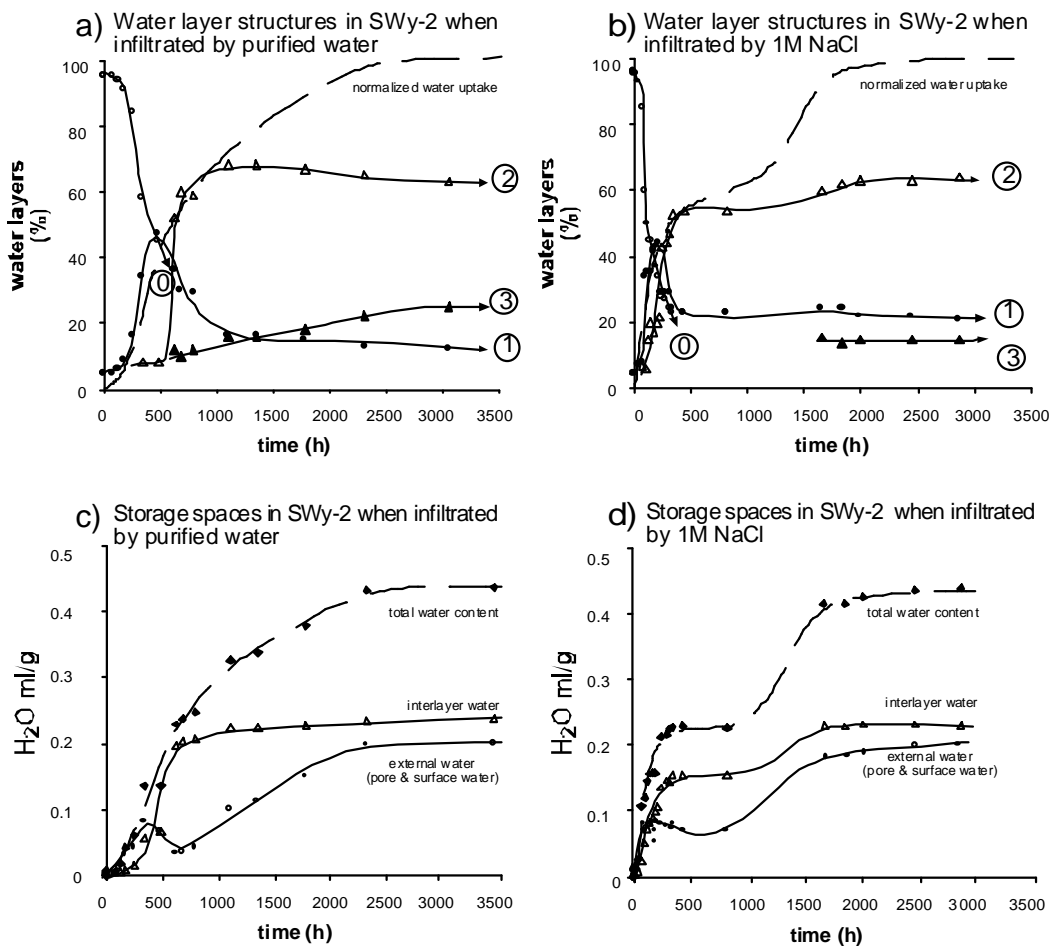


Fig. 4.3.4. Development of water layers in Na-exchanged purified montmorillonite (SWy-2). a) During infiltration of purified water and b) during infiltration of 1M NaCl. c) Storage sites for solution when infiltrated by purified water and d) by 1M NaCl. Values for weight of NaCl corrected.

The corresponding storage sites determined by subtracting the interlayer from the total water are shown for both samples (Fig. 4.3.4c+d). In the case of the pure water infiltrated

sample, the curve for interlayer water uptake indicates that a relative stable state is achieved after 625h with an intake of 0.20ml/g (Fig. 4.3.4c). After 1104h, the amount increased only slightly to 0.24ml/g making up around 54% of the total water uptake (table 4.3.2). The curve for external water (combined surface- and pore water) indicates rapid uptake followed by a short temporary decrease between 625 and 790h. This decrease reflects, most likely, the transfer of pore water to hydrate interlayer space without a higher rate of new water inflow. The expansion of non-interlayer sites continues after the stabilization of interlayers and reaches its stable state at 2314h after incorporating 0.20ml/g of solution.

	Total water [ml/g]	Interlayer water [ml/g]	Saturation time (h)	Rate (ml/g/h)	External water [ml/g]	Saturation time (h)	Rate (ml/g/h)
SWy-2- H ₂ O	0.44	0.24	1104	2.2E-04	0.20	2314	8.6E-05
SWy-2- NaCl	0.43*	0.23	1653	1.4E-04	0.20	2450	8.2E-05

Table 4.3.2. Water uptake into the different storage sites of SWy-2 montmorillonite. *Weight after NaCl correction.

The first 500h of the pure water experiment reveal important information on the hydration mechanism. As the 1-WL hydrates are formed, the rate of interlayer swelling is not quick enough to use all available water and, therefore, excess surface- and pore water are present. At this stage, the largest amount of interlayer water is accommodated within 2-WL structures. However, during the development of the 3-WL structure, a significant amount of water is used up from pores and this leads to the decrease observed in the external water uptake curve. Another additional mechanism to explain this pattern of water uptake is that during hydration the particle size decreases (Fig. 4.3.5).

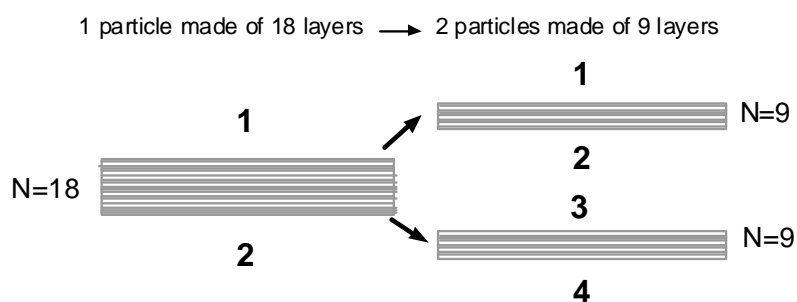


Fig. 4.3.5. Schematic representation of the formation of new external surfaces associated with decreasing particle thicknesses. N=number of layers per particle (stack).

Such a decrease in particle thickness, commonly observed during hydration, is associated with the transformation of interlayer into external particle surfaces. This is achieved by simple splitting and detachment of layers during water uptake, probably related to internal stresses generated by particle expansion. This latter mechanism would be expected to lead to a relative increase in the gradient of the non-interlayer curve relative to the interlayer water uptake as the particles swell, split and increase the surface area of the wet clay powder.

In the case of the sample infiltrated with 1M NaCl, a similar pattern of water transfer is observed (Fig. 4.3.4d) as a temporary stable state is reached after 340h (0.16ml/g) for the interlayer water and a temporal increase for external water after ~280h (0.08ml/g) for the non-interlayer water. As for the pure water infiltrated sample, the curve for non-interlayer water increases rapidly, indicating that solution is first accommodated on external surfaces and within pores before being incorporated into the interlayer space. During the last period of the experiment (after 1653h), interlayer expansion ceases with 0.23ml/g, whereas values for external water are slightly lower with 0.20ml/g (table 4.3.2).

The fact that the values for both the water and 1M NaCl infiltrated sample are similar indicates that the higher ionic strength does not affect the net hydration state. However, the rates are different, with more continuous hydration in case of the water infiltrated sample. Pores might be kept open and facilitate inflow as a high ionic strength inhibits possible osmotic swelling and the closure of pores by non-coherent particle expansion (Lagaly, 1993; Hofmann et al., 2004; Lagaly, 2006).

4.3.2.2. Organization of interlayer water (ordering) in SWy-2

Fig. 4.3.6 shows the ordering probabilities of the different WL structures which developed in the stable state condition (from 625h onward) for the water- and 1M NaCl-hydrated samples. In the case of the water hydrated sample (Fig. 4.3.6a), high probabilities (>0.5) occur for the same WL lying adjacent to each other. This applies particularly to the 1-WL (p11 between 0.6 and 0.7) and 2-WL (p22 ranging from 0.65 to 0.86) structures. The high probability to find a 2-WL adjacent to another 2-WL structure is expected to increase simply as a function of the abundance of this hydrate (around 60%). Similarly, it is also relatively probable that 3-WLs are found adjacent to the abundant 2-WL (0.4-0.6) and other 3-WL structures (p33 0.34-0.5). However, it is less common to find the 1-WL adjacent to 2-WL. These characteristics are best seen in the salt solution infiltrated experiment (here shown from 1650h onwards) where highest probabilities occur for 2-WL to adjacent to 2-WL (p22 is over

0.8, Fig. 4.3.6b), which corresponds well to the high abundance of this 2-WL structure. The probability that 1-WL follows 1-WL is also relatively high but it is not as common as in the pure water infiltrated sample.

Generally, the ordering of WLs in the hydrated powders is largely a function of the relative abundance of WL structures. For random stacking (R0), the layer probabilities would be a direct function of layer abundance. For example, 2-WL structure with an abundance of 60% has the same probability for p12, p22 and p32 which is 0.6. Any ordering in the arrangement of water layers is revealed by normalizing probabilities to random stacking, as shown in Fig. 4.3.6c+d. In both pure and saline water experiments, the probability of combinations of the same structure is relatively enhanced over the random case (positive values for p11, p22 and p33). Therefore, the combination of different structures is generally not favoured (negative values for p32, p12), except for the p31 pair in montmorillonite hydrated in saline water. Some differences are also seen when comparing the pure water with the NaCl solution infiltrated sample. The former is characterized by high p11 and p33 probabilities, the latter by high p11 and p22 probabilities. This pattern provides evidence for clustering of hydrating layers during local homogeneous uptake of water along layers of equivalent layer charge.

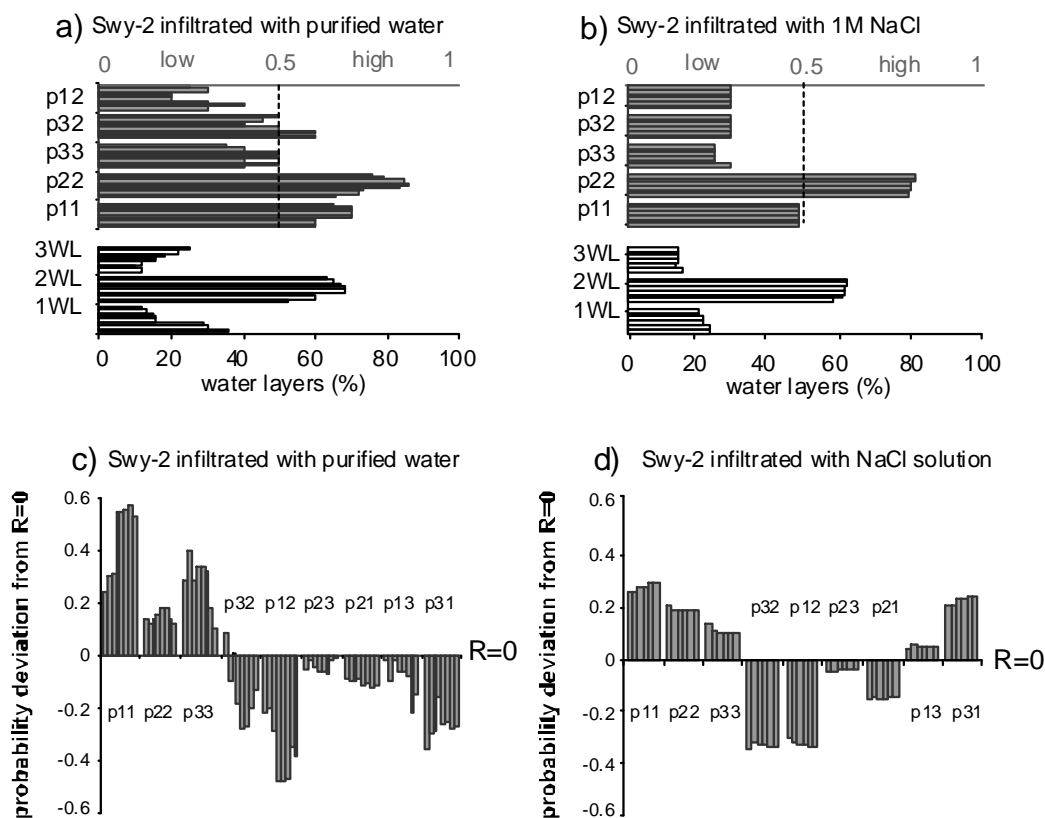


Fig. 4.3.6. Ordering of mixed water layer structures (grey bars) expressed as probabilities (p) and the corresponding water layer abundance (empty bars) for SWy-2 a) infiltrated by water b) infiltrated by NaCl. c) Stacking probability plotted for SWy-2 expressed as the deviation from the random stacking state ($R=0$) when infiltrated by purified water and d) for SWy-2 infiltrated by NaCl solution.

4.3.2.3. Particle thickness and theoretical surface area in SWy-2

In Fig. 4.3.7a+b the changes in N are presented for water and 1M NaCl-solution infiltrated samples. The mean values for N are obtained by matching measured profiles against calculated diffraction patterns. The N values can also be used to estimate relative changes in surface area (m^2/g), referred to as the theoretical specific surface area (SSA; table 4.3.4 and details in appendix).

The initial measurement of the purified water experiment was best fitted with a mean of 18 layers per particle ($N=18$). This value serves as a reference value and corresponds to a “dry” BET surface area of $27.64\text{m}^2/\text{g}$. The mean particle thickness rapidly decreased during the first 480h of water uptake and then stabilized at 12 layers per particle stack until 1780h, which corresponds to a SSA value of $41.5\text{m}^2/\text{g}$. A further decrease to 9 layers per stack and a SSA of $55.3\text{m}^2/\text{g}$ occurs by the end of the experiment (3500h) when the steady state is reached. Here, the hydrated smectite particles have half the thickness of the dry particles and twice their surface area.

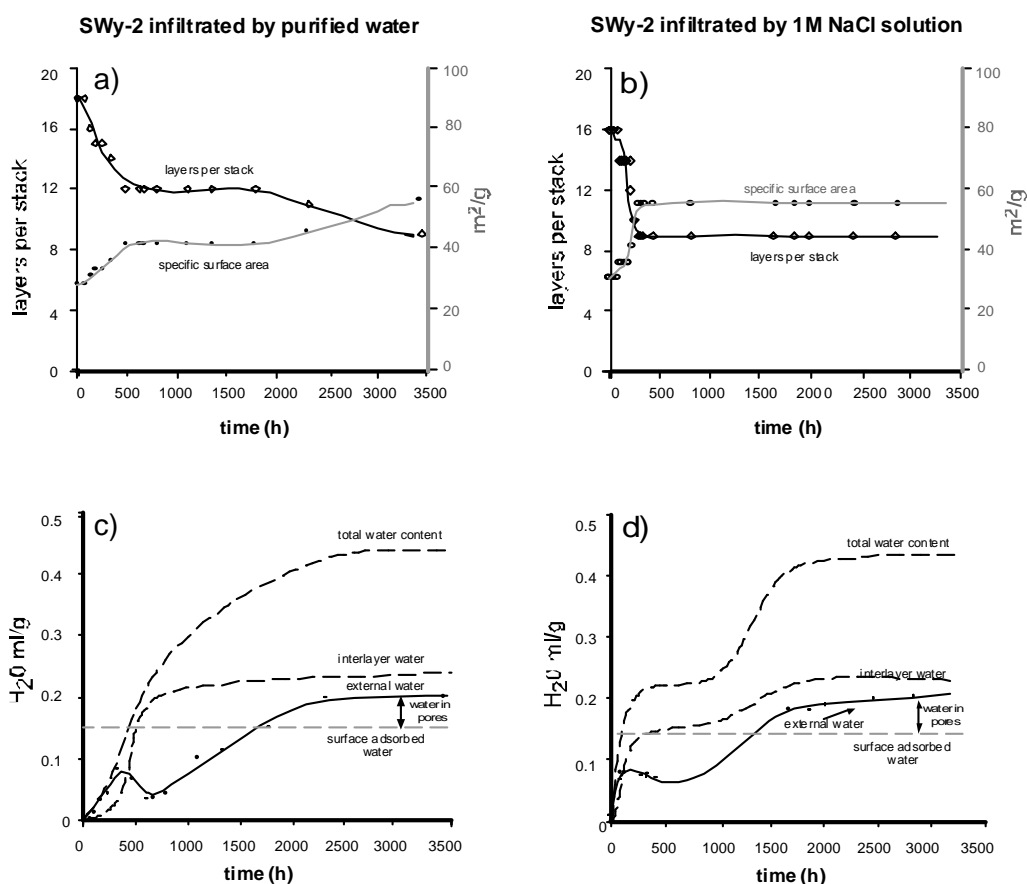


Fig. 4.3.7. Plot showing the change in the number of layers per stack and the corresponding increase of surface area with time a) for SWy-2 infiltrated by purified water and b) by 1M NaCl. c) Shows the distribution of stored water and the estimated amount of surface adsorbed water for the saturated stable state (indicated as a horizontal dotted line) assuming a concentration of 4mmol/g. The distance between the surface adsorbed water line and the external water curves (marked by a vertical arrow) represents the amount of bulk pore water at the end of the hydration experiment.

The sample infiltrated by salt solution has a slightly lower initial number of layers per stack and shows rapid decrease in N during hydration (Fig. 4.3.7.b). Within the first 340h, N decreases from 16 to 9 and corresponds to a surface area increase from 31.1 to 55.3m²/g. In this experiment, no intermediate plateau in the N curve was observed as it was seen for pure water. The nonlinear decrease shows a simple curve and attains a stable, saturated state at a rate ten times faster than for pure water. Despite the more rapid change in N , there is no difference between the average particle thickness of the smectite saturated in salt solution or pure water. Therefore, the theoretical final surface area is for both experiments the same (~55m²/g). These values are, due to the confined volume conditions, significantly lower than those obtained for free swelling Na-montmorillonite, where up to 850m²/g could be theoretically reached (Schramm & Kwak, 1982; Michot & Villieras, 2006).

An estimation of the contribution of surface adsorbed water to the measured external (non-interlayer) water was calculated by assuming that 4mmol/g of water is required to cover the initial surface area of 27.64m²/g with one sheet of H₂O molecules (Bérend et al., 1995). Fig. 4.3.7c+d shows the amount of water stored in the smectite clay and the dotted lines indicate the amount of surface adsorbed water as calculated for the stable state. In both cases (Fig. 4.3.7c+d), the surface adsorbed water would account for almost the entire “external” water (which is the combined surface and pore water) indicating that only a small portion of water filled porosity remains (table 4.3.4). However, it is important to note that all the above described quantifications of surface areas and the amount of surface adsorbed water are just approximations and they serve only as estimations to compare the behaviour of equally treated samples and should not be treated as absolute values equivalent to analytically measured parameters.

	Layers per stack initial	Layers per stack final	External surface area Initial [m ² /g]	External surface area final [m ² /g]	Stabilization time [h]	Surface adsorbed water * [ml/g]	Excess water [ml/g] (pore water)
SWy-2-H ₂ O	18	9	27.64	55.3	3440 (480)	0.14	0.06 (30%)
SWy-2-NaCl	16	9	31.13	55.3	340	0.14	0.06 (30%)

Table 4.3.3. Average number of layers per stack and the corresponding theoretical surface area. *Calculated assuming 4mmol/g. The dry BET surface area is 27.64m²/g.

4.3.3. Influence of initial packing density and water content on the hydration behaviour of MX80 bentonite

4.3.3.1. Dynamics of water layer development in MX80

The influence of initial packing density and hydration state on the hydration dynamics of smectite-rich clay was investigated using MX80 bentonite. Fig. 4.3.8 shows the change in water-layer abundance during hydration for 3 different MX80 samples of varying packing density and initial water contents that were infiltrated with solution of low ionic strength (I<0.001M). Although the sample in Fig. 4.3.8a was dehydrated for 2 weeks in the oven at 110°C (table 4.1.1.), some 1-WL (5%) and 2-WLs (4%) were present at initial measurements.

During the first 300h of the experiment, all non-hydrated smectite interlayers were completely replaced by the developing 1- and 2-WL structures. Both reached a maximum of 35%, after 490h for 1-WL and after 681h for 2-WL. The 3-WL structure developed relatively early by replacing 1-WLs and, at the final stages of the experiment, it reached an abundance of 30%. The 4-WL structure was also detected and formed by replacing the 2-WLs. The shape of the XRD profiles also indicated the presence of even thicker hydrated structures, which were best fitted by assuming a d-value of $\sim 22.8\text{\AA}$. For reasons of simplicity, this structure is referred to as a 5-WL structure, although the precise nature of this hydrated layer is not clear. This d-value might also result from the ordering effects of thinner water layers (e.g. a superstructure formed from adjacent ca 11.4\AA layers). At the end of the saturation experiment, the powder contained 9% of apparent 5-WLs, 30% of 4-WLs and 61% of 3-WLs.

The abundance of water layers in the more densely packed powder (1.43g/cm^3) changed in a similar way with hydration of dehydrated layers (94% of 0-WL) to form a mixture of 1- to 3-WL and, eventually, 2- to 4-WL structures (Fig. 4.3.8b). However, in comparison to the less compacted MX80 bentonite, the thickness of hydrated layers (mixture of 3-, 2- and 4-WLs compared to 3-, 4- and 5- for 1.35g/m^2) was notably smaller and the rate of hydration slower, with a stable state of total water uptake attained after more than 5000h. The 2-WL was for most of the hydration process the dominant structure increasing in abundance up to 70% followed by a subsequent decrease to 14%. The 3-WL structure developed slowly and continuously to form the dominant structure at (quasi)-stable state with a value of 78% together with 8% of the 4-WL structure. A “5-WL” structure was not observed in this more strongly compacted sample. Both a reduction in water layer thicknesses and a slower rate of hydration was expected for the more strongly packed samples because of reduced pore space and, thus, restricted volume for inflow and particle expansion.

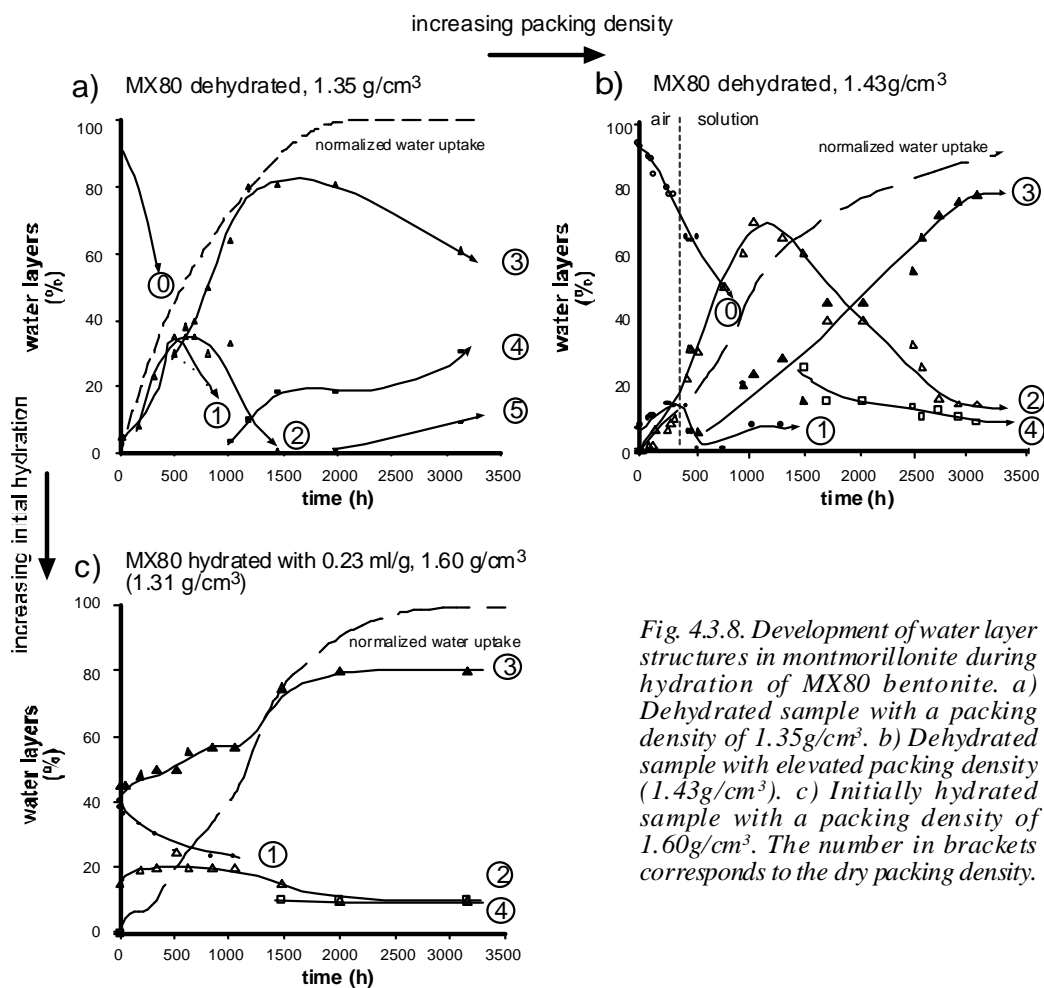


Fig. 4.3.8. Development of water layer structures in montmorillonite during hydration of MX80 bentonite. a) Dehydrated sample with a packing density of 1.35g/cm^3 . b) Dehydrated sample with elevated packing density (1.43g/cm^3). c) Initially hydrated sample with a packing density of 1.60g/cm^3 . The number in brackets corresponds to the dry packing density.

The pre-hydrated MX80 bentonite (containing $\sim 0.23\text{ml/g}$ of water) showed a significantly different pattern of interlayer hydration to that of the two dehydrated bentonite samples (Fig. 4.3.8c). The packing density of this sample was higher when including the pre-absorbed water (1.60g/cm^3) but corresponded to dry packing density of 1.31g/cm^3 . Therefore, the initial hydration state was notably different from the other two samples, with a mixture of 40% 1-WLs, 15% 2-WLs and 45% 3-WL structures. The subsequent pattern of water-layer development was less complicated with a gradual increase of 3-WL which was always the most abundant structure (80% at stable state after $\sim 2000\text{h}$ of hydration time). This gradual increase corresponded with a gentle decrease of the 1- and 2-WL, whereas, after $\sim 1500\text{h}$, a 4-WL structure occurred (ca. 10% abundance) and remained unchanged until the end of the experiment.

The relative abundance of WL structures formed in the pre-hydrated bentonite is most similar to the more highly compacted dehydrated sample of 1.43g/cm^3 . The water incorporated into the smectite (prior to packing the powder into the reaction-cell) was added

into interlayer sites inducing particle expansion. Therefore, the sample behaved according to its “wet” packing density (1.60g/cm^3) like a highly compacted material with reduced permeability.

Comparing the mean thicknesses of the different initial and final WL structures for the three samples showed, as expected, similar values for the hydrated and densely packed dehydrated MX80 (1.43g/cm^3 , table 4.3.4). In contrast, the two dehydrated samples had similar values for the difference in mean lattice layer thickness which reflects the dimension of the hydrated interlayer (Δd 9.45\AA and 8.25\AA as opposed to 2.7\AA for the hydrated sample).

		MX80 dehydrated		MX80 dehydrated		MX80 hydrated	
<i>Packing density</i>		1.35 g/cm^3		1.43 g/cm^3		1.6 g/cm^3	
<i>Water layers</i>	<i>d-value</i>	Initial	Final	Initial	Final	Initial	Final
0	9.6	0.91		0.94			
1	12.2	0.05		0.06		0.4	
2	15.2	0.04			0.14	0.15	0.10
3	18.5		0.61		0.78	0.45	0.80
4	20.2		0.3		0.08		0.10
5	22.8		0.09				
<i>Mean thickness of d (Å)</i>		9.95	19.4	9.95	18.2	15.6	18.3
Δd (Å)		9.45		8.25		2.7	

Table 4.3.4. Water layer abundance (%) and the difference in mean lattice layer thickness in Å between the initial and final state of hydration.

4.3.3.2. Organization of interlayer water (ordering) in MX80

An example of the ordering probabilities for the different WL structures formed during hydration is given for the dehydrated MX80 bentonite at two different stages of hydration (Fig. 4.3.9a-d). At the beginning of hydration (the first 480h), the probability that a dehydrated structure lies adjacent to another dehydrated structure is always very high with a p_{00} between 0.57 and 0.94. Other combinations that have high probabilities are the 1-WL and 2-WL structures adjacent to dehydrated layers with p_{10} and p_{02} values both between 0.7 and 0.9. During the final stages of water intake (between 1700 and 5040h), the 3-WL structure dominates with abundances between 45 and 81% (Fig. 4.3.9b) resulting therefore in high p_{33} values, ranging between 0.56 and 0.91. Although the amount of the 2-WL structures decreases during hydration, the probability that 2-WL structures are neighbours is consistently high (p_{22} 0.6-0.7). The 4-WL structure is more frequently located adjacent to other thick hydrated structures than to thinner ones, with p_{44} values between 0.4 and 0.5 and p_{43} values of 0.5.

Ordering of the WL structures is displayed as a deviation from the random (R0) case for the initial and final stages of hydration in the MX80 bentonite (Fig 4.3.9c+d). Little variation is seen from the random stacking state during the initial stages, with layer probabilities not exceeding 0.31. Systematic deviations from random are only seen in some cases with positive values for p11 and p22 and negative values for p21 and p12.

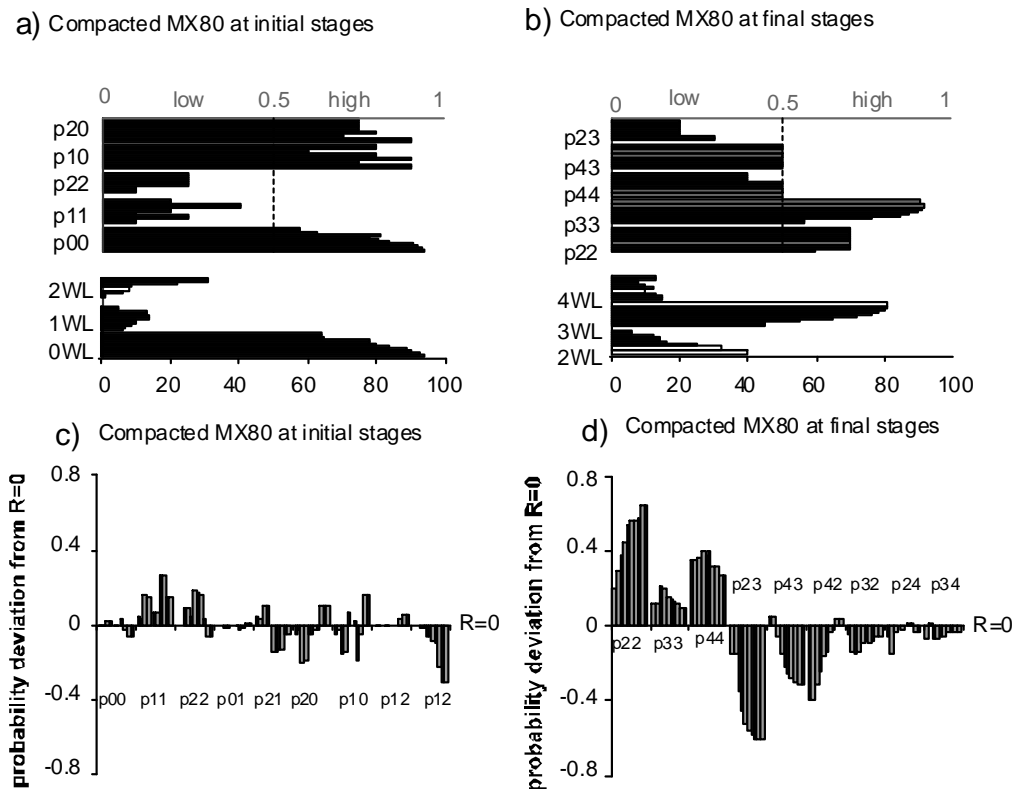


Fig. 4.3.9. Ordering of mixed water layer structures (grey bars) expressed as probabilities (p) and the corresponding water layer abundance (black empty bars). a) Initial stages of the experiment and b) the final stages. Expressed as the deviation from the random stacking state (R=0). c) Initial stages and d) final stages.

In contrast, clearly reproducible deviations from the random case occur at final stages of the experiment (Fig 4.3.9.). As observed in the case of SWy-2 (cp. Fig. 4.3.6), enhanced probabilities occur for adjacent WL structures of the same thickness, with positive values for p22 (0.2-0.64), p33 (0.09-0.22) and p44 (0.27- 0.4). In contrast, well defined “negative” probabilities characterize all combinations of different WL structures. This is especially the case for the probability that 2-WL is followed by 3-WL (p23 between -0.15 and -0.61), that 4-WL is followed by 3-WL (p43 up to -0.31) and that 4-WL is followed by 2-WL (p42 up to -0.41). For other combinations, the deviations are less reproducible and close to the zero line indicating random ordering.

Based on the described variation, it is clear that as hydration proceeds, the water layer structures become increasingly ordered as the structured water arranges itself in a state that is closer to equilibrium. The degree of ordering attained is likely to be strongly influenced by electrostatic forces that attract water molecules and are, moreover, induced by internal stresses due to particle expansion in a confined volume reaction system.

4.3.3.3. Water uptake into different storage sites in MX80

Fig. 4.3.10 shows the curves for total water uptake and the calculated amount of water stored in interlayer and external storage sites. The most water was incorporated by the dehydrated, less compacted MX80 bentonite (Fig. 4.3.10a). At the stable saturated state, (after 3130h) the total water accounts for 0.54ml/g (table 4.3.5) with a relatively fast inflow rate of $1.4\text{E-}04\text{ml/g/h}$. Although the sample was dehydrated prior to the experiment, some water (0.09ml/g) was still present in interlayer spaces. During the early stage of hydration, the external water makes up the major proportion with 0.16ml/g after ~310h. This external water located in pores serves as a reservoir before absorption into interlayer spaces (a similar pattern of water uptake was observed for SWy-2, Fig 4.3.4). After 490h the interlayer water uptake dominates and reaches a stable state after 1449h with a maximum of 0.32ml/g. Interlayer water makes up ~59% on the total water budget with an average hydration rate of $2.2\text{E-}04\text{ml/g/h}$ whereas the surface- and pore water accounts only for 0.22ml/g (41%) of the total water intake.

In the case of the more strongly compacted MX80 powder (1.43g/cm^3), the total water uptake and the amount of water adsorbed into interlayers were almost identical for the first 2000h of the experiment (Fig. 4.3.10b). The time axis was chosen to be compatible to the other experiments but, in this hydration run, it actually took more than 5000h to achieve stable state conditions. This resulted in a particularly slow rate of water inflow ($7.1\text{E-}05\text{ml/g/h}$) that reached a total water intake of 0.36ml/g. Interlayer water dominated during the first 3720h of hydration with 0.28ml/g water accounting for more than 77% on the total water. Residual external water (surface and pore) makes up ~22% of the water budget (0.08ml/g). This small amount of surface- and pore water can be attributed to the higher packing density characterized by lower sample porosity.

The pre-hydrated sample contained 0.18ml/g interlayer water and 0.05ml/g external water (total: 0.23ml/g) at the beginning of the experiment (Fig. 4.3.10c). The surface and pore water stayed relatively constant at 0.05ml/g and most of the water intake was stored within

interlayer sites. After 1470h, the interlayer water was complete with 0.27ml/g, which made up ~82% of the water inflow.

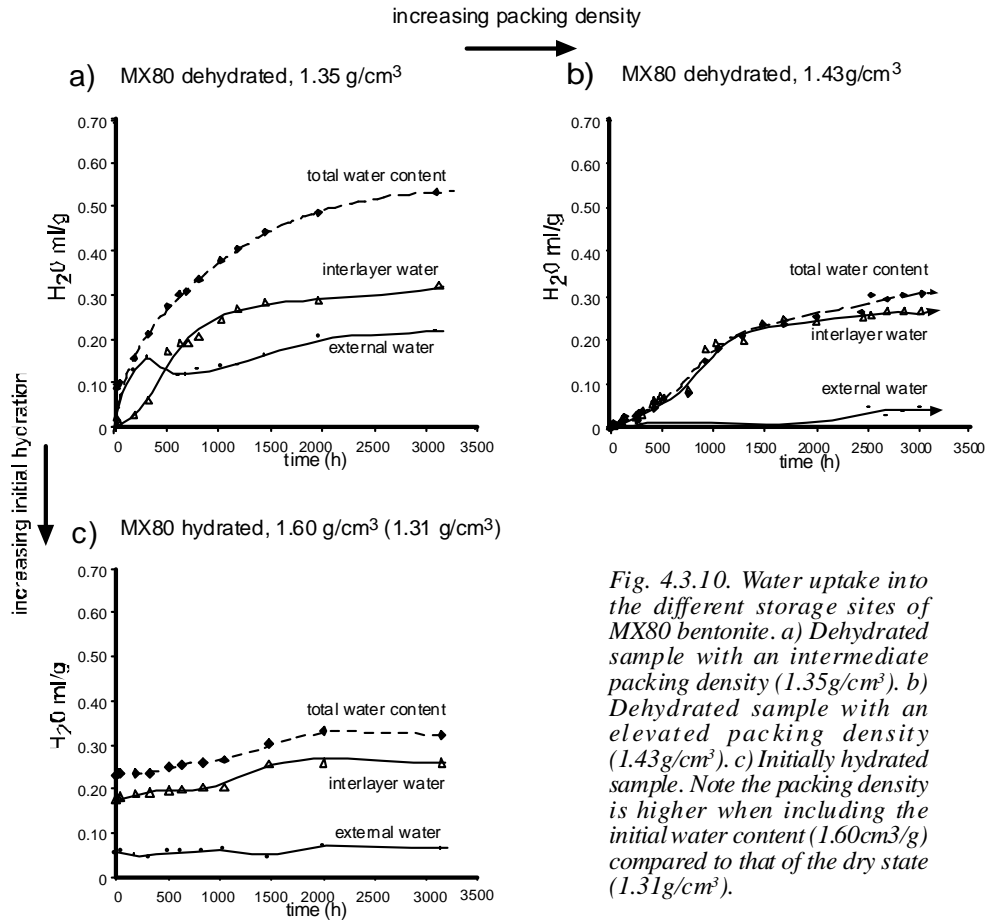


Fig. 4.3.10. Water uptake into the different storage sites of MX80 bentonite. a) Dehydrated sample with an intermediate packing density (1.35g/cm³). b) Dehydrated sample with an elevated packing density (1.43g/cm³). c) Initially hydrated sample. Note the packing density is higher when including the initial water content (1.60cm³/g) compared to that of the dry state (1.31g/cm³).

	MX80-dehydrated 1.35 g/cm ³	MX80-dehydrated 1.43 g/cm ³	MX80-hydrated 1.6-1.31 g/cm ³
Total water			
Initial amount (ml/g)	0.09	0.005	0.23
Saturation time (h)	3130	5040	1998
Final amount (ml/g)	0.54	0.36	0.32
Rate (ml/g/h)	1.4E-04	7.1E-05	5E-05
Interlayer water			
Saturation time (h)	1449	3720	1470
Uptake (ml/g)	0.32	0.28	0.27
Proportion (%)	59.3	77.7	81.8
Rate (ml/g/h)	2.2E-04	7.5E-05	1.8E-04
External (surface and pore) water			
Saturation time (h)	1997	3720	1998
Uptake (ml/g)	0.22	0.08	0.05
Proportion (%)	40.7	22.3	18.2
Rate (ml/g/h)	1.1E-04	1.6E-06	5.8E-05

Table 4.3.5. Experimental results used to calculate the rates of water uptake into the various storage sites of MX80 montmorillonite as a function of different packing densities and initial hydration states.

The storage of water in the pre-hydrated bentonite seemed to show more similar characteristics to the strongly packed dehydrated samples. The “wet” powder packed at higher density (1.60g/cm^3) incorporated less external water than the more weakly compacted dehydrated sample (1.35g/cm^3) and in comparison with the strongly packed dehydrated sample (1.42g/cm^3), the storage sites were occupied in a similar way. This behaviour indicated that a wetted bentonite powder shows equivalent sealing capacities as similarly packed dehydrated samples while pre-hydrated bentonites will have the disadvantage of sudden volume loss and clay cracking when dried (Delage et al., 1998; Cui et al., 2002).

4.3.3.4. Particle thickness and theoretical surface area in MX80

Changes in particle thickness and theoretical surface area during hydration for the two dehydrated MX80 bentonites are displayed in Fig. 4.3.11. The surface area calculated assuming a particle thickness of 19 layers corresponds to a BET surface area of $30\text{m}^2/\text{g}$ (table 4.3.6). In the case of the less compacted sample (1.35g/cm^3 , Fig. 4.3.11a), the particle thickness decreased from 15 to 3 layers and the surface area increased from theoretically $38\text{m}^2/\text{g}$ (already slightly hydrated) to around $190\text{m}^2/\text{g}$ by the end of the experiment (Fig. 4.3.11a). This difference indicates a 5 fold increase in surface area in the near-saturated state.

The more strongly compacted powder also showed a decrease in particle thickness, here from 19 to 7 layers (Fig. 4.3.11b). This corresponded to a theoretical increase in surface area from ca. 30 to $81\text{m}^2/\text{g}$, which was less than a threefold increase. The smaller increase in surface area during hydration and the higher abundance of interlayer water in this sample (Fig. 4.3.11b) suggests particle splitting, and the generation of new external surfaces and pore spaces is not a significant mechanism in the more strongly compacted clay.

	Layers per stack		External surface area* [m^2/g]		Stabilisation time [h]	Total external water [ml/g]	Maximal surface water [ml/g]		Surface availability [%]	
	Initial	final	initial	final			4mmol $\text{H}_2\text{O/g}$	2.5mmol $\text{H}_2\text{O/g}$	4mmol $\text{H}_2\text{O/g}$	2.5mmol $\text{H}_2\text{O/g}$
MX80- 1.35 g/cm^3	15	3	38	190	1977	0.22	0.46	0.29	47.8	75.8
MX80- 1.43 g/cm^3	19	7	30	81	1704	0.06	0.2	0.12	30	50
MX80- hydrated	9	5	63	115	1998	0.05	0.27	0.17	18.5	29.4

Table 4.3.6. Results used to estimate the amount of surface water based on decreasing layers per stack. *Assuming a mean of 19 layers per stack at dry state.

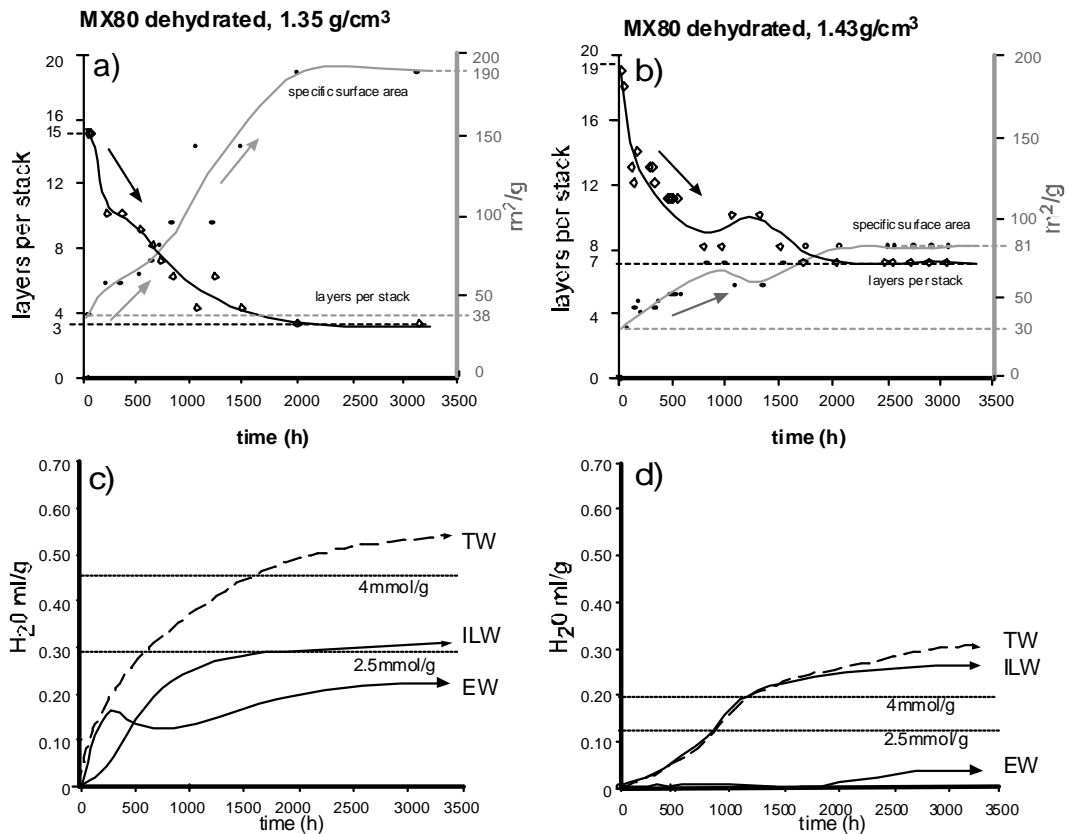


Fig. 4.3.11. Plot showing the change in the number of layers per stack and the corresponding increase of surface area with time for dehydrated and compacted MX80 powder. a) Dehydrated and compacted MX80 powder (1.35 g/cm³). b) Dehydrated and highly compacted MX80 powder (1.43 g/cm³). Estimation of surface adsorbed water according to increased smectite surface area for c) dehydrated and compacted MX80 powder (1.35 g/cm³) and d) dehydrated and highly compacted MX80 powder (1.43 g/cm³). Dotted lines indicate the calculated amount of water corresponding to the stable saturated state assuming 4 or 2.5 mmol/g required to cover the external surface area. TW-total water; ILW-interlayer water; EW-external water (combined surface and pore water).

The relative contribution of the increased surface area to the sorption of surface water was calculated assuming that 4 and 2.5 mmol/g of water were needed to cover the external surfaces at the stable state (Fig. 4.3.11c+d). 4 mmol/g were considered more typical for dispersed Na-montmorillonite (Bérend et al., 1995) whereas 2.5 mmol/g was reported for Ca-montmorillonite (Cases et al., 1997). As noted for the SWy-2 sample, these values should be just taken as a reference to compare equally treated samples, since the published data was not obtained using similar experimental conditions.

For both samples, the theoretical possible amount of water sorbed on external surfaces exceeded the available external water when using both values (4 and 2.5 mmol/g). (The external water was obtained by subtracting interlayer water, obtained from CALCMIX calculations). Because of the confined volume, water is unable to enter the system and to

saturate the surfaces as in an open system. Therefore, in the case of the less compacted sample (Fig. 4.3.11c), a higher proportion of surfaces could be saturated with the available external water compared to the strongly compacted sample. Calculating for 2.5mmol/g, the maximal portion of saturated external surface was 73% for the less compacted sample vs. 42% for the more compacted one. In comparison to the SWy-2, where excess water was available to fill pore spaces, the access for water in MX80 is limited.

4.3.4. Hydration behaviour of bentonite in natural solution

4.3.4.1. Dynamics of water layer development in IBECO and TIXOTON

The hydration experiments infiltrated with ground water and Atlantic sea water were conducted to quantify the uptake and storage in Na-activated IBECO and Ca-activated TIXOTON bentonite when infiltrated by ground- and Atlantic sea water. The development of water layer structures is given in Fig. 4.3.12a-d. In the case of the ground water infiltrated IBECO powder, the initial hydration state comprised 31% 0-WL, 59% 1-WL and 10% 2-WL (Fig. 4.3.12a). During ground water inflow, rapid growth of the 2-WL structure occurred at the expense of both 0- and 1-WL. Between 400-600h of inflow, the 0-WL disappeared, the 1-WL structure stabilized at ~ 30% and the 2-WL state reached its maximum abundance at 60%. After 600h of hydration, the 2-WL transformed into the 3-WL state, a reaction which was completed by ~1400h. Following this change, the hydration condition reached a steady state composed of ~ 70% 3-WL and ~ 30% 1-WL. No 4-WL structure was detected in this experiment.

In sea water, the interlayer hydration of IBECO occurred over a shorter time period than in ground water (Fig. 4.3.12b). The abundance of 0- and 1-WLs rapidly decreased during the initial hours of hydration and disappeared within the first 300h of hydration time. During this period, both 2-WL and 3-WL formed rapidly, and reached a steady state condition between 200-400h consisting of 55% 2-WL, 40% 3-WL and 5% 4-WL components.

In the case of the Ca-activated TIXOTON powder, the initial hydration state was higher, consisting of 15% 1-WL, 70% 2-WL and 5% 3-WL (Fig. 4.3.12c). No 0-WL structure was detected in this sample material. During the first phase of ground water inflow both 1 and 2-WLs rapidly decreased during the first 30h of hydration, with the formation of the 3-WL state, reaching a maximum (~60% abundance) after 40h. A 4-WL state appeared at this stage

of the experiment, corresponding to the disappearance of the 1-WL, the continued decline of 2-WL, and the reduction of the 3-WL structure. A steady state system was achieved after 150h of hydration and comprised 11% 2-WL, 42% 3-WL and 47% 4-WL. When hydrated in sea water, the 1- and 2-WL structures decreased rapidly and the formation of 3 and 4-WLs during the initial 60h of hydration could be observed (Fig. 4.3.12d). After 120h, the 2-WL structure showed about the same abundance as in ground water (~10%) and the 3-WL structure increased to ~ 60%. However, in the steady state condition, the 3-WL phase remained dominant, and was accompanied by 27% of 4-WLs.

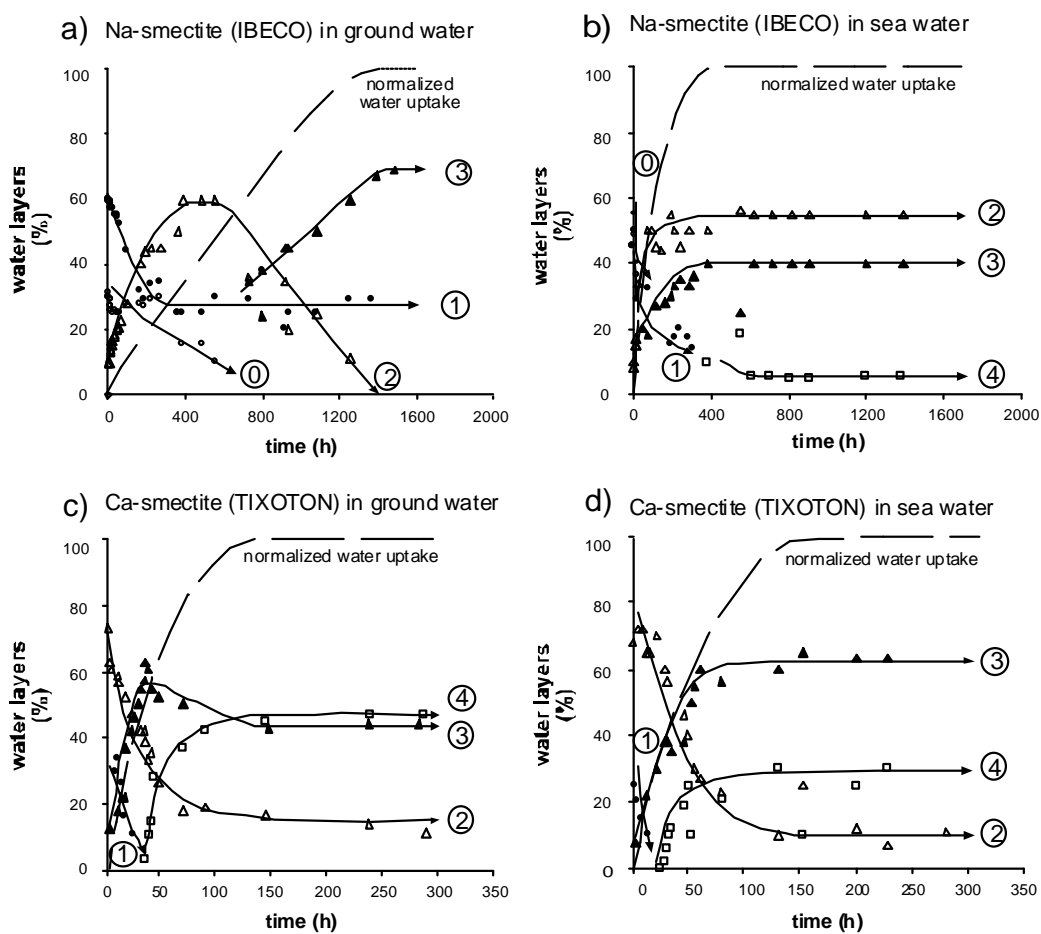


Fig. 4.3.12. Water layer development in smectite contained in bentonite powders. a) IBECO infiltrated by ground water. b) IBECO infiltrated by sea water. c) TIXOTON infiltrated by ground water. d) TIXOTON infiltrated by sea water. Ionic strength for ground and sea water is 0.0013 and 0.64M, respectively. Modified after Warr & Berger (2007).

Values of mean thickness (d-values) for the initial and final water layer distribution are given in table 4.3.7 for both the ground- and sea water infiltrated IBECO and TIXOTON samples. Both IBECO bentonite samples had similar final mean thicknesses (16.64Å in ground- and 16.77Å in sea water) that was lower compared to values for TIXOTON with 18.9

vs. 18.6Å. This is in accordance with results for different interlayer cations (cp. Fig. 4.3.3.) and can be attributed to the fact that IBECO is Na-activated and TIXOTON Ca-activated.

		<i>IBECO</i> <i>Ground water</i>		<i>IBECO</i> <i>Sea water</i>		<i>TIXOTON</i> <i>Ground water</i>		<i>TIXOTON</i> <i>Sea water</i>	
<i>Water layers</i>	d-value	Initial	Final	Initial	Final	Initial	Final	Initial	Final
0	9.6	0.31		0.45					
1	12.2	0.59	0.29	0.45		0.15		0.25	
2	15.2	0.1	0.01	0.1	0.55	0.7	0.11	0.7	0.11
3	18.5		0.7		0.4	0.05	0.42	0.05	0.62
4	20.2				0.05		0.47		0.27
<i>Mean d-value (Å)</i>		11.7	16.64	11.33	16.77	13.4	18.9	14.6	18.6
<i>Difference Δd (Å)</i>		4.94		5.44		5.5		4	

Table 4.3.7. Water layer abundance (%) and the difference in mean lattice layer thickness in Å between the initial and final state of hydration for bentonites infiltrated by natural solution.

4.3.4.2. Water uptake into different storage sites in IBECO and TIXOTON

The quantification for interlayer and non-interlayer water are given in Fig. 4.3.13 with corresponding uptake rates in table 4.3.8. In this case, the calculation was based on CALCMIX fitting of XRD-patterns of samples that already contained some interlayer water and all curves were normalized to a starting water content of zero at the beginning of each experiment. Thus, the presented hydration curves represent the quantification of water inflow and not the total water content of the bentonite, which is higher than the values given.

In the case of Na-bentonite, the total inflow of ground water, the growth of interlayer water and the incorporation of external water showed the same general linear increase. The interlayer water hydrated at an average rate of 1.5E-04ml/g/h over 1368h but a slight flattening of the curve started after around 1250h (Fig. 4.3.13a). The external water hydrated at a similar rate 1.2E-04ml/g/h over 1368h but, in this case, a clear linear trend was maintained. After 1500h, the proportion of interlayer water made up 54% of the total water inflow.

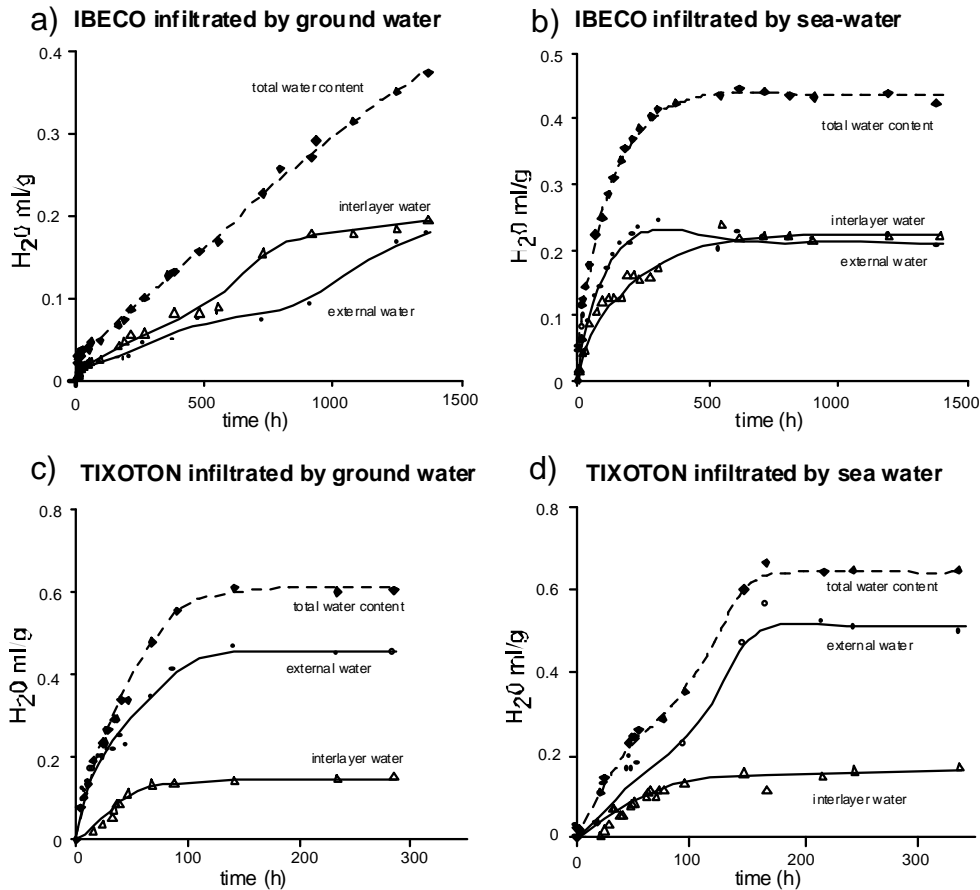


Fig. 4.3.13. Partitioning of water storage sites in bentonites infiltrated by natural solutions. The weight of seawater was corrected for the amount of dissolved ions. Modified after Warr & Berger (2007).

The sea water intake curves reveal a different behaviour from the ground water experiments with non-linear intake rates (Fig. 4.3.13b). Rapid uptake leads to the formation of a relative stable plateau after only 552h for the external water (average rate $3.6E-04$ ml/g/h) and after 720h for interlayer hydration (average rate $3.1E-04$ ml/g/h). 52% of interlayer water and 48% of external water were observed at the end of the experiment (values for higher weight of the sea water were corrected). This uptake was much more rapid than the NaCl infiltrated SWy2 sample (cp. Fig. 4.3.6) and was most likely due to the decreased packing density.

	IBECO in ground water	IBECO in sea water	TIXOTON in ground water	TIXOTON in sea water
Interlayer water				
Saturation time (h)	1368	720	87	146.3
Uptake (ml/g)	0.2	0.22	0.15	0.15
Proportion (%)	54	52	24	23
Rate (ml/g/h)	1.5E-04	3.1E-04	1.7E-03	1.0E-03
External water (surface and pore water)				
Saturation time (h)	1368	552	142	167.6
Uptake (ml/g)	0.17	0.20	0.46	0.49
Proportion (%)	46	48	76	77
Rate (ml/g/h)	1.2E-04	3.6E-04	3.2E-03	2.9E-03

Table 4.3.8. Experimental results used to calculate the rates of water uptake into the various storage sites of Na- and Ca-bentonites. The weight of sea water was corrected for salt content.

The proportion of external water was visibly higher in the Ca-bentonite experiments (Fig. 4.3.13 c-d). In ground water, most of the total content was stored as surface and pore water (76%), which formed at an average rate of 3.2E-03ml/g/h. The interlayer water intake was already completed (hydration rate of 1.7E-03ml/g/h) when the total intake ceased after 142h. When infiltrated with sea water, the amount stored as external water made up around 77% of the total water inflow resulting, therefore, equivalent to the ground water infiltrated sample. The interlayer water curve flattened after 100h (hydration rate of 1.0E-03ml/g/h) and indicated no change after 146h, whereas significant volumes of surface and pore water continued to build up until ceasing at ~ 167h (hydration rate of 2.9E-03ml/g/h).

4.3.4.3. Particle thickness and surface area estimates in IBECO and TIXOTON

The Na-montmorillonite containing IBECO infiltrated with natural ground water showed the same initial and final number of layers per stack as infiltrated by sea water, decreasing from 15 to 5 (Fig. 4.3.14a+b). Accordingly, the values for the initial surface area for both samples were 66.4m²/g and at the final stages 199.2m²/g. The major difference between the two samples was the time needed to achieve stable state. When infiltrated by ground water it took 1250h until a stable state was formed, whereas, in the case of salt water infiltration, the system stabilized already after 214h (that is more than 5 times quicker). The same trend was visible for the Ca-montmorillonite-containing TIXOTON bentonite when infiltrated by ground- and sea water (Fig.4.3.14c+d). In both cases, the particle thickness decreased from 14 to 7 layers per stack and the corresponding surface area increased from 132 to 265m²/g. When

infiltrated by ground water, a stable state was achieved after 142h, whereas, salt water infiltration led to a stable state after less than 5h (3 times less time).

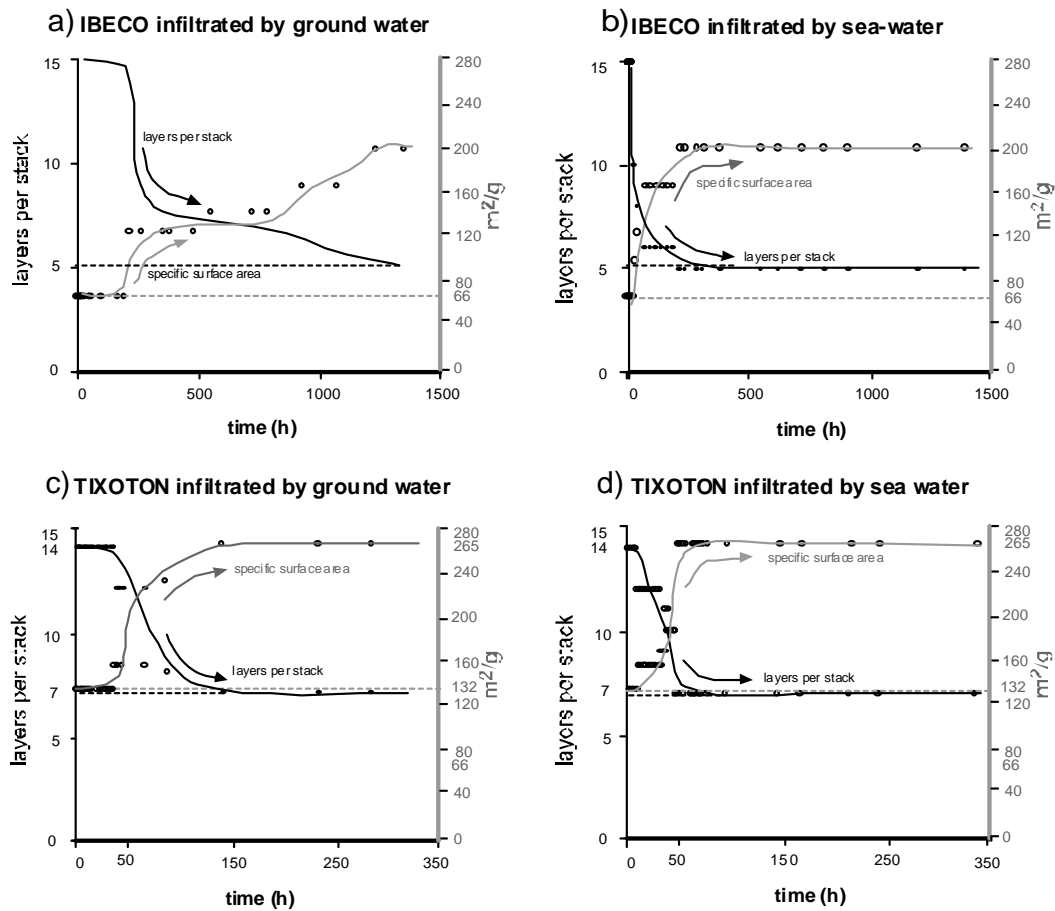


Fig. 4.3.14. Changes in the number of layers per stack and the corresponding surface areas of montmorillonite contained in bentonite (a-d).

4.4. Discussion

The hydration of smectite clay is a process that occurs at a range of different scales including the lattice interlayers, the external surfaces of particles, the voids between particles in “clusters” and the voids between such clusters (Fig. 4.4.1). The sorption or trapping mechanisms of water during the hydration of swelling clays varies based on sample properties and the experimental conditions applied. Here, the various controls on smectite hydration are addressed and discussed in the light of the experimental results and are included in the model of scale-dependent hydration as shown in Fig. 4.4.1.

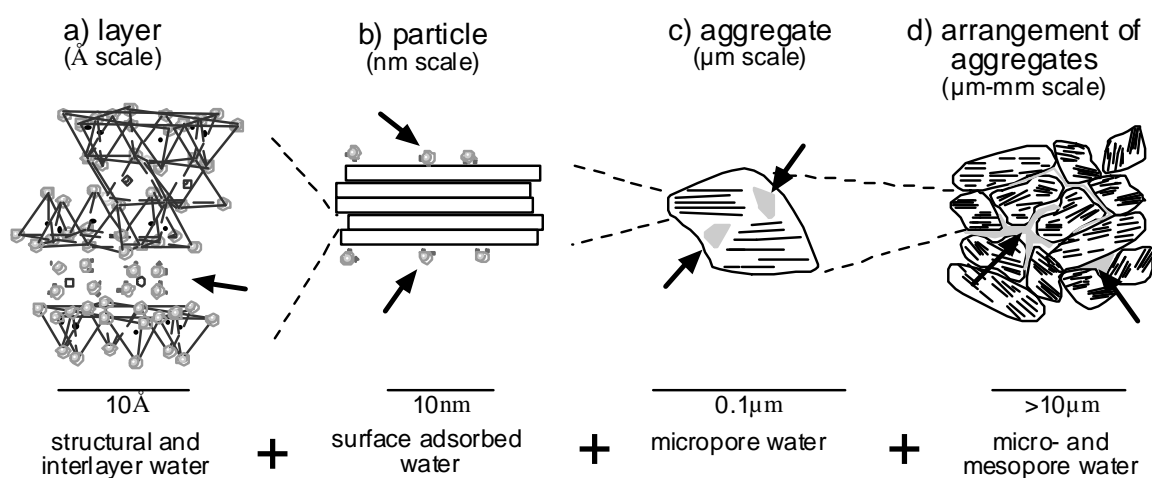


Fig. 4.4.1. Different hydration sites in a smectite powder as a function of scale. a) Interlayer, b) surface of particles composed of several layers, c) aggregates composed of several particles and d) arrangements of aggregates. The aggregate model shown in c is modified after Suzuki et al. (2005). Hydration sites are marked with arrows.

4.4.1. The influence of the type of smectite and solution chemistry

Layer-scale

The type of smectite has the major influence on the swelling behaviour at all scales, whereas the most important factor is the type of interlayer cation. This primarily controls the structure of water layers sorbed in the interlayer related to the charge distribution and hydration energy of the cation in question (Mooney et al., 1952; MacEwan & Wilson, 1980; Sposito & Prost, 1982; Brigatti et al., 2006). The hydration energy is related to important cationic properties such as ionic size and valency (Montes-Hernandez et al., 2003a) and therefore the larger monovalent Na ion has a much lower hydration energy ($\Delta H_{\text{hyd}}\text{Na} = -405$

kJ/mol; Huheey 1993) compared to the smaller, divalent Ca ($\Delta H_{\text{hydCa}} = -1592$ kJ/mol). This effect is visible by the slower interlayer water uptake in case of all Na-containing smectites (SWy-2, MX80-bentonite and IBECO-bentonite, table 4.3.1).

For example the Na-activated IBECO bentonite hydrated in ground water showed the slowest rate of hydration and was not completely saturated even after the 1500h duration of the experiment. In contrast, the interlayer uptake of the Ca-activated TIXOTON bentonite infiltrated by the same solution was accomplished after just 80h. Although differences in packing density occur between these samples (TIXOTON bentonite 0.94 g/cm^3 vs. 1.15 g/cm^3 for IBECO), which influences access of water to interlayer sites, the dominant factor controlling the enhanced uptake rate of the Ca-smectite is considered to be the higher hydration energy. Whereas the interlayer uptake rates for all Na- smectites vary between $1.4\text{E-}04$ and $7.5\text{E-}05$, the Ca-varieties show values enhanced by a factor of 10 with rates between 1.0 and $1.7\text{E-}03$ (table 4.4.1).

Material	IBECO seal 80*		TIXOTON-TE ⁺		MX80 (BF100)*			SWy-2*		Nau-1 ⁺
	Na-activated bentonite		Ca-activated bentonite		bentonite			Purified montmorillonite		Purified nontronite
packing density [g/cm ³]	1.15	1.14	0.94	0.94	1.43	1.35	1.60 (dry 1.31)	1.37	1.36	1.08
Ionic strength of infiltrating solution [mol/l]	0.0013	0.639	0.0013	0.639	0.0001	0.0109	0.0109	0.0001	1	0.0001
Interlayer uptake rate [ml/g/h]	$1.5\text{E-}04$	$3.1\text{E-}04$	$1.7\text{E-}03$	$1.0\text{E-}03$	$7.5\text{E-}05$	$2.2\text{E-}04$	$1.8\text{E-}04$	$2.2\text{E-}04$	$1.4\text{E-}04$	$<1.2\text{E-}03$

Table 4.4.1. Calculated rates of water uptake into the interlayer spaces of various *Na- and ⁺Ca- smectites. The samples are of varying packing density and where infiltrated with a range of ionic solutions

Particle-scale

The type of interlayer cation has additionally an influence on particle scale (Fig. 4.4.1) because the number of average layers per clay stack varies for the different types of smectite. For example, the number of layers per particle is reported to be higher for Ca-smectite (average ~10 layers per stack when hydrated) as opposed to the thinner stacks composed of 3 to 5 layers for Na-varieties (Cases et al., 1997; Pusch, 2006b). This trend is partially visible when comparing the Ca-activated TIXOTON and the Na-activated IBECO where the latter shows a decrease to 5 layers per stack and the TIXOTON to 7, independent of the infiltrated solution (Fig. 4.3.15). However, these differences are less pronounced than described in the

literature (Schramm & Kwak, 1982; Pusch, 2006a) and appears to be strongly dependent on the packing density when particle separation is restricted by limited pore volume.

The solution chemistry also clearly influences smectite hydration on a particle scale. It has been reported that a higher ionic strength of infiltrated solution leads to increased rates of hydration by influencing the micro texture of clay particles. During particle aggregation, voids in the micro porosity are not closed (Pusch, 2001a). This mechanism occurs during the initial states of solution uptake by Na-smectite (SWy-2 montmorillonite and the Na-activated IBECO-bentonite) where both external (surface- and pore-water) and interlayer water show enhanced uptake rates (Fig. 4.3.2). The Ca-activated TIXOTON bentonite showed slower uptake when infiltrated with sea water compared to the ground water infiltrated sample (ionic strength of 0.64M as opposed to 0.0013M). Due to the presence of the divalent Ca in the interlayers, this sample has already a tendency to form aggregates and the effect of solution concentration is not as pronounced as for Na-smectite.

Responsible for sealing is, however, the amount of interlayer water that was in both cases (Na and Ca-smectite) not observed to be affected by the higher ionic strength. In the case of SWy-2 infiltrated by 1M NaCl the interlayer water did not significantly differ from the water infiltrated sample (table 4.3.2) and in the case of IBECO-bentonite, the interlayer water was even enhanced when infiltrated by sea water as opposed to ground water (table 4.3.8). These results indicate that the saline solution has no serious detrimental effects on intracrystalline swelling of Na-smectite, as previously noted by Hofmann et al. (2004).

4.4.2. Progressive hydration in solution under confined volume conditions

All hydration experiments in this study were conducted using aqueous solutions as opposed to conditions of relative humidity. Therefore differences in the mechanisms and kinetics of hydration can be expected. It is generally well documented that the smectite clays (in particular montmorillonite) show a step-wise hydration behaviour as the water activity is improved under conditions of increasing air humidity (Collins et al., 1992; Chipera et al., 1997; Ferrage et al., 2005b). This stepwise hydration behaviour is commonly attributed to apparent energy levels as hydration shells are formed around interlayer cations (Karaborni et al., 1996; Cases et al., 1997). In contrast the build-up of structured interlayer water in percolating solutions is observed to be a more continuous process. In general, water-layers do not appear spontaneously in high abundance, as seen with increasing humidity, but form

steadily as part of a progressive layer expansion process as seen during the hydration of the Wyoming bentonite sample, SWy-2 (Fig. 4.3.4 a+b) or the MX80 bentonite (Fig. 4.3.8).

In some hydration experiments the occurrence of apparent plateaus may be better explained by transport fluctuations during the inflow of water rather than to variations in hydration energy. A stepwise behaviour was observed for SWy-2 when hydrated with a solution of increased ionic strength (1M NaCl, Fig. 4.3.2.a). This apparent hydration step could result from precipitation of salts from the solution that blocked infiltration but might be as well due to the increased rate of infiltration whereby less time is available to organize the preferred coordination of interlayer water molecules. In the case of the sea water infiltrated, Ca-activated TIXOTON bentonite, an apparent hydration step is also visible (Fig. 4.3.2). One possible explanation here is that cation exchange reactions such as K exchanging Ca led to a reduction in the number of water layers.

However, such variations in the rate of interlayer water uptake and the occurrence of apparent hydration steps should be interpreted with caution as these fluctuations can also result as an artefact of the calculation procedure applied in this study. In the CALCMIX program, that was used to quantify the abundance of water layers, only combinations of 3 different WL structures can be fitted simultaneously, whereas in some transitional states it is probable that more WLs coexist. For example, the immediate appearance of abundant 3-WL structures in some bentonites (e.g. 35%, as seen for Na-activated IBECO, Fig. 4.3.12a) is considered to be such an artefact as these thick hydrated interlayers are more likely to form continuously by progressive layer growth, which could not be resolved by the CALCMIX approach.

Influence of the confined volume conditions on a layer scale

The confined volume was seen to have, as expected, a significant influence on the hydration behaviour of the smectites on all scales. Concerning the interlayer hydration (layer-scale, Fig. 4.4.1) the generation of significant swelling pressures can limit particle expansion (Pusch, 2001b; Komine, 2004; Komine & Ogata, 2004; Pusch, 2006a). This is visible in the number of water layers formed with increasing packing density of the MX80 bentonite (Fig. 4.3.8). The more strongly compacted sample (initial packing density 1.43g/cm^3 , Fig. 4.3.8b) shows a final combination of 2-, 3- and 4-WL whereas for the less compacted sample (1.35g/cm^3 , Fig. 4.3.8a) 3-, 4- and 5-WL are developed.

The suppression of water layers due to an increased packing density is also well illustrated by considering the mean thickness of hydrated interlayers such as presented in table 4.3.4 for the MX80 samples. Both the pre-dried more densely packed MX80 ($1.43\text{g}/\text{cm}^3$) and the wet MX80 sample ($1.60\text{g}/\text{cm}^3$) show similar final mean thicknesses with 18.2-18.3Å whereas the more loosely packed powder ($1.35\text{g}/\text{cm}^3$) accommodates thicker structures with a mean thickness of 19.4Å. The other investigated bentonites exhibit as well features that can be attributed to the confined volume. The stable configuration of saturated Na-activated IBECO was a mixture of 1- and 3-WLs; a structural arrangement commonly described for the interlayer hydration of Na cations under high humidity conditions (Karaborni et al., 1996). The absence of a 4-WL structure in the saturated state of this experiment is attributed to the buildup of swelling pressure within the sealed cell, which inhibited further layer expansion (Fig. 4.3.12).

Influence of the confined volume on a particle scale

Furthermore the volume of the system is seen to influence particle and aggregate processes (Fig. 4.4.1). Classical studies have characterized smectite and bentonite hydration in free swelling systems (Norrish, 1954; Norrish & Quirk, 1954; Laird et al., 1995; Wilson et al., 2004) in which Na-montmorillonite can by osmotically swell and increase the interlayer space until the particles lose their coherence and form a amorphous gel (Lagaly 1993; 2006). Accordingly, the external surface area can reach several hundreds of m^2 (Schramm & Kwak, 1982; Lagaly, 2006; Michot & Villieras, 2006). However, in confined volume conditions the formation of gels is inhibited and probably occurs only locally in restricted void space. In theoretical calculations, based on the reduced particle thickness, the surface area yield the highest values for MX80 at $\sim 190\text{m}^2/\text{g}$, which corresponds to a mean number of 3 layers per particle (table 4.3.6). However, under confined volume conditions such calculated values for surface area are not directly applicable because the particles cannot expand freely (Fig. 4.4.3 c+d). For example the area provided by external surfaces of the less compacted MX80 bentonite could theoretically accommodate up to 0.4ml/g but only 0.22ml/g is contained as external water because the volume is restricted.

For purified Na-exchanged SWy-2 montmorillonite, however, the values of theoretically adsorbed surface water and available external water are in good agreement (Fig. 4.3.7). In this case the numbers of layers per stack do not decrease as strong as for MX80 samples although the packing densities are similar (between 1.35 and $1.37\text{m}^2/\text{g}$). This might indicate that the relative strong decrease in particle thickness observed for MX80 is due to sample

heterogeneities and non clay mineral impurities which provide local voids that allow more free expansion (Fig. 4.4.3e). The SWy-2 sample, in contrast, is notably more homogenous (grain size separated $<1\mu\text{m}$, Na-exchanged, almost completely dehydrated). Here is noted that in a confined volume system the surface area is not necessarily entirely available, for example to adsorb toxins.

Generally it should be noted that the surface area calculations are based on values for number of layer per stack which were included in the peak fitting of the CALCMIX program that should be considered as a best approximation rather than absolute values. However the results show that it is not applicable to consider values of several hundreds of square meters in confined volume conditions but it is as well not recommended to assume a constant surface area for hydrating smectite.

Influence of the confined volume on aggregates (bulk textural scale)

The effect of texture and micro porosity in confined volume can be seen in samples with sufficiently low uptake rates ($< 1\text{E-}04\text{ml/g/h}$). These experiments reveal relatively rapid pore water intake which serves as a reservoir that is subsequently redistributed to occupy interlayer space (Fig. 4.3.4.c and 4.3.10a). It is considered likely that smectite particles adjacent to the same pore space take up similar amounts of water and form clusters with the same water layer abundance (Fig. 4.4.3e). The formation of such hydration clusters is indicated by the increasing ordering of WL structures observed during hydration. Water layer distributions in the confined volume experiments show an enhanced probability that structures of the same thickness lie adjacent to each other (Fig. 4.3.6c, 4.3.9d). This contrasts the general assumption of random ordering for swelling in relative humidity ($R=0$) and as well the $R=1$ ordering that was described to occur on a particle scale in experiments done by Moore and Hower (1986). Here ordered arrangements of different thicknesses were observed to be more stable.

The difference between Na- and Ca-smectites tends to decrease with increasing packing density because the importance of micro texture becomes increasingly negligible with compaction as noted by Pusch (2001b; 2006a). This was observed concerning the final amount of water uptake that was seen to be strongly dependent on interlayer cation at low packing densities and almost independent at higher densities (Fig. 4.3.3). Although during hydration the degree of homogenization increases and texture changes play an important role attaining a uniform hydration behaviour, the confined volume studies conducted by Pusch (2001b) revealed that density variations persist. He showed that even at very high packing

densities, softer and more pervious zones are formed by partly or completely interconnected "external" voids that are filled with more or less dense clay gels. A schematic representation of the hydration on the bulk texture scale for Na- and Ca-smectite under confined volume conditions is presented in Fig. 4.4.2.

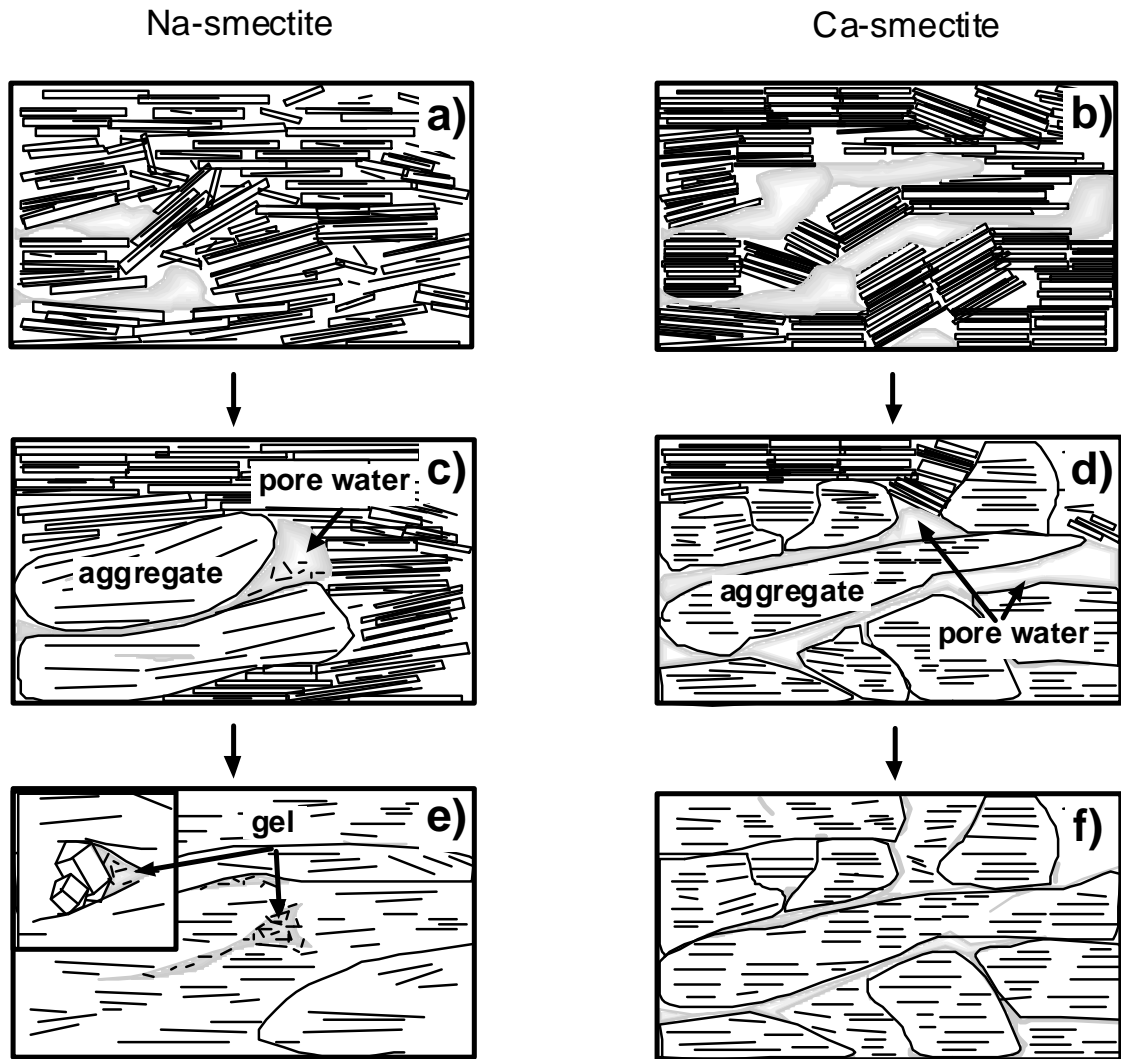


Fig. 4.4.2. Schematic sketch of water uptake and hydration of smectite in confined volume conditions (bulk textural scale). a+b) Initial stages of hydration dominated by pore water intake. c+d) Pore water serves as a reservoir for interlayer expansion leading to the formation of hydration aggregates. e+f) Interlayer hydration and local particle separation leads to the expansion of aggregates and pore closure. In the case of Na-smectite (e) the formation of gels fill remaining pore spaces and voids associated with mineral impurities (inserted image).

Differences between Na-smectite and Ca-smectite at initial stages are the smaller number of layers par stack in the case of Na-smectite and a poorer connectivity of the porespace, whereas Ca-smectite is characterized by thicker stacks and a better connectivity (Fig.

4.4.2a+b). Therefore pore water enters the Ca-smectite more rapidly compared to the Na-smectite. Where water came in contact with the powder, hydration aggregates are formed (Fig. 4.4.2c+d). Because of the increased expansion of Na-smectite aggregates, the access for water is restricted and the rate of intake relative to the Ca-smectite decreased. At saturated state the formation of gels in voids seals the Na-smectite, whereas in the case of Ca-smectite some porosity remains (Fig. 4.4.2e+f).

4.4.3. The influence of initial conditions

Initial variations in sample conditions, namely packing density, pore-size distributions and particle orientation (texture) have been shown to influence hydration behaviour to a large extent (Wilson et al., 2004). The influence of packing density is for example visible in the case of MX80 where the more densely packed sample incorporate less total water into the powder compared to the dry and more loosely packed powder (Fig. 4.3.10a+b). Despite these differences in total water uptake, the amount of water in the interlayer is almost the same, indicating the higher porosity accommodates the additional external water measured. It is also evident that if the initial hydration is elevated the increased wet packing density is higher and the amount of available pore space for additional water uptake becomes restricted (Fig. 4.3.10c).

The incorporation of water in the powder prior to conducting the hydration experiment results in a similar behaviour compared to the equivalent highly compacted dry sample. However once the sample dries after the period of experimentation a significant macro porosity is expected to be created. The initial state of pore structure and particle orientation was not quantified as part of this study but these variations between samples are considered to be relative low compared to those presented in other studies (Wilson et al., 2004). A consistent and reproducible method was used to introduce the powders into the reaction-cell before hydration and therefore textural differences were minimized. Textural variations present are more likely to represent the natural state of the clay powder rather than introduced during loading of the cell. Such heterogeneities are typical of bentonite powders, which contain non-platy minerals (table 3.1) and a range of grain size distributions. In contrast, the separated fine grained clay mineral fractions appear to be more homogenous in nature due to their close to monomineralic content and reduced range of grain size.

4.4.4. Implications of confined volume laboratory analogue for understanding natural systems

The varying amounts of external and interlayer water incorporated into saturated bentonites is expected to have significant effects on the rate of elemental transfer, and can be described by combining equations of free diffusion and surface adsorption (Bourg et al., 2003). Successful numerical modelling of elemental transport, including the migration of radionuclides (Bors et al., 1997) in the repository setting is reliant on the type of quantitative data presented here. Loosely bound, external water is more likely to be lost at lower temperatures during any subsequent heating and dehydration event, which might occur in the vicinity of radioactive waste containers. This contrasts with the more strongly bound interlayer water that is released at temperatures of generally 100°C and higher (Farmer & Russel, 1971; MacEwan & Wilson, 1980; Bray et al., 1998).

The separation of interlayer and true particle surface adsorption is also required to improve knowledge of these potential reaction sites in sorption and desorption processes. In confined volume swelling of compacted bentonite it is observed that the decrease in particle thickness and the corresponding increase in surface area is somewhat restricted compared to the uninhibited particle swelling in solution. Therefore transport calculations involving reactive surface areas based on free swelling experiments would lead to significant errors in the estimations. On a qualitative level it is also essential to consider the scale of hydration involved, particularly when evaluating reaction or exchange rates on the layer-, particle- or bulk textural-scale.

Based on the result represented in table 4.4.2 the water uptake rates calculated for the different experiments can be used to estimate the time required to saturate a bentonite barrier of 1m thickness. As expected, materials that contain mostly Na-smectite (IBECO, MX80 and SWy-2) have relatively low saturation velocities (between ~ 2 and $5E-09$ m/s) and therefore the time required to attain the stable state varies between 6.5 and 24 years. In the case of the IBECO bentonite the increased ionic strength has a notably strong effect on the saturation time with only 1.8 years required to reach this state. This is almost 5 years less time than when hydrated with ground water. Using finer grained monomineralic smectite separates appears to successfully slow down the rate of water inflow. Separates of the SWy-2 Wyoming montmorillonite hydrated with 1M NaCl required 9.5 years to reach saturation compared to 11 years when hydrated with purified water. These differences highlight the influence of clay microstructure on the solution infiltration rate that is seen to be more pronounced in the less

compacted, bulk IBECO (the ~1.15 compared to ~1.37g/cm³ packed sample). The influence of the initial packing density is as well visible in the decreased hydration velocity of the more strongly compacted MX80 sample (1.43g/cm³). An inflow rate of 1E-09m/s yields the longest time required to saturate the 1m barrier with 24 years. This compares to the 14.9 years needed for the less compacted equivalent (1.35g/cm³) based on an inflow rate of 2E-09m/s. Here, the decreased degree of compaction (5.6%) leads to the 1.6 times increase in hydration time. The hydration velocity for the Ca-smectite based bentonites varied between 2 and 8E-08m/s and therefore hydration of 1m material would need between 8months (0.67 years) and 1.4 years. For these samples, the hydration behaviour is notably less sensitive to the composition of the infiltrating natural solution. The industrially available TIXOTON would require just 8-10 months to saturate the barrier irrespective of whether hydrated in sea water or ground water.

	IBECO		TIXOTON		MX80		SWy-2		Nau-1	
	Ground water	Sea water	Ground water	Sea water	dehydrated 1.35 g/cm ³	dehydrated 1.43 g/cm ³	Hydrated 1.6 g/cm ³	Purified water	NaCl	Purified water
Saturation velocity [m/s]										
<i>Interlayer water</i>	5E-09 (6.5 y)	9E-09 (3.4 y)	8E-08 (0.14y)	5E-08 (0.69y)	5E-09 (6.9y)	2E-09 (17.7 y)	5E-09 (7 y)	6E-09 (5.3 y)	4E-09 (7.9 y)	2E-08 (1.38)
<i>External water</i>	5E-09 (6.5 y)	1E-08 (2.6 y)	5E-08 (0.67 y)	4E-08 (0.8 y)	3E-09 (9.5 y)	2E-09 (17.7 y)	3E-09 (9.5 y)	3E-09 (11 y)	3E-09 (11.7y)	--
<i>Total water</i>	5E-09	2E-08	5E-08	4E-0	2E-09	1E-09	3E-09	3E-09	3E-9	2E-08
Time to saturate 1m of compacted smectite [years]										
Total	6.5	1.8	0.67	0.8	14.9	24	9.5	11	9.5	1.4

Table 4.4.2. Calculated saturation velocities for the different clays powders used in this study. The time to saturate 1m of compacted smectite is calculated based on the distance across the reaction cell (24mm) and the time required to reach the fully hydrated state.

CHAPTER 5

-

BACTERIAL INFLUENCE ON SMECTITE HYDRATION

CHAPTER 5 BACTERIAL INFLUENCE ON SMECTITE HYDRATION

Abstract

This chapter presents experimental results on the interaction between smectite (NAu-1, SWy-2 and MX80) and the facultative anaerobic, heterotrophic *Shewanella putrefaciens* in two types of model conditions: i) Low solid to liquid ratio in agitated oxygenated conditions and ii) high solid to liquid ratio in anaerobic conditions. The former was chosen to study smectite-bacteria interaction in a solution dominated environment where the reaction rates are most enhanced. The latter was designed to simulate the subsurface case expected in planned underground repository waste sites. Bacterial cell counts in the low solid to liquid ratio batch reactor experiments revealed the prolonged survival of *S. putrefaciens* with smectite compared to growth in commonly used laboratory media. Compared to the sterile control, the pH of the bacteria containing smectite-solution was found to be dependent on the growth phase with lower pH values recorded during initial stages of the experiment (lag and exponential phase) when protons are produced during aerobic respiration. The final death phase showed a more alkaline pH due to reduced buffering of the cells in combination with the release of lyses products. Variations in solution chemistry detected by ICP-OES indicated the consummation and/or partial binding of elements, especially in the case of nontronite where the concentration of Ca and Fe was observed to decrease. The final concentration of cations in solution measured at the end of the experimental run showed enhanced values compared to initial measurements which is attributed to elemental release during lyses, however Ca was assumed to remain in the exopolymeric substance (EPS). Microscopic investigations (confocal microscopy, ESEM and TEM coupled to EDX) showed the association of biofilm and smectite-aggregates, the prolonged persistence of biofilm and the partial dissolution of nontronite surrounded by Si-rich gels and EPS. In contrast, the MX80 bentonite was not seen to be affected by bacterial activity. The presence of bacteria in compacted Na-smectite samples hydrated under confined volume conditions was seen to enhance total water uptake and to increase the number of water layers detected in the clay interlayer. Additional water was seen to be stored as external water in nontronite whereas, in the case of Na-smectite, both

interlayer water and external water uptake were seen to be enhanced. The characterization of reaction products showed the presence of sulphate and phosphate phases in the bacteria containing nontronite sample which indicates changed redox conditions. Intensity differences in texture preparations indicate textural changes whereas differences in the response to heat and chemical treatment suggest the presence of organic coatings and enhanced layer charge properties. Bacteria containing MX80 (Na-smectite) showed dissolution of accessory phases, namely calcite and eventually pyrite, and the synchronous precipitation of lepidocrocite and green rust. The different response to the bacterial activity is attributed to variations in composition and texture since nontronite contains high amounts of divalent Ca that facilitates the attachment of *S. putrefaciens* to the smectite surface by cationic “binding”. Fe(III) appears to provoke the production of chelators trapping the Fe and increasing the overall degree of mineral dissolution. The reduction of Fe also serves, additionally, as TEA (terminal electron acceptor) under anaerobic conditions. Due to its composition, montmorillonite is less affected by chemical alteration but it is sensitive to microstructural changes, including the aggregation of clay particles in voids created by cells lyses. Therefore it can be concluded that the influence of bacteria on smectite hydration in confined volume systems is highly dependent on the precise crystal chemistry of the clay and its microstructure which results in a variety of different alteration mechanisms. Even though the bacteria are not considered to stay alive over a significant period of time, detrimental effects induced during initial activity have been shown to remain for at least 1½ years and should be taken into account when considering future applications.

5.1. Introduction

Bacteria inhabit most environments of the Earth's surface and upper crust and are well known to interact with mineral surfaces where nutrients often accumulate (Brown et al., 1977; Ellwood et al., 1982; Bright & Fletcher, 1983; Van Loosdrecht et al., 1990; Lehman et al., 2001). Due to electrostatic interactions between bacterial cells and positively charged minerals, they are easily attached and often concentrated (Maurice & Warren, 2006). In soils, bacteria tend to be specifically associated with clay minerals because they are, relative to the bulk soil, enriched in ions, water, and organic matter (Theng & Orchard, 1995; Tazaki, 2006). At the same time, ion exchange reactions, especially with smectite clays, contribute to buffering the pH and stimulate bacterial growth (Stotzky, 1966a; Stotzky & Rem, 1966; Stotzky, 1967).

The attachment of the (normally negatively charged) bacteria to the negatively charged clay minerals is often aided by the formation of exopolymeric substances (EPS, Little et al. (1997)) that are considered to change surface charge properties of clays (Maurice & Warren, 2006). EPS are also known to induce particle aggregation as well as to enhance mineral dissolution associated with biofilm assemblages (Welch & Vandevivere, 1994; Labille et al., 2005; Jaisi et al., 2007). Moreover certain elements, such as Si and Fe can accumulate in the EPS and were reported to induce smectite crystallization as suggested for clays in deep sea sediments (Ueshima & Tazaki, 2001).

Many important bacterial reactions in soils and sediments take place at the aerobic-anaerobic interface (Roden et al., 2004) where organic matter supports large biotic O₂ demands that consume the supply faster than it can be replaced (Magonigal et al., 2003). As molecular oxygen diffuses more slowly through water than through air, anaerobic environments are often associated with water bodies (e.g. wetlands, rivers, lakes, estuaries, coastal marine sediments and water columns, aquifers). In the case of an underground repository, after the system is closed, the conditions will rapidly switch from initially aerobic to reducing conditions because oxygen will be rapidly consumed (Montes-Hernandez et al., 2005a). Therefore it is essential to study bacteria related reactions both in presence and absence of oxygen.

The bacteria *Shewanella putrefaciens* is a facultative anaerobe and can respire under both conditions. In the absence of oxygen, they use other electron acceptors to gain energy, such as Fe(III). This species is insoluble in pure water at neutral pH and, as a consequence, the bacteria are forced to use the Fe(III) that is present in Fe-bearing minerals such as ferrihydrite,

hematite, goethite and clay minerals (Stucki et al., 1987; Roden & Zachara, 1996; Dong et al., 2000; Zachara et al., 2002; Dong et al., 2003b; Bonneville et al., 2004; Stucki, 2006)

The dissimilatory reduction of Fe(III) in smectites, especially in nontronite, has been shown to drastically alter the properties of the clay. Kim et al. (2004) observed, for example, that in batch experiments *Shewanella sp.* triggered the transformation of smectite to illite. The reduction of the Fe(III) in the octahedral sites of the smectite lattice led to a greater charge discrepancy and to a net increase in negative layer charge. This charge subsequently collapsed the interlayer space, reduced the thickness of the hydrated interlayer and increased cation (K^+) fixation (Kostka et al., 1999; Stucki et al., 2000; 2003; Kim et al., 2004; Komadel et al., 2006; Stucki, 2006).

Recent studies on Fe-smectites also showed that bacterial modifications can include partial dissolution of the clay particles (Kostka et al., 1999; Dong et al., 2003a). It is suggested that either Fe(III) reduction causes a charge imbalance in smectite that can trigger mineral dissolution or bacterially produced substances, such as organic acids and chelators, dissolve the mineral prior to Fe-reduction (O'Reilly et al., 2006). In the latter case, Fe(III) would be released into solution and become accessible for dissimilatory microbial reduction. Here, the production of specific iron chelators (siderophores) is a common process in order to make iron more bioavailable (Neilands, 1989; Gram, 1994; Hersman et al., 2000).

In aerobic conditions, bacteria do not need to reduce metals for it is energetically much more efficient to reduce oxygen (Madigan et al., 2003). Based on investigations of polluted aquifers, Bennett and coworkers (1996) proposed that microbes selectively dissolve minerals based on their nutrient requirements. Laboratory experiments, showed that P- and Fe-bearing silicates and glasses are colonized and dissolved when the contained elements act as limiting nutrients (Rogers et al., 1998; Rogers & Bennett, 2004). In the case of smectites, it is their unique ability to adsorb or exchange cations that make them a potentially rich nutrient source for bacteria (Stotzky, 1966a; , 1967).

A large proportion of clay-bacterial interactions take place under confined volume conditions as is the case in soils or engineered systems like nuclear waste repositories. In Chapter 4, it was shown that the hydration behaviour of smectites under confined volume conditions is notably different from the free swelling system. However, the effects that bacteria have under such conditions have not been well studied yet. Any consumption of cations or changes in layer charge properties could have strong effects on the hydration capacity of swelling clays.

In this study, the experiments were therefore designed to quantify the impact of the bacteria *Shewanella putrefaciens* on the swelling behaviour of two types of smectites, nontronite and montmorillonite, (SWy-2 and MX80) in two types of experiments: i) Agitated batch experiments with low solid to liquid ratio in oxygenated conditions and ii) the subsurface environment with a high solid to liquid ratio, diffusion controlled transport, and anaerobic conditions. The latter was again constructed to serve as a laboratory analogue for the underground storage of nuclear waste (Chapter 4). In situ X-ray diffraction monitoring techniques of reaction processes combined with mineralogical and geochemical investigation of the reaction products reveal the importance of bacteria activity in swelling clay systems.

5.2. Analytical procedure

5.2.1. Agitated batch experiments

Batch experiments of smectites in solution were designed to quantify the impact of the bacteria *Shewanella putrefaciens* on both pure clay separates (monomineralic) and bentonite mixtures (polymineralic). Nontronite (NAu-1) and montmorillonite were prepared as purified separates (SWy-2) and a MX80-bentonite powder was selected from an industrial source. The clay was first pre-sterilized in the oven at 110°C for 3h and then dispersed in sterilized water (sterilized by autoclaving at 121°C for 15 min). A portion of sterilized clay (0.01 and 0.04g/ml) was then incubated with washed bacteria cultures prepared with varying cell densities (see table 5.3.1). Simultaneously abiotic control experiments were conducted for comparison. Clay-bacterial suspensions were continuously mixed with an agitator or magnetic stirrer. At selected intervals samples were extracted for ICP-OES analysis using a sterile syringe and filtered using a 0.2µm polycarbonate filter. The extracted samples were then acidified using concentrated HNO₃ and stored in a dark cool place prior to analysis. The pH was controlled using a pH-meter on pre-sampled aliquots of the suspensions in order to prevent contamination. Bacterial density was determined by viable cell counts (Chapter 3) in order to monitor their response to the smectitic material. Bacterial solutions were examined by ESEM, which allowed direct imaging of the material in the hydrated state. Samples were pipetted onto self-adhesive conductive carbon stickers that were placed on the aluminum SEM sample holder. This procedure was done as rapidly as possible only minutes before placing into the microscope. The chamber pressure was set between 5.9-6 torr (0.0078-0.008

bar) and temperatures between 8°C and 22°C resulting in a relative humidity between 55 and 75%.

In order to study the composition of the bacteria and the nature of clay-bacteria interaction at the small scale, transmission electron microscopy (TEM) was undertaken coupled with energy dispersive X-ray spectroscopy (EDX). For study, dried dispersed samples were prepared by directly pipetting dilute suspensions onto copper grids and then left to dry under room conditions. For investigation of the solid reaction-cell samples, the material was first dispersed in de-ionized water and then diluted (several 10 fold dilutions). Suspended clay samples extracted from the batch experiments were diluted 10 to 100 times. Quantifications of microchemical analysis were done without correction for carbon introduced during coating of the grid. Textural (oriented) clay samples were also prepared from the batch control experiments for XRD characterization of mineralogical changes following clay-bacteria interaction.

5.2.2. Confined volume experiments using reaction-cell XRD

In situ reaction-cell XRD was applied to monitor the influence of *S. putrefaciens* on clay under confined volume conditions. Powdered material (~ 5g) of nontronite and montmorillonite containing MX80-bentonite was added to 0.6-0.8ml of bacteria containing water or a culture medium (density 10^8) and mixed with a sterile spatula. The clay-bacterial mixture was then loaded into the reaction-cell and pressed in order to control porosity (see appendix for procedure). As an internal standard for X-ray diffraction, delaminated kaolinite was added to the upper surface and worked into the sample powder using a razor blade. Once sealed with a capton foil, the reaction-cells were measured by XRD in order to obtain a reference profile representing zero reaction time. During hydration the frequency of measurements was adapted to the reaction rate but kept to a minimum to limit radiation damage of bacteria. After each irradiation the chambers were resealed by the pressure cap and the experimental solution reattached to allow percolation from the Teflon© bottle located at the top of the chamber (Fig. 5.2.1). Anaerobic conditions were controlled applying the GEN-bag anaerobic system provided by BioMerieux©, which consists of generators that produce CO₂.

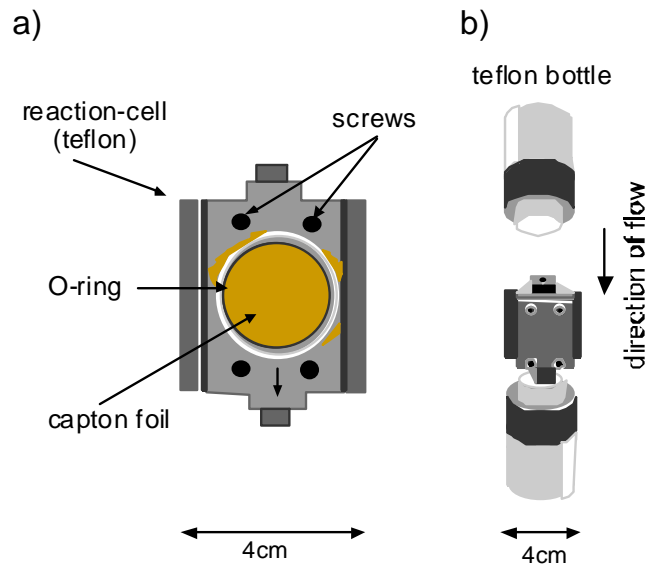


Fig. 5.2.1. a) Schematic representation of the reaction-cell device (without upper sealing plate). b) Set up for flow-through experiments with solution bottles attached. At any stage of the hydration experiment, the reaction-cell in a) can be placed in the X-ray diffractometer for measurement.

5.2.3. Analyses of reaction products

After completion of the experiment runs, the hydrated reaction products were extracted from the reaction-cell device and investigated for changes in composition and mineral content. For solution chemistry measurements, between 0.2-0.5g of the clay paste were removed from the freshly opened reaction-cells, dispersed and diluted 20 times in Millipore® water (e.g. 0.2g of paste was diluted with 4ml of water to give a concentration of 50mg clay per ml solution). The samples were homogenized using an ultra sonic bath (2 times for 15 minutes) and allowed to sediment for 24h. After repeated ultra sonic treatment, the samples were centrifuged (3500 rpm for 15 minutes), filtrated ($< 0.22\mu\text{m}$) and acidified using concentrated HNO_3 . The same procedure was applied for HCl extraction where, instead of water, 1N HCl was used as the leaching agent. Samples for Fe(II) measurements were dissolved in 0.5N HCl (0.5N HCl extraction method) and incubated for 12 hours to extract Fe(II). Solutions were filtered and then analyzed by ICP-OES.

Viable cell counting (Chapter 3) was applied on clay samples extracted from the reaction-cell by suspending known amounts of solids in corresponding amounts of water (e.g. 0.3g and 3ml) prior to serial dilutions and plate testing. TEM in combination with EDX was applied on

diluted, well dispersed samples that were directly pipetted onto copper grids. Qualitative evaluation of changes in layer charge was verified on cation-exchanged samples (MgCl_2 , KCl, Chapter 3) and investigated using conventional texture XRD.

5.3. Results

5.3.1. Bacterial growth in a clay suspension

Fig. 5.3.1a shows the change in abundance of colony forming units (cfu) of *S. putrefaciens* in the smectite suspensions over the period of experimentation (ca. 50 days). For the three samples of smectite studied (nontronite and two types of Na-montmorillonites: MX80 and SWy-2), two densities of dispersed clay suspensions are presented with 0.01 and 0.04g clay per ml. For comparison, population curves for two culture media were also determined. LB (Luria Bertrani) is an undefined, nutrient rich medium and MM (Minimal Medium) represents a defined medium where only the minimums of nutrients are supplied (Myers and Nealson, 1988, compositions in Chapter 3). The bacterial starting densities used at the beginning of the experiment are given in table 5.3.1. A more schematic representation of the population curves is given in Fig. 5.3.1b, showing the recognizable classical phases of development and their duration (numbers in italics). All mixtures were continuously agitated.

Sample	cfu/ml
Nontronite (Nau-1) 0.04g/ml	$3.8 \cdot 10^4$
Nontronite (Nau-1) 0.01g/ml	$5.8 \cdot 10^4$
Na,Ca montmorillonite (MX80) 0.04 g/ml	$5.7 \cdot 10^4$
Na,Ca montmorillonite (MX80) 0.01 g/ml	$3.8 \cdot 10^4$
Na montmorillonite (SWy-2) 0.04 g/ml	$7.5 \cdot 10^4$
Na montmorillonite (SWy-2) 0.01 g/ml	$3.7 \cdot 10^2$
Luria Bertrani Medium (LB)	$1.2 \cdot 10^3$
Minimal Medium (MM)	$2.3 \cdot 10^2$

Table 5.3.1. Starting densities of bacteria used in the experiments expressed as colony forming units per ml clay suspension (cfu/ml).

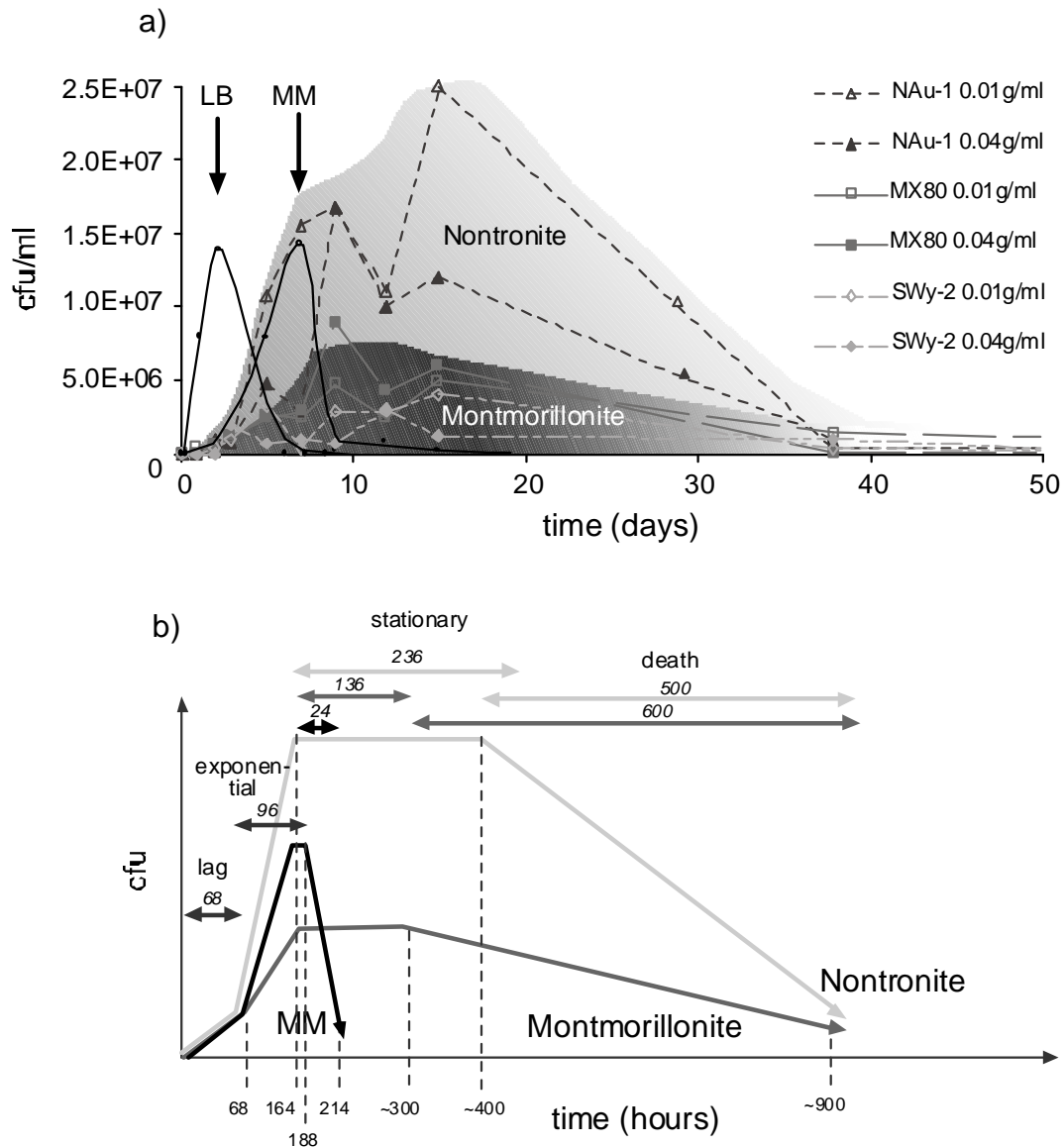


Fig. 5.3.1. a) Growth curves of *S. putrefaciens* in culture media (solid black lines, LB indicates Luria Bertrani medium and MM the minimal medium defined by Myers & Nealson (1988)) and smectite suspensions of two different mineral concentrations. The light grey background indicates the population span for the nontronite (NAu-1) culture and the dark grey background for the two montmorillonite rich samples MX80 and SWy-2. Bacterial populations are measured as colony forming units per ml of suspension (cfu/ml) plotted against reaction time (days). b) Schematic representation of the growth curves showing the main differences in the duration of recognized phases (numbers in italics).

The shape of the population curves is considered to be typical of bacterial growth in a batch culture where nutrients are not replaced and waste products are not removed. The curves show four more or less distinct phases known to characterize a typical growth cycle (Madigan et al., 2003). An initial lag phase is characterized by a low growth rate and is normally present if the bacteria have to adapt to new conditions. During this time, enzymes that are required to synthesize essential metabolites are produced. Following the initial lag,

the culture actively grows and each cell divides to produce an exponential rate (exponential phase). As nutrients become limited and waste products built up, the culture passes into a stationary phase. During the stationary phase, the number of cells generated is balanced by mortality (cryptic growth). Finally, due to the critical lack of nutrients and a high concentration of toxic waste products, the bacteria cells fail to reproduce and the culture passes into the so called death phase (Madigan et al., 2003).

No lag phase was observed for bacteria grown in the LB culture as this is an inoculum medium in which the cells had already developed all the necessary enzymes. Exponential growth started immediately followed by a presumably short stationary phase (too short to detect in this experiment) and then a rapid decline in cfu during a 4 day long death period. A similar curve is produced during growth in the MM, but an initial 3 day lag (68h) is required for adaptation. Similar gradients in the lag stage are also observed in the *S. putrefaciens* cultures grown in all smectite suspensions. The lag is longest in the montmorillonite suspensions (compared to the defined MM culture and the nontronite suspension). This indicates that the bacteria are successful in generating the enzymes, but that it is more difficult for them to adjust to the montmorillonite suspensions than to the culture medium or Fe-smectite.

The exponential growth phase of most cultures started after 3 days but differences in the gradient of the slope are observed. Steep slopes occur for growth in MM and nontronite media and relatively flat ones for montmorillonite based samples. These slopes can be used to calculate the time required to double the population (table 5.3.2, for details see appendix). The population doubling time in the nontronite suspension is with ~21.5h similar to that calculated for the MM (~18.5h). In contrast, the value for montmorillonite cultures (e.g. MX80) is significantly higher and with ~83h, is more than 4 times longer. These calculated doubling times are, however, highly dependent on recognizing the transition to the stationary phase and should be treated as estimates.

Sample	Initial cell number [cfu/ml]	Maximal cell number [cfu/ml]	Slope	Generation time (g) [h]
Nontronite 0.04	6.96E05	1.65E07	0.014	21.5
MX80 0.04	1.08E06	1.40E06	0.0036	83.3
Minimal Medium	3.96E05	1.42E07	0.016	18.5
Luria Bertrani	4.4E03	1.39E07	0.077	3.8

Table 5.3.2. Data used to calculate the time required to double bacterial population during the exponential growth phase here referred to as the generation time (g) in hours. The initial

and final cell numbers correspond to the beginning (68h) and end (164h, see Fig. 5.3.1.b) of the exponential phase and were used to calculate the slope.

Compared to LB medium it takes 5 times longer for the culture to double its population in the MM culture or nontronite solution. Bacterial growth in the Na-montmorillonite suspensions takes even more time, with generation times that are around 20 times longer compared to that observed in LB medium. As the conditions of incubation were the same for all samples, it is likely that the concentration of nutrients is the major factor limiting the growth rates. One possible reason for the slower increase in cfu in the case of montmorillonite is the extensive osmotic swelling that occurs in these gel-like suspensions (see Chapter 2). Electrostatic repulsions within this gel structure restrict access to the montmorillonite and thus to nutrients.

The major differences between the bacterial growth curves for smectite suspensions and culture media are the character and duration of stationary and death phases. The stationary stage was estimated to begin after 164h (1 week after the experiment started) for all clay suspensions and to finish after ~300h (~13 days) for the montmorillonite and after ~400h (~17 days) for the nontronite samples (Fig 5.3.1.b). Both stationary and death phases for clay suspensions are significantly longer than observed in the culture media. The length of the stationary phase observed within media cannot be accurately determined but the data indicates that it must be short (maximum at 24h). The death phase is accomplished within 6 days for LB medium and within 10 days for MM. In contrast, the death phase in smectite suspensions is much longer in duration with over 500h for nontronite and 600h for montmorillonite suspensions. Compared to the MM, this is 20 to 25 times longer and could be due to two major factors: i) a slower release of nutrients by the clay due to gradual dissolution and ii) simultaneous sorption of toxic waste products produced by the bacteria, especially during the death phase.

Generally, the numbers of cfu present in the various mineral cultures vary with suspension density. In the case of monomineralic samples (nontronite and SWy-2 montmorillonite), the number of cfu is enhanced when the suspension is more diluted. Based on maximal values for cfu, the dilute nontronite sample supports twice the number of bacteria and the dilute SWy-2 sample three times the population. Most likely, this is due to the enhanced viscosity of the more concentrated suspensions that decreases the bacterial mobility. In contrast, the number of cfu developed in the MX80 bentonite is enhanced by about two times when the solution is denser probably because of the additional supply of accessory minerals that serve as nutrients.

The overall supply of nutrients that are derived from the smectite particles depends on the mineral composition, the mechanism of dissolution and the quantity released into solution. Rapid exchange of interlayer cations, predominantly Ca and Na, is expected and their availability is dependent on solution chemistry and CEC. Stoichiometrical dissolution of smectites has only been reported for very acidic pH values (Metz et al., 2005) but these conditions do not apply to the experiments conducted in this study. However, in order to compare the relative cation contents of the clays with the nutrient media, the dissolved contents are displayed in table 5.3.3 assuming 100% dissolution. Major differences between the clay solution and the media are the potentially higher concentrations of virtually all cations in the smectites (Si, Al, Fe, Mg, Ca and Na), except K, which is enhanced in the medium.

Element [% oxide]	Nontronite (NAu-1) [g/l]	Montmorillonite SWy-2 [g/l]	Montmorillonite MX80 [g/l]	Minimal Medium [g/l]	Luria Bertrani Medium [g/l]
Si	2.49	2.94	2.69	0.0001	0.0019
Al	0.54	1.04	0.99	0	0.0001
Fe	2.39	0.25	0.42	0	0.0004
Mg	0	0.18	0.13	0.0045	0.002
Ca	0.24	0.12	0.10	0.0096	0.003
Na	0.01	0.11	0.16	0.0215	-
K	0	0.04	0.05	0.1940	0.30
P	0	0	0.01	0.3620	0.13

Table 5.3.3. The amount of cationic nutrients available in g/l for the different smectites if particles were completely dissolved (100%).

During the death phase, the sorption capacity of the clays is of special importance and is basically influenced by two important parameters: the specific surface area and the cation exchange capacity. The montmorillonites studied here have a specific surface area that is almost 3 times lower (about 30 m²/g, see 3.1 Chapter 3) than the nontronite sample (~84m²/g) and, thus, have notably lower sorption capacities. However, an increase in surface area does occur during the osmotic swelling of Na-montmorillonite particles as the layers loose their coherence during layer expansion. The cation exchange capacities of all samples are similar at ca. 70 meq/100g (Chapter 3).

5.3.2. Effects of bacterial action on smectite solution chemistry

The solution chemistry of key growth experiments was controlled at selected time intervals and both H^+ activity (pH) and the concentration of the main cations (Al^{3+} , Ca^{2+} , Fe_{tot} , K^+ , Mg^{2+} , Na^+ , Si^{4+}) measured. Smectite suspensions (density of 0.01g clay per ml distilled water) were inoculated with washed bacteria (density $5E07$ cfu/ml) giving initial bacteria densities in cfu/ml as follows: SWy-2 montmorillonite $2.12E05$, MX80 Montmorillonite $3.55E05$, and NAu-1 nontronite: $1.78E05$ cfu/ml. If not indicated otherwise, all experiments were conducted in the presence of oxygen.

5.3.2.1. pH variations

Fig. 5.3.2 provides an overview of the pH evolution over the period of experimentation for all unbuffered clay suspensions with and without bacteria. The initial smectite suspensions have slightly alkaline pH values ranging from 9.8 to 8.12 that shift to a narrower range of 9.5 to 8.01 as they approach a stable state after 27 days. The montmorillonite suspensions have generally higher pH values than the nontronite which might be due to proton sorption and increased buffering of the montmorillonite clays (Bauer et al., 2001; Hofmann et al., 2004). In all samples, the bacteria containing suspensions have, from the beginning, lower pH values than the sterile controls. This probably reflects the introduction of acids, together with the bacteria present in the growth medium, which were not removed during washings or were released by the bacteria after the washings.

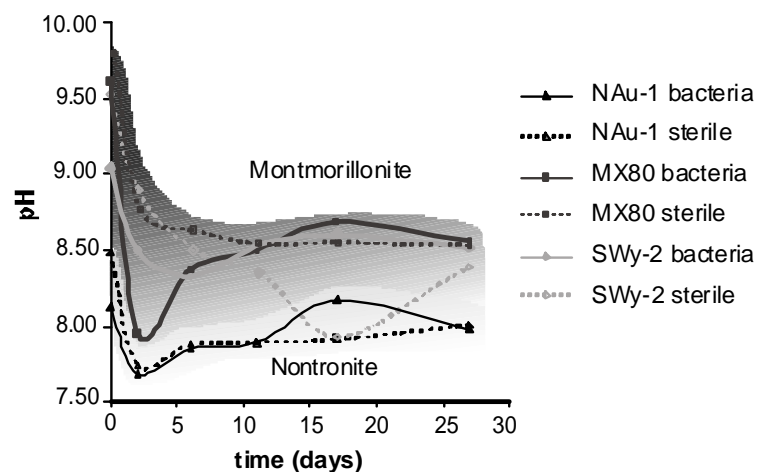


Fig. 5.3.2. Changes in pH over time for the different smectite suspensions (density 0.01g/ml). Montmorillonite suspensions are highlighted with a dark background, nontronite suspension with a light grey one. Filled symbols indicate the presence of bacteria, empty ones present sterile controls.

Fig 5.3.3.a-c shows the pH evolution separately for the individual samples, each with the corresponding bacterial growth curve. For both the bacteria-containing and the sterile samples, the initial pH values are higher than the final measurements. In this pH range ($\text{pH} > 6$), the edges are negatively charged and are available for cation exchange reactions (Lagaly, 1993). The coupled deprotonation (release of H^+) at the edges of the smectite particles thus leads to a relative decrease in pH.

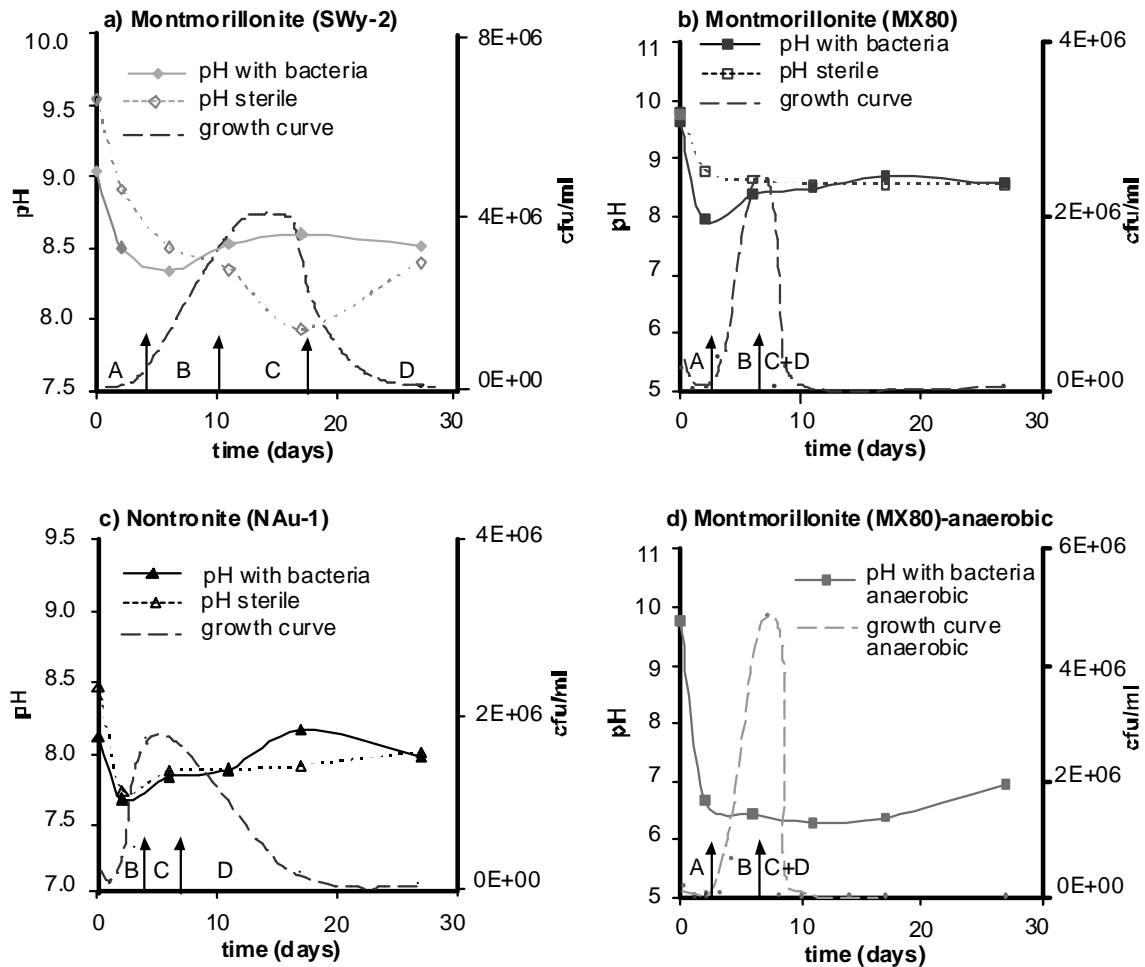


Fig. 5.3.3. Changes in pH over time for a-b) montmorillonite suspensions (aerobic), c) the nontronite (NAu-1) suspension (aerobic) and d) the montmorillonite (MX80) suspension (anaerobic). Filled symbols with solid lines indicate the evolution of pH values for samples containing bacteria; the empty symbols with dotted lines represent sterile controls. The corresponding growth curves are presented as dashed lines, and the recognized phases marked with vertical arrows: A-lag, B-exponential, C- stationary and D-death.

In case of the SWy-2 montmorillonite (Fig 5.3.3.a), the sterile control already shows a higher pH value at the initial stage than the bacteria containing sample (9.53 as opposed to 9.04). This is followed by a successive decrease of the pH during the first 6 days. The pH of the sterile control shows a further decrease after 17 days, reaching the lowest value of 7.93,

followed by an increase to 8.4 after 27 days. Successive measurements (not shown) indicate stable state conditions were reached with no further changes in pH. In contrast, the pH of the bacteria-containing samples shows a consistent increase after ~ 6 days and these are notably higher values than the sterile control. This period corresponds to a large portion of the exponential growth phase (B), the stationary phase (C) and the initial stages of the death phase (D).

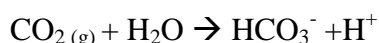
Both the bacteria-containing and the bacteria free MX80 montmorillonite suspensions show the same trend of rapidly decreasing pH during the first 2 days. The pH decrease to 7.9 in the bacteria-containing sample is the lowest observed during experimentation with a decrease of 19% as opposed to 13% change in the abiotic control. This corresponds to the beginning of the exponential growth phase (indicated as B in Fig. 5.3.3.b). This phase is accomplished after ca. 7 days and the death phases start almost immediately without a recognizable stationary phase. At the end of the death phase (after already 10 days), the pH stabilizes. This rapid decrease of bacteria is notably different from that observed in the system shown in Fig 5.3.1a and can be attributed to differences in the degree of agitation.

In the nontronite sample (Fig 5.3.3.c), the presence of bacteria results in a 5% lower pH value compared to the sterile control (8.1 as opposed to 8.5 for the abiotic sample). The lowest pH values were measured after 2 days with 7.74 for the sterile and 7.68 for the biotic sample. Unlike for the montmorillonite samples, the pH of the nontronite suspension does not correspond with the exponential growth phase (B) and the abiotic control shows the same trend. A difference between the sterile and biotic sample is only visible after 17 days when a relative pH increase occurring in the bacteria-containing sample is observed. During this time, the culture is in the final stage of the death phase (D).

The influence of anaerobic conditions on the pH is shown in Fig 5.3.3d for the MX80 montmorillonite sample. The used anaerobic bags produce CO₂ and, according to the equilibrium with the pCO₂, the pH is lowered producing more acidic suspensions (as low as 6.36 - 6.60). At the end of experimentation, near neutral conditions (6.95) are approached. This corresponds to a relative decrease of 32% compared to the starting pH (pH 9.7) within the first 2 days. The growth curve in the anaerobic example follows the same trend as in the aerobic suspension but the influence of the bacteria on the pH is masked by the CO₂ produced by the bags.

The relative differences in pH (expressed in %) between bacteria-containing experiments and the sterile controls are presented in Fig. 5.3.4. Negative values indicate a relatively lower pH and positive values reflect a higher pH compared to the sterile control. In this plot, the

zero line reflects no difference between bacterial and abiotic experiments. All bacteria containing samples were characterized by a relatively more acidic pH at the beginning of experiments (increase of H^+) and a more alkaline state during the intermediate to final stages of experimentation (decrease of H^+). The enhanced H^+ concentration observed during initial phases corresponds with the lag and exponential growth phase during which the bacteria are actively adapting and the production of biomass is highest. Here, the production of carbonic acid formed during respiration (or in case of the anaerobic experiments the artificial production of CO_2) contributes to a H^+ production according to the reaction



Additionally, the production of organic acids (such as oxalate, formate and propionate) also leads to a decrease in pH as reported for soils, sediments and aquifers (Barker et al., 1997).

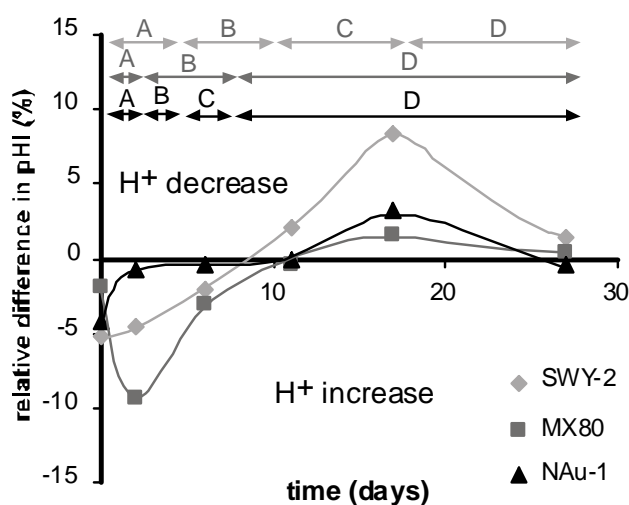


Fig. 5.3.4. Relative difference in the pH of bacteria containing smectite suspensions from the abiotic control expressed as a %. The phases of growth (A-D) are indicated as shown in Fig 5.3.2. Abbreviations for the growth phases: A-lag, B-exponential, C-stationary and D-death.

Although the pH for all solutions follows the same trend, being less alkaline at the beginning and more alkaline during the final stages, there are notable differences in the magnitude of bacterially induced pH differences between the different clays (Fig. 5.3.4). A relatively low deviation from the sterile control is visible for the nontronite that is quickly

approaching pH values of the sterile control (zero line). The bacterial density is already relatively high at this stage (1.71E05 cfu/ml) and the production of acids is likely to be active, suggesting that nontronite is quite successful in buffering the pH. After 17 days (peak in positive deviation), the amount of cfu is already decreasing (1.28E05 cfu/ml). In contrast, the amount of bacteria in SWy-2 is with 1E05 cfu/ml less than in nontronite but the negative deviation after 2 days is more pronounced (around 5 % less alkaline than the sterile control). Additionally, after 17 days (positive deviation of almost 9%), the number of cfu is enhanced with 3.84E06 per ml indicating that the pH changes are not dependant on the amount of cfu. Moreover, it seems that the pH deviations are linked to the presence of bacteria even when they are not viable because a similar pattern is visible for the MX80 although the culture accomplished the death phase much earlier.

5.3.2.2. Nontronite cation release into solution

The cation release from nontronite clay into purified water monitored by ICP-OES is presented in Fig. 5.3.5a. Concentrations of Al^{3+} , Si^{4+} , Ca^{2+} and $\text{Fe}_{(\text{tot})}$ were measured in the sterile nontronite suspension (0,01 g/ml) after 2h (light grey columns) and 264h (dark grey columns) of solution agitation. The dotted columns present the theoretical stoichiometric release of cations for comparison.

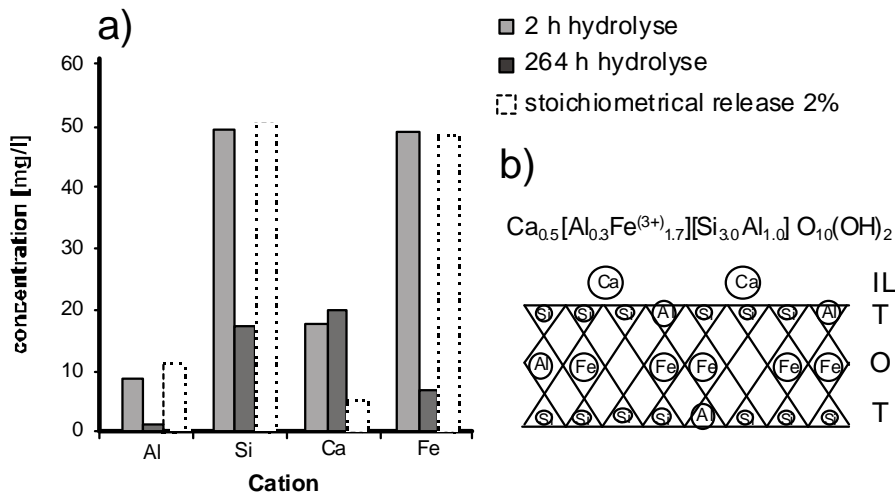


Fig. 5.3.5. a) The concentration of cations released from nontronite into purified water. Light grey columns indicate cation release into the solution after 2h of dispersion, dark grey columns after 264h. Columns in dotted lines correspond to 2% theoretical stoichiometrical cation release. b) Mineral formula and a schematic representation of cation sites in layered smectite structure (non-stoichiometric). Abbreviations: IL- interlayer, T- tetrahedral sites and O- octahedral sites.

The cation concentrations after 2h show some release of Al, Fe and Si that corresponds well to the stoichiometrical values indicating that both the tetrahedral and octahedral layers of some small nontronite grains dissolve (ca 2%) (Fig. 5.3.5b). In contrast, the concentration of the interlayer Ca^{2+} is ~3 times higher than the stoichiometric concentration, which can be attributed to rapid exchange with K^+ or H_3O^+ ions. The Ca concentration remained high after 264h (11 days) and corresponds to 8 % exchange of the total of exchangeable Ca (assuming this is the only interlayer cation). The concentrations of Al, Si and Fe in the suspension show a general decrease after the 264h period with respect to the first measurement. These decreases are (expressed in mg/l) Al^{3+} : 8.5 to 1.1 (~8 times less), Si^{4+} : 48.5 to 16.8 (~3 times less) and $\text{Fe}_{(\text{tot})}$: 48.3 to 6.6 (~7 times less). The Si:Al ratio in solution increases from around 5 (stoichiometric) to 15 as the relative amount of silica in solution increases with respect to Al. Higher amounts of Si relative to Al would indicate the preferred dissolution of tetrahedral edges sites (Bosbach et al., 2000; Bickmore et al., 2001) but could be, as well, due to Al precipitation from solution (values correspond to less than 1 % of nontronite dissolution). The iron released from the octahedral sites is here mostly trivalent (divalent is rapidly oxidized) and therefore does not stay in solution at pH 8 but is expected to precipitate as Fe(III) oxides.

The release of cations into bacteria containing nontronite-bearing solution (bacterial density $1.78\text{E}05\text{cfu/ml}$) is plotted in Fig. 5.3.6. Filled columns indicate the measured concentrations and empty columns represent the differences (depletions) relative to the sterile control (shown in Fig 5.3.5). The first measurements, after 2h, show some Si^{4+} , Ca^{2+} and $\text{Fe}_{(\text{tot})}$ dissolved in solution and virtually no Al^{3+} (light grey columns). After 264h, also no Al is detectable, whereas the concentration of Si^{4+} is slightly enhanced. Ca remains constant and $\text{Fe}_{(\text{tot})}$ shows a slight decrease. During this experiment, all the measured cations in solution have a lower concentration than the abiotic control indicating bacterial induced depletions of all measured elements. The largest differences are seen after just 2h of mixing: 12 times less Al (-7.8mg/l), 5 times less Si (-38.8mg/l) and 12 times less Fe (-44.4 mg/l) compared to the abiotic control. Values for Ca are around 2 times lower after 2h (-9.9mg/l) and around 2.5 times lower after 264h (-12.3mg/l). The concentrations of Al and Si after 264h approach that of the sterile control whereas, in the case of Fe, the differences are maintained with 4.6mg/l or 3 times less Fe in the bacteria containing samples.

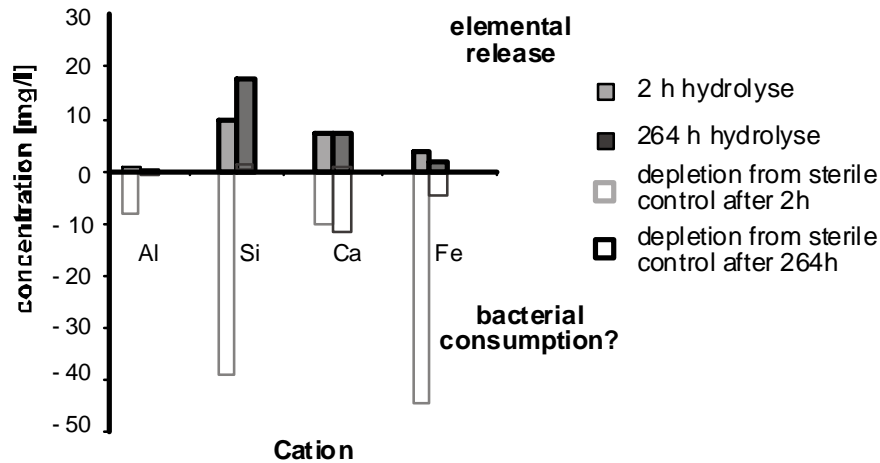


Fig. 5.3.6. The concentration of cations in solution derived from the bacteria containing nontronite suspension after 2h (filled light grey columns) and 264h (filled dark grey columns). Empty columns indicate the amount of depletion compared to the cation concentration of the sterile control.

The depletion of cations in the extracted solution of the *S. putrefaciens*-nontronite mixture may relate to: i) less dissolution and release of cations into solution, ii) cationic consumption (including complexation and “binding”) by bacteria or iii) temporal storage as precipitates or within biofilm. The most likely explanation for the lower cation concentrations is “consumption” by the bacteria, especially during the initial phases of growth, when nutrients are required the most. This explains well the lower concentrations of Ca and Fe but does not explain the decrease in Al, which is toxic to most bacteria and is therefore likely not to be consumed. In contrast, precipitation reactions in the case of Si and Al are the most probable explanation for the decrease in concentration of these elements.

The less pronounced difference in cation concentrations between sterile and bacteria containing suspensions observed after 11 days appears to be related to the death of bacterial cells (see corresponding growth curves in Fig. 5.3.3). As the experimental system is closed, cations that were consumed by bacteria can re-enter the solution during cell breakdown (lyses). This is not the case expected for cations stored in biofilm, as the polysaccharide often persists when the cells are already dead and disintegrating. As described by Leon-Morales et al. (2007) the storage of Ca^{2+} in biofilm at the same time aids to stabilize the extracellular structure. In this case, the relative lower amount of Ca might be associated to rapid biofilm formation, as it is already after just 2h relatively depleted.

5.3.2.3. Montmorillonite cation release into solution

The concentrations of the released cations Al^{3+} , Ca^{2+} , $\text{Fe}_{(\text{tot})}$, Mg^{2+} , Na^+ and Si^{4+} measured in sterile montmorillonite-bearing solutions (10 g of MX80 and Swy-2 per ml, respectively) is shown in Figs 5.3.7 - 5.3.8. The theoretical cation release that would correspond to the stoichiometry is also plotted as open dotted columns. The first measurement after 2h shows the enhanced release of the interlayer cations Ca and Na for both types of montmorillonites (SWy-2 and MX80) into the solution (Fig. 5.3.7b and 5.3.8b). Also relatively high amounts of Fe are detected and in contrast to the nontronite sample, only small amounts of Al or Si are released into solution.

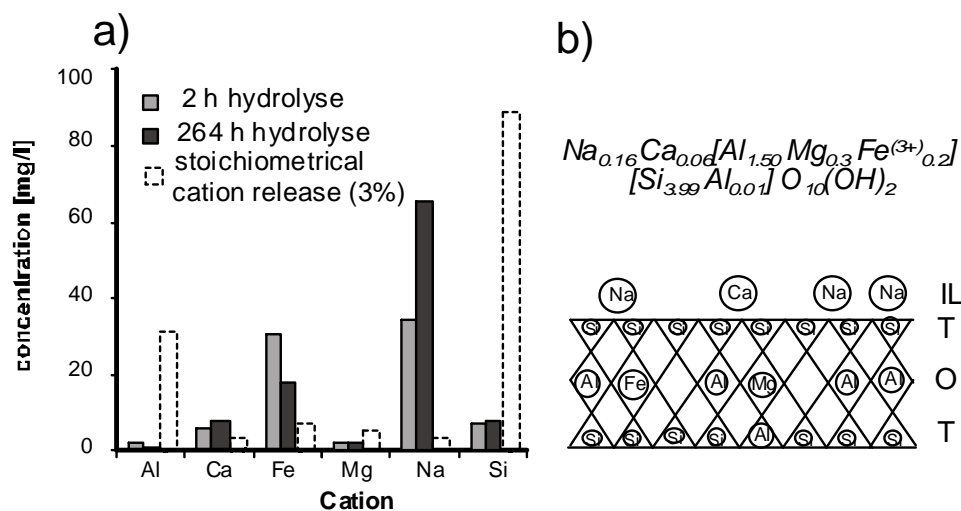


Fig. 5.3.7. The concentration of cations released from Wyoming montmorillonite (SWy-2) into purified water after 2h (light grey columns) and 264h (dark grey columns). Columns in dotted lines represent stoichiometrical cation release. b) Mineral formula and a schematic representation of cation sites in the smectite structure (non-stoichiometric). Abbreviation: IL- interlayer, T- tetrahedral sites and O- octahedral sites.

After 264h (11 days) of reaction, most of the cations are present in higher concentrations compared to the first measurement. Only Fe is relatively lower in concentration, which suggests that some precipitation occurs. Changes of the interlayer cation concentration expressed with respect to the first measurement show 14% more Ca and 37% more Na for the MX80 sample. For SWy-2, even higher amounts of Ca and Na are released (22% and 47%, respectively). Fe is present in lower concentrations in the SWy-2 suspension compared to the MX80 and its content decreases by 41% after the 11-day period. In the case of MX80, the corresponding decrease is only 7%. This rapid release of interlayer cations is quite similar to the behaviour of nontronite solution. The Fe detected in solution might be derived from the

octahedral sites of the smectite clay but the other octahedral coordinated cations, such as Mg, are not detected in the stoichiometrically equivalent concentrations suggesting another Fe source. Traces of chlorite in SWy-2 might be an explanation as reported for the bulk material (Chipera & Bish, 2001). However, as these are purified separates, it is not likely and the Fe source could be an artefact. In MX80, traces of pyrite are known to occur in the bulk material (0.5%, Sauzeat et al. (2001)). The relatively constant Fe values for this industrial bentonite powder in solution indicate relatively continuous Fe release. In the case of the SWy-2 sample, a portion of the Fe appears to be precipitated during the experiment.

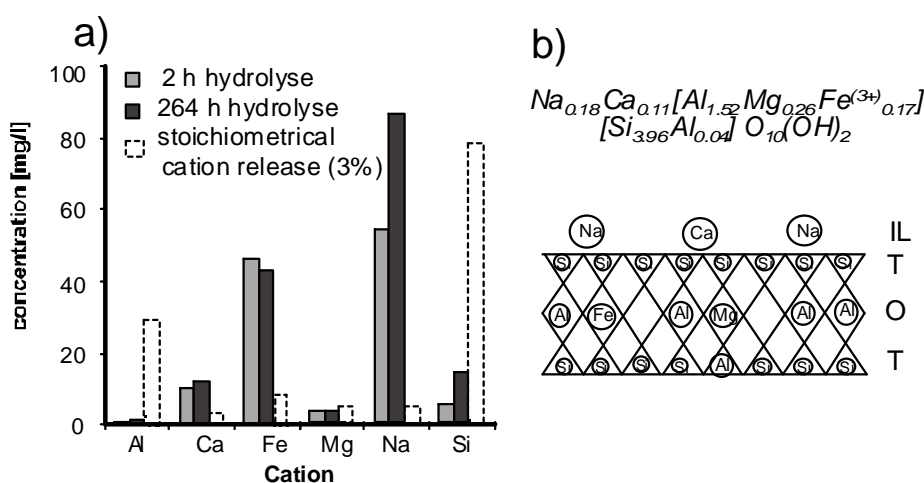


Fig. 5.3.8. a) The concentration of cations released from montmorillonite (contained in MX80) into purified water after 2h and 264h. Columns in dotted lines correspond to 3% theoretical stoichiometrical cation release. b) Mineral formula and a schematic representation of cation sites in the smectite structure (non-stoichiometric). Abbreviation: IL- interlayer, T- tetrahedral sites and O- octahedral sites.

The cations released in bacteria-containing suspensions (bacterial populations of $3.5E05$ and $2.12E05$ cfu/ml for MX80 and SWy-2) are plotted after 2h and 264h for both montmorillonites in Figs. 5.3.9 and 5.3.10. Compared to the abiotic control, the values measured after 2h show roughly the same pattern indicating the quick release of interlayer cations and Fe with only a small release of Si and Al. After 264h, the concentration of interlayer cations is enhanced and the Fe reduced. The cation difference for MX80 compared to the sterile control (empty columns in Fig. 5.3.9) reveal a decrease in Ca (13 and 17% after 2 and 264h) and Fe (13 and 24% after 2 and 264h, respectively). In contrast, a slight increase is observed for Na (5% after 264h) and Si (36 and 15% after 2 and 264h). In the SWy-2 bacterial experiment almost all cations show enhanced concentrations in the presence of bacteria. Ca is higher by 72 and 34% after 2 and 264h respectively, whereas Fe is enhanced to

56 and 45%, Mg by 53 and 34% and Na by 31 and 4%. Only Al and Si show negative values after the 2h time intervals with reductions of 43 and 40% for the two elements respectively.

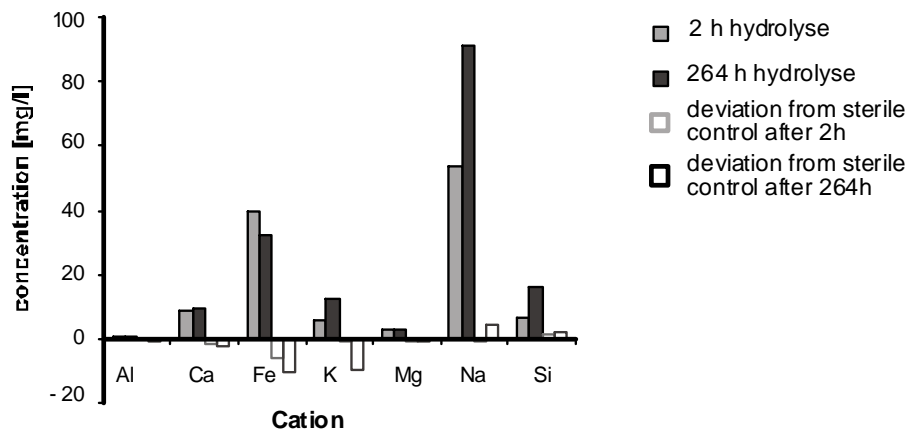


Fig. 5.3.9. The concentration of cations in solution derived from bacteria containing MX80 suspension. Empty columns indicate the amount of depletion compared to the cation concentration of the sterile control. In the case of Ca, Fe and K less cations are dissolved in solution when bacteria are present. Na and Si in contrast are slightly enhanced.

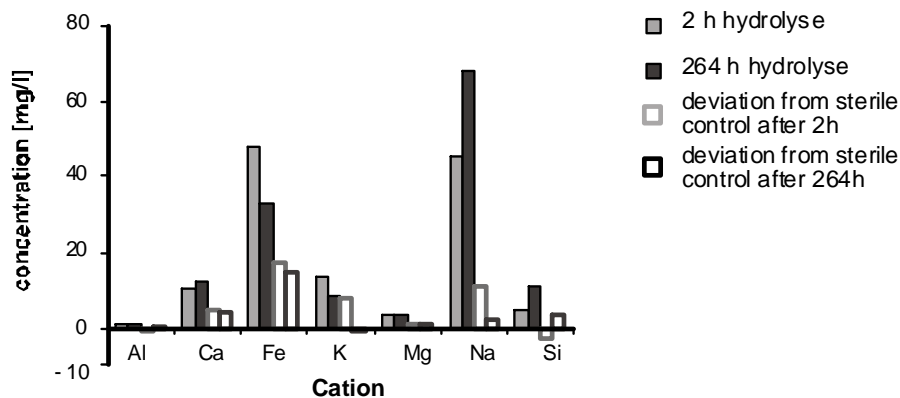


Fig. 5.3.10. The concentration of cations in solution derived from bacteria containing SWy-2 suspension. Empty columns indicate the amount of depletion compared to the cation concentration of the sterile control. Virtually all cations in solution are present in higher concentrations when bacteria are present.

The lower concentrations of Ca and Fe in solution of MX80 can be interpreted to reflect “consumption” by bacteria. Na is a nutrient for *S. putrefaciens* but is not depleted in any of the samples and might indicate a continuous supply from the interlayer sites. In the case of SWy-2, virtually all cations are enhanced when bacteria are present; this is especially true for Ca and Fe. The active growth of the culture (compare with Fig. 5.3.1) results in nutrient requirements and no other nutrients than the clay are supplied. With SWy-2, the rate of

dissolution might exceed the rate of consumption, leading to excess of cations. At least partly, this can be attributed to the small particle size ($<0.2 \mu\text{m}$) of the purified sample where relatively more edge sites for proton attack are available (Nagy, 1995) and bacterially mediated alteration is enhanced (Vandevivere et al., 1994; Welch & Vandevivere, 1994; Barker et al., 1998).

5.3.3. Microscopic Analysis

5.3.3.1. The role of biofilm: Confocal microscopy and ESEM

In order to evaluate the role of biofilm, both optical and electron microscopy were undertaken on selected samples. Fig. 5.3.11a shows a confocal microscope image of MX80 bentonite that was incubated 1 week with a fresh culture of *S. putrefaciens*.

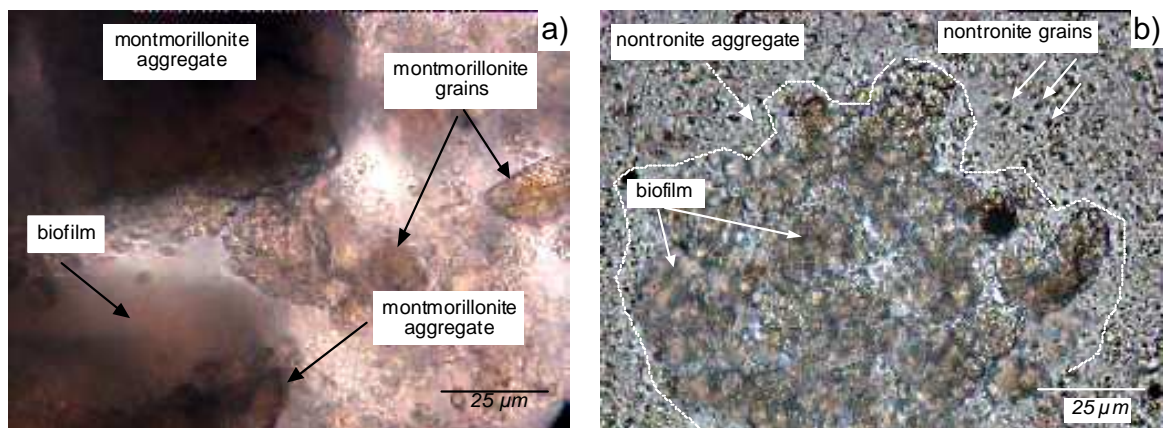


Fig. 5.3.11. Confocal transmitted light microscopy image of smectite incubated with *S. putrefaciens*. a) MX80 and b) nontronite. Biofilm appears within aggregates as diffuse structure.

The dark areas in the upper and lower left are montmorillonite aggregates, whereas single montmorillonite particles are visible in the centre. Especially in the darker regions, diffuse structures visible are attributed to patches of biofilm as described in other studies (Aouad, 2006). Fig. 5.3.11b shows a confocal microscope image of nontronite incubated with the bacteria under the same conditions. The grains of the nontronite are much smaller and the diffuse biofilm is concentrated around clay aggregates. In general, it is relatively difficult to distinguish biofilm from viable bacterial colonies because the smectite sorbs the staining products such as calcufluor and ethidium bromide for epifluorescence microscopy (see example in appendix).

Biofilm structures are well visible in the bacteria suspensions studied by ESEM. Examples of biofilms formed in a pure *S. putrefaciens* culture in minimal medium are given in Figs. 5.3.12a (fresh biofilm) and 5.3.12c (2 week old biofilm).

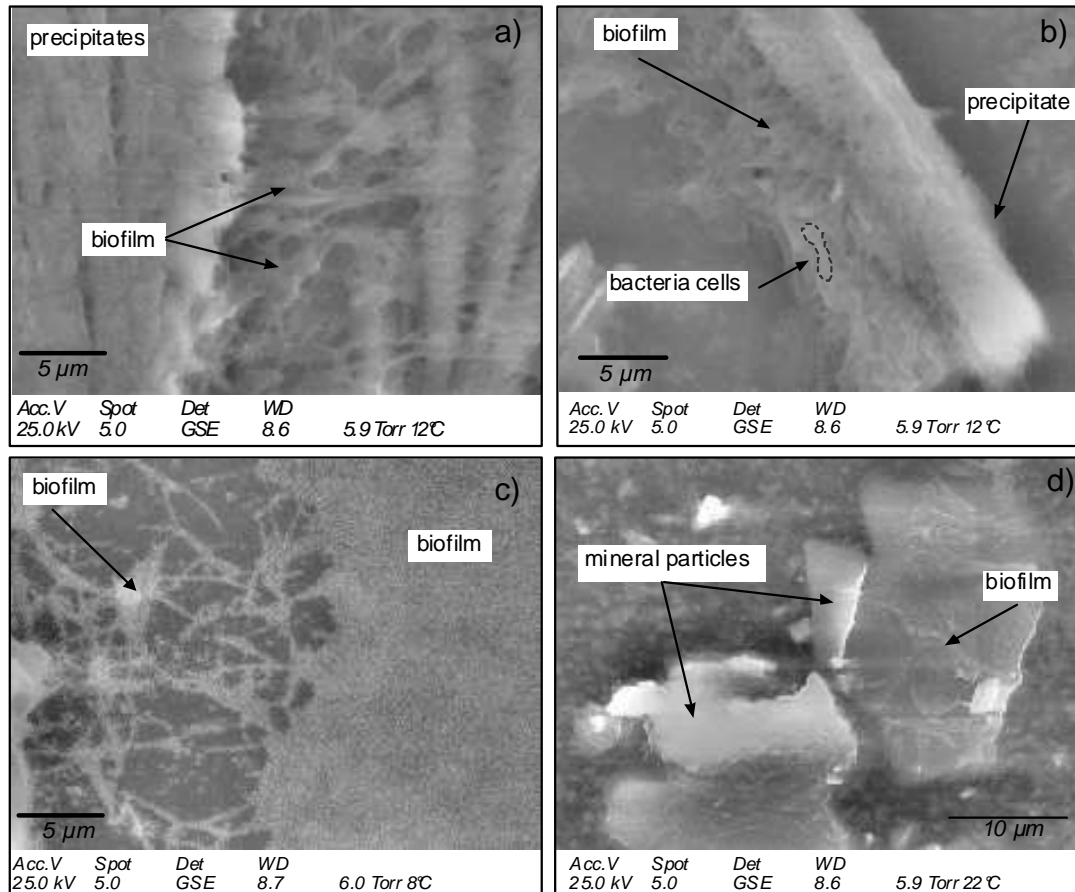


Fig. 5.3.12. a) ESEM image of a two day old *S. putrefaciens* culture forming biofilm around precipitates from the medium. b) Bacteria incorporated in biofilm attached to a phosphate needle that precipitated from the medium. c) ESEM image of a two week old culture after the majority of cells have died. The biofilm is still visible. d) ESEM picture of biofilm forming on mineral particles.

In the fresh biofilm, the net-like arrangement is associated with the needle-shaped precipitates from the medium and seems to be built by single cells attached to each other (Fig 5.3.12b). Those single cells are generally difficult to distinguish from each other because of the thick biofilm surrounding them (see dotted line in Fig 5.3.12b). In the 2 weeks old biofilm shown in Fig. 5.3.12c, no single cells are distinguishable. The biofilm is either present as fibrous, net-like structures (in the left part of the image) or as a relative homogenous mass, as shown in the right part. Fig. 5.3.12d shows two large mineral particles (supposedly quartz) with traces of biofilm on the surface. It seems that the cells colonized the surface and at the same time excreted substances that trace the former presence of the living cells.

5.3.3.2. Microscale interaction and microchemistry investigated by TEM

The TEM microphotograph of a pure culture of *S. putrefaciens* in Fig. 5.3.13a shows relatively large cells (average length 4 μm , width around 0.5 μm) that are in close vicinity to each other and arranged with end-to-end contacts. An EDX microanalyse of the cell in the center shows relatively high values for Na (3.4wt.% Na₂O), Mg (0.3wt.% MgO), P (3.4wt.% P_{tot}) S (1.2wt.% S_{tot}), and Ca (4.7wt.% CaO) that are typical compounds of the bacteria and partly due to the consumption of the incubation medium (table 3.4 in Chapter 3). The exception is K, which is contained in the medium in high amounts (~0.2g/l) but was detected only in small quantities in the bacteria cell (0.3 wt.% K₂O).

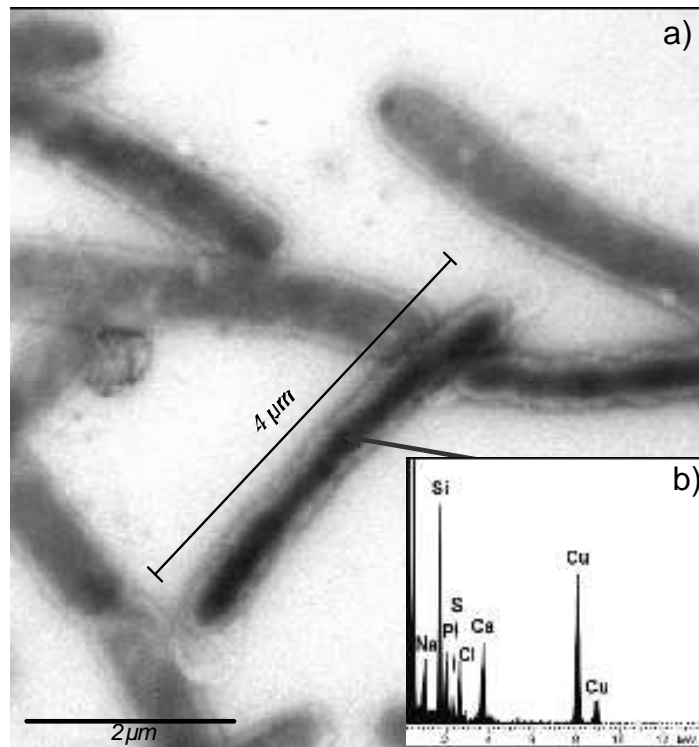


Fig. 5.3.13. a) TEM microphotograph of *S. putrefaciens* cultivated in minimal medium. b) EDX microanalysis of part of the cell marked by an arrow. The analysis shows high amounts of Na, P, S and Ca, as well as a Cu peak from the sample grid.

The measured composition of the cells is highly depending on the medium that was used for incubation. Fig. 5.3.14 shows a TEM microphotograph of a *S. putrefaciens* cell that was incubated in Fe-rich medium prior to washing and analyses. Compared to the control analysis of the grid (Fig. 5.3.14b), the cell shows typical enrichments in P (4.6 wt.% P_{tot}), S (1.2 wt.%

S_{tot}), Ca (1.5 wt.% CaO) and Fe (3.6wt.% Fe_{tot}) that might be present as coatings. As for the other examples, the cells incubated in this medium are relatively large, here around $3\mu\text{m}$.

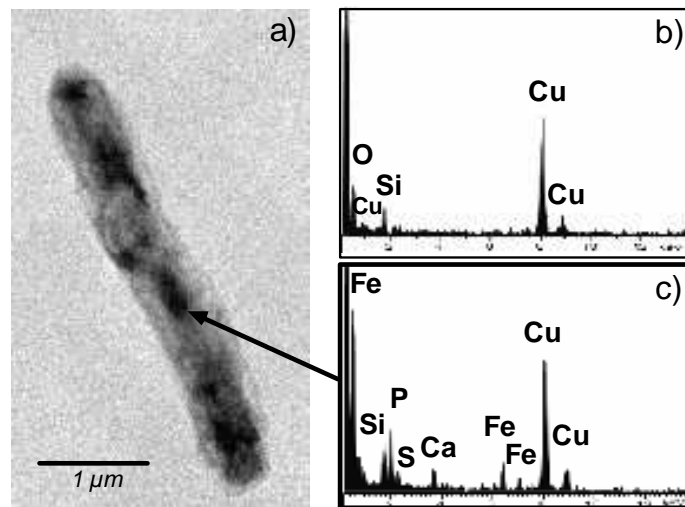


Fig. 5.3.14. a) TEM microphotograph of *S. putrefaciens* cultivated in Fe-rich minimal medium. b) EDX microanalysis of the coated grid. c) EDX microanalysis of the cell showing the bacterium to contain elements of the medium. The dark areas of the cell are Fe-rich (the Cu-peak is from the sample grid).

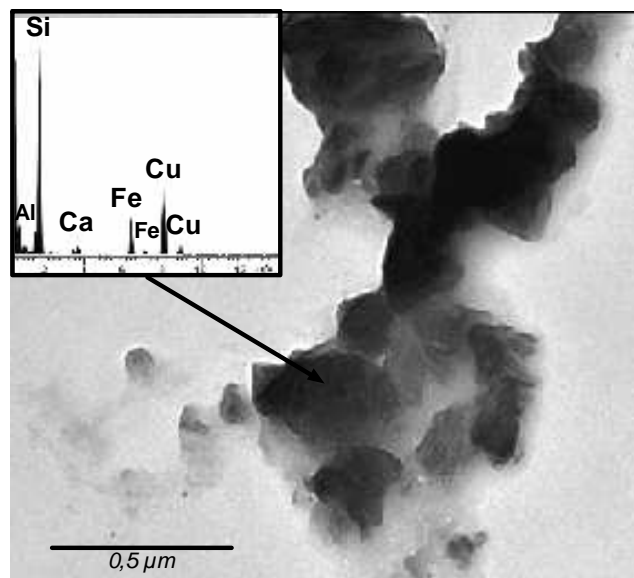


Fig. 5.3.15. TEM microphotograph and corresponding EDX spectra of nontronite particles. Microanalysis shows typically high amounts of iron (12.1 wt% Fe_{tot}). Quantification was done without correcting for C content derived from the sample coating. The Cu-peak comes from the sample grid.

In order to evaluate possible effects of bacteria on the clay, pure samples of nontronite were incubated with and without bacteria for a period of 10 days. A TEM image of the sterile nontronite sample is presented in Fig. 5.3.15 showing an aggregate formed by small

individual particles between 0.1 and 0.5 μm in size. Microchemical quantification of the particle shows the typically high values of Fe (12.1 wt.% Fe_{tot}) and the relative low values of Al (3.27 wt.% Al_2O_3) for nontronite. Ca is as well abundant (with 1.9 wt.% CaO) and mostly derived from the clay, whereas the small amount of Na (0.4 wt.% Na_2O) is probably derived from the experimental solution (Chapter 3).

The bacteria containing nontronite sample, after 10 days of bacterial activity, is shown in Fig. 5.3.16. Compared to the sterile one, the bacteria incubated sample shows particles with only diffusely defined edges surrounded by a homogenous, substance.

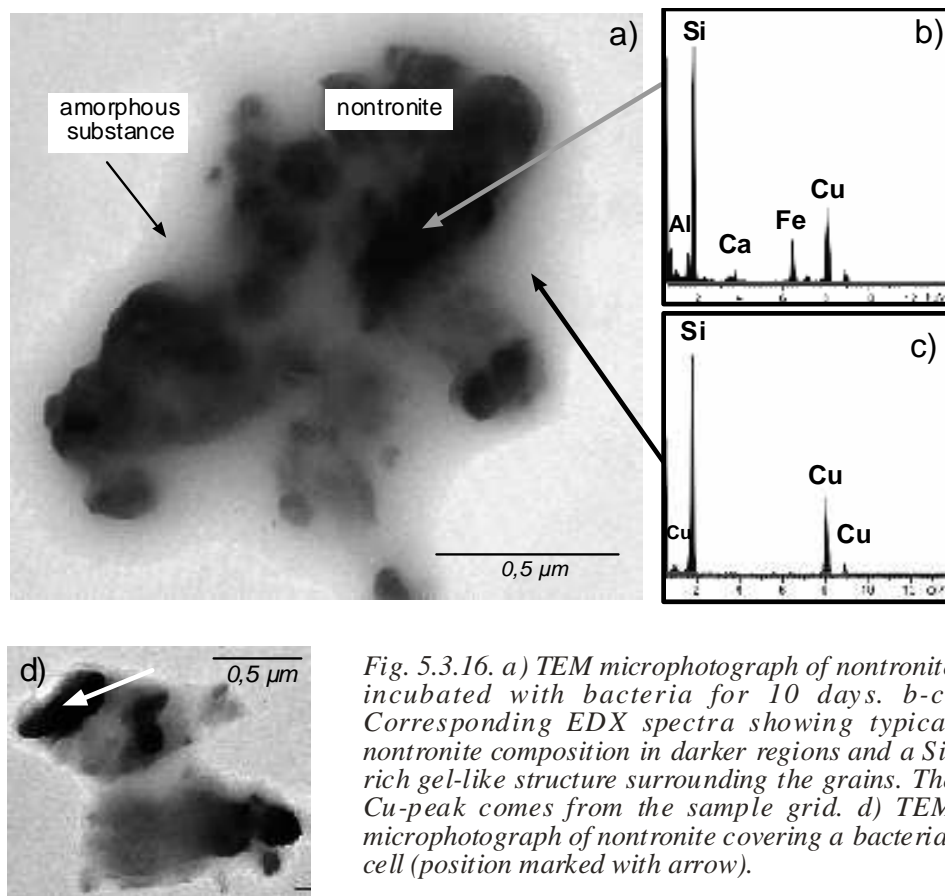


Fig. 5.3.16. a) TEM microphotograph of nontronite incubated with bacteria for 10 days. b-c) Corresponding EDX spectra showing typical nontronite composition in darker regions and a Si-rich gel-like structure surrounding the grains. The Cu-peak comes from the sample grid. d) TEM microphotograph of nontronite covering a bacterial cell (position marked with arrow).

Dark field imaging (not shown) confirmed the amorphous character. Corresponding microchemical analysis show high values of Fe (10.2 wt.% Fe_{tot}) and low concentrations of Al (2.8 wt.% Al_2O_3) in the electronically denser regions (Fig 5.3.16b). Additionally, a small amount of Ca was detected (1.3 wt.% CaO). In contrast, the analyses for the amorphous material around the particles show only traces of Fe and Ca (0.5 wt.% Fe_{tot} and 0.6 wt.% CaO, not indicated in spectra), no Al, and is mostly composed of Si (46.3 wt.% SiO_2 ; Fig. 5.3.16c). The *S. putrefaciens* cells in the clay are difficult to distinguish due to their much smaller size

(length $\sim 0.5\mu\text{m}$) compared to bacteria grown in pure cultures. The cells are mostly hidden within clay aggregates. Fig. 5.3.16d shows a bacteria cell partly covered by the nontronite particles as confirmed by the microchemical analyze that shows small amounts of P (0.4wt% P_{tot}) and S (0.4 wt.% S_{tot}) that are not present in the other analyses. The structure and composition of the amorphous substance surrounding the clay grains implies it is more likely a transitional gel material formed by partial dissolution of the nontronite as described in other studies (O'Reilly et al., 2006; Furukawa & O'Reilly, 2007). Additionally, the presence of EPS associated to the partly dissolved grains was described (Jaisi et al., 2007) but cannot be clearly confirmed due to the lack of P and or S in the analyze.

No significant differences are visible between the sterile samples and the ones incubated with bacteria for 10 days with MX80 bentonite.

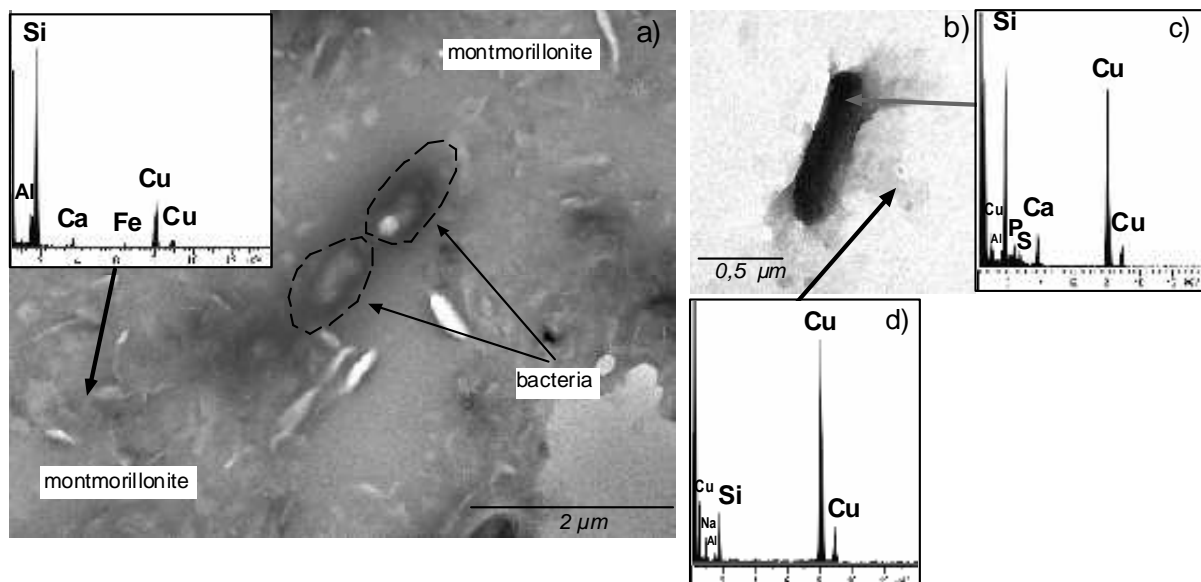


Fig. 5.3.17. a) TEM microphotograph of montmorillonite (MX80) showing relicts of a bacterial cell. The corresponding EDX spectrum shows typical values for montmorillonite. b) TEM microphotograph of bacteria cultivated in the presence of MX80 bentonite. The image shows a bacterial cell with montmorillonite wrapped around it. c) EDX spectrum of the cell. d) EDX spectrum of the montmorillonite.

The TEM image in Fig. 5.3.17a shows a typical example of montmorillonite clay with a diffuse mass marking the position of swelled particles. The darker objects in the center are most likely relicts of bacterial cells. Microchemical analyses show the presence of Na (2.3 wt.% Na_2O), relatively high amounts of Ca (3.2 wt.% CaO) and some Fe (0.5 wt.% Fe_{tot}). In some of the analyzed samples, bacteria are visible outside of the aggregates. Fig. 5.3.17b shows a close association between a bacterium and surrounding montmorillonite grains. The composition of the cell contains the elements P, S and Ca (P is 1 wt% P_{tot} , S is 1.6 wt.% S_{tot}

and Ca is 3.3 wt.% CaO; Fig. 5.3.17c). As seen in the nontronite sample, the bacteria are relatively small with lengths of around 0.5 μ m. The analyses of the clay grains contain Al, Si and Na, which are the major cations of montmorillonite (Fig 5.3.17d).

5.4. Bacteria - compacted clay interaction under confined volume conditions

5.4.1. In situ monitoring of smectite hydration by reaction-cell X-ray diffraction

The influence of *S. putrefaciens* on the following aspects are reported in this section, i) the smectites capacity for water uptake ii) the development and organization of water layer (WL) structures incorporated into the interlayers and iii) the partitioning of solution into the different storage sites (Chapter 4). Results in this section are given for nontronite and montmorillonite (MX80). Additionally changes in mineral assemblage of the bulk sample were studied.

5.4.1.1. Bacterial effects on total water uptake

Compacted nontronite powder (1.34 g/cm³) shows a high rate of water uptake in the absence of bacteria reaching a stable state after only ~72h (Fig. 5.4.1a). During this period, a total of 0.17ml/g entered the experimental reaction-cell. The equivalent bacteria-containing nontronite powder (packing density 1.37 g/cm³, inoculated with 2.8E06 cfu per g, table 5.4.1) show a slightly higher and slower water intake, reaching the steady state of 0.19ml/g after 840h. The uptake rates are accordingly higher for the sterile sample (2.4E-03ml/g/h) compared to 2.3E-04ml/g/h (table 5.4.2). At the end of the experiment, the bacteria containing sample shows a slightly higher amount of solution intake and contains 0.185ml/g compared to the sterile sample with 0.182ml/g.

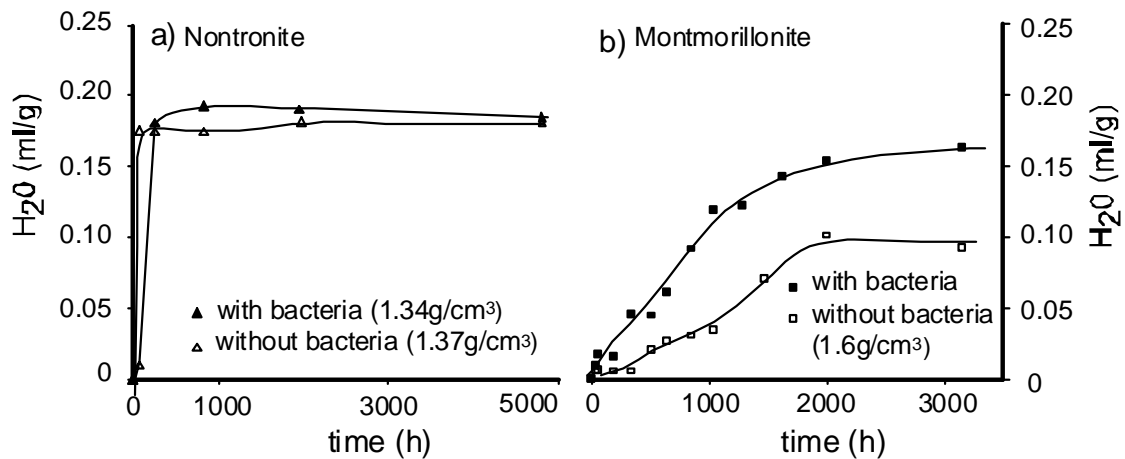


Fig. 5.4.1. Total water uptake into smectite powder determined by weight.

For montmorillonite (Fig 5.4.1b), the uptake is notably slower and less solution enters the powder. The sterile powder shows 0.10ml/g of solution intake after 1998h compared to 0.16ml/g after 3100h with bacteria (initial density $5.7E04$ cfu/g), and water inflow rates of $5.0E-05$ ml/g/h and $5.2E-05$ ml/g/h, respectively. As seen for nontronite, the total water uptake with bacteria is enhanced but this effect is more pronounced in the montmorillonite, with ~37% more uptake than during sterile clay hydration.

For nontronite, the bacteria appear mostly to influence the rate of total water uptake (lowering uptake rate) whereas for montmorillonite the amount of total uptake is the most affected (enhancing uptake).

	Solution	Ionic strength	Bacterial density initial (cfu/g)	Bacterial density during experiment (cfu/g)
<i>Nontronite</i>	MM	0.039	$2.8E06$	$4.6 E06$ (after 2000h)
<i>Montmorillonite</i>	Salt Solution	0.011	$5.7E04$	$4E06$ (after 600h)

Table 5.4.1. Ionic strength of solutions and bacterial densities.

5.4.1.2. Bacterial effect on interlayer water uptake

The water layer distribution was obtained from the X-ray diffraction patterns using CALCMIX as described in Chapter 3. Fig. 5.4.2 shows the development of water layer (WL) structures expressed in % against time (hours) for nontronite (a+b) and montmorillonite (c+d) with and without bacteria.

Effect on nontronite interlayer water uptake

For sterile nontronite, the initial hydration state consisted of a mixture of the following water-layer (WL) structures: 45% 3-WL, 44% 2-WL and 11 % 0-WL (Fig. 5.4.2a). The curve for normalized solution uptake (normalized to the maximal uptake after 1 year, data not shown) shows rapid intake corresponding to the formation of the 1 and 3-WLs. These structures are formed at the expense of the 2-WL structure and replace the initially non hydrated structure (0-WL). During the experiment, the abundance of WL structures reaches a stable state after 2000h and, after 5000h (~ 30 weeks) of experimentation the water layers have a final composition of 62% 3-WL, 29% 2-WL and 9 % 1-WL. In the bacteria-containing sample, the initial water layer structures show slightly higher hydration states than the sterile control, composed of 45% 3-WL, 35% 2-WL and 2 % 4-WL (Fig. 5.4.2b). These differences most likely represent some initial hydration during the addition of the water-bearing bacterial preparation. During hydration and the initial stage of rapid uptake into the experimental reaction-cell, the 3 and 4- WL structures develop largely at the expense of the 2-WLs. At the end of the experimental run, the 3-WL dominates with 85%, the 4-WL decreases slightly to 10% and the 2-WL has only 5% abundance at the steady state. The addition and presence of bacteria during nontronite hydration led to the presence of thicker water layer structures, with the dominance of 3- and 4-WLs and to more prolonged changes in the hydration state than the sterile control. Compared to the 2000hours needed to reach the steady state condition, the bacteria containing nontronite had not stabilized after 5000h of experiment time.

Effect on montmorillonite (MX80) interlayer water uptake

In the case of the montmorillonite (contained in MX80), the development of the water layer structures is slower and more complex. For the sterile sample (Fig. 5.4.2.c), the initial state comprises 45% 3-WL, 15% 2-WL and 40 % 1-WL. The 1-WL structure decreases continuously until disappearing completely after 1038h, when the 4-WL structure (10%) develops. The 2-WL remains stable as long as the 1-WL is present and, subsequently decreases until stabilizing at 10% after 1038h. The 3-WL continuously increases from the beginning of hydration and stabilizes after 1998h as the most abundant structure (80 %). The highest rates of total water uptake (normalized curve) correspond to the initial increase in 2-WLs during the first hours of hydration and the more persistent increase in 3-WLs occurring up to 1500h.

When bacteria are present, the 1 and 2-WLs (each with initial 30% abundance, Fig. 5.4.2d) decrease more rapidly than observed in the sterile sample and both structures are

replaced by thicker hydrated structures. Here, the 1-WL decreases to $\sim 17\%$ and its disappearance matches with the formation of 4-WL (starting with 18%) after 630h. In the case of the 2-WL, it decreases down to 5% and disappears after 1279h. This corresponds with the formation of a structure at $\sim 22.4\text{\AA}$ (for reasons of simplicity referred to as 5-WL structure) that remains constant at 5%. As seen for the sterile sample, the 3-WL structure dominates but develops more quickly in the presence of bacteria. The stable state is reached in a third of the time, after just $\sim 630\text{h}$, and stabilizes with 68% 3-WL, 27% 4-WL and 5% 5-WL structures. The total water intake also continues after stabilization of the interlayer structure (after 2500h), showing a similar behaviour to the abiotic (sterile) sample.

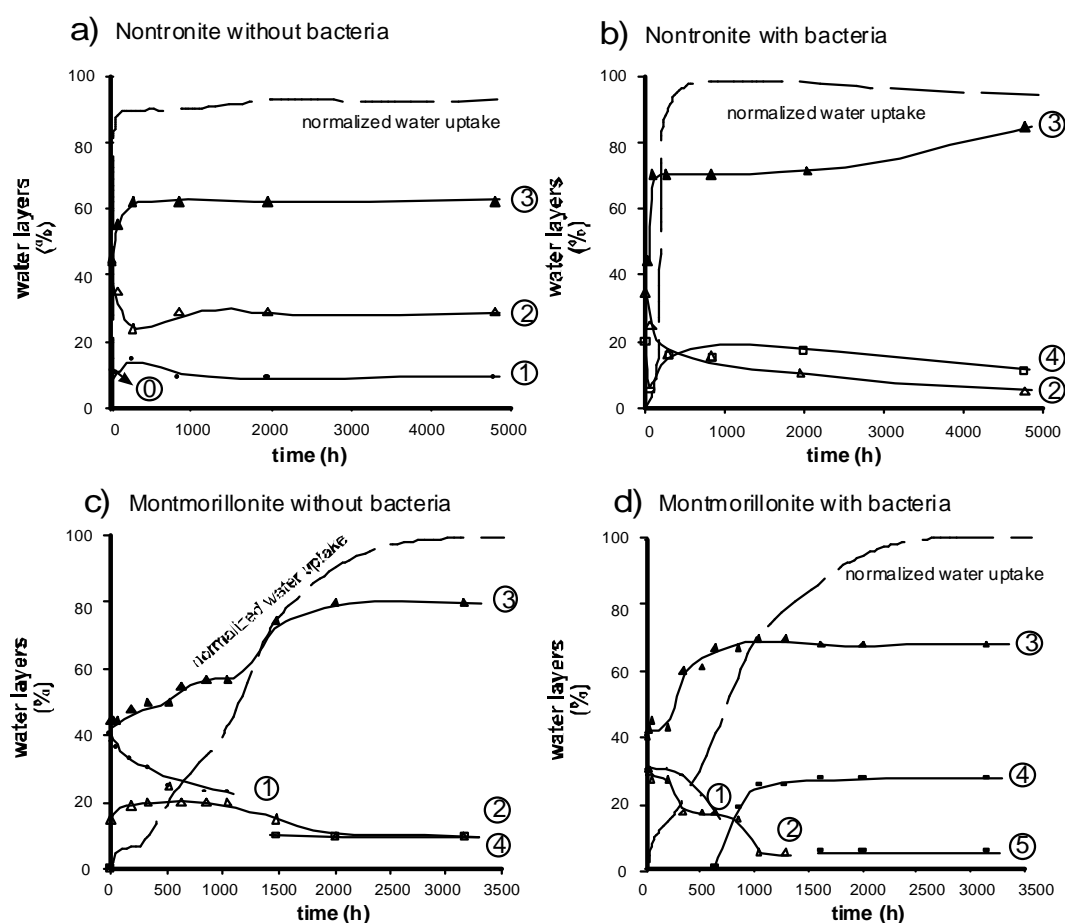


Fig. 5.4.2. a-b) Abundance of water layers for nontronite (NAu-1) and montmorillonite (MX80) without and with *S. putrefaciens*, expressed in percent (%) vs. the reaction time (in hours). Encircled symbols indicate the number of water layers within the hydrating interlayer. The dashed lines show the normalized total water uptake determined by weight.

The thicker water structures formed in montmorillonite in the presence of bacteria follow the same trend observed in the nontronite clay. Expressing the WL distributions as mean thicknesses (d-values) shows generally higher initial values for nontronite (16.1 and 17.7\AA for

the sterile and bacteria containing sample) than for the montmorillonite (15.6 and 15.7Å for the sterile and bacteria containing sample, table 5.4.2). Subtracting the initial mean thicknesses from the values representing the final stage of swelling yields a mean d-value difference (Δd). The Δd values of the bacteria containing samples are higher confirming the formation of more space consuming WL structures, whereas the difference between the sterile and bacteria containing samples notably is more pronounced for montmorillonite.

		Nontronite				MX80			
		Sterile		With bacteria		Sterile		With bacteria	
<i>Water layers</i>	<i>d-value</i>	<i>Initial</i>	<i>Final</i>	<i>Initial</i>	<i>Final</i>	<i>Initial</i>	<i>Final</i>	<i>Initial</i>	<i>Final</i>
0	9.6	0.11							
1	12.2		0.09	0.35	0.05	0.4		0.30	
2	15.2	0.44	0.29	0.45	0.80	0.15	0.10	0.30	
3	18.5	0.45	0.62	0.20	0.15	0.45	0.80	0.40	0.68
4	20.2						0.10		0.27
5	22.8								0.05
<i>Mean thickness (Å)</i>		16.1	17	17.7	18.5	15.6	18.3	15.7	19.2
Δd		0.9		1.05		2.7		3.5	

Table 5.4.2. Water layer abundance (%) and corresponding basal lattice d-values for sterile and *Shewanella*-bearing nontronite and MX80 bentonite clays.

Organization (ordering) of interlayer water in nontronite

The organization of WL structures with and without bacteria is shown in Fig. 5.4.3, normalized to the random case. The deviation from $R=0$ for the sterile and bacteria containing nontronite is given in Fig. 5.4.3a and b. Without bacteria, the deviation from random stacking is positive for the same WL structures indicating an elevated probability for this arrangement. Highest values are obtained for the probability that 1-WL follows 1 (p_{11} : 0.61-0.81) but, as well, p_{22} is a probable combination (p_{22} : 0.51-0.66). Values for p_{33} are lower (0.23-0.38) but show, relative to the random case, a higher probability. Accordingly, other combinations are less probable (e.g. p_{32} ranging between -0.17 and -0.30; p_{23} ranges between -0.45 and -0.57). When bacteria are present, the deviations from R_0 are less systematic. Combinations for the same WL structures are favoured as a tendency (e.g. p_{22} , but maximum is only 0.25). The only combination that seems to have a systematic higher probability is that 4-WLs are followed by 3 (p_{43} with highest values of 0.75). As the system with bacteria is generally more hydrated, a direct comparison is difficult. However, with increasing hydration a systematically increase in ordering was observed (Chapter 4) indicating that the presence of bacteria induces the observed fluctuations.

Organization (ordering) of interlayer water in montmorillonite (MX80)

In case of the MX80, the deviations are generally more systematic (Fig. 5.4.3.c +d) and values are lower compared to the nontronite indicating the tendency towards random stacking. Without bacteria, the probabilities for the same WL structures to be adjacent to each other is however slightly lower than the random case (maximum value for p22 is -0.2). In contrast, slightly enhanced probabilities are visible for 3-WL followed by 2-WL (p32 ranging from 0.06 to 0.25), and for 2-WLs followed by 1-WL (p21 ranging between 0.12 and 0.47). The probability of 1-WL is followed by 3-WL is also higher than random (p13 ranging from 0.03 to 0.25).

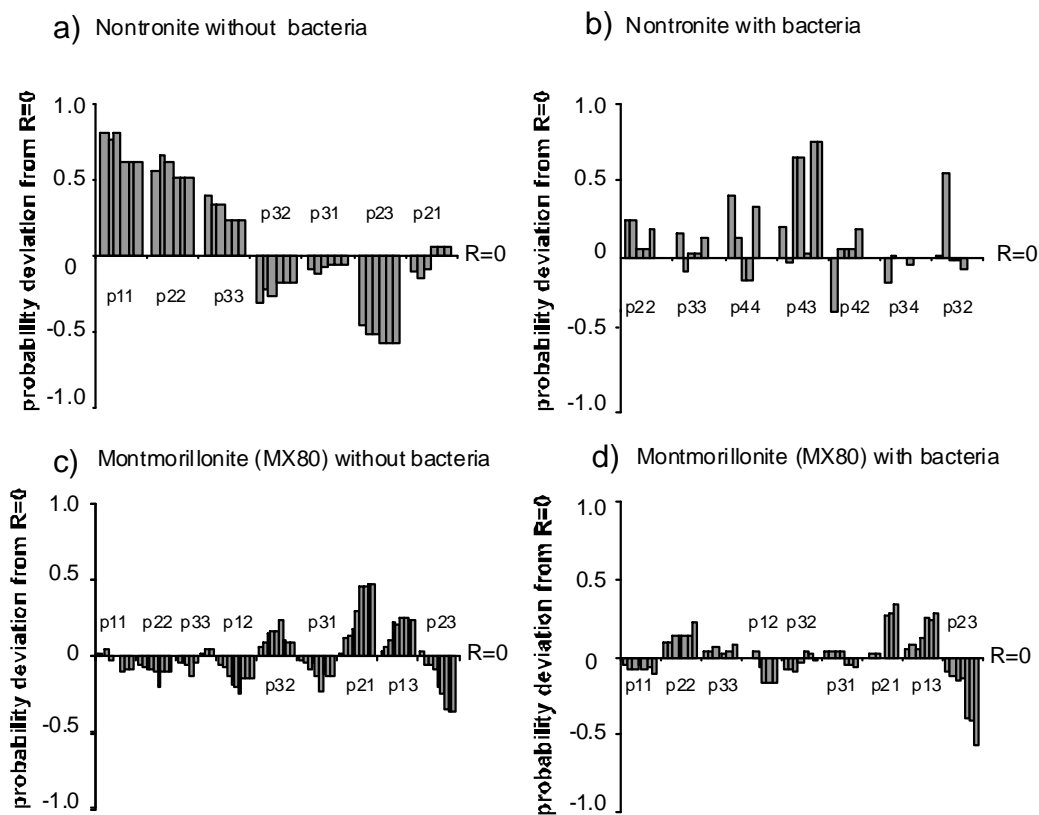


Fig. 5.4.3. Ordering of mixed water layer structures expressed as a deviation from the R0 (random) stacking state for a) nontronite without bacteria, b) nontronite with bacteria, c) montmorillonite (MX80) without bacteria, and d) montmorillonite (MX80) with bacteria.

This pattern indicates a preferred stacking order of 3-WL-1-WL-2-WL. When bacteria are present, the deviations from random are, for most of the combinations, less pronounced. The probability that 2-WL is followed by the same 2-WL is slightly enhanced (p22 ranges between 0.1 and 0.23) as is the 2-WL followed by 1-WL (p21 maximally 0.34) and the 1-WL

is followed by the 3-WL (p13 between 0.05 and 0.28). The combination 2-WL followed by 3-WL (maximum value for p23 is -0.57) is not very probable. Therefore the preferred stacking order with bacteria in montmorillonite is as a tendency toward 2-WL-1-WL-3-WL structures, having like in the abiotic sample, the 1-WL in the center.

5.4.1.3. Bacterial effects on the storage of water

Measured and calculated water contents for nontronite (a+b) and montmorillonite contained in MX80 (c+d) are plotted in Fig. 5.4.4. The amount of interlayer water was calculated from the relative abundances of water layer structures obtained by CALCMIX in combination with published data (Bérend et al., 1995; Cases et al., 1997; Jänchen et al., 2006; Milliken & Mustard, 2007). For details, see Chapter 3 and the appendix. Subtracting this values from the total water uptake (determined by weight; cp. Fig 5.4.1.) gives the non-interlayer water (displayed as surface and pore water). Significant amounts of solution were introduced during the mixing process of clay and bacteria (each containing 0.25ml solution with or without bacteria per g clay). Therefore, the initial water is included in Fig 5.4.4.

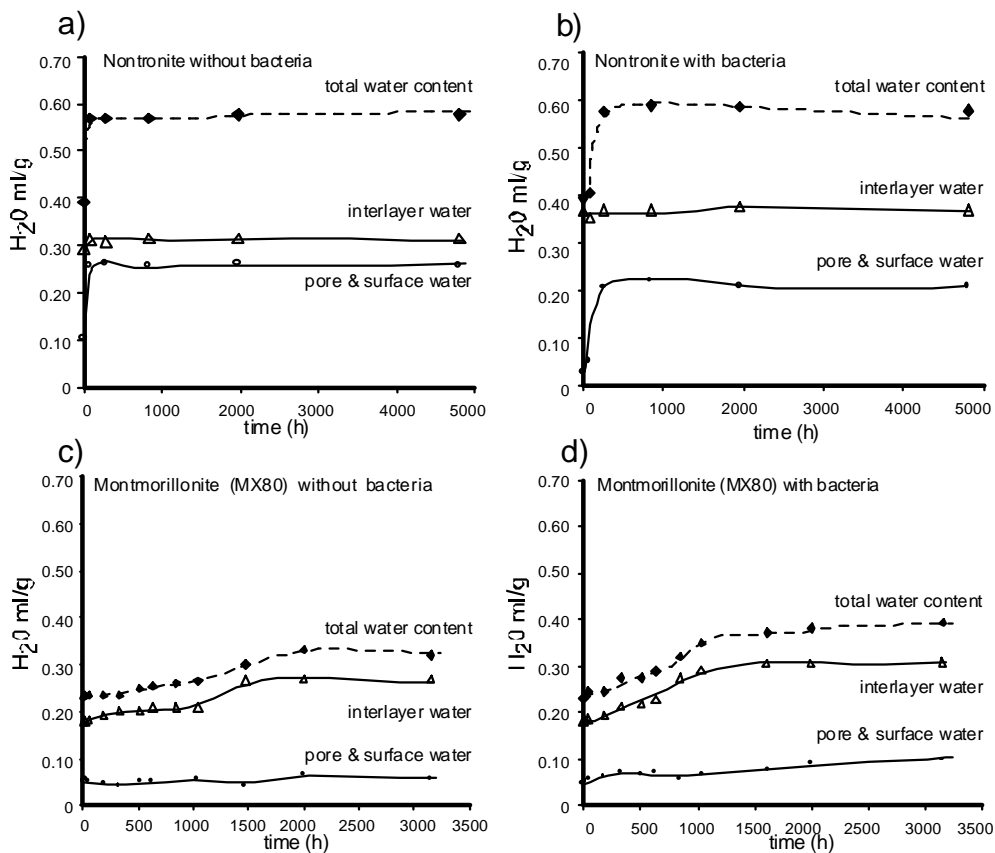


Fig. 5.4.4. a-d. Storage of water in interlayer and non-interlayer sites from nontronite (NAu-1) and montmorillonite (MX80) without and with *S. putrefaciens*.

Water storage in nontronite

The initial total water content in the sterile and bacterial containing nontronite clay was almost identical, with values of 0.39ml/g and 0.40ml/g, respectively (table 5.4.3). After complete hydration of the two samples, the total water content also reached comparable levels with 0.58ml/g, representing ~67-69% of the water uptake since the first measurements started. A significant difference is visible between the initial values of interlayer water contained in the sterile and bacteria-containing sample (0.27ml/g in contrast to 0.36ml/g). At initial states, the proportion of interlayer water on total water is 69.2% for the sterile sample and 90% for the bacteria-containing sample.

With the sterile sample, around 15% of the water inflow is stored as structured interlayer water and taken in at a rate of 4.6E-05ml/g/h during 863h. The same period is needed to complete non-interlayer water uptake resulting at a rate of 1.6E-04ml/g/h. The sample with bacteria shows generally higher values of uptake (Fig. 5.4.4 b), a larger proportion of interlayer water and a reduced level of surface- and pore water. However, no additional water is taken into the interlayers but only into non-interlayer sites. This non-interlayer uptake is accomplished within 839h at a rate of 2E-04ml/g/h. The addition of bacteria to the clay before packing into the reaction-cell appears to have caused more interlayer swelling in the initial state, which inhibits further interlayer uptake into the system. However, absolute values of interlayer water are higher than those measured in the sterile sample.

	Nontronite	Nontronite with bacteria	Montmorillonite	Montmorillonite with bacteria
<i>Total water</i>	<i>Initial / Final</i>	<i>Initial / Final</i>	<i>Initial / Final</i>	<i>Initial / Final</i>
Content [ml/g]	0.39 / 0.58	0.40 / 0.58	0.23 / 0.32	0.23/ 0.39
<i>Interlayer water</i>				
Content [ml/g]	0.27 / 0.31	0.36 / 0.38	0.19 / 0.27	0.19/ 0.30
Proportion [%]	69.2 / 53.4	90 / 65.5	82.6/ 84.4	82.6 / 76.9
Saturation time [h]	863	-	1470	1615
Uptake rate [ml/g/h]	4.6E-05	-	1.8E-04	6.8E-05
<i>Non-interlayer water</i>				
Content [ml/g]	0.12 / 0.26	0.04 / 0.20	0.05 / 0.05	0.04/ 0.09
Proportion [%]	30.8 / 46.6	10 / 34.5	17.4 / 15.6	17.4 / 23.1
Saturation time [h]	863	839	-	3151
Uptake rate [ml/g/h]	1.6E-04	2E-04	-	3.2E-05

Table 5.4.3. Experimental results used to calculate the rates of water uptake into the various storage sites of nontronite and MX80 montmorillonite clays with and without bacteria.

Water storage in montmorillonite (MX80)

The montmorillonite, in contrast to the nontronite clay, takes the majority of water into the interlayers (between 76.9 and 84.4%). In the sterile and bacteria containing montmorillonite samples, the proportions of total, interlayer and non-interlayer (surface and pore) water are the same in the initial state prior to water inflow (Fig 5.4.4c+d). The 0.23ml/g initial total water content is distributed as 82.6% interlayers (0.19ml/g) and 17.4% non-interlayer (0.05g/ml). A significant difference in the total water content between the sterile and bacteria samples is observable after hydration is complete, with higher amount of water incorporated in the presence of bacteria (0.39ml/g as opposed to 0.32ml/g). The additional 0.07ml/g is distributed almost equally between the interlayer and non-interlayer sites (0.03ml/g and 0.04ml/g, respectively). Therefore the presence of bacteria in montmorillonite sample leads to a general enhancement of water content at all sites.

Changes in particle thickness

Because of the initially elevated hydration state, the number of layers per particle is, in the case of the nontronite sample, already low at the beginning (N=7 with bacteria and 8 without). For MX80, the number of layers per stack is 9 for both initial samples, which during hydration decreases to 3 for the bacteria containing sample and to 5 in the sterile sample (table 5.4.4). Theoretically, this corresponds to an enhanced surface area when bacteria are present (190m²/g as opposed to 114m²/g for the sterile sample) that could accommodate larger volumes of water than actually observed. Based on these values, a maximal of ~29% surfaces participation is estimated in the sterile system and, when bacteria are present, the participation is 31%.

	Layers per stack initial	Layers per stack final	External surface area Initial [m ² /g]	External surface area final [m ² /g]	Maximal surface adsorbed water [ml/g]	Maximal participation of surface [%]
MX80 with bacteria	9	3	63.4	190	0.46*/0.29**	19.6*/31**
MX80 sterile	9	5	63.4	114.1	0.27*/0.17**	18.5*/29.4**

*Table 5.4.4. Mean number of layers per stack and corresponding theoretical surface area for MX80 montmorillonite with and without bacteria. *Assuming 19 layers per stack for the “dry” state and *4 and **2.5 mmol H₂O/g for the amount of adsorbed surface water.*

5.4.2. Characterization of reaction products

5.4.2.1. Powder XRD

Powder XRD of nontronite

The whole rock XRD patterns of the nontronite clay (initial and final measurements) for bacteria containing and sterile samples are presented in Fig. 5.4.5 a and b.

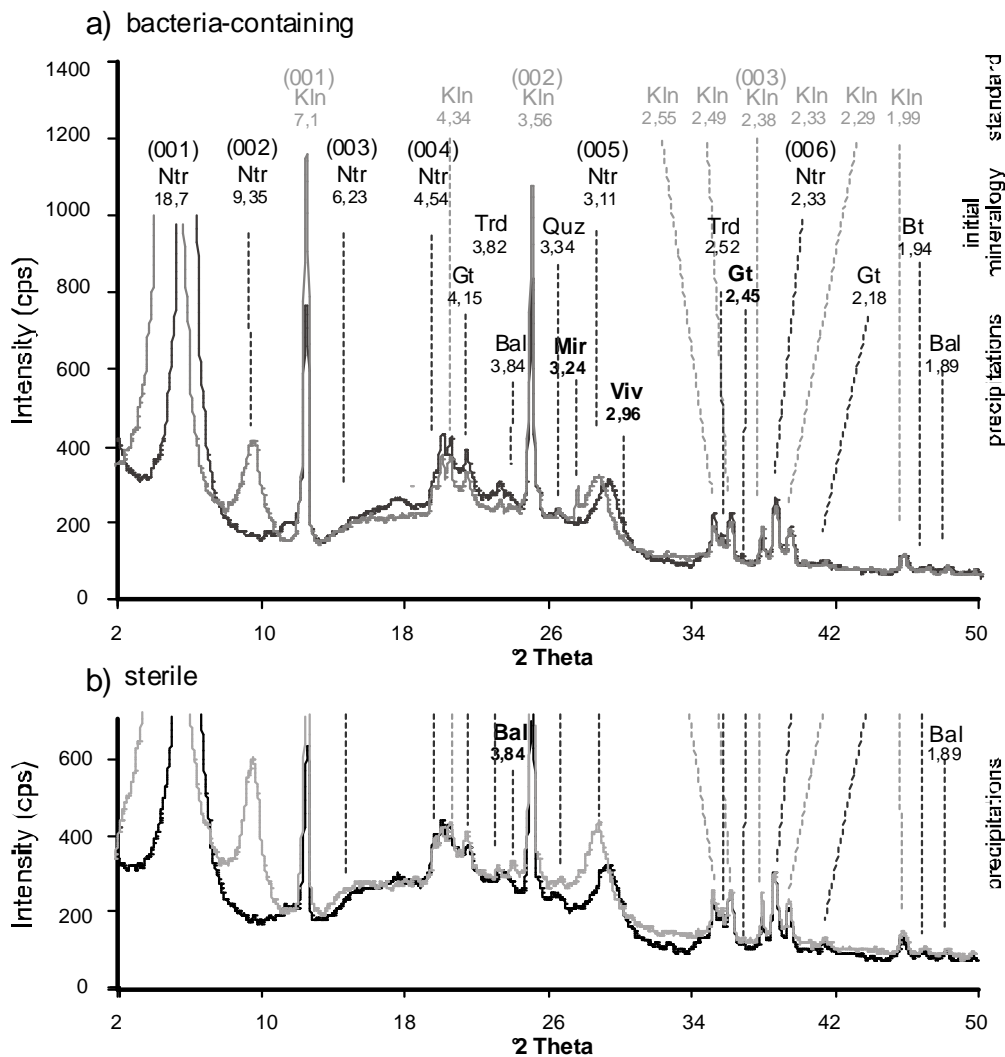


Fig. 5.4.5. a) XRD patterns of initial (black) and final (grey) bacteria containing nontronite powders extracted from the reaction-cell experiments. Basal reflections of hydrated nontronite (Ntr) and the internal standard kaolinite (Kln) are indicated with corresponding d-values in Å. Additionally both samples contain goethite (Gt), tridymite (Trd), biotite (Bt) and precipitations of the Al-sulphate basaluminite (Bal). Mirabilite (Mir) and vivianite (Viv) are only contained in the final reaction products (bold). b) XRD patterns of the initial sterile nontronite (black) and the final measurements made at the end of the experiment (grey). The final reaction products show enhanced basaluminite precipitation (bold).

The kaolinite (indicated in grey) which was added to the upper surface of the pressed powder sample as an internal standard and shows sharp multiple reflections at 7.1Å (001) and 3.56Å (002). The reflections of nontronite (presented for the hydrated state) correspond to a predominantly 3-WL hydrate and are positioned at 18.7Å (001), 9.35Å (002), 6.23Å (003), 4.54Å (004) 3.11Å (006) and 2.33Å (007). Additionally, tridymite (reflections at 3.82Å and 2.52Å), biotite (1.94Å) and goethite (4.15Å and 2.18Å) are detected in the sample pattern. The Al-hydroxo-sulfate basaluminite ($\text{Al}_4(\text{OH})_{10}\text{SO}_4$) is present in both samples with reflections at 3.84Å and 1.89Å. In the bacteria containing sample (Fig. 5.4.4.a), mirabilite ($\text{Na}_2\text{SO}_4 \cdot 10\text{H}_2\text{O}$) is visible with a reflection at 3.24Å which is most probably precipitated from the medium. Additionally, some vivianite ($\text{Fe}_3(\text{PO}_4)_2 \cdot 8(\text{H}_2\text{O})$) is present with a peak at 2.96Å.

Powder XRD of montmorillonite (MX80)

Selected whole rock XRD patterns of the hydrating sterile MX80 bentonite clay, are presented in Fig. 5.4.6.

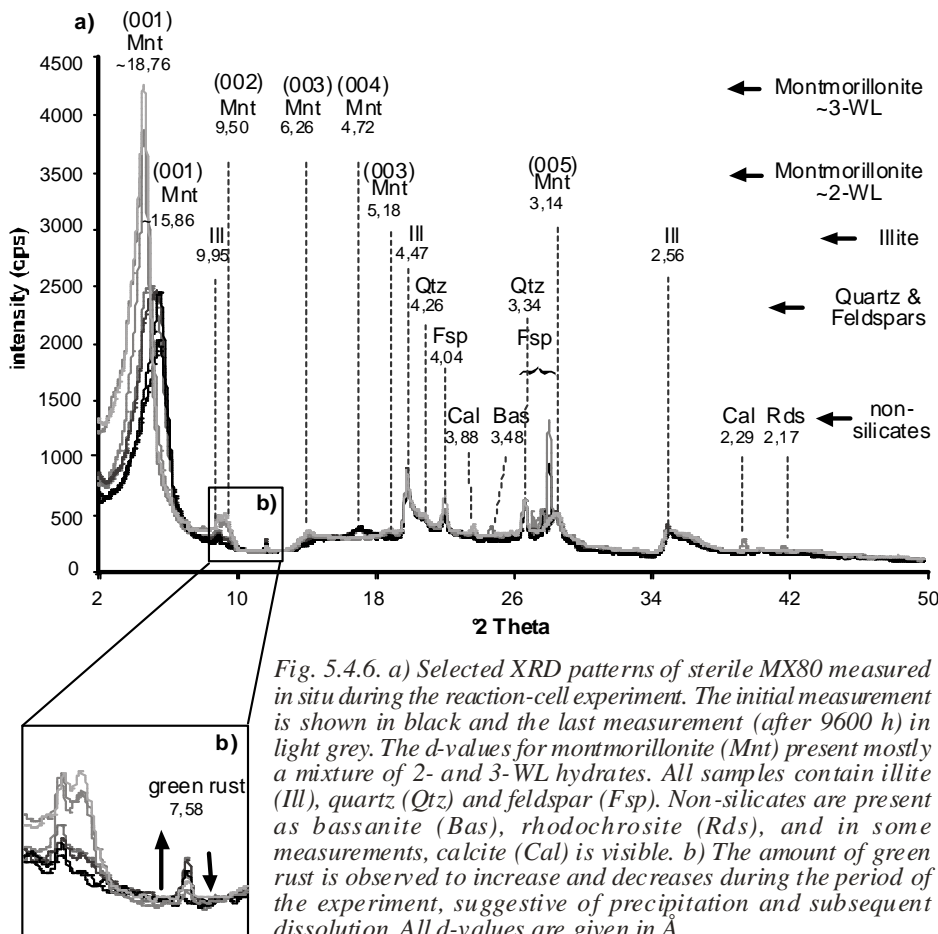


Fig. 5.4.6. a) Selected XRD patterns of sterile MX80 measured in situ during the reaction-cell experiment. The initial measurement is shown in black and the last measurement (after 9600 h) in light grey. The d-values for montmorillonite (Mnt) present mostly a mixture of 2- and 3-WL hydrates. All samples contain illite (Ill), quartz (Qtz) and feldspar (Fsp). Non-silicates are present as bassanite (Bas), rhodochrosite (Rds), and in some measurements, calcite (Cal) is visible. b) The amount of green rust is observed to increase and decreases during the period of the experiment, suggestive of precipitation and subsequent dissolution. All d-values are given in Å.

As the montmorillonite hydrates, the d-values of the basal reflections change continuously and are simplified to a 2 and 3 water layer structure end-member. Reflections for predominantly 2-WL are present at 15.88Å (001), 5.18Å (003), 3.14Å (005) whereas the 3-WL endmember occurs at 18.76Å (001), 9.5Å (002), 6.26Å (003) and 4.72Å (004) (for details of the WL structures see Fig. 5.4.2 c+d).

An illite-type mica is visible in all measurements with strong reflections at 9.95Å (001), and 4.47Å (002). The change in intensity of the illite (001) reflection is due to superposition with the montmorillonite (002) reflection at 9.50Å and not due to an increase in illite content (Fig. 5.4.6b). Other silicates that are present in both the initial and final reaction states are quartz (reflections at 4.26Å and 3.34Å) and feldspar (albite end-member) with several reflections that are not all indicated (e.g. 4.04Å, 3.22Å, 3.17Å and 3.14Å). Some of the feldspar reflections are only visible in some measurements, as their intensity is highly orientation dependent.

Non-silicate reflections are present in some measurements but are not present in all patterns, such as the calcite (CaCO_3 , visible reflection at 3.88Å and 2.29Å), rhodochrosite (MnCO_3 , visible reflection at 2.17Å) and calcium sulfate bassanite ($\text{CaSO}_4 \cdot 0.5\text{H}_2\text{O}$, visible reflection at 3.48Å). These minerals are considered to represent local precipitates from solutions that are readily re-dissolved during local changes in the saturation level of dissolved Ca, Mn and SO_4 . The only non-silicate showing a clear sequence of crystallization is an iron carbonate hydroxide ($\text{Fe}_6(\text{OH})_{12}(\text{CO}_3)$) referred to as “green rust” which is identifiable by a strongest reflection at 7.58Å (Fig. 5.4.6b). This reflection is not present at initial (almost dry) states, but occurs with fluctuating intensities throughout experimentation indicating active Fe dissolution and precipitation reactions. This reaction product was also described in other studies (Sauzeat et al., 2001) but it appears to be most easily detected under hydrated conditions.

Fig 5.4.7a shows selected XRD patterns for the bacteria containing MX80 bentonite in the reaction-cell over a time span of 3150h. As for the sterile sample, the dominant reflections are montmorillonite (reflections are indicated for 2 and 3 water layers), an illite-type mica (10.0Å 4.48Å 2.56Å), quartz (4.26Å and 3.34Å) and feldspar (mostly albite). The reflection of an iron carbonate hydroxide is present in all measurements except the first. The intensity of the peak at 7.58Å remains stable during the whole experiment (Fig. 5.4.7b). Unlike the sterile sample, a reflection of lepidocrocite ($\gamma\text{-FeOOH}$) visible at 2.46Å shows a sequential increase in intensity that indicates continuous precipitation (Fig. 5.4.7c). Another sequence is visible for calcite (2.48Å) with decreasing intensity. This is even more visible for the

reflection at 1.91Å, showing the highest intensity at the beginning with a successive decrease in intensity followed by a complete disappearance within the first 190h of experimentation (Fig. 5.4.7d). The reflection of rhodochrosite (visible reflection at 2.17Å) is, like the bassanite reflection at 2.99Å, not visible in all samples.

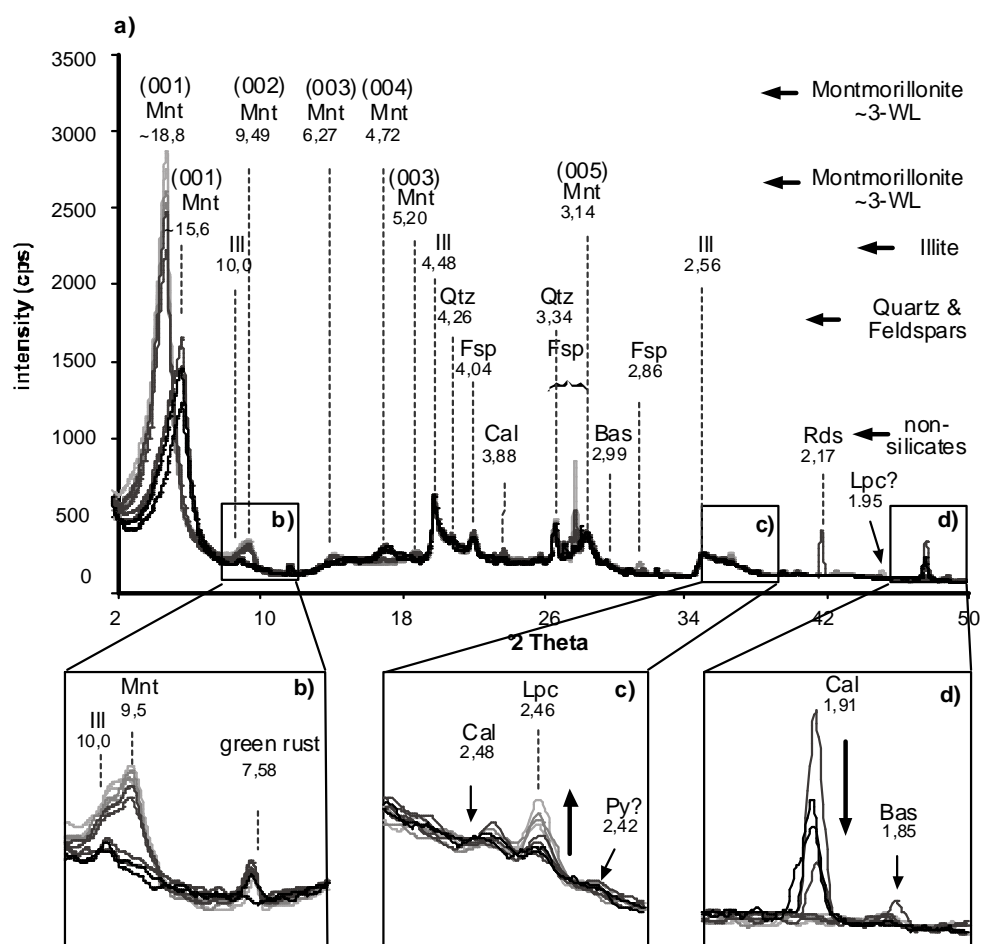


Fig. 5.4.7. a) Selected XRD patterns of bacteria containing MX80 measured in situ during the reaction-cell experiment. The initial measurement is shown in black and the last measurement (after 3150 h) in light grey. The d-values for montmorillonite (Mnt) present mostly a mixture of 2- and 3-WL hydrates. All samples contain illite (Ill), quartz (Qtz) and feldspar (Fsp). Non-silicates are bassanite (Bas), rhodochrosite (Rds) and in some measurements calcite (Cal). Reflections indicating dissolution/precipitation are shown in the magnified images: b) increase of green rust c) increase of lepidocrocite (Lpc) and d) decrease of calcite (Cal). The 2.42 Å peak of pyrite (Py) is perhaps present in c). All d-values are given in Å.

5.4.2.2. XRD-texture characterization of samples

Sample powders extracted from the reaction-cell holders after completion of the hydration cycle were measured as laboratory texture preparations to investigate changes in basal

reflections. These samples were both measured in the untreated state and after saturation with cations (KCl and MgCl₂) and organic complexes, (ethylene glycol and glycerol) used to characterize the clay samples. For nontronite, the texture sample of the original material that was not incubated in the reaction-cell chamber was prepared as a reference.

Texture characterization of nontronite

Fig. 5.4.8a shows the XRD patterns for the air dried (AD) and ethylene glycol (EG) saturated samples prepared from the original material, as well as from the sterile reaction-cell and the bacteria containing reaction-cell.

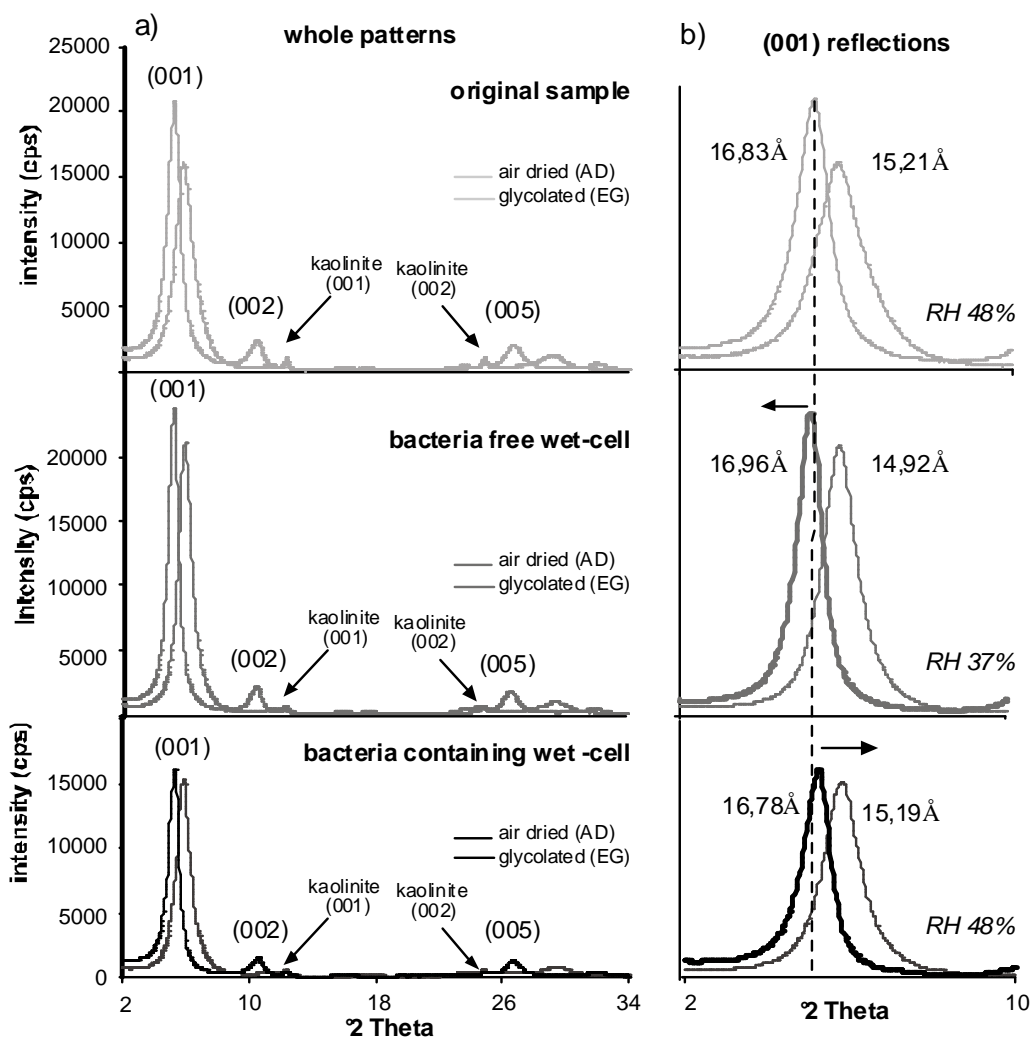


Fig. 5.4.8. a) XRD patterns of air dried (AD) and glycolated (EG) texture preparations of the original nontronite sample (upper sketch, light grey), of the sample extracted from the sterile reaction-cell (middle dark grey) and the sample extracted from the *S. putrefaciens* containing reaction-cell (black). b) Enlarged image of the (001) reflection with d-values. The numbers in italics indicate the relative air humidity (RH) for air dried samples at the time of measurement.

The basal reflections of ethylene glycol treated nontronite are the most characteristic of this mineral with an intense (001) basal reflection and relatively intense (002) reflections (005), typical for the high amounts of Fe in the octahedral sites (Moore & Reynolds, 1997). The other basal reflections are those of Kaolinite standard. No precipitates or other mineral phases are detectable either in the sterile or in the bacteria-containing samples.

In Fig 5.4.8b, the (001) nontronite reflections are shown for air dried and ethylene glycol saturated samples. The air dried state of the samples shows only minor differences in d-values with a range from 14.91 to 15.25Å, which can be attributed to variations in relative humidity that was elevated in case of the original and bacteria containing samples (both with 48%) as opposed to the sterile sample that was equilibrated in 37% RH. These d-values confirm that after the 1½ year experiment period, the interlayer cation is still divalent (supposedly Ca²⁺). In contrast, the d-values of glycolated samples are independent of the relative humidity and all reflections show an expected shift towards higher d-values due to the intercalation of the molecule. Compared to the glycolated original sample (see dotted line in Fig. 5.4.8b), the sterile reaction-cell sample shows a d-value slightly higher than the original, indicating an increased accessibility for the EG-molecule (16.96 vs. 16.83Å). The value for the bacteria containing sample shows a lower d-value (16.78Å) and a reduced accessibility for the molecule that might be due to coatings of organic matter.

Measurements of the full-width-at-half-maximum (FWHM) of the glycolated (001) reflection show higher values for the bacteria containing sample compared to the sterile control (0.744 vs. 0.705°, table 5.4.5) but both confined volume derived samples show lower values than the original one (0.867°). Higher FWHM values indicate a broader peak and, in the case of the original sample, this might indicate the presence of very small grains that are contributing to the peak broadening. In contrast the reaction-cell samples, the sharper peaks (lower values for FWHM) could indicate some dissolution of such grains. The bacteria containing sample shows a peak broadening relative to the sterile control, suggestive of decreased particle size. Values for the FWHM and d-values do not correlate (plot not shown), which indicates that differences in broadening are independent of EG saturation state. Generally, the XRD maximal peak intensity for the bacteria-containing sample is lower compared to the sterile reaction-cell. Most likely the bacteria cause textural changes by producing lower basal intensities due to a poor preferred orientation.

	Original sample			Sterile reaction-cell sample			Bacteria containing reaction-cell sample		
	<i>d</i> -value (Å)	Intensity (cps)	*FWHM°	<i>d</i> -value (Å)	Intensity (cps)	FWHM°	<i>d</i> -value (Å)	Intensity (cps)	FWHM°
<i>Air dried</i>	15.21	9504	1.287	14.92	2098	0.957	15.19	1520	1.029
<i>Ethylene glycol</i>	16.83	1075	0.867	16.96	2389	0.705	16.78	1610	0.744
<i>MgCl₂+glycerol</i>	14.83	2651	0.921	14.64	1520	0.888	14.25	1240	0.890
80°C				14.02	1551	1.289	14.12	1649	1.258
120°C				11.08	3927	1.880	11.29	3909	2.033
160°C				9.90	4088	1.125	9.93	4295	1.189
200°C				9.81	4283	1.049	9.78	4590	1.021

Table 5.4.5. XRD peak characteristics (001 reflection) of nontronite materials after various chemical and physical treatments. *FWHM= full width at half maximum.

A qualitative evaluation of layer charge was undertaken by exchanging the samples with Mg followed by glycerol saturation. If the charge approaches vermiculitic values, this treatment leads to a shift of the (001) reflection towards lower *d*-values (Brown & Brindley, 1984; Moore & Reynolds, 1997). Fig. 5.4.9 shows the diffraction patterns of the Mg exchanged and glycerol saturated sterile sample, as well as the bacteria-containing reaction-cell samples and the original sample.

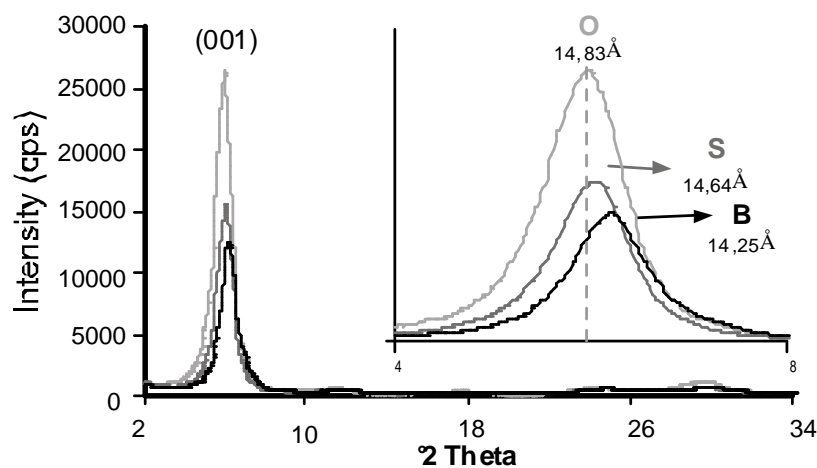


Fig. 5.4.9. XRD patterns of Mg-exchanged and glycerol-saturated texture preparations extracted from sterile (S) and bacteria containing (B) reaction-cell experiments. The enlarged image shows the position of 001 reflections and their corresponding *d*-values. The light grey pattern represents the Mg-exchanged and glycerol-saturated original sample (O) that was taken as a reference.

As the nontronite has in general a relatively high layer charge (~0.5 per half unit cell), the original sample shows relatively low d-values (14.83Å as opposed to the 17Å of typical smectites). The d-value of the sterile reaction-cell sample shows a decrease to 14.64Å, whereas the d-value of the bacteria-containing sample decreases relatively strongly to 14.25Å. The latter value is typically vermiculitic (14.2-14.3Å, Brown & Brindley 1984) and indicates an increased layer charge.

As both reaction-cell samples were anoxic over a long period (1½ years), the changed redox conditions already might have led to an increased layer charge. The bacteria containing sample shows an additional increase that may be linked to additional dissimilatory Fe-reduction due to bacterial respiration. However, a cation fixation (K^+) within smectite interlayers or neo-formation of illite (Kim et al., 2004) was not observed in these samples indicating that the layer charge did not exceed 0.8 per unit cell.

In order to test the presence of organics in the interlayer space, the samples were successively heated up to 200°C and the d-values measured at selected stages. As water leaves the structure relatively easily, differences in the response to the heat treatment can help to identify organic contaminations that, depending on the compound, leaves the structure at higher temperatures typically more than 105°C, (Birkel et al., 2002). Fig. 5.4.10 shows the XRD patterns of the samples from sterile and bacteria containing reaction-cells for 3 different temperatures compared to the AD state (Fig. 5.4.10a). After heating to 80°C for 24h (Fig. 5.4.10b), the reflections show a strong decrease in maximal intensity and a shift towards lower d-values (14.02Å for the sterile and 14.12Å for the bacteria-containing sample). The difference in d-value between the sterile and bacteria containing sample is slightly enhanced in the measurement after heating to 120°C (Fig. 5.4.10c) with lower d-values for the sterile sample (11.08Å vs. 11.29Å). Heating to 160°C leads almost to a complete loss of interlayer water and both d-values shift to around 9.90Å (Fig. 5.4.10d). After heating to 200°C (not shown in plot) the d-values change to 9.81Å and 9.78Å for the sterile and bacteria containing samples (table 5.4.5), and the complete loss of interlayer water is accomplished.

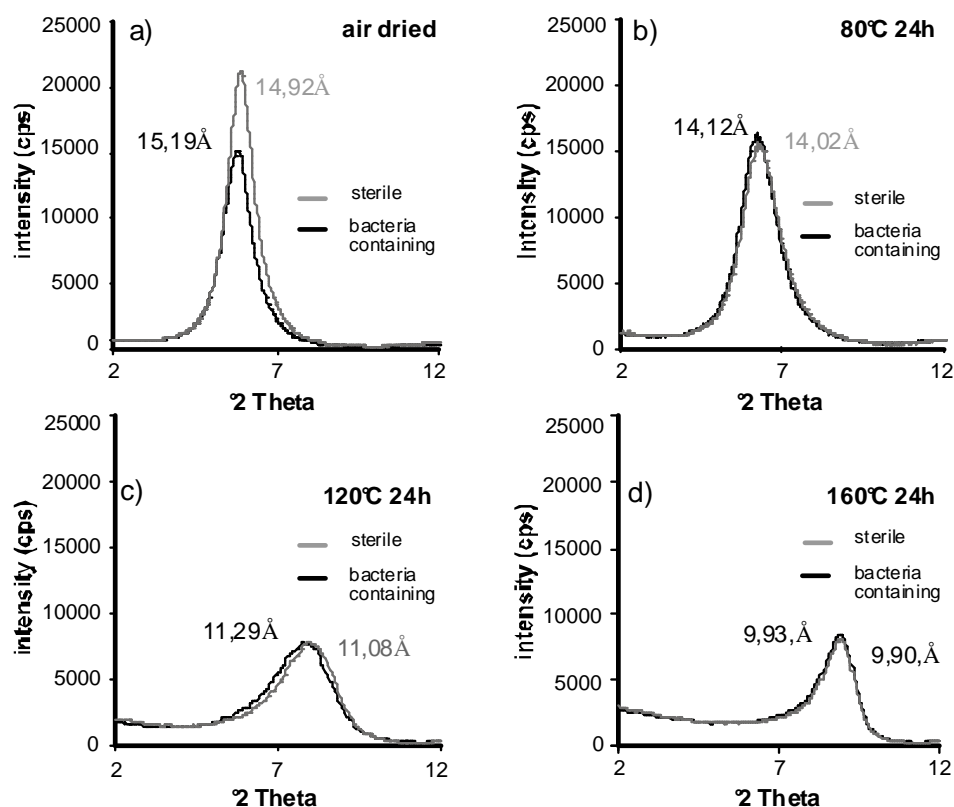


Fig. 5.4.10. XRD patterns of nontronite reaction-cell experiments with and without bacteria. a) Air dried, b) heated to 80°C, c) heated to 120°C and d) heated to 160°C.

Slight differences in d-values in the range of 0.1 Å are observed at 80 and 120°C which, although small, might indicate minor contamination with organic matter in the case of the bacteria-containing sample. As organic molecules are usually relatively large, they are not likely to be present in the interlayer space but as coatings that restrict the dehydration, as seen in the bacteria-containing sample. The identical d-values after heating to 200°C exclude artefacts such as different sample thickness. Another possibility is that the enhanced layer charge leads to a more vermiculite-like behaviour as they generally lose their water later than smectites and have collapse at temperatures more than 600°C (MacEwan & Wilson, 1980).

Texture characterization of montmorillonite (MX80)

The reaction-cell derived MX80 samples were prepared as texture samples, without separating the clay fraction. No differences are visible in the diffraction pattern of the sterile and bacteria MX80 samples (Fig. 5.4.11). The d-values are very similar for the (001) reflections at 12.58 Å and 12.56 Å, respectively (see Fig. 4.11b). At a relative humidity between 42 and 45%, these d-spacings still correspond to montmorillonite with predominantly

Na as the interlayer cation (MacEwan & Wilson, 1980). The presence of bacteria in those samples did not lead to significant exchange of interlayer cations.

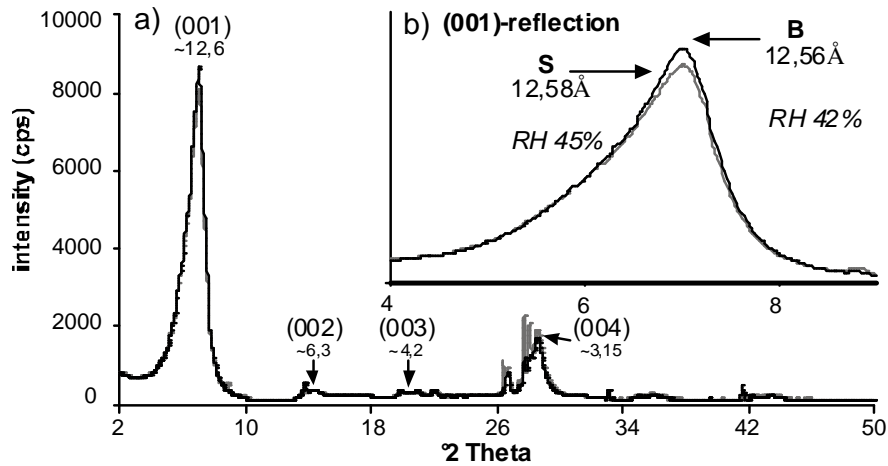


Fig. 5.4.11. a) XRD patterns of montmorillonite (MX80 sample) measured as air dried texture slides prepared from the sterile (grey) and bacteria containing (black) reaction-cells. The numbers in brackets indicate the order of diffracting basal planes (00l series of montmorillonite) and their corresponding d-values in Å. b) Enlarged image of the (001) reflection. The numbers in italics indicate the relative air humidity (RH) during measurement.

The effect of heat treatment on the material is shown in Fig. 5.4.12. Compared to the air dried samples (Fig. 5.4.12a), the heat treated preparations show a strong decrease in intensity and both peaks shift to lower d-values (9.74Å for the sterile and 9.69Å for the bacteria-containing sample already after 80°C). Successive heating up to 200°C showed no significant changes (table 5.4.6.) The collapse of the structure to ~ 9,7Å after heating lies between the typical values for Na⁺ (9.6Å) and Ca²⁺ (9.8Å) in the interlayers, indicating the probable presence of both cations. In case of MX80, the bacteria had no effect on the properties of the montmorillonite and no intercalation of any organic compounds is visible.

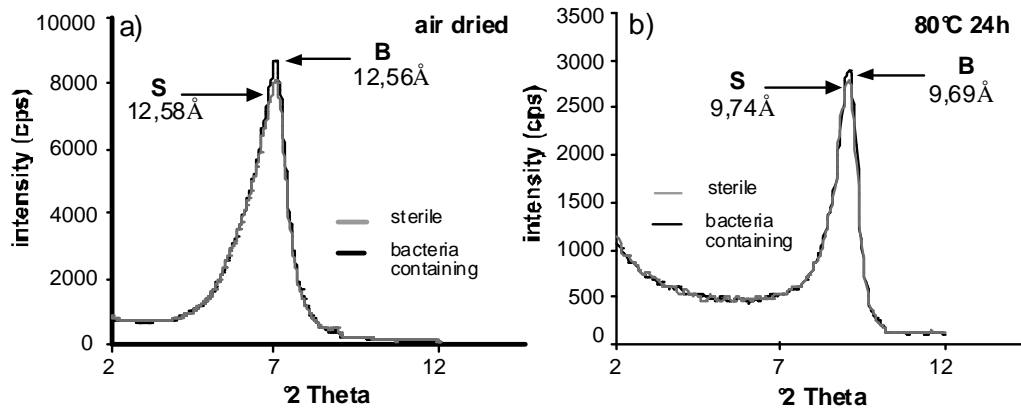


Fig. 5.4.12. a) XRD patterns of montmorillonite (MX80) measured as air dried texture slides prepared from the sterile (S, grey, RH 45%) and bacteria containing (B, black, RH 42%) reaction-cells. b) XRD patterns of the collapsed interlayer structure after heat treatment (24h 80°C).

	Sterile reaction-cell sample			Bacteria containing reaction-cell sample		
	<i>d</i> -value (Å)	Intensity (cps)	FWHM°	<i>d</i> -value (Å)	Intensity (cps)	FWHM°
<i>Air dried</i>	12.58	6969	1.247	12.56	8016	1.190
<i>Ethylene glycol</i>	16.91	7195	0.520	16.87	7837	0.509
80°C	9.74	1397	0.808	9.69	1466	0.777
120°C	9.70	1409	0.764	9.69	1470	0.778
160°C	9.69	1447	0.751	9.63	1521	0.733
200°C	9.67	1505	0.762	9.67	1603	0.749

Table 5.4.6. XRD peak characteristics (001 reflection) of MX80 montmorillonite after various chemical and physical treatments.

5.4.2.3. Chemistry of solution extractions

The long-term effect of bacteria on the solution chemistry was measured on solution extractions. Therefore, aliquots of samples taken from the reaction-cell experiments were dispersed in a leaching solution (water and/or HCl) and measured with ICP-OES. The relative contribution of experimental solutions, infiltrated during the reaction-cell experiments, to the leaching solution was calculated. Significant values are only visible for K^+ , which contributes with ~10mg/l (table 5.4.7). As well, cations contained in the Millipore© water used for extraction contribute to the measured concentrations with 0.84mg/l Mg contained in the purified water. All other cations in the solution derive mainly from the clay and/or bacteria, if present.

Ion	nontronite (MM)		montmorillonite (salt solution)		Millipore water
	Composition [mg/l]	contribution to leaching [mg/l]	Composition [mg/l]	contribution to leaching [mg/l]	
Na	46	1.01	0.25	5.5E-3	0.11
K	486	10.7	180	3.96	0.147
Mg	24	0.53			0.837
Ca	20	0.44	20	0.44	2.2

Table 5.4.7. Contribution of experimental solutions (minimal medium in the case of nontronite and salt solution in the case of MX80) to cationic content of leaching solutions.

Nontronite

The absolute values for cation release into water are shown in Fig. 5.4.13a for both the bacteria containing and bacteria free nontronite (initial experimental solution was MM). Compared to the sterile control the cation contents are enhanced when bacteria are present (e.g. 7.9% more Al^{3+} with 329 vs. 303mg/l, 10.5% more Ca^{2+} with 467 vs. 418mg/l and 6.7% more Fe_{tot} with 675 vs. 630mg/l). The exception is the silica, which is not present to a significantly higher amount (285mg/l with bacteria and 284 mg/l in the sterile sample). In order to estimate the cation release in terms of dissolution, the values are displayed normalized to a theoretical stoichiometric dissolution of 10% (Fig. 5.4.13b). Positive values indicate a higher cation release, negative values a lower cation release and zero would indicate 10% dissolution. Al^{3+} , Ca^{2+} and total iron are released into solution to a higher amount than the reference. All three cations are enhanced when bacteria are present. Si, in contrast, is barely found in solution (value corresponds to $\sim 1.4\%$ of mineral dissolution).

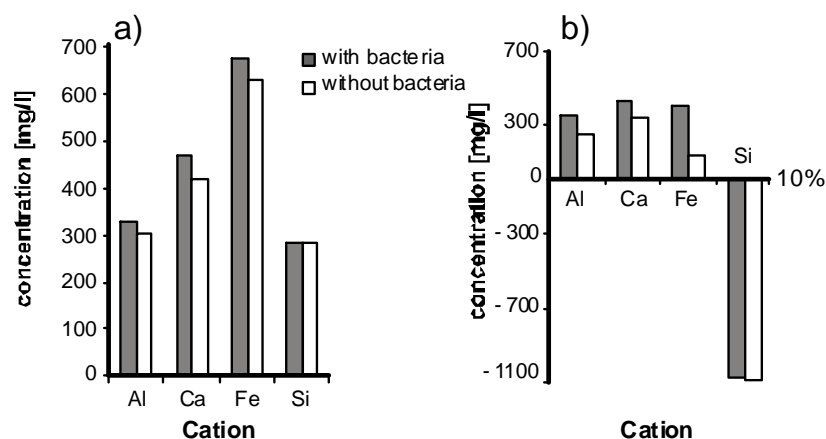


Fig. 5.4.13. Concentration of cations leached into solution of samples taken from nontronite reaction-cell experiments (with and without bacteria). a) Absolute concentrations, b) normalized to 10% of stoichiometric cation release (zero line).

Metal cations were also measured in the acid extract that, due to the low pH, allows them to stay in solution and not to precipitate as insoluble oxides. Fig 5.4.14 shows the cations released into acid compared to water. Al is enhanced to 42-47% and Fe to 52-58% and, in both cases, the amount of cations is higher when bacteria are present. Additionally, the difference between the biotic and abiotic release is more pronounced. In HCl, the bacteria induced release is enhanced by a factor of ~1.19-1.21 for Al and Fe relative to the sterile control, whereas in water, the difference is by a factor of 1.08-1.07 for Al and Fe, respectively. As the experiments were running over a long time period, the Al and the Fe were, in all probability, precipitated at earlier stages (the presence of Al-sulfate and Fe-phosphate was detected in XRD patterns). The HCl treatment dissolved these precipitates and therefore the amount of Al can be taken as an indicator of the amount of clay dissolution for there are no other sources for this element in these samples (corresponding dissolution of 23.1% which is 3.7% more than for the sterile sample with 19.4%).

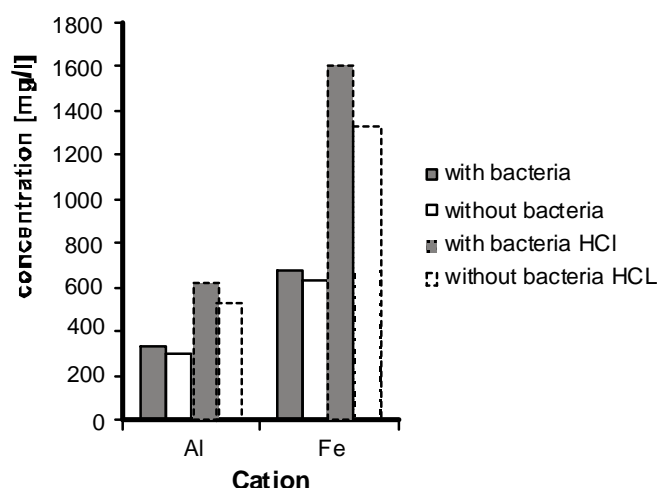


Fig. 5.4.14. A comparison between the concentrations of cations extracted from nontronite using water (solid lines) and HCl (dashed lines). The results show higher cationic content for HCl leaching especially for Fe. Generally bacteria containing samples (grey columns) release more cations into solution than bacteria free (white columns).

In the nontronite structure, Al is situated in tetrahedral sites and partially substitutes Si (responsible for the layer charge deficiency). It is not likely that only the Al sites are dissolved, thus the Al should represent the true dissolution of the tetrahedral lattice even when Si is detected to a lesser extent. Fe in solution is sensitive to redox state and it is described

separately. Nevertheless, it is visible that the total Fe concentration in acid is enhanced and always present in higher amounts when bacteria are present.

Montmorillonite (MX80)

Cation release of the long-term MX80-montmorillonite sample into Millipore® water is shown in Fig. 5.4.15a for both the bacteria containing and the sterile sample. Generally, the difference between the biotic and abiotic samples is less pronounced compared to the nontronite. No difference is visible for Al, which is generally not found in high amounts (around 38mg/l in both cases). The interlayer cations Na and Ca are typically released to a higher extent in both cases and are slightly less in the presence of bacteria with 2% less Na (450 vs. 469mg/l) and Ca (393 vs. 401mg/l). The only cation that is released into water to a higher amount in the presence of bacteria is Fe, with an enhanced concentration of about 8% (71 vs. 65mg/l).

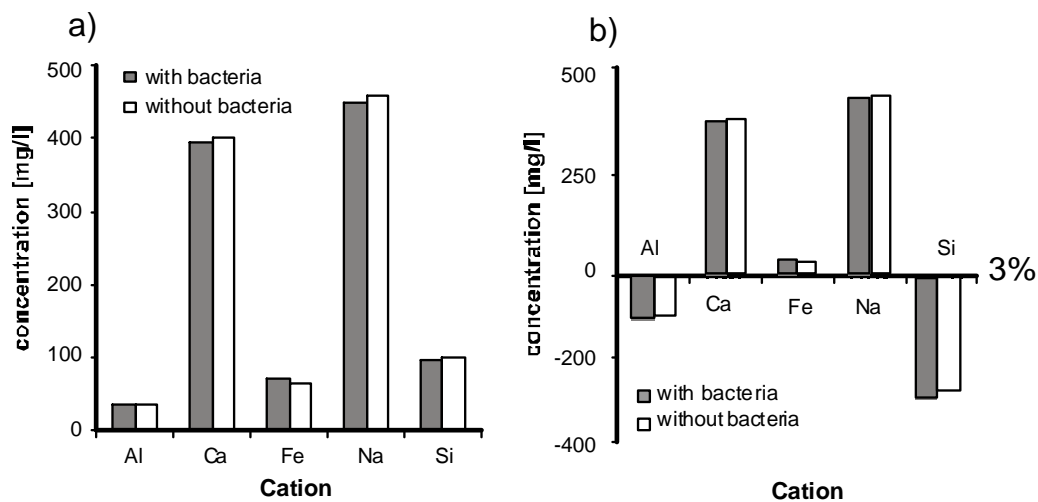


Fig. 5.4.15. Concentration of cations leached into solution of samples taken from the MX80 montmorillonite reaction-cell experiments (with and without bacteria). a) Absolute values obtained from ICP-OES analyses. b) Normalized to 3% stoichiometric cation release (zero line).

Fig. 5.4.15.b shows the relative amounts of cations released into solution normalized to a 3% stoichiometrical release as a reference (represented by the zero line). Positive values are basically obtained for the interlayer cations Ca, and Na. Fe is also shows positive values (correspond to 5% dissolution). Low concentrations are obtained for Al and Si indicating a true dissolution of less than 1% with a stable Si/Al ratio (~2.5 as opposed to initial 2.7). Cation release into HCl (Fig. 5.4.16.) shows, however, higher values for Al when bacteria are

present. The Si/Al ratio (Si not shown in plot) shifts to 1.3, indicating a higher release of Al into solution. Fe is enhanced as well in the acid leaching when bacteria are present. This indicates that the bacterial effect on metal release into solution is masked by precipitation (precipitation of green rust and lepidocrocite visible in XRD patterns) and is only seen in high pH extracts. Other cations show no significant differences with HCL.

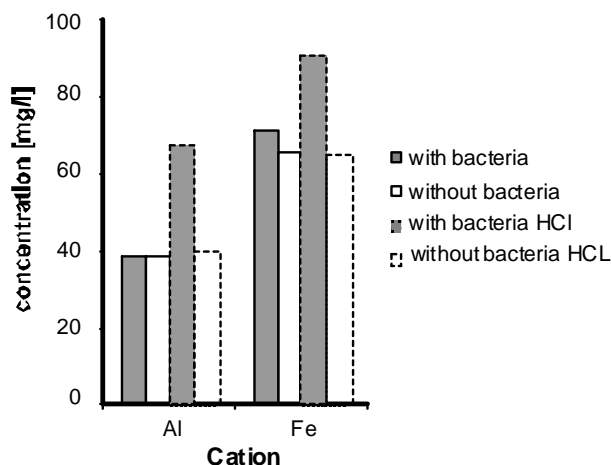


Fig. 5.4.16. Comparison between the concentrations of cations extracted from montmorillonite using water (solid lines) and HCl (dashed lines). The results show higher cationic content for HCl leaching analysis of bacteria containing montmorillonite samples. Without bacteria (white columns) the values are comparable to the water extracts.

Like in nontronite, the interlayer cations in montmorillonite are easily released in solution. Even the enhanced amount of Al in the acid leaching indicates that maximal dissolution does not exceed 1.4%. Fe is released to a higher amount and might be as well derived from the traces of the pyrite contained in the samples, as sulfate measurements suggest this to some extent (data not shown). Generally, the MX80 structure seems to be less affected by the experiments than the nontronite, especially visible by the low amount of Si and Al dissolved.

5.4.2.4. The role of Fe-reduction under confined volume conditions

Fig 5.4.17 shows the Fe(II) production measured in HCl extractions of samples taken from the reaction-cell experiments with and without bacteria. These are compared to values taken from Andrade et al.(2002) and Kim et al. (2003; 2004) for initial Fe(II) values (empty dotted column) and from Kim et al. (2004) for final values after clay bacteria interaction (filled dotted column). Both confined volume samples show, relative to the initial content of 0.21mmol/g, enhanced Fe(II) concentrations. In the bacteria containing sample, the amount of Fe(II) is enhanced with 0.57mmol vs. 0.47 in the sterile control. This value is relatively low

compared to batch experiments conducted by Kim and co-workers (2004) that yielded 1.2mmol/g. Expressed in % of reduced iron relative to the total iron content (4.3mmol/g, table 5.4.8), the bacteria containing sample indicates a reduction of 13.4%. However, already the anaerobic conditions induced a partial reduction that is visible for the sterile control sample.

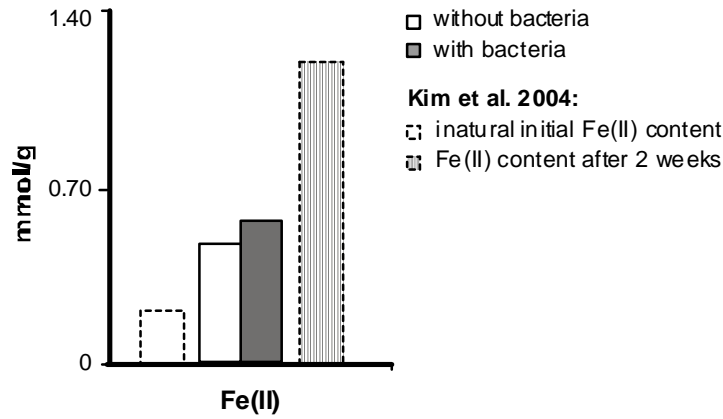


Fig. 5.4.17. Measured Fe(II) values for reaction-cell extractions (solid lines) with and without bacteria. Dotted columns represent values taken from the literature, which show initial Fe(II) concentration (empty column) and that after clay-bacteria interaction in batch experiments (Kim et al. 2004, striped column).

Fe ₂ O ₃ +FeO [wt %]	Fe(III) +Fe(II) [wt%]	Fe _{tot} /g clay [mmol]	max. initial Fe (II) [mmol/g]
34.2	23.9	4.3-4.5**	0.21*

Table 5.4.8. Theoretical iron content of the nontronite sample (NAu-1) as described by Keeling et al. (2000),*Andrade et al. (2002); Kim et al.(2004) and **O'Reilly et al.(2005).

In order to quantify the amount of Fe(II) that can be attributed to bacterial activity, the difference relative to the sterile controls is plotted in Fig. 5.4.18 for the bacteria containing reaction-cell and two batch experiments. Positive values indicate enhanced, and negative values decreased Fe(II), relative to the sterile controls. The reaction-cell sample (no viable cells were present at the time of measurement) shows enhanced Fe(II) values with 21.2%, which is more Fe(II) than the sterile control indicating enhanced iron reduction. This is different from observations in experiments containing viable cells as seen from the Fe(II) values of two batch experiments. Both examples show, with respect to the sterile control, negative values due to Fe-consumption. This is the case for the anaerobic experiment which has 7.5% less Fe(II) compared to the sterile control (0.27mmol with bacteria and 0.29mmol without bacteria vs. an initial concentration maximal 0.21mmol/g). This trend is, as expected,

enhanced for the aerobic sample where Fe(II) is consumed and due to oxygen respiration is not produced by Fe-reduction.

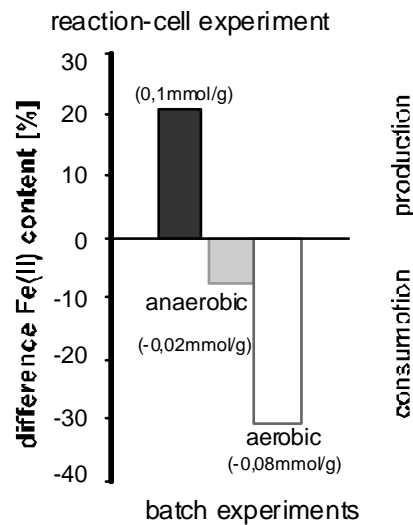


Fig. 5.4.18. Relative differences in Fe(II) content for the bacteria-containing reaction-cell experiments in % (dark grey column) when normalized to the sterile control. Anaerobic batch cultures (light grey column) and aerobic batch cultures (empty column). The numbers in brackets represent the absolute differences in mmol/g.

As discussed in Chapter 5.3, the bacteria consume or sorb cations during their growth and, even if Fe-reduction occurs due to respiration, the released Fe(II) is partly stored by bacteria or within biofilms. This iron is, therefore, not detected in the analyses as long as the cells are intact. In the case of the reaction-cell experiments, no viable *S. putrefaciens* cells were detected after the 1½ years of experiment, and therefore Fe(II) that was eventually consumed or attached to cells re-enters the system.

5.4.2.5. Microscopical observations of long-term experiments

During the long-term confined volume experiments, systematic monitoring by microscopy was not possible however, some limited observations were done after around 7 weeks. An example is given in Fig 5.4.19a that shows a TEM-microphotograph of bacteria containing nontronite incubated under confined volume conditions for around 52 days. The kaolinite standard is present as hexagonal platelets and nontronite is visible as a particle with a relatively well defined shape in the upper right of the image. The EDX microchemical data shows the typically high values of Fe (44.4 wt.% Fe_{tot}) and Si (57 wt.% SiO) and some Ca (2.1 wt.% CaO; Fig. 5.4.19b). A bacterial cell showing beginning lyses is present in the left

part where microchemical analysis shows the presence of S (0.9 wt.% S_{tot}) and Cl (5.3 wt.%), that is typically associated with the bacteria. Additionally, elements derived from the smectite such as Si (2.6 wt.% SiO), Ca (2.5 wt.% CaO) and Fe (1.5 wt.% Fe_{tot}) are present (Fig. 5.4.19c). Here, it is not clear to what extent the analysis is influenced by the surrounding clay, or clay that is attached to the cell. However, the relative high values for Ca in comparison to low values of Si indicate an accumulation of elements on or in the bacterial cell. A gel-like structure, like previously observed in batch experiments (5.3), was not observed in this sample.

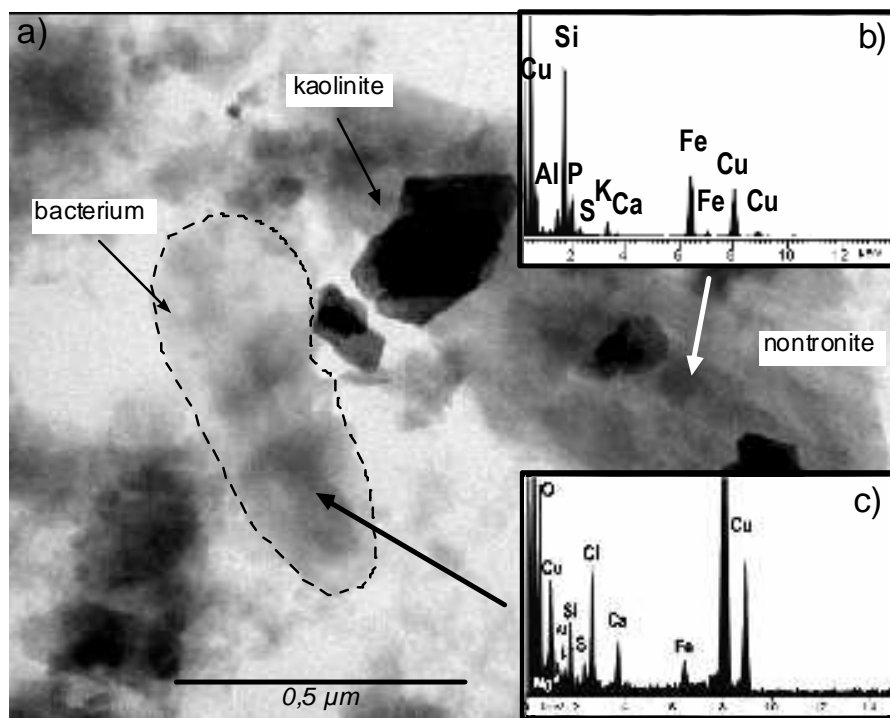


Fig. 5.4.19. a) TEM microphotograph of nontronite and *S. putrefaciens* taken from reaction-cell experiment. The size of the bacterium does not exceed 0.7 μm in length and is partly damaged. b) EDX microanalysis of the nontronite grain shown in a) contains Si, Al, Fe, Ca and K. c) EDX microanalysis of the bacterial cell showing the same cations along with additional S and Cl due to the presence of bacteria. The Cu is derived from the sample grid.

It should be noted that imaging bacteria in reaction-cell experiments is difficult as they are, compared to batch experiments, very small, present in low numbers and normally covered by clay. However, it can be seen that under this confined volume conditions, *S. putrefaciens* survived several weeks (1½ month) and that they consumed most likely cations derived from the clay.

5.5. Discussion

5.5.1. The influence of smectite on bacterial activity

The influence of smectite on the bacteria growth is basically a function of the physico-chemical properties of the clay and the requirements of the bacteria. The basic chemical necessities for the growth of *S. putrefaciens* are the supply of nutrients, energy and water in an environment of moderate pH.

Nutrients & energy

It was shown that microorganisms selectively colonize mineral surfaces that contain required nutrients indicating that the bacteria clearly profit from their proximity to the solid surface (Bennett et al., 1996; Rogers et al., 1998; Bennett et al., 2001). This is visible in the growth experiments where, independently of the type of smectite, *S. putrefaciens* survived despite smectite been the only available substrate (Fig. 5.3.1). Additionally, this species is observed to quickly adapt its metabolism to use smectite as a substrate. This is visible in the similar lag and exponential growth phase when incubated with nontronite and minimal medium (MM), where the latter is especially adapted to the needs of *S. putrefaciens* (Fig. 5.3.1). The continuous supply of cations appears to be particularly beneficial for the culture, especially those derived from nontronite that providing high amounts of Fe and Ca.

Particularly important is carbon, which was not supplied in the growth experiments but, as *S. putrefaciens* is heterotroph, it does need a source of pre-existing organic materials. Raw bentonite materials, such as MX80, often contain organic carbon (0.19% C_{org}, Sauzeat et al. 2000) and, in this case, the C_{org} values (0.02 and 0.08g/l for a suspension density of 0.01 and 0.04g/ml, respectively) lie between the values of the carbon-rich culture media (> 2g/l) and the carbon-poor sediments in natural environments (0.001-0.015g/l, Roszak & Colwell, 1987). The amount of carbon in the powdered MX80 bentonite sample might explain why the number of cfu/ml is enhanced with the increasing clay concentration in solution, for this enhances the amount of accessory minerals and organic substances (table 3.1).

The purified smectite samples, in contrast, are not expected to contain significant amounts of C_{org} because they were (due to grain size separations) washed several times. Nevertheless, the bacteria were observed to stay alive for significant periods of time (> 4 weeks). One possibility is that during the stationary phase, starved cells release C_{org} and aid

the growth of surviving cells (Dean & Hinshelwood, 1966; Postgate, 1976). To a certain amount, this could recycle the carbon in the system compensating the relative lack in the purified samples.

The fact that smectites generally have enormous surface areas per gram powder should be beneficial in solutions because bacteria can stay attached to surfaces that accumulate nutrients. This is advantageous, especially when nutrients become short in supply and *S. putrefaciens* is -despite flagellum- not likely to be very motile in order to economize energy.

Although smectites serve as a substrate for *S. putrefaciens*, the exposure to the clay induces stress. Bacteria incubated with smectite were, for example, seen to be drastically reduced in cell size compared to cultures incubated in growth medium (Fig. 5.3.17). This has been reported for bacteria in natural environments with limited nutrients that attained larger sizes when cultured in the laboratory and can be taken as a clear sign for nutrient stress (Dawson et al., 1981; Roszak & Colwell, 1987). The probable cause of this stress is that smectite does not contain all the necessary concentrations of nutrients for fully developed growth. This effect is even more enhanced in the compacted clay under confined volume conditions although nutrients are present in higher concentrations. In this environment the high solid liquid ratio clearly restricts the motility of bacteria.

The role of surfaces on nutrient supply

The increase in external surface area observed during the free swelling of smectite in batch solution provides more opportunities for bacteria to attach to these mineral surfaces. The osmotic swelling of Na-montmorillonite induces extensive particle delamination along individual silicate interlayers (Schramm & Kwak, 1982; Lagaly, 1993; , 2006) and therefore presents additional and freshly exposed external surface area. Additional surface area can be beneficial for bacterial growth as the reactive surface area is a fundamental factor enhancing mineral dissolution leading to additional cationic supply (Lasaga, 1995; Nagy, 1995). On the other hand, the osmotic swelling of Na-montmorillonite can form a colloidal suspension that is not favourable for bacteria movement because of the strong electrostatic repulsions between the both negatively charged bacteria and clay surfaces (Fig. 5.5.1). In the presence of divalent cations, these repulsions can be overcome, as in the nontronite suspension containing relatively higher concentrations of Ca^{2+} (Lagaly, 1993; , 2006).

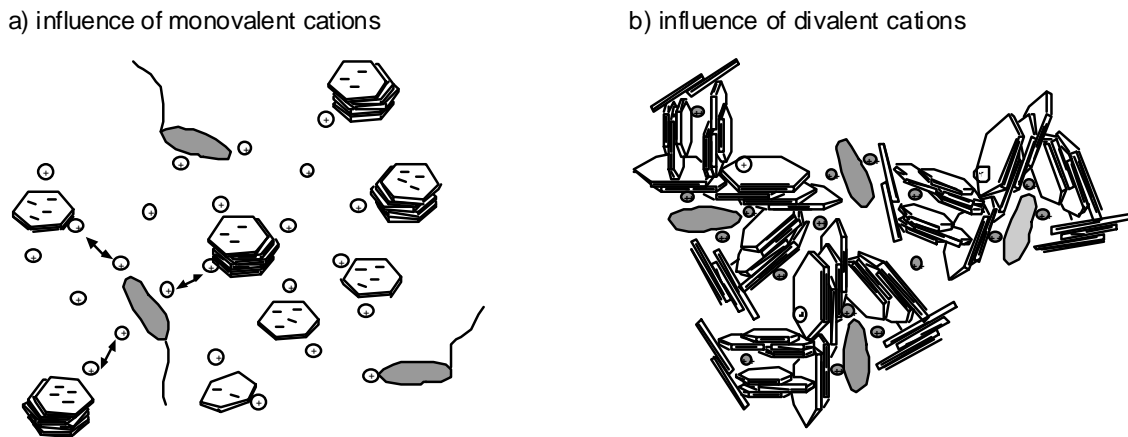


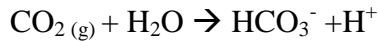
Fig. 5.5.1. The behavior of smectite and bacteria in solutions. a) With monovalent cations the electrostatic repulsion keeps clay and bacteria in suspension. b) The presence of divalent cations serve as bridges and allow the formation of aggregates.

The survival of bacteria is prolonged in all smectite solutions compared to growth in standard culture media and shows especially long stationary and death phases. This indicates that the smectite containing system respond better to requirements linked to cell death and lyses than the smectite free system. Most likely this is due to the high surface area providing numerous sorption sites for lyses products that are released during the death phase (e.g. organic molecules including complex acids (Lee &Fein, 2000)).

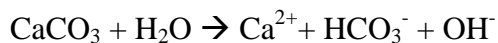
The external surface area of smectite under confined volume conditions also increases during hydration as the mean number of lattice layers per stack (i.e. particle thickness) decreases (Chapter 4). However, the fact that the swelling creates new X-ray scattering diffraction domains (detected by the broadening of XRD reflections) does not necessarily imply that the newly formed surfaces participate as reactive surfaces, as this would be the case in the batch solution experiments. The percentage of surface participation during the hydration of sterile and bacteria-containing montmorillonite (MX80) in the confined volume system was estimated from the theoretical amount of water that could be adsorbed and the amount determined from the experimental results (table 5.4.4). These are very general estimations, however a 100% contribution of all available surfaces was never observed because the smectites layers cannot expand freely. This implies that the advantageous effect of high smectite surface areas occurring in batch solutions is not maintained for bacteria in compacted clays that are hydrated under confined volume conditions.

Smectites and pH control

In experiments conducted under aerobic conditions bacteria clearly produce CO₂ by respiring oxygen. According to the simplified reaction below, the aerobic respiration leads to the production of protons and a decrease in pH:



The influence of aerobic respiration is visible during the initial stages of the batch solution experiments when a rapid decrease in pH is seen to exceed the normal pH drop caused by deprotonation at smectite edge sites. The availability of such edge sites buffers and stabilizes the pH of the solution (Lagaly, 1993; Apelo & Postma, 1994). The closest match to the sterile control with the quickest pH adaptation was observed in the nontronite solution, which is probably due to a higher concentration of edge-sites in this <0.5 micron grain size fraction (Lagaly, 1993). In the case of the coarser polymineralic MX80 bentonite, the pH is buffered to a lesser extent (Fig. 5.3.3.b). Here, the strong pH decrease within the first two days can be attributed to dissolution of traces of pyrite, which when oxidized, releases protons (Lowson, 1982; Nordstrom, 1982). In contrast, the more alkaline condition reached once the stable state was attained (pH ca. 8.6) can be attributed to calcite dissolution leading to OH⁻ production according to the reaction:



In addition to well documented interaction of clays and H⁺ ions, the bacterial cell walls can also become protonated and, thus, influence the measured pH (Haas, 2004; Claessens, 2006). During respiration, cells pump protons into the wall matrix which, in turn, can protonate surface functional groups and render them electrically neutral (Koch, 1986; Haas, 2004). In contrast, dead cells no longer induce a proton gradient, so the cell wall tends to become more anionic and capable of accommodating protons (Urrutia et al., 1992). The effect of these reactions is evident during the later stages of the solution experiments where the pH of all solutions increases with respect to the sterile control (Fig. 5.3.5). When lysis is complete, however, the pH returns to the value of the sterile control.

5.5.2. Physical and chemical influence of bacteria on smectite clay

The effects that bacteria can have on the properties of smectites are closely linked to their activity and, therefore, their viability. Bacterial activity can directly influence these clays by consuming mineral derived compounds, aided by the production of organic substances like chelators or EPS. Respiration has both indirect effects on smectite (solution Eh and pH is changed) as well as direct effects in the case of anaerobic metal respiration because the layer charge is changed. Finally, a number of textural effects in smectite powders can be attributed to bacterial activity, particularly those linked to binding and the formation of particle aggregates. Here, biofilm can persist long after cell death and have long term textural effects even after all bacterial activity has ceased.

5.5.2.1. Complexation and binding of potential nutrients and effects on smectite

Nontronite

Fe is the principle cation in the octahedral layers of the mineral nontronite with an abundance of ca. 34 wt.% (Fe_{tot}). It was noted that a bacterial colonization of the mineral surfaces is a systematic process involving chelators, especially to complex Fe (Rogers & Bennett, 2004). Fe is an important macronutrient and, as a key component in cytochromes, it plays a major role in cellular respiration (Madigan et al., 2003). In the batch solution experiments containing both nontronite and *S. putrefaciens*, the Fe was clearly depleted with respect to the sterile control (Fig. 5.3.6). As Fe(III) has a low solubility in water at near neutral pH and, it should be quickly lost from the aqueous phase and precipitated as oxides and/or hydroxides. However, when bacteria were present, an enhanced depletion of Fe in the solution was observed that could be due to iron coatings formed at the bacteria cells surface (Ehrlich, 1999; Coby & Picardal, 2005).

Additionally, the production of iron binding ligands (siderophores) could aid the formation of Fe-complexes localized on the cell where they are available for transport into the cell (Birkel et al., 2002; Faraldo-Gomez & Sansom, 2003). Such binding ligands are reported to be formed in abundance during active exponential growth (Kalinowski et al., 2000) and have been described for the *S. putrefaciens* strain used in this study (Gram, 1994). As siderophores are usually produced in Fe(III)-limiting conditions, the high Fe content of nontronite (Fe_{tot} ~34 wt.%) might at first glance be considered unsuitable for the formation of

Fe binding ligands. However, the metal in the octahedral sites is only slowly released. Moreover this “potentially” available iron might induce the production of chelating agents as it was described for *Pseudomonas mendocina* strains where only in presence of Fe-oxides the production of iron chelators was enhanced (Hersman et al., 1995; Hersman et al., 2000).

Independent of organic ligands is the depletion of Ca in nontronite suspensions. As water hydrates the interlayer sites and interlayer cations become highly reactive, undergo rapid exchange with the infiltrating solution (Banfield & Hamers, 1997; Barker et al., 1997) and become available for bacterial adsorption (Stotzky, 1966a). This effect is visible in nontronite solution experiments where the presence of bacteria was observed to rapidly deplete the concentration of Ca in solution (Fig. 5.3.6). Investigations with TEM coupled with EDX microanalyses indicate that smectite derived Ca is concentrated in or on *S. putrefaciens* cells (e.g. Fig. 5.3.17.). This was also observed for the MX80 montmorillonite, although the amount of interlayer Ca was relatively low compared to nontronite.

The concentration of Ca at bacterial surfaces may simply occur by electrostatic forces. As a divalent cation, Ca has a relatively high affinity to be strongly adsorbed on bacterial surfaces and was described by Beveridge (1989) for *Bacillus subtilis* as “binding”. Since both bacteria cells and smectite surfaces are (at near neutral pH) negatively charged, the Ca can help to bridge the equally charged surfaces, particularly in solution of higher ionic strength where the thickness of the diffuse ion layer is suppressed (Ellwood et al., 1982; Banfield & Hamers, 1997).

Because the electrostatic mechanism of Ca binding is only active as long as the bacteria cells are intact, cations should be reintroduced into the system when cells undergo lyses. However, this is not observed and Ca stays continuously depleted in solution even when cells are dead (Fig. 5.3.6). Precipitations associated with Ca (e.g. calcite) were not detected, which could explain the depletion, but abundant EPS were visible both by confocal and electron microscopy (Fig. 5.3.11, 5.3.12 and 5.3.16a). As the EPS are seen to persist after cell death (e.g. Fig. 5.3.12c), the prolonged storage of Ca in the EPS is likely and helps at the same time to stabilize the biofilm structure (Körstgens et al., 2001; Konhauser, 2007). However, longer term experiments of 1 ½ years length showed enhanced values of virtually all cations (Fig. 5.4.13). This indicates that even the biofilm structure decomposes with time and the sorbed elements are indeed eventually remobilized.

5.5.2.2. Effects of bacterial respiration on smectite

As discussed above, aerobic respiration can affect the properties of smectites by leading to a decrease in pH that is known to be the major factor concerning mineral dissolution rates (Lasaga, 1995; Nagy, 1995; Barker et al., 1997). This pH decrease is visible in batch solution experiments during the initial stages even though values that would significantly contribute to dissolution (e.g. a pH lower than 5 and higher than 9, Blum & Lasaga (1988)) were only temporally observed (e.g. MX80, Fig. 5.3.3.).

Effects of respiration on nontronite

Under anaerobic confined volume conditions oxygen is not available and another terminal electron acceptor (TEA) is required. *S. putrefaciens* is capable of reducing the Fe(III) that is contained in the nontronite structure and induces significant alteration of this mineral as shown in the various studies using batch cultures (agitated low solid to liquid ratio experiments). Dissimilatory Fe(III) reduction in the octahedral sites modifies the charge imbalance, resulting in higher layer charge and stronger cation fixation (Stucki et al., 1987; Stucki et al., 2003; Kim et al., 2004; Stucki & Kostka, 2006). These factors are closely linked to interlayer hydration characteristics and should be taken into account. In other studies, the bacterially-induced reduction of Fe was described to occur both before and after mineral dissolution (Dong et al., 2003a; O'Reilly et al., 2006).

Indications of a layer charge increase due to Fe-reduction in the confined volume nontronite experiments are provided from XRD texture preparations of Mg-exchanged and glycerol saturated samples. The low (001) basal d-spacing (14.25Å) of these samples indicates higher layer charges equivalent to those of vermiculite swelling clays (Fig. 5.4.9). The sterile control sample also showed lower basal d-spacings (14.64Å) indicative of an increased layer charge that are caused by the anaerobic conditions, however, the degree of alteration is less intensive. Fe-reduction is also visible in the chemical results where the production of Fe(II) is detected in both bacterial and sterile conditions (Fig. 5.4.17). The relative increase of Fe(II) due to bacterial respiration and Fe reduction is probably linked to partial dissolution of the nontronite particles. However, the values for reduced iron are relatively low for the confined volume experiments because i) the reaction rate is low (high solid to liquid ratio without agitation) and ii) the clay restricts the movement of the bacteria. Fe-reduction only takes place under anaerobic conditions and most oxygen poor environments are compacted, confined volume systems with high solid to liquid ratios, such as soils, aquifers and engineered systems like waste repositories. The constraints presented from the

reaction-cell laboratory analogue are considered to provide more useful estimates for predicting the rates of Fe-reduction under repository conditions than those based on batch solution experiments,

5.5.2.3. Bacterially induced dissolution of nontronite

Both the described mechanisms of complexation/binding and bacterial respiration have recognisable effects on the nontronite. Moreover the presence of specific organic ligands is known to trigger the overall dissolution of minerals and could be an explanation of the partial dissolution of nontronite (Banfield & Hamers, 1997; Barker et al., 1997; Kostka et al., 1999; Banfield & Welch, 2000). Clear signs of this bacterially induced dissolution are visible by the relative Si-depletion in nontronite when compared to the sterile control (Fig. 5.3.7). The rapid dissolution and the release of Si are most obvious during the initial stages of the solution experiments. Microscopic investigations reveal the formation of a Si rich amorphous phase surrounding nontronite particles (Fig. 5.3.16). This relationship suggests partial mineral dissolution followed by precipitation when the system is supersaturated with respect to silicic acid. These observations are in accordance with recently published observations on nontronite-*S. oneidensis* interaction by Furukawa & O'Reilly (2007). The nontronite samples may however contain a certain amount of quartz even in the <0.5µm fraction (Keeling et al., 2000) and it is possible that these small grains dissolve rapidly and precipitate as an amorphous phase. In this case, the Si is not only derived from the tetrahedral sites of the smectite.

In Fig. 5.5.2, a schematic representation illustrates the overall effect that bacteria have on nontronite. At unstable edge sites Fe(III) is mobilized and most likely trapped by organic ligands that keep the iron in solution (5.5.2a). At the same time Ca is released from the interlayer sites and serves as bridges between the bacteria and the clay, and thus facilitating the access (5.5.2b). The complexed Fe is transported to the cells and might be either transported into the cell or be present as coatings on the surface. Increasing dissolution of the nontronite leads to Si-release that is precipitated in the EPS associated with the smectite and the bacteria.

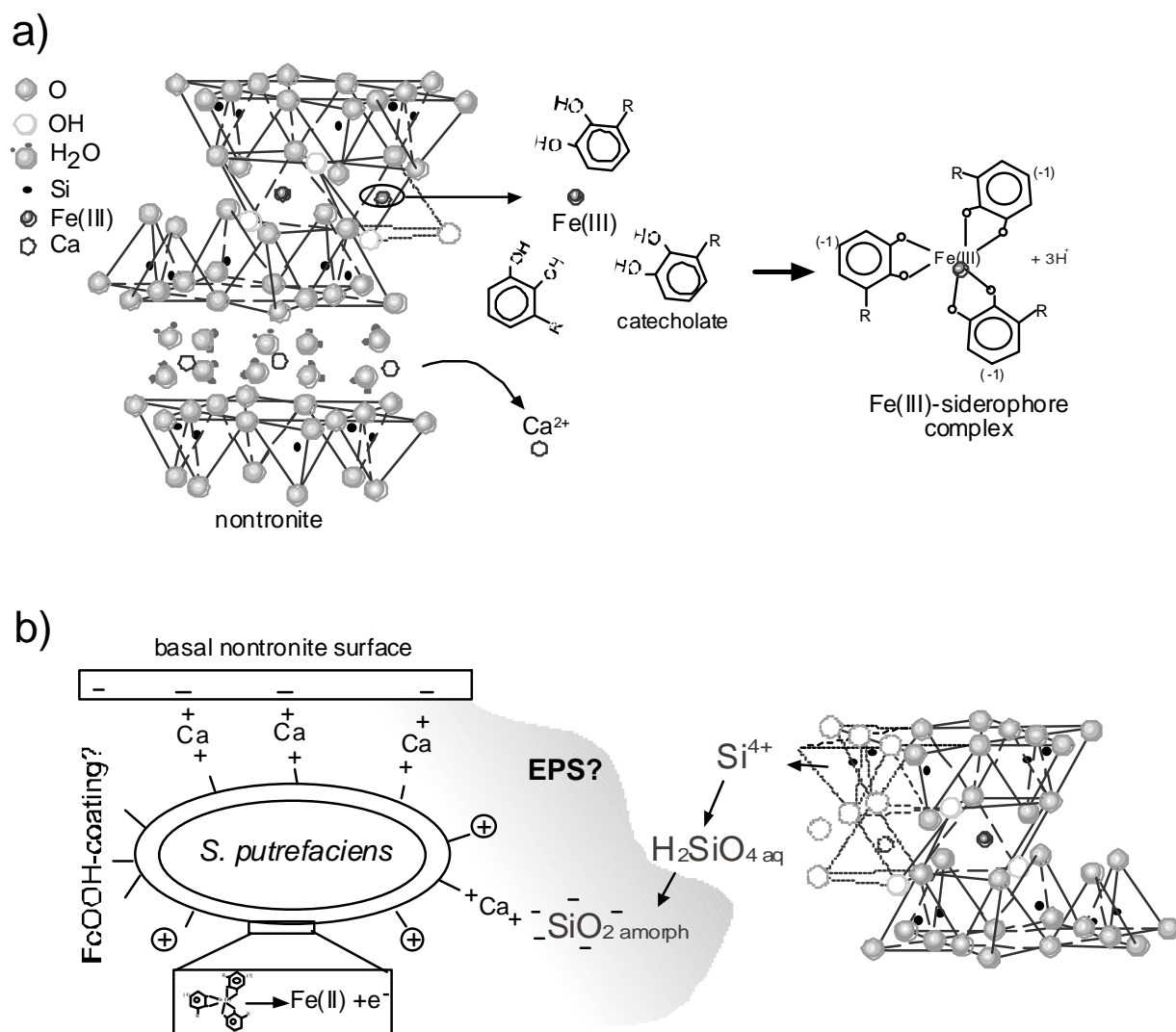


Fig. 5.5.2. Schematic sketch showing the interaction of nontronite and *S. putrefaciens* at the lattice layer scale. a) Octahedrally coordinated Fe(III) is mobilized at unstable edge sites and the Ca from interlayer sites is released into solution. Bacterially produced ligands (here catecholates) form siderophore complexes with Fe(III) as the central cation (modified after Konhauser, 2007). b) Calcium acts as a bridge between clay and bacteria. The complex is transported to the cell, the Fe(III) is dismantled and reduced or is involved in the formation of Fe(III)-coatings at the cell surface. As the complexation leads to continuous dissolution, Si is released and precipitated as amorphous silica, which is presumably associated with EPS.

Tetrahedrally coordinated Al is also depleted from nontronite during initial stages of the batch solution experiments but it re-enters the solution during the final phase. Al is, like Fe, known to form bridges between bacterial cells and Si, as it was reported for *B. subtilis* by Fein and co-workers (2002). It is therefore likely that the metals are partly associated with active cells and released when the cells die. The relative depletion of Si and Al observed at the beginning of the experiment and the re-introduction into the system during the decline of the

bacteria population confirms this as a possible mechanism. Analyses of the long term confined volume experiments also show enhanced Al release in the (formerly) bacteria – containing sample, which confirms that dissolution mechanisms are also dominant. Unlike Si, no other source of Al exists in these samples. As both the *S. putrefaciens* cells and associated biofilm are not likely to persist the 1½ year’s period of experimentation, any adsorbed or bound cations are re-introduced into the system.

5.5.2.4. Textural alteration

Whereas chemical alteration was basically observed in bacteria containing nontronite, textural alteration is observed for both nontronite and montmorillonite (MX80) sample. The interaction of bacteria and smectite is known to be an aggregate forming process, particularly when associated with EPS production (Jaisi et al., 2007). Such mechanisms of aggregate formation are confirmed by microscopic investigations of the smectite-in-solution experiments where EPS are seen to be closely associated with the clustering and attachment of both bacteria and clay particles (cp. Fig. 5.3.12 and 5.3.13). Other indicators of particle aggregation are seen in the confined volume experiments where the basal intensities of smectite X-ray diffraction peaks are consistently lower in the presence of bacteria indicating poor particle orientation.

Both in compacted MX80 and nontronite clay, the presence of bacteria appear to create additional local porosity. In nontronite this additional pore space leads to a reduced ordering of the water layer structures (Fig. 5.4.3). Such fluctuations in stacking probabilities might represent unsystematic heterogeneities in water supply caused by bacterial water uptake. In contrast, the sterile sample shows a more systematic pattern indicating hydration of layers in clusters, as documented by the abiotic experiments (Chapter 4). For MX80, the effects are even more pronounced with enhanced water intake and the formation of thicker water layer structures that require more volume (Fig. 5.4.2). As packing densities are the same in MX80 experiments, the additional space is attributed to bacterial activity that causes i) formation of aggregates due to organic matter and clay interaction and ii) new porosity due to lyses. Additionally, the dissolution of accessory minerals in MX80 may contribute to additional pore space. A schematic representation is given in Fig. 5.5.3. During initial stages of hydration the bacteria are present in pore spaces and attached to mineral surfaces via binding cations (Fig. 5.5.3a). As the smectite hydrates and the pores get closed the bacteria are likely to produce EPS in order to protect themselves (5.5.2b). With increasing compaction the

bacteria die and disintegrate providing additional porespace, whereas the EPS remains, is associated with aggregates and accumulates cation (Fig. 5.5.3c).

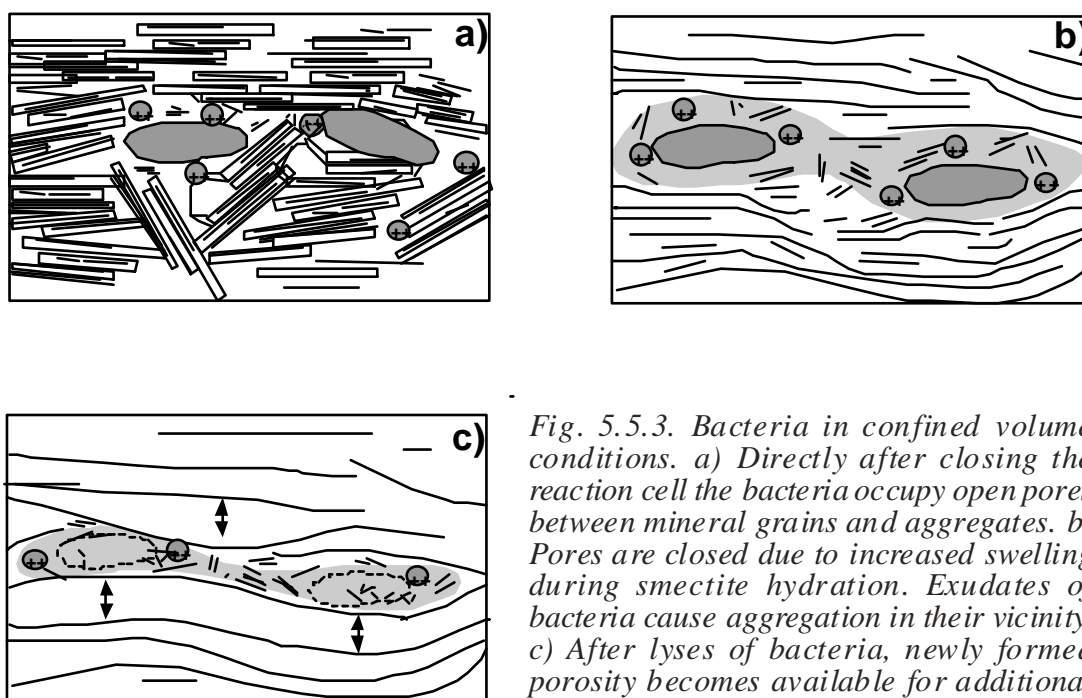


Fig. 5.5.3. Bacteria in confined volume conditions. a) Directly after closing the reaction cell the bacteria occupy open pores between mineral grains and aggregates. b) Pores are closed due to increased swelling during smectite hydration. Exudates of bacteria cause aggregation in their vicinity. c) After lyses of bacteria, newly formed porosity becomes available for additional swelling.

The amount of new pore space created by lyses should, however, not be overestimated. Simplifying the bacteria to be a water-filled prolate spheroid with an average dimension of $2 \times 0.5 \times 0.5 \mu\text{m}$ (size of a femtoliter, fl) one bacterium can be estimated to have a volume of ca. $0.26 \mu\text{m}^3$. The resulting increase in porosity occurs in the dimension of nanoliters and is, therefore, not of a magnitude to be detected in the methods applied. The breakdown of the cells alone does not contribute significantly to the porosity and it is more likely that a combination of aggregation, cell death and mineral dissolution are the main factors enhancing the available pore spaces (see biomineralization in appendix).

5.5.3. Concluding remarks

Generally, it is noted that the interaction between *S. putrefaciens* and smectite is very complex and several mechanisms are observed that depend on a number of physical and chemical variables. In the case of nontronite, the mineral properties are altered whereas for montmorillonite, the observed changes concern more the spatial organization and microstructure, but provoke no chemical alteration.

Batch experiments containing larger volumes of solution and lower proportions of clay clearly do show increased reaction rates and hence a more advanced state of reaction process. This type of study enhances knowledge of bacteria-smectite-solution interactions, allowing recognition of specific mechanisms and the fate of smectite derived cations. Basic mechanisms, such as complexation and binding, are likely to operate in compacted clays hydrated in confined volume conditions and the precise kinetics of these reactions under such conditions are more applicable to underground waste repositories. Therefore the reduced rates of reactions derived from the confined volume experiments are considered to be much more useful for predictive modeling of compacted clay systems.

CHAPTER 6

-

IMPLICATIONS OF SMECTITE HYDRATION IN BIOTIC AND ABIOTIC ENVIRONMENTS

CHAPTER 6 IMPLICATIONS OF SMECTITE HYDRATION IN ABIOTIC AND BIOTIC ENVIRONMENTS

6.1. Environmental processes and the importance of laboratory analogue experiments

The approach of studying environmental processes at and close to the Earth's surface classically combines direct investigations of natural systems, laboratory experiments and numerical modelling. As experiments conducted in the laboratory can be closely monitored and controlled, qualitative and quantitative data are provided which help constrain selected processes and aid our understanding of larger scale, complex natural and engineered systems (Wogelius & Vaughan, 2000). Laboratory experiments can therefore provide useful analogues that simulate the key processes operating in natural systems.

In this study, a flow-through reaction-cell (known as a "wet-cell") was successfully applied to study the progressive hydration of compacted swelling clays during the infiltration of aqueous solutions under confined volume conditions. This experimental setup is suggested to provide a useful analogue for predicting hydration behaviour in an underground waste repository site, where bentonite (smectite-rich) clays are likely to be used as a low permeability seal. Many of the conditions expected to occur in the underground repository were simulated in the experiments, including i) a range of high solid to liquid ratios, ii) hydration under anaerobic conditions and iii) both abiotic and biotic (bacteria containing) systems as well as both diffusive and advective mechanisms of transport. This approach was combined with the more traditional batch experimental approach required to study low solid to liquid ratios and agitated systems.

From the results of this thesis, it is evident that the hydration mechanisms dominant in batch experiments are not necessarily active in the confined volume state. This aspect is often ignored in many published studies (Komine, 2004; Komine & Ogata, 2004). For example, the hydration of Na-montmorillonite is dominated by osmotic swelling in solutions of low electrolyte concentration (Lagaly, 1993; , 2006) whereas, under confined volume conditions, the space for expansion is significantly limited and therefore the interlayer distance required for tactoid formation ($>20\text{\AA}$) is difficult to achieve. Based on the results obtained with the reaction-cell experiments it can be stated that the phenomenon of osmotic swelling is only locally observable and the majority of Na-smectite undergo restricted expansion associated

with the build up of swelling pressure. Local osmotic swelling in Na-smectite is likely to occur by gel formation in open pores. This process is of importance because gels lead to lower hydraulic conductivity and will also influence the rate and nature of elemental transport (Pusch, 2001b; Pusch, 2006b). Here, an important aspect is the connectivity of such gels that might facilitate diffusive transport (Pusch & Weston, 2003). Additionally, in contrast to smectite particles, gels are isotropic and, thus, transport is independent of the fabric. Such gels also readily form aggregates when in contact with solutions of elevated ionic strength (Fig. 4.3.2.) or in presence of bacterial exudates, as discussed in Chapter 5 (e.g. Fig. 5.3.11 and Fig. 5.4.4.c+d). These kind of textural changes are clearly seen to enhance permeability and the storage of external (non-interlayer) water in many of the experiments conducted.

Another important point is that the activity of bacteria is notably different for compacted smectite under confined volume conditions when compared to freely dispersed smectite in batch solution. It was observed that smectites in batch solutions have numerous beneficial effects on bacterial growth and survival. These effects are linked to their composition and exchange properties of key elements that are important for bacteria (Fig. 5.3.1, table 6.1). Some cations (e.g. Ca and Fe) act as nutrients whereas Fe(III) additionally, serves as terminal electron acceptor (TEA) for respiration. In the case of bentonites, the accessory minerals are also dissolved and contribute to the nutrient supply, such as pyrite (in MX80) that serves as a source for both Fe and S.

Other important properties of smectite aiding bacterial growth are: their variable edge charge, which can buffer the pH of the solution, and the high specific surface area that is available to adsorb toxic waste derived from metabolic activity (Dean & Hinshelwood, 1966; Postgate, 1976; Roszak & Colwell, 1987). However, in compacted clays, hydrated under confined volume conditions, the effects of buffering and/or adsorption are probably not the most significant factors influencing bacterial growth on the local scale (table 6.1). The results presented here indicate that the restricted transport properties of the compacted clay are the largest inhibiting factor. In the hydrating state, the available pore space becomes so restricted, and probably disconnected, that the bacteria become immobile and cannot access distant nutrients. In such a state, the bacteria-clay contacts become the principle sites of nutrient transfer, once the cations in the surrounding pore water have been depleted. Another factor leading to a decrease in the rate of transport within hydrating clay is the decreasing rate of water inflow when the sample reaches its saturation state. At the beginning of a clay hydration, water is drawn in relatively rapidly by suction (adhesive and cohesive properties of

capillary surfaces) but as it approaches saturation, the rate of water inflow is significantly reduced (Agus & Schanz, 2006; Pusch, 2006a; Erzin & Erol, 2007).

	In solution	Effect on bacteria in solution	Effect on bacteria in confined volume
Bulk bentonite composition			
Accessory minerals	Dissolution possible depending on conditions	Effect positive: Provide energy and nutrients (C _{org} , S and Fe(III))	Effect locally positive (see effect in solution)
Smectite composition			
Cations in structure	Partial release into solution possible	Effect positive: Serve as nutrients and TEA (Fe(III))	Effect locally positive (see effect in solution)
Physical and chemical properties of smectite			
Negative layer charge	Hydration Na-smectite: osmotic swelling	No Effect: Water not limiting factor Effect negative: Osmotic swelling of Na-smectite might induce electrostatic interactions (repulsion)	Effect negative: Competition for water; Creation of swelling pressure
CEC	Exchange	Effect positive: Provides cationic nutrients (Ca, Na); Ca aids binding	Effect locally positive (see effect in solution)
Variable edge charge	Buffering	Effect positive: Stabilizes pH	Effect insignificant (only local)
Specific surface area	Sorption (increasing)	Effect positive: Attachment site for bacteria, accumulates nutrients and sorbs toxins	Effect insignificant Due to limited expansion surfaces not accessible

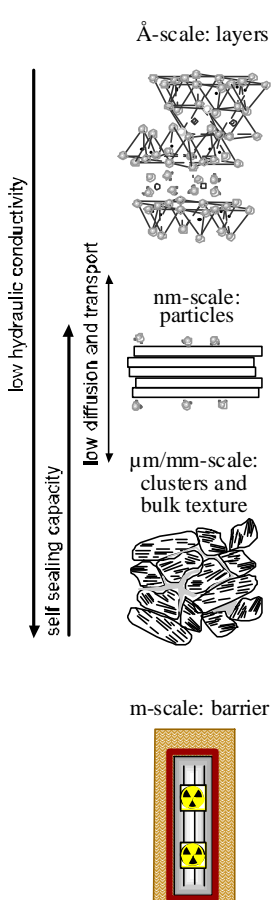
Table 6.1. A summary of the effects clay minerals have on bacterial growth in batch experiments (solution dominated system) and compacted confined volume experiments (mineral-dominated). TEA = Terminal electron acceptor.

Moreover, the key property of smectites, namely the ability to expand upon hydration, can be assumed to be highly detrimental for bacterial activity because of the high swelling pressures that are generated (100-1000kPa, Pusch 2006). Although the cell walls serve as a protection and can withstand significant turgor pressures (internal pressure of *E. coli* is estimated to be ca 200kPa (Madigan et al., 2003)), it is likely that the swelling pressure has a detrimental effect during hydration (table 6.1).

The experimental results on smectite-bacteria interaction clearly provide important information concerning the effects of smectite on bacterial survival. In the following section, the effects that bacteria have on modifying the properties of smectites materials are addressed. The results from progressive smectite hydration in a confined volume are discussed by considering behaviour in abiotic and biotic (*S. putrefaciens* bearing) conditions and their implications for underground nuclear waste disposal are explored.

6.2. Application of confined volume experiments: constraints for backfill hydration

The key requirement that an underground repository has to fulfil is to eliminate the risk of radionuclide transport from nuclear waste to the biosphere (OECD, 1999; ANDRA, 2005; OECD, 2006; Pusch, 2006a; 2006b). A smectite based material is considered to be suitable as backfill, basically, because of its properties that are dependent on the hydration capacity namely the i) low hydraulic conductivity, ii) the self sealing capacity and iii) a low diffusion and transport capacity for radionuclides (Pusch, 2006b). As discussed in Chapter 4, the hydration of smectite and related characteristics involves water retention on a range different scales and this should be taken into account when evaluating possible detrimental effects on a bentonite backfill. Table 6.2 compiles the main mechanisms of hydration as a function of different scales and summarizes the observed biotic and abiotic effects.



Basic mechanism upon hydration	Abiotic effects		Biotic effects	
	Na-montmorillonite	Ca-montmorillonite	Na-montmorillonite	Ca-nonttronite
Solvation of interlayer cations leads to interlayer hydration and expansion	High ionic strength led to formation of thicker WL structures because of increased porosity	High ionic strength compresses diffuse double layer around IL cations leading to thinner WL structures	Enhanced interlayer expansion due to increased porosity	Partial dissolution and changes in layer charge
Number of layers per particle decreases and external surfaces might be formed (less than in open systems)	Higher packing density restricts particle separation	No effect visible	Decreased number of layers per particle due to increased porosity	Decreased sorption capacity if partially dissolved
Expansion of particle-clusters and formation of gels lead to the closure of pore space	High ionic strength causes gels to aggregate and to increase porosity Increased packing leads to closure of pores	Not determined	Bacterial induced formation of aggregates creating additional porosity	Bacterial induced formation of aggregates and partial clay dissolution
Possible effects on a bentonite barrier	- HC lower than Ca-smectite - HC increased by ionic strength	- HC higher than Na-smectite - generally less affected by solution chemistry	- self sealing capacity disturbed by formation of aggregates - transport facilitated by enhanced porosity	-HC enhanced by chemical alteration (layer charge) - transport facilitated by dissolution and formation of aggregates

Table 6.2. Compilation of bentonite clay backfill properties and possible abiotic and biotic effects as a function of scale. IL = Interlayer water WL = Water layer HC = Hydraulic conductivity.

6.2.1. Predicting the rates of clay barrier saturation

The low hydraulic conductivity is one of the key properties of bentonites and it is essential that it is maintained when applied as a back fill material (Hermann-Stengele & Plötze, 2000; Karnland & Sandén, 2000; Pusch, 2006b; Pusch et al., 2007). This property is basically a consequence of the interlayer hydration that leads to particle expansion, which results in the closure of the available pore space. The pathways for solution transport are thus restricted on all scales as indicated by the vertical arrow in table 6.2. The major control on interlayer hydration appears to be the type of smectite used, and in particular the hydration energy of interlayer cation present, which controls the amount and rate of interlayer water uptake (Norrish, 1954; MacEwan & Wilson, 1980; Montes-Hernandez et al., 2003a). For example, compared to Na-smectite the uptake for Ca-smectite was observed to be more rapid and thicker hydrated interlayers were formed (e.g. Fig. 4.3.3, Fig. 4.3.12). The slow hydration rate in the case of Na-smectites revealed that the interlayer hydration is, in turn, highly dependant on the initial porosity because water that is entering the confined volume reaction-cell is first accommodated in pores that then serve as reservoir to fill the interlayer space (4.3.4. c+d, 4.3.10a). During the later stages of hydration, interlayers were seen to be the dominant storage site for water in all Na-smectite dominated systems providing a constant low hydraulic conductivity when infiltrated with water of a low ionic concentration.

In contrast, despite the higher hydration energy of Ca, water in Ca-activated bentonite was predominantly stored as external water (surface- and pore water) and not within interlayers. This behaviour is attributed to the differences in the microstructure on the aggregate and bulk texture scale whereby the thicker particles of Ca-smectite yield an enhanced porosity. This porosity is reduced during interlayer swelling, but is not completely sealed due to the absence of osmotically driven swelling and local gel formation as in Na-smectites (Chapter 4, fig. 4.4.3). Changes in the textural properties of Na-smectite clays are intimately linked with the enhancement of saturation velocity during the infiltrations of solutions with elevated ionic strength (Chapter 4, fig. 4.3.13). Such an enhancement can be attributed to the aggregation of clay particles, combined with the suppression of osmotic swelling. Despite these effects, the total amount of structured interlayer water taken in during hydration is still enhanced in the case of Na-smectite compared to Ca-smectite, whereas the quantity of external water (surface- and pore water) is relatively reduced (Chapter 4, fig. 4.3.13 b+d). This is the main reason Na-smectite that shows lower rates of water saturation

compared to Ca-smectite (e.g. $1.7E-08$ for IBECO vs. $4.0E-08$ m/s for TIXOTON) even in solutions of high ionic strength.

Values for water inflow were used to calculate the time that is required to saturate a compacted bentonite (table 4.4.2). Accordingly, a barrier of 1m industrial Na-bentonite (IBECO) infiltrated by sea water is saturated after 1.8 years, whereas the same thickness of industrial Ca-bentonite (TIXOTON) is saturated in less than 1 year (Fig. 6.1). The effect of the packing density can also be seen when comparing the different Na-bentonite MX80 samples: the lowest rates of water saturation are obtained for the dehydrated higher compacted sample (1.43 g/cm^3) that yields a saturation time of 24 years. In contrast, a pre-hydrated sample would need 10 years to accommodate its infiltrating solution (Fig. 6.1). However, the velocities required to saturate the barrier are, due to suction forces, much higher than the expected values for hydraulic conductivity at the saturated state ($< 1E-10$ m/s) (Jo et al., 2004) where transport through 1m of saturated barrier takes hundreds of years.

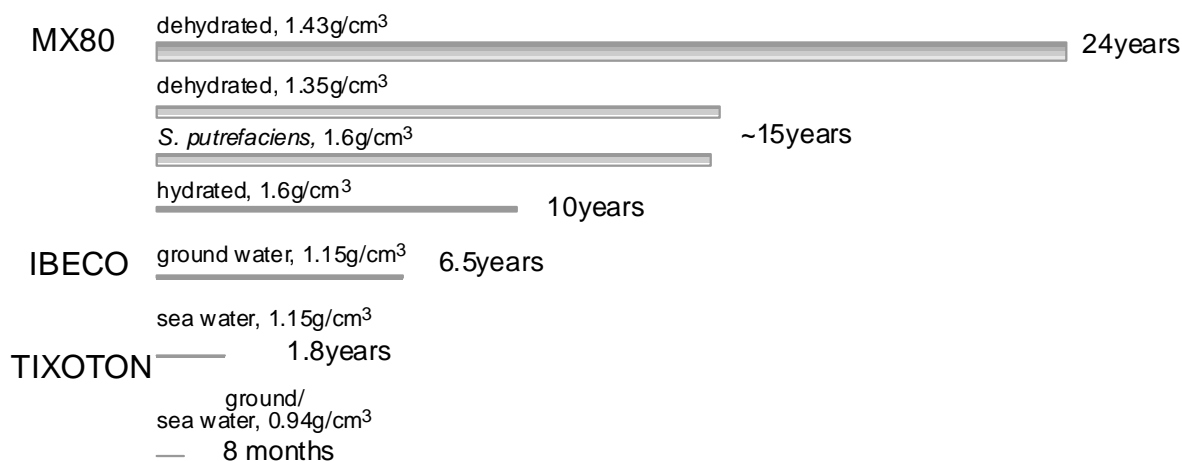


Fig. 6.1. Schematic sketch of the time required to saturate a 1m thick bentonite barrier as a function of initial packing density and the difference types of solutions infiltrated.

The experiments presented in chapter 5 clearly show that bacteria influence interlayer hydration by effecting the texture of smectite particles, particularly on the aggregate/ bulk texture scale (table 6.2). Their presence locally enhances the formation of aggregates (associated with the formation of exopolymeric substance (EPS)) and enhances additional pore space available for interlayer expansion, especially in the case of Na-smectite (Chapter 5, fig. 5.4.4 c+d). An additional mechanism was observed in the case of the Fe-rich Ca-smectite (nontronite) in the presence of *S. putrefaciens*. This bacteria enhanced the dissimilatory reduction of Fe(III) in octahedral structure which leads to an increase in the

layer charge (Chapter 5, fig. 5.4.9 and fig. 5.4.17). As the layer charge is responsible for interlayer hydration, Fe-reduction would be expected to be highly detrimental for the sealing capacity of the backfill clay and could lead to enhanced rates of water uptake and higher rates of elemental transport. However, in the confined volume experiments these effects were not observed because the bacterially induced Fe-reduction was only locally active. Contrarily, the rate of hydration was seen to be decreased when bacteria were present ($7.9\text{E-}09$ vs. $9.3\text{E-}08$ m/s), which could be caused by the clogging effects of EPS or other organic substances.

A scenario that would be highly detrimental to the sealing capacity of the clay barrier would be substantial smectite dissolution. This is most evident in the Fe-rich Ca-smectite (nontronite) batch reactions (high solution content) (Chapter 5, fig. 5.3.16) and to a lesser extent in compacted material hydrated under confined volume conditions (see section 5.5.2.4.) Such a material is, generally, not considered to be used as backfill but it is likely to form by solution alteration of bentonite in contact with the steel (Fe) containers (Wilson et al., 2006). According to the obtained results, the partial alteration of smectite in the presence of Fe-reducing bacteria could decrease the hydration capacity of this material considerably if bacterial action is sustained over significant periods of time. However, the extent of Fe-reducing bacteria activity is likely to be less significant on a repository scale compared to small-scaled laboratory experiments where relatively high populations of bacteria were introduced. Less abundant bacterial populations are certainly expected to be characteristic of the saturated underground backfill. Because the bacteria are not mobile under such conditions, they are not considered to survive or evolve over long periods of time (Pedersen, 2000; Pedersen et al., 2000). Any detrimental effects induced by the presence of bacteria would only occur in permeable, open portions of a bentonite barrier, such as along microcracks caused during hydration-dehydration cycles (Montes-Hernandez et al., 2003b). In such sites, bacterially-induced dissolution could become an important contributing mechanism to the breakage of the bentonite seal.

To summarize, the rate of water uptake is a function of a range of multi-scale hydration mechanisms that are highly dependent on the type of smectite. Because of microstructural characteristics, Ca-smectite exhibit higher rates of hydration but these types of clays are notable less sensitive to changes in solution chemistry. Bacterially induced textural and chemical alteration has the potential of enhancing the rates of water uptake whereas EPS production appears to aid the sealing of smectite based material.

6.2.2. Diffusion and transport capacity for radionuclides

Because of the restricted hydraulic conductivity it is generally assumed that diffusion controlled processes are dominant in compacted bentonite (Bors et al., 1997; Molera et al., 2003; Pusch, 2006b). As cations can be more easily fixed on the negatively charged clay surfaces it is further assumed that anion diffusion will be more operative (Oscarson et al., 1994) including the transport of anionic forms of long-lived radionuclides such as ^{129}I and ^{99}Tc (Molera et al., 2003). Both adsorption of cation and anion diffusion processes are largely controlled by the availability of sorption sites and are present on the hydrated surfaces and edges of smectite clays. Therefore, quantifications of the water budget, stored in interlayers on surface and within pore spaces provide here some useful constraints. During hydration, it was observed that the external surface area increases but to a lesser extent when the packing density is increased. In the case of dehydrated and compacted MX80 bentonite, surface calculations based on the decrease of layers per stack led to a value of around $80\text{m}^2/\text{g}$ at a packing density of $1.43\text{g}/\text{cm}^3$; this is half the surface area than the less compacted sample ($1.35\text{g}/\text{cm}^3$, Chapter 4). It is clear from these results that any modeling requiring an estimation of smectite surface area should consider that this variable is highly dependent on the state of hydration.

6.3. Limitations of the study: challenges for further research

This study aimed to simulate the hydration of compacted smectite under confined volume conditions and to characterize, by in situ XRD measurements both biotic and abiotic effects. Experiments were designed to constrain the importance of a range of initial characteristics, such as packing density and initial hydration state as well as experimental conditions such as different infiltrating solutions and the presence or not of bacteria. The packing densities studied was restricted to the range of $0.94\text{-}1.6\text{g}/\text{cm}^3$, and therefore the state of compressed bentonite blocks ($> 1.8\text{g}/\text{cm}^3$), that are especially developed to maximize sealing, were not tested. This provides scope for further in situ hydration experiments. In the same way, the effects of hydration-dehydration cycles, occurring during solution inflow and subsequent drying, could also be investigated using the reaction-cell approach, as these effects are only

well documented in conditions of varying humidity (Montes-Hernandez et al., 2003a; Montes-Hernandez et al., 2003b). Additionally further study on the effects of varying solution chemistry is possible as there are important constraints required on the rates of mineral dissolution in compacted smectite when influenced by the percolation of more corrosive acid and alkaline solutions (Bauer & Velde, 1999; Bauer et al., 2001).

The influence of bacteria was simplified by studying only one “model” species *Shewanella putrefaciens*. These are well studied bacteria capable of respiring in both aerobic and anaerobic conditions and have the important ability of reducing Fe(III) and modifying the crystal-chemistry of Fe-smectite (Kostka et al., 1996; Gates et al., 1998; Kim et al., 2004; Stucki & Kostka, 2006). However in natural and engineered systems, it is clear that such monocultures do not exist and bacteria coexist in consortia that are better adapted. For example, in the industrial available MX80-bentonite several species are naturally present and can be cultivated from the dry powder. These include spore-forming genera and species such as *Bacillus subtilis*, *Bacillus cereus* and *Brevibacillus brevis* as well as desiccation-resistant species such as *Pseudomonas stutzeri* (Pedersen, 2000). Additional bacteria species will be introduced via the ground water (Meike & Stroes-Gascoyne, 2000). As a result of this natural diversity, it is an enormous challenge to study the role of these indigenous consortia in influencing the hydration behaviour and transport properties of the smectite-based bentonite seal.

A general limitation in applying the results of laboratory experiments is the problem of extrapolating over the long time period that underground waste repositories should remain sealed (1Ma) which is determined by the long lifetime of certain radionuclides (Madsen, 1998; OECD, 1999; , 2006; Pusch, 2006b). Taking into account that this is about the time span between the first occurrence of fossil hominids and today, gives an impression about the “controllability” of a repository site (Asfaw et al., 2002). Therefore, continuous and careful research is essential and should not aim to provide quick solutions to complex problems.

GENERAL
CONCLUSIONS

GENERAL CONCLUSIONS

- The reaction-cell (“wet-cell” device) employed in this study, developed by Warr & Hoffman (2004) provides an efficient laboratory analogue for monitoring in situ the hydration of compacted smectite clays in percolating solution. The confined volume nature of this reaction cell is considered to simulate more closely the conditions smectite clays will experience in an engineered underground waste repository site. This experimental setup was successfully applied to investigate smectite hydration in both abiotic and biotic (bacteria containing) conditions by in situ X-ray diffraction study, combined with gravimetric measurement with minimal disturbance of the sample set up.
- Combining XRD-peak calculations by using the CALCMIX software (Plançon & Drits, 1999) plus water vapour adsorption data (Cases et al., 1992; Bérend et al., 1995; Cases et al., 1997; Jänchen et al., 2006) allowed successful quantification of the amount of water stored in both interlayer and non-interlayer (surface and pore) sites (Warr & Berger, 2007). Additionally, the changes in particle thickness were calculated and qualitatively used to estimate changes in smectite surface area during hydration. As these analytical results are time dependent, based on up to 25 measurements per experiment, the dynamic changes in hydration state could be well defined.
- The combination of classical microbiological and mineralogical methods (viable cell counts, XRD, SEM, TEM and ICP-OES) was successfully applied to study *S. putrefaciens* and smectite interaction under conditions of varying solution to mineral ratios (including variable agitated batch reactors).
- In compacted Na-smectite powders, hydration proceeded first by saturating external sites (surface- and pore water) and then by redistributing this water into interlayer sites. Knowledge of water storage as a function of solution chemistry and as packing density is important for predicting smectite hydration in underground bentonite backfill and to assess barrier performance in terms of the rate of water inflow, sealing capacity and sorption and/or transport of radionuclides. Additional constraints for the numerical modeling of material transport are provided based on the experimentally

determined mechanisms and on the rates of water intake and dynamic changes in the textural and surface properties of the clay minerals.

- The process of bulk clay hydration occurs at different scales, ranging from the Angstrom (lattice-layer) to the bulk (micron to mm) structure, including particles, clusters of particles and arrangements of clusters (aggregates). The hydration mechanism on the lattice scale is mostly influenced by the type of interlayer cation present, whereas the bulk texture of the material is largely affected by the ionic strength of the infiltrating solution.
- *S. putrefaciens* grown in smectite suspensions showed enhanced numbers in colony forming units and prolonged survival compared to growth in standard culture medium (LB and minimal media). This beneficial effect is attributed to the sustainable supply of cationic nutrients, organic carbon, the buffering capacity of clay minerals, and their large surface areas that accumulate nutrients, serve as attachment sites and adsorb toxic waste. In the biotic systems, the pH was seen to depend on the growth phase, with a lower pH observed during the initial stages (lag and exponential phase). This is attributed to proton production during anaerobic respiration. In contrast, during the final stages (the death phase) of growth, more alkaline pH values are observed that is related to the reduced buffering of the bacterial cells and the release of lyses products.
- The rate of bacterially induced smectite alteration/dissolution in batch solutions, as monitored by ICP-OES, showed depletion of the main cations in the nontronite extracted solution. This is attributed to the initial consumption and/or binding of cations by *S. putrefaciens*. Constant depletion of Ca occurs, most likely, due to the production of EPS. The release of other cations during the later stages of the batch experiments is attributed to cell lyses. When compared to the sterile control, the compacted smectites within the confined volume reaction-cell showed enhanced cation release in bacteria-containing nontronite solutions. This was especially evident for Fe values after acid leaching and it corresponded to partial dissolution of nontronite as confirmed by TEM coupled to EDX. This dissolution was observed to be closely associated with the formation of Si-rich gels and EPS. Characterization of the reaction products from confined volume experiments showed the presence of redox sensitive phases and an enhanced layer charge for nontronite due to Fe(III) reduction. Solutions extracted from the MX80 bentonite experiments showed less difference between bacteria containing and sterile samples. The increased release of Al by acid leaching corresponds to a maximal of 1.4% partial smectite dissolution.

- The presence of *S. putrefaciens* caused abundant textural changes, as observed by microscopic investigations (confocal microscopy, ESEM) associated with the formation of smectite-aggregates and biofilm. In confined volume conditions, the presence of bacteria in Na-smectite clay was seen to enhance both the uptake of interlayer water and the amount of externally stored surface- and pore water. In this type of compacted smectite, an increase in the total thickness of hydrated interlayers occurs due to bacterial enhancement of sample porosity (XRD and CALCMIX). In the case of nontronite, additional water was stored as external water indicating a similar enhancement of porosity but, here, the rate of water inflow into the reaction cell decreases in the presence of *S. putrefaciens* indicating the probable clogging of the pores by biofilm. The presence of these bacteria during nontronite hydration also led to a decrease in the ordering of water layers indicating increased heterogeneities.
- The interaction between *S. putrefaciens* and the different types of smectites tested clearly encourages the growth of bacteria in clay solutions. Their role in providing a cationic nutrient supply, energy sources and reactive mineral surfaces are linked to the key smectite properties that are most active in free swelling environments. However, under confined volume conditions these effects are significantly limited by the hindered mobility of bacteria and the buildup of swelling pressures. The most detrimental effects occurred in the nontronite clay because of chemical alteration most likely triggered by chelators and other bacterially produced substances.

Concerning the possible application of bentonites as backfill material, it can be concluded that the bacteria, present during the initial stages of water inflow, will certainly influence the hydration behaviour and modify the properties of the clay barrier, especially by bacterially produced substances that reside after the cells death (chelators, EPS). Therefore, although it is generally considered that bacteria might not survive in a hydrating bentonite (except in the form of spores), their presence should be taken into account when predicting the hydration and sealing properties of smectite-based material. In order to study bacteria–mineral interactions, in both natural and engineered systems, an interdisciplinary approach and the understanding of multi-scale processes are essential to design and control safer clay barrier systems.

RÉFÉRENCES

- Agus, S. S. and T. Schanz (2006). Drying, wetting, and suction characteristic curves of a bentonite-sand mixture. Geotechnical Special Publication.
- ANDRA (2005). Dossier 2005 - Argile, Andra, France.
- Andrade, S., R. Hypolito, H. H. G. J. Ulbrich and M. L. Silva (2002). "Iron(II) oxide determination in rocks and minerals." *Chemical Geology* 182(1): 85-89.
- Aouad, G. (2006). Influence de *Pseudomonas aeruginosa* sur la dégradation de silicates: incidence sur la stabilité de matrices de confinement de déchets et d'un mâchefer industriel. Ecole et Observatoire des Science de la Terre UMR7517. Strasbourg, Université Louis Pasteur: 137.
- Aouad, G., J. L. Crovisier, V. A. Geoffroy, J. M. Meyer and P. Stille (2006). "Microbially-mediated glass dissolution and sorption of metals by *Pseudomonas aeruginosa* cells and biofilm." *Journal of Hazardous Materials* 136(3): 889-895.
- Apelo, C. and D. Postma (1994). Geochemistry Groundwater and Pollution. Rotterdam, Balkema.
- Asfaw, B., W. H. Gilbert, Y. Beyene, W. K. Hart, P. R. Renne, G. WoldeGabriel, E. S. Vrba and T. D. White (2002). "Remains of *Homo erectus* from Bouri, Middle Awash, Ethiopia." *Nature* 416(6878): 317-320.
- Bailey, S. W. (1980). Structure of Layer Silicates. In: Crystal Structures of Clay Minerals and their X-Ray Identification. G.W. Brindley and G. Brown. London, Mineralogical Society. 5: 1-125.
- Banfield, J. F. and R. J. Hamers (1997). "Processes at minerals and surfaces with relevance to microorganisms and prebiotic synthesis." *Reviews in Mineralogy* 35: 116-122.
- Banfield, J. F. and S. A. Welch (2000). Microbial controls on the mineralogy of the environment. In: Environmental Mineralogy. David J. Vaughan and R.A. Wogelius. Budapest, Eotvos University Press. 2: 173-196.
- Barker, W. W., S. A. Welch and J. F. Banfield (1997). "Biogeochemical weathering of silicate minerals." *Reviews in Mineralogy* 35: 419-428.
- Barker, W. W., S. A. Welch, S. Chu and J. F. Banfield (1998). "Experimental observations of the effects of bacteria on aluminosilicate weathering." *American Mineralogist* 83(11-12 PART 2): 1551-1563.
- Bauer, A., T. Schäfer, R. Dohrmann, H. Hoffmann and J. I. Kim (2001). "Smectite stability in acid salt solutions and the fate of Eu, Th and U in solution." *Clay Minerals* 36(1): 93-103.
- Bauer, A. and B. Velde (1999). "Smectite transformation in high molar KOH solutions." *Clay Minerals* 34(2): 259-273.
- Bennett, P. C., F. K. Hiebert and W. J. Choi (1996). "Microbial colonization and weathering of silicates in a petroleum-contaminated groundwater." *Chemical Geology* 132(1-4 SPEC. ISS.): 45-53.
- Bennett, P. C., J. R. Rogers, W. J. Choi and F. K. Hiebert (2001). "Silicates, silicate weathering, and microbial ecology." *Geomicrobiology Journal* 18(1): 3-19.
- Bérend, I., J. M. Cases, M. François, J. P. Uriot, L. Michot, A. Masion and F. Thomas (1995). "Mechanism of adsorption and desorption of water vapor by homoionic montmorillonites: 2. The Li⁺, Na⁺, K⁺, Rb⁺ and Cs⁺- exchanged forms." *Clays & Clay Minerals* 43(3): 324-336.
- Bergaya, F. and G. Lagaly (2006). Chapter 1 General Introduction: Clays, Clay Minerals, and Clay Science. In: Developments in Clay Science. F. Bergaya, B.K.G. Theng and G. Lagaly, Elsevier. Volume 1: 1-18.
- Beveridge, T. J. (1989). Metal ions and bacteria. In: Metal ions and bacteria. R.D. TJ Beveridge. New York, Wiley: 1-29.
- Bickmore, B. R., D. Bosbach, M. F. Hochella Jr, L. Charlet and E. Rufe (2001). "In situ atomic microscopy study of hectorite and nontronite dissolution: Implications for phyllosilicate edge surface structures and dissolution mechanisms." *American Mineralogist* 86(4): 411-423.
- Birkel, U., G. Gerold and J. Niemeyer (2002). Abiotic reactions of organics on clay mineral surfaces. In: Developments in Soil Science. A. Violante, P.M. Huang, J.M. Bollag and L. Gianfreda. Amsterdam, Elsevier. 28A: 437-448.
- Blum, A. and A. Lasaga (1988). "Role of surface speciation in the low-temperature dissolution of minerals." *Nature* 331(6155): 431-433.

- Bonneville, S., P. Van Cappellen and T. Behrends (2004). "Microbial reduction of iron(III) oxyhydroxides: effects of mineral solubility and availability." *Chemical Geology* 212(3-4): 255-268.
- Bors, J., A. Gorny and S. Dultz (1997). "Sorption Characteristics of Radioiodide on Organophilic Bentonite." *Radiochimica Acta* 78(1): 117-121.
- Bosbach, D., L. Charlet, B. Bickmore and Hochella M.F, Jr. (2000). "The dissolution of hectorite: In-situ, real-time observations using atomic force microscopy." *American Mineralogist* 85(9): 1209-1216.
- Bourg, I. C., A. C. M. Bourg and G. Sposito (2003). "Modeling diffusion and adsorption in compacted bentonite: a critical review." *Journal of Contaminant Hydrology* 61(1-4): 293-302.
- Bowman, J. P. (2005). Genus XIII. *Shewanella*. In: Bergey's Manual of Systematic Bacteriology. D.J. Brenner, N.R. Krieg, J.T. Stanley and G.M. Garrity. New York, Springer: 480-491.
- Bradbury, M. H. and B. Baeyens (2003). "Porewater chemistry in compacted re-saturated MX-80 bentonite." *Journal of Contaminant Hydrology* 61(1-4): 329-338.
- Bradley, W. F., R. E. Grim and G. F. Clark (1937). "A study of the behavior of montmorillonite on wetting." *Z. Kristallogr.* 97: 260-270.
- Bray, H. J., S. A. T. Redfern and S. M. Clark (1998). "The kinetics of dehydration in Camontmorillonite: An in situ X-ray diffraction study." *Mineralogical Magazine* 62(5): 647-656.
- Brigatti, M. F., E. Galan and B. K. G. Theng (2006). Chapter 2 Structures and Mineralogy of Clay Minerals. In: Developments in Clay Science. F. Bergaya, B.K.G. Theng and G. Lagaly, Elsevier. Volume 1: 19-86.
- Bright, J. J. and M. Fletcher (1983). "Amino acid assimilation and respiration by attached and free-living populations of a marine *Pseudomonas* sp." *Microbial Ecology* 9(3): 215-226.
- Brown, C. M., D. C. Ellwood and J. R. Hunter (1977). "Growth of bacteria at surfaces: Influence of nutrient limitation." *FEMS Microbiology Letter* 1(3): 163-166.
- Brown, G. and G. W. Brindley (1984). Crystal Structures of Clay Minerals and their X-Ray Identification. London, Mineralogical Society.
- Cases, J. M., I. Bérend, G. Besson, M. François, J. P. Uriot, F. Thomas and J. E. Poirier (1992). "Mechanism of adsorption and desorption of water vapor by homoionic montmorillonite. 1. The sodium-exchanged form." *Langmuir* 8(11): 2730-2739.
- Cases, J. M., I. Bérend, M. François, J. P. Uriot, L. J. Michot and F. Thomas (1997). "Mechanism of adsorption and desorption of water vapor by homoionic montmorillonite: 3. The Mg²⁺, Ca²⁺, Sr²⁺ and Ba²⁺ exchanged forms." *Clays and Clay Minerals* 45(1): 8-22.
- Chipera, S. J. and D. L. Bish (2001). "Baseline studies of the clay minerals society source clays: Powder X-ray diffraction analyses." *Clays and Clay Minerals* 49(5): 398-409.
- Chipera, S. J., J. W. Carey and D. L. Bish (1997). Controlled-humidity XDR analyses: application to the study of smectite expansion/contraction. In: Advances in X-ray Analysis. J. Gilfrich. New York, Plenum Press. 39: 713-722.
- Claessens, J. W. (2006). Surface chemistry and acid-base activity of *Shewanella putrefaciens*: Cell wall charging and metal binding to bacterial cell walls. Earth Science-Geochemistry. Utrecht, Utrecht University: 127.
- Coby, A. J. and F. W. Picardal (2005). "Inhibition of NO₃⁻ and NO₂⁻ reduction by microbial Fe(III) reduction: Evidence of a reaction between NO₂⁻ and cell surface-bound Fe²⁺." *Applied and Environmental Microbiology* 71(9): 5267-5274.
- Collins, D. R., A. N. Fitch and C. R. A. Catlow (1992). "Dehydration of vermiculites and montmorillonites: a time-resolved powder neutron diffraction study." *Journal of Material Chemistry* 2(8): 865-873.
- Corliss, J. B., J. Dymond and L. I. Gordon (1979). "Submarine thermal springs of the Galapagos Rift." *Science* 203: 1073-1083.
- Cuadros, J. and S. P. Altaner (1998). "Characterization of mixed-layer illite-smectite from bentonites using microscopic, chemical, and X-ray methods: constraints on the smectite-to-illite transformation mechanism." *American Mineralogist* 83(7-8): 762-774.
- Cui, Y. J., M. Yahia-Aissa and P. Delage (2002). "A model for the volume change behavior of heavily compacted swelling clays." *Engineering Geology* 64(2-3): 233-250.

- Dawson, M. P., B. A. Humphrey and K. C. Marshall (1981). "Adhesion: A tactic in the survival strategy of a marine vibrio during starvation." *Current Microbiology* 6(4): 195-199.
- Dean, A. C. R. and C. N. Hinshelwood (1966). Growth, funktion and regulation in acterial cells. Oxford, Claredon Press.
- Delage, P., M. D. Howat and Y. J. Cui (1998). "The relationship between suction and swelling properties in a heavily compacted unsaturated clay." *Engineering Geology* 50(1-2): 31-48.
- Delay, J., A. Vinsot, J. M. Krieguer, H. Rebours and G. Armand (2007). "Making of the underground scientific experimental programme at the Meuse/Haute-Marne underground research laboratory, North Eastern France." *Physics and Chemistry of the Earth* 32(1-7): 2-18.
- DiChristina, T. J., R. G. Arnold, M. E. Lidstrom and M. R. Hoffmann (1988). "Dissimilative iron reduction by the marine eubacterium *Alteromonas putrefaciens* strain 200." *Water Science and Technology* 20(11-12): 69-79.
- Dong, H., J. K. Fredrickson, D. W. Kennedy, J. M. Zachara, R. K. Kukkadapu and T. C. Onstott (2000). "Mineral transformation associated with the microbial reduction of magnetite." *Chemical Geology* 169(3-4): 299-318.
- Dong, H., J. E. Kostka and J. Kim (2003a). "Microscopic evidence for microbial dissolution of smectite." *Clays and Clay Minerals* 51(5): 502-512.
- Dong, H., R. K. Kukkadapu, J. K. Fredrickson, J. M. Zachara, D. W. Kennedy and H. M. Kostandarithes (2003b). "Microbial reduction of structural Fe(III) in illite and goethite." *Environmental Science and Technology* 37(7): 1268-1276.
- Drits, V., J. Srodon and D. D. Eberl (1997). "XRD measurement of mean crystallite thickness of illite and illite/smectite: Reappraisal of the Kubler index and the Scherrer equation." *Clays and Clay Minerals* 45(3): 461-475.
- Drits, V. A., D. D. Eberl and J. Srodon (1998). "XRD measurement of mean thickness, thickness distribution and strain for illite and illite-smectite crystallites by the Bertaut-Warren-Averbach technique." *Clays and Clay Minerals* 46(1): 38-50.
- Dud'a, R., L. Rejl and D. Slivka (1992). La Grande Encyclopedie des Mineraux. Paris, Librairie Gründ.
- Eberl, D. D., R. Nuesch, V. Sucha and S. Tsipursky (1998). "Measurement of fundamental illite particle thicknesses by X-ray diffraction using PVP-10 intercalation." *Clays and Clay Minerals* 46(1): 89-97.
- Ehrlich, H. L. (1996). Geomicrobiology. New York, Marcel Dekker.
- Ehrlich, H. L. (1999). "Microbes as Geologic Agents: Their Role in Mineral Formation." *Geomicrobiology Journal* 16(2): 135 - 153.
- Ellwood, D. C., C. W. Keevil, P. D. Marsh, C. M. Brown and J. N. Wardell (1982). "Surface-associated growth." *Philosophical transactions of the Royal Society of London. Series B: Biological sciences* 297(1088): 517-532.
- Elsass, F. (2006). Chapter 12.8 Transmission Electron Microscopy. In: Developments in Clay Science. F. Bergaya, B.K.G. Theng and G. Lagaly, Elsevier. Volume 1: 939-963.
- Elzea, J. M. and H. H. Murray (1990). "Variation in the mineralogical, chemical and physical properties of the Cretaceous Clay Spur bentonite in Wyoming and Montana (USA)." *Applied Clay Science* 5(3): 229-248.
- ENRESA (2007). Full-scale High Level Waste Engineered Barriers (FEBEX). Grimsel Test Site (GTS)- www.grimsel.com.
- Erzin, Y. and O. Erol (2007). "Swell pressure prediction by suction methods." *Engineering Geology* 92(3-4): 133-145.
- Faraldo-Gomez, J. D. and M. S. P. Sansom (2003). "Acquisition of siderophores in Gram-negative bacteria." *Nat Rev Mol Cell Biol* 4(2): 105-116.
- Farmer, V. C. and J. D. Russel (1971). "Interlayer complexes in layer silicates." *Transactions of the Faraday Society* 67: 2737-2749.
- Fein, J. B., S. Scott and N. Rivera (2002). "The effect of Fe on Si adsorption by *Bacillus subtilis* cell walls: Insights into non-metabolic bacterial precipitation of silicate minerals." *Chemical Geology* 182(2-4): 265-273.

- Ferrage, E., B. Lanson, N. Malikova, A. Plançon, B. A. Sakharov and V. A. Drits (2005a). "New insights on the distribution of interlayer water in bi-hydrated smectite from X-ray diffraction profile modeling of 001 reflections." *Chemistry of Materials* 17(13): 3499-3512.
- Ferrage, E., B. Lanson, B. A. Sakharov and V. A. Drits (2005b). "Investigation of smectite hydration properties by modeling experimental X-ray diffraction patterns: Part I: Montmorillonite hydration properties." *American Mineralogist* 90(8-9): 1358-1374.
- Flemming, H. C. (1995). "Sorptions sites in biofilms." *Water Science and Technology* 32(8): 27-33.
- Fox, G. E., K. R. Pechman and C. R. Woese (1977). "Comparative cataloging of 16S ribosomal ribonucleic acid: molecular approach to procaryotic systematics." *International Journal of Systematic Bacteriology* 27(1): 44-57.
- Fredrickson, J. K. and T. C. Onstott (1996). "Microbes deep inside the earth." *Scientific American* 275(4): 68-73.
- Fredrickson, J. K., J. M. Zachara, D. L. Balkwill, D. Kennedy, S. M. W. Li, H. M. Kostandarithes, M. J. Daly, M. F. Romine and F. J. Brockman (2004). "Geomicrobiology of high-level nuclear waste-contaminated vadose sediments at the Hanford Site, Washington State." *Applied and Environmental Microbiology* 70(7): 4230-4241.
- Furukawa, Y. and S. E. O'Reilly (2007). "Rapid precipitation of amorphous silica in experimental systems with nontronite (NAu-1) and *Shewanella oneidensis* MR-1." *Geochimica et Cosmochimica Acta* 71(2): 363-377.
- Garavito, A. M., P. De Canniere and H. Kooi (2007). "In situ chemical osmosis experiment in the Boom Clay at the Mol underground research laboratory." *Physics and Chemistry of the Earth* 32(1-7): 421-433.
- Gates, W. P., A. M. Jaunet, D. Tessier, M. A. Cole, H. T. Wilkinson and J. W. Stucki (1998). "Swelling and texture of iron-bearing smectites reduced by bacteria." *Clays and Clay Minerals* 46(5): 487-497.
- Gates, W. P., P. G. Slade, A. Manceau and B. Lanson (2002). "Site occupancies by iron in nontronites." *Clays and Clay Minerals* 50(2): 223-239.
- Gauthier, G., M. Gauthier and R. Christen (1995). "Phylogenetic analysis of the genera *Alteromonas*, *Shewanella*, and *Moritella* using genes coding for small-subunit rRNA sequences and division of the genus *Alteromonas* into two genera, *Alteromonas* (emended) and *Pseudoalteromonas* gen. nov., and proposal of twelve new species combinations." *International Journal of Systematic Bacteriology* 45(4): 755-761.
- Gorshkov, A. I., V. A. Drits, G. A. Dubinina, O. A. Bogdanova and A. V. Sivtsov (1992). "The role of bacterial activity in the formation of hydrothermal Fe- Mn-formations in the northern part of the Lau Basin (south-western part of the Pacific Ocean)." *Izvestiya - Akademiya Nauk, Seriya Geologicheskaya* 9: 84-93.
- Gram, L. (1994). "Siderophore-mediated iron sequestering by *Shewanella putrefaciens*." *Applied and Environmental Microbiology* 60(6): 2132-2136.
- Grim, R. E. (1962). Applied Clay Mineralogy. New York, McGraw-Hill.
- Gustafsson, B. G. (2004). "Sensitivity of Baltic Sea salinity to large perturbations in climate." *Climate Research* 27(3): 237-251.
- Haas, J. R. (2004). "Effects of cultivation conditions on acid-base titration properties of *Shewanella putrefaciens*." *Chemical Geology* 209(1-2): 67-81.
- Haas, J. R., T. J. Dichristina and R. Wade (2001). "Thermodynamics of U(VI) sorption onto *Shewanella putrefaciens*." *Chemical Geology* 180(1-4): 33-54.
- Harvey, C. C. and G. Lagaly (2006). Chapter 10.1 Conventional Applications. In: Developments in Clay Science. F. Bergaya, B.K.G. Theng and G. Lagaly, Elsevier. Volume 1: 501-540.
- Haycox, J. R., W. S. Pettitt, D. S. Collins and R. P. Young (2006). Validating 3-D numerical models of rock fracture with laboratory and field scale studies. 5th ICEG Environmental Geotechnics: Opportunities, Challenges and Responsibilities for Environmental Geotechnics - Proceedings of the ISSMGE 5th Int. Congress.
- Herbert, H. J. and H. C. Moog (1999). "Cation exchange, interlayer spacing, and water content of MX-80 bentonite in high molar saline solutions." *Engineering Geology* 54(1-2): 55-65.

- Hermann-Stengele, R. and M. Plötze (2000). Suitability of mineral for controlled landfill and containment. In: Environmental Mineralogy. David J. Vaughan and R.A. Wogelius. Budapest, Eotvos University Press. 2: 291-331.
- Hersman, L., T. Lloyd and G. Sposito (1995). "Siderophore-promoted dissolution of hematite." *Geochimica et Cosmochimica Acta* 59(16): 3327-3330.
- Hersman, L. E., A. Huang, P. A. Maurice and J. H. Forsythe (2000). "Siderophore production and iron reduction by *Pseudomonas mendocina* in response to iron deprivation." *Geomicrobiology Journal* 17(4): 261-273.
- Hofman, H. (2003). Einfluss konzentrierter Salzlösungen auf die physiko-chemischen Eigenschaften quellfähiger Tonminerale: Konsequenzen für den Einsatz von Bentonit als Versatzmaterial in einem Endlager für schwach- bis mittelradioactive Abfälle in Salzformationen. Naturwissenschaftlich-Mathematische Gesamtfakultät. Heidelberg, Ruprecht-Karls-Universität: 189.
- Hofman, U. and W. Bilke (1936). "Intercrystalline swelling of montmorillonite." *Kolloidzeitschrift* 77: 239-251.
- Hofmann, H., A. Bauer and L. N. Warr (2004). "Behavior of smectite in strong salt brines under conditions relevant to the disposal of low- to medium-grade nuclear waste." *Clays and Clay Minerals* 52(1): 14-24.
- Hofmann, U., R. Fahn and A. Weiss (1957). "Thixotropie bei Kaolinit und innerkristalline Quellung bei Montmorillonit - Wirkung der austauschfähigen Kationen, der Flüssigkeit und der Elektrolyte einer wäßrigen Lösung." *Kolloid-Zeitschrift* 151(2): 97-115.
- Horgan, G. W. (1999). "An investigation of the geometric influences on pore space diffusion." *Geoderma* 88(1-2): 55-71.
- Huber, R., M. Kurr, H. W. Jannasch and K. O. Stetter (1989). "A novel group of abyssal methanogenic archaeobacteria (*Methanopyrus*) growing at 110°C." *Nature* 342(6251): 833-834.
- Huheey, J. E. (1993). Inorganic Chemistry: Principles of structure and Reactivity. New York, Harpers Collins College Publishers.
- Ivanov, M. V. and G. I. Karavaiko (2004). "Geological Microbiology." *Microbiological Reviews* 73(5): 493-508.
- Jaisi, D. P., H. Dong, J. Kim, Z. He and J. P. Morton (2007). "Nontronite particle aggregation induced by microbial Fe(III) reduction and exopolysaccharide production." *Clays and Clay Minerals* 55(1): 96-107.
- Jänchen, J., D. L. Bish, D. T. F. Möhlmann and H. Stach (2006). "Investigation of the water sorption properties of Mars-relevant micro- and mesoporous minerals." *Icarus* 180(2): 353-358.
- Jo, H. Y., C. H. Benson and T. B. Edil (2004). "Hydraulic conductivity and cation exchange in non-prehydrated and prehydrated bentonite permeated with weak inorganic salt solutions." *Clays and Clay Minerals* 52(6): 661-679.
- Jolley, D. M. (2002). Radionuclide uptake and transport on microbes in potential repository drifts at Yucca Mountain, Nevada. Materials Research Society Symposium - Proceedings.
- Jorand, F., B. M. R. Appenzeller, M. Abdelmoula, P. Refait, J. C. Block and J. M. R. Genin (2000). "Assessment of vivianite formation in *Shewanella putrefaciens* culture." *Environmental Technology* 21(9): 1001-1005.
- Kalinowski, B. E., L. J. Liermann, S. Givens and S. L. Brantley (2000). "Rates of bacteria-promoted solubilization of Fe from minerals: A review of problems and approaches." *Chemical Geology* 169(3-4): 357-370.
- Karaborni, S., B. Smit, W. Heidug, J. Urai and E. Van Oort (1996). "The swelling of clays: Molecular simulations of the hydration of montmorillonite." *Science* 271(5252): 1102-1104.
- Karland, O. (2003). "Session 3: Introduction and Conclusions by Session Chairman." *Applied Clay Science* 23(1-4): 167.
- Karland, O. and T. Sandén (2000). Long Term Test of Buffer Material at Aspö Hard Rock Laboratory, Sweden. Materials Research Society Symposium - Proceedings.
- Karland, O., T. Sandén, L.-E. Johannesson, T. Eriksen, M. Jansson, S. Wold, K. Pedersen and B. Rosborg (2000). Long term test of buffer material Final report on the pilot parcels. SKB Technical Report TR-00-22.

- Kawano, M. and K. Tomita (2001). "Microbial biomineralization in weathered volcanic ash deposit and formation of biogenic minerals by experimental incubation." *American Mineralogist* 86(4): 400-410.
- Keeling, J. L., M. D. Raven and W. P. Gates (2000). "Geology and characterization of two hydrothermal nontronites from weathered metamorphic rocks at the Uley Graphite Mine, South Australia." *Clays and Clay Minerals* 48(5): 537-548.
- Kim, J., H. Dong, J. Seabaugh, S. W. Newell and D. D. Eberl (2004). "Role of Microbes in the Smectite-to-Illite Reaction." *Science* 303(5659): 830-832.
- Kim, J. W., Y. Furukawa, T. L. Daulton, D. Lavoie and S. W. Newell (2003). "Characterization of microbially Fe(III)-reduced nontronite: Environmental cell-transmission electron microscopy study." *Clays and Clay Minerals* 51(4): 382-389.
- Kim, J. W., Y. Furukawa, H. Dong and S. W. Newell (2005). "The effect of microbial FE(III) reduction on smectite flocculation." *Clays and Clay Minerals* 53(6): 572-579.
- King, F., M. Kolar, S. Stroes-Gascoyne, P. Bellingham, C. H. U. James and P. V. D. Awe (1999). Modelling the activity of sulphate-reducing bacteria and the effects on container corrosion in an underground nuclear waste disposal vault. Materials Research Society Symposium - Proceedings.
- King, F., M. Kolar, S. Stroes-Gascoyne and P. Maak (2004). Model for the microbiological corrosion of copper containers in a deep geologic repository. Materials Research Society Symposium Proceedings.
- Klug, H. P. and L. E. Alexander, Eds. (1954). X-ray diffraction procedures for polycrystalline and amorphous materials.
- Koch, A. L. (1986). "The pH in the neighborhood of membranes generating a protonmotive force." *Journal of theoretical biology* 120(1): 73-84.
- Kohler, B., A. Singer and P. Stoffers (1994). "Biogenic nontronite from marine white smoker chimneys." *Clays & Clay Minerals* 42(6): 689-701.
- Komadel, P., J. Madejova and J. W. Stucki (2006). "Structural Fe(III) reduction in smectites." *Applied Clay Science* 34(1-4): 88-94.
- Komine, H. (2004). "Simplified evaluation for swelling characteristics of bentonites." *Engineering Geology* 71(3-4): 265-279.
- Komine, H. and N. Ogata (2004). "Predicting swelling characteristics of bentonites." *Journal of Geotechnical and Geoenvironmental Engineering* 130(8): 818-829.
- Konhauser, K. (2007). Introduction to Geomicrobiology. Oxford, Blackwell Publishing.
- Körstgens, V., H. C. Flemming, J. Wingender and W. Borchard (2001). "Influence of calcium ions on the mechanical properties of a model biofilm of mucoid *Pseudomonas aeruginosa*." *Water Science and Technology* 43(6): 49-57.
- Kostka, J. E., E. Haeefele, R. Viehweger and J. W. Stucki (1999). "Respiration and dissolution of iron(III)-containing clay minerals by bacteria." *Environmental Science and Technology* 33(18): 3127-3133.
- Kostka, J. E., J. W. Stucki, K. H. Nealson and W. U. Jun (1996). "Reduction of structural Fe(III) in smectite by a pure culture of *Shewanella putrefaciens* strain MR-1." *Clays and Clay Minerals* 44(4): 522-529.
- Kronhauser, K. (2007). Introduction to Geomicrobiology. Oxford, Blackwell Publishing.
- Kühnel, R. A. and S. J. van der Gaast (1993). "Humidity controlled diffractometry and its applications." *Advances in X-ray Analysis* 36: 439-449.
- Labille, J., F. Thomas, M. Milas and C. Vanhaverbeke (2005). "Flocculation of colloidal clay by bacterial polysaccharides: Effect of macromolecule charge and structure." *Journal of Colloid and Interface Science* 284(1): 149-156.
- Lagaly, G. (1993). Reaktionen des Tonminerale. In: Tonminerale und Tone: Struktur, Eigenschaften und Einsatz in Industrie und Umwelt. J. K. and L. G. Darmstadt, Steinkopff Verlag: 89-167.
- Lagaly, G. (2006). Chapter 5 Colloid Clay Science. In: Developments in Clay Science. F. Bergaya, B.K.G. Theng and G. Lagaly, Elsevier. Volume 1: 141-245.
- Laird, D. A., C. Shang and M. L. Thompson (1995). "Hysteresis in crystalline swelling of smectites." *Journal of Colloid and Interface Science* 171: 240-245.

- Lasaga, A. C. (1995). Fundamental approaches in describing mineral dissolution and precipitation rates. In: Chemical Weathering Rates of Silicate Minerals, Reviews in Mineralogy. A.F. White and S.L. Brantley, Mineralogical Society of America. 31: 23-81.
- Lee, J.-U. and J. B. Fein (2000). "Experimental study of the effects of *Bacillus subtilis* on gibbsite dissolution rates under near-neutral pH and nutrient-poor conditions." *Chemical Geology* 166(3-4): 193-202.
- Lee, J. V., D. M. Gibson and J. M. Shewan (1977). "A numerical taxonomic study of some pseudomonas like marine bacteria." *Journal of General Microbiology* 98(2): 439-451.
- Lee, K., J. E. Kostka and J. W. Stucki (2006). "Comparisons of structural Fe reduction in smectites by bacteria and dithionite: An infrared spectroscopic study." *Clays and Clay Minerals* 54(2): 195-208.
- Lehman, R. M., F. S. Colwell and G. A. Bala (2001). "Attached and Unattached Microbial Communities in a Simulated Basalt Aquifer under Fracture- and Porous-Flow Conditions." *Appl. Environ. Microbiol.* 67(6): 2799-2809.
- Leon Morales, C. F., M. Strathmann and H. C. Flemming (2007). "Influence of biofilms on the movement of colloids in porous media. Implications for colloid facilitated transport in subsurface environments." *Water Research* 41(10): 2059-2068.
- Liermann, L. J., A. S. Barnes, B. E. Kalinowski, X. Zhou and S. L. Brantley (2000a). "Microenvironments of pH in biofilms grown on dissolving silicate surfaces." *Chemical Geology* 171(1-2): 1-16.
- Liermann, L. J., B. E. Kalinowski, S. L. Brantley and J. G. Ferry (2000b). "Role of bacterial siderophores in dissolution of hornblende." *Geochimica et Cosmochimica Acta* 64(4): 587-602.
- Likos, W. J. (2004). "Measurement of crystalline swelling in expansive clay." *Geotechnical Testing Journal* 27(6): 540-546.
- Little, B. J., P. A. Wagner and Z. Lewandowski (1997). "Spatial relationships between bacteria and mineral surfaces." *Reviews in Mineralogy* 35: 154-159.
- Lloret, A. and M. V. Villar (2007). "Advances on the knowledge of the thermo-hydro-mechanical behaviour of heavily compacted "FEBEX" bentonite." *Physics and Chemistry of the Earth* 32(8-14): 701-715.
- Lloyd, J. R. (2003). "Microbial reduction of metals and radionuclides." *FEMS Microbiology Reviews* 27(2-3): 411-425.
- Lovley, D. R. (1991). "Dissimilatory Fe(III) and Mn(IV) reduction." *Microbiological Reviews* 55(2): 259-287.
- Lovley, D. R., D. E. Holmes and K. P. Nevin (2004). "Dissimilatory Fe(III) and Mn(IV) reduction." *Advances in Microbial Physiology* 49: 219-286.
- Lovley, D. R., E. J. P. Phillips, Y. A. Gorby and E. R. Landa (1991). "Microbial reduction of uranium." *Nature* 350(6317): 413-416.
- Lowenstam, H. A. (1981). "Minerals formed by organisms." *Science* 211(4487): 1126-1131.
- Lower, S. K., M. F. Hochella Jr and T. J. Beveridge (2001). "Bacterial recognition of mineral surfaces: Nanoscale interactions between *Shewanella* and α -FeOOH." *Science* 292(5520): 1360-1363.
- Lowson, R. T. (1982). "Aqueous oxidation of pyrite by molecular oxygen." *Chemical Reviews* 82(5): 461-497.
- MacDonell, M. T. and R. R. Colwell (1985). "Phylogeny of the vibrionaceae, and recommendation for two new genera, listonella and shewanella." *Systematic and Applied Microbiology* 6(2): 171-182.
- MacEwan, D. M. C. and M. J. Wilson (1980). Interlayer and Intercalation Complexes of Clay Minerals. In: Crystalstructure of Clay Minerals and their X-ray Identification. G.W. Brindley and G. Brown. London, Mineralogical Society. 5: 197-242.
- Madigan, M. T., J. M. Martinko and J. Parker (2003). Brock biology of microorganisms. 10th ed. Upper Saddle River, Pearson Prentice Hall.
- Madsen, F. T. (1998). "Clay mineralogical investigations related to nuclear waste disposal." *Clay Minerals* 33(1): 109-129.

- Marcos, N. (2002). "Lessons from nature - The behaviour of technical and natural barriers in the geological disposal of spent nuclear fuel." *Acta Polytechnica Scandinavica, Civil Engineering and Building Construction Series*(124).
- Marshall, K. C., R. Stout and R. Mitchell (1971). "Selective sorption of bacteria from seawater." *Canadian Journal of Microbiology* 17(11): 1413-1416.
- Marshall, M. J., A. S. Beliaev, A. C. Dohnalkova, D. W. Kennedy, L. Shi, Z. Wang, M. I. Boyanov, B. Lai, K. M. Kemner, J. S. McLean, S. B. Reed, D. E. Culley, V. L. Bailey, C. J. Simonson, D. A. Saffarini, M. F. Romine, J. M. Zachara and J. K. Fredrickson (2006). "c-type cytochrome-dependent formation of U(IV) nanoparticles by *Shewanella oneidensis*." *PLoS Biology* 4(8): 1324-1333.
- Martin, P. L. and J. M. Barcala (2005). "Large scale buffer material test: Mock-up experiment at CIEMAT." *Engineering Geology* 81(3): 298-316.
- Maurice, P. A. and L. A. Warren (2006). Introduction to geomicrobiology: Microbial interactions with minerals. *CMS Workshop Lectures*. 14: 1-35.
- McNeil, B. L. (1970). "Prediction of Interlayer Swelling of Clays in Mixed-Salt Solutions." *Proceedings of the Soil Science Society of America* 34(2): 201-206.
- Megonigal, J. P., M. E. Hines, P. T. Visscher, D. H. Heinrich and K. T. Karl (2003). Anaerobic Metabolism: Linkages to Trace Gases and Aerobic Processes. In: *Treatise on Geochemistry*. Oxford, Pergamon: 317-424.
- Meike, A. and S. Stroes-Gascoyne (2000). Review of Microbial Responses to Abiotic Environmental Factors in the Context of the Proposed Yucca Mountain Repository. [UCRL-ID-141064](#). U.S.D.o. Energy, Lawrence Livermore National Laboratory
- 212.
- Meleshyn, A. (2005). Monte Carlo Simulationen zur Untersuchung von Quell- und Sorptionsprozessen in Wyoming-Montmorillonite im Hinblick auf seine Verwendung als Barrierematerial in Endlagern für radioactive Abfälle. Hannover, University of Hannover: 86.
- Méring, J. (1946). "The hydration of montmorillonite." *Transactions of the Faraday Society* 42: 205-219.
- Méring, J. (1949). "L'interférence des Rayons X dans les system à stratification désordonnée." *Acta Crystallographica* 2: 371-377.
- Mermut, A. R. and A. F. Cano (2001). "Baseline studies of the clay minerals society source clays: Chemical analyses of major elements." *Clays and Clay Minerals* 49(5): 381-386.
- Mermut, A. R. and G. Lagaly (2001). "Baseline studies of the clay minerals society source clays: Layer-charge determination and characteristics of those minerals containing 2:1 layers." *Clays and Clay Minerals* 49(5): 393-397.
- Metz, V., K. Amram and J. Ganor (2005). "Stoichiometry of smectite dissolution reaction." *Geochimica et Cosmochimica Acta* 69(7): 1755-1772.
- Meunier, A., B. Lanson and D. Beaufort (2000). "Vermiculitization of smectite interfaces and illite layer growth as a possible dual model for illite-smectite illitization in diagenetic environments: A synthesis." *Clay Minerals* 35(3): 573-586.
- Michot, L. J. and F. Villieras (2006). Chapter 12.9 Surface Area and Porosity. In: *Developments in Clay Science*. Faiza Bergaya, B.K.G. Theng and G. Lagaly, Elsevier. Volume 1: 965-978.
- Milliken, R. E. and J. F. Mustard (2007). "Estimating the water content of hydrated minerals using reflectance spectroscopy. II. Effects of particle size." *Icarus* 189(2): 574-588.
- Molera, M., T. Eriksen and M. Jansson (2003). "Anion diffusion pathways in bentonite clay compacted to different dry densities." *Applied Clay Science* 23(1-4): 69-76.
- Monsalvo, R., L. de Pablo and M. L. Chàvez (2006). "Hydration of Ca-montmorillonite at basin conditions: A Monte Carlo molecular simulation." *Revista Mexicana de Ciencias Geológicas* 23(1): 84-95.
- Montes-Hernandez, G., J. Duplay, L. Martinez, Y. Geraud and B. Rousset-Tournier (2003a). "Influence of interlayer cations on the water sorption and swelling-shrinkage of MX80 bentonite." *Applied Clay Science* 23(5-6): 309-321.
- Montes-Hernandez, G., J. Duplay, L. Martinez and C. Mendoza (2003b). "Swelling-shrinkage kinetics of MX80 bentonite." *Applied Clay Science* 22(6): 279-293.

- Montes-Hernandez, G., B. Fritz, A. Clement and N. Michau (2005a). "Modelling of geochemical reactions and experimental cation exchange in MX80 bentonite." *Journal of Environmental Management* 77(1): 35-46.
- Montes-Hernandez, G., B. Fritz, A. Clement and N. Michau (2005b). "A simplified method to evaluate the swelling capacity evolution of a bentonite barrier related to geochemical transformations." *Applied Geochemistry* 20(2): 409-422.
- Montes-Hernandez, G., N. Marty, B. Fritz, A. Clement and N. Michau (2005c). "Modelling of long-term diffusion-reaction in a bentonite barrier for radioactive waste confinement." *Applied Clay Science* 30(3-4): 181-198.
- Mooney, R. W., A. G. Keenan and L. A. Wood (1952). "Adsorption of water vapor by montmorillonite. II. Effect of exchangeable ions and lattice swelling as measured by X-ray diffraction." *Journal of the American Chemical Society* 74(6): 1371-1374.
- Moore, D. M. and J. Hower (1986). "Ordered interstratification of dehydrated and hydrated Na-smectite." *Clays & Clay Minerals* 34(4): 379-384.
- Moore, D. M. and R. C. Reynolds (1997). X-Ray Diffraction and the Identification and Analysis of Clay Minerals 2nd Edition. New York, Oxford University Press.
- Müller-Vonmoos, M. and E. E. Kohler (1993). Geotechnik und Entsorgung. In: Tonminerale und Tone: Struktur, Eigenschaften und Einsatz in Industrie und Umwelt. J. K. and L. G. Darmstadt, Steinkopff Verlag: 312-357.
- Muller, D., C. Medigue, S. Koechler, V. Barbe, M. Barakat, E. Talla, V. Bonnefoy, E. Krin, F. Arsene-Ploetze, C. Carapito, M. Chandler, B. Cournoyer, S. Cruveiller, C. Dossat, S. Duval, M. Heymann, E. Leize, A. Lieutaud, D. Lievremont, Y. Makita, S. Mangenot, W. Nitschke, P. Ortet, N. Perdrial, B. Schoepp, P. Siguier, D. D. Simeonova, Z. Rouy, B. Segurens, E. Turlin, D. Vallenet, A. Van Dorsselaer, S. Weiss, J. Weissenbach, M. C. Lett, A. Danchin and P. N. Bertin (2007). "A tale of two oxidation states: bacterial colonization of arsenic-rich environments." *PLoS genetics* 3(4).
- Murray, H. H. (1977). "Industrial Minerals Outlook for the Paper Industrie." *TAPPI* 60(8): 70-72.
- Muurinen, A. and J. Lehtikoinen (1999). "Porewater chemistry in compacted bentonite." *Engineering Geology* 54(1-2): 207-214.
- Myers, C. R. and K. H. Nealson (1988). "Bacterial manganese reduction and growth with manganese oxide as the sole electron acceptor." *Science* 240(4857): 1319-1321.
- Myers, C. R. and K. H. Nealson (1990). "Respiration-linked proton translocation coupled to anaerobic reduction of manganese(IV) and iron(III) in *Shewanella putrefaciens* MR-1." *J. Bacteriol.* 172(11): 6232-6238.
- Nadson, G. A. (1903). Mikroorganizmy kak geologicheskije deyateli (Microorganisms as Geological Agents). St. Petersburg, Tip. Saikina.
- Nagelschmidt, G. (1936). "The structure of montmorillonite." *Z. Kristallogr.* 93: 481-487.
- Nagy, K. L. (1995). "Dissolution and precipitation kinetics of sheet silicates." *Reviews in Mineralogy and Geochemistry* 31(1): 173-233.
- Nazina, T. N., I. M. Kosareva, V. V. Petrunyaka, M. K. Savushkina, E. G. Kudriavtsev, V. A. Lebedev, V. D. Ahunov, Y. A. Revenko, R. R. Khafizov, G. A. Osipov, S. S. Belyaev and M. V. Ivanov (2004). "Microbiology of formation waters from the deep repository of liquid radioactive wastes Severnyi." *FEMS Microbiology Ecology* 49(1): 97-107.
- Neilands, J. B. (1989). Siderophore systems in bacteria and fungi. In: Bacteria in Nature. J.S. Poindexter and E.R. Leadbetter. New York, Plenum Press: 141-163.
- Nordstrom, D. K. (1982). Aqueous pyrite oxidation and the consequent formation of secondary iron minerals. In: Acid Sulphate Weathering. K. J.S., F. D.S. and H. L.R. Madison, Soil Science of America Special Publication. 10: 37-56.
- Norrish, K. (1954). "Crystalline Swelling of Montmorillonite: Manner of Swelling of Montmorillonite." *Nature* 173(256-257).
- Norrish, K. and J. P. Quirk (1954). "Crystalline swelling of montmorillonite: Use of Electrolytes to Control Swelling." *Nature* 173: 255-256.
- O'Driscoll, M. (1988). "Bentonite: overcapacity in need of markets." *Industrial Minerals* 250: 43-67.
- O'Driscoll, M. (1989). "US Pacific Northwest: an outpost of industrial mineral wealth." *Industrial Minerals* 259: 19-55.

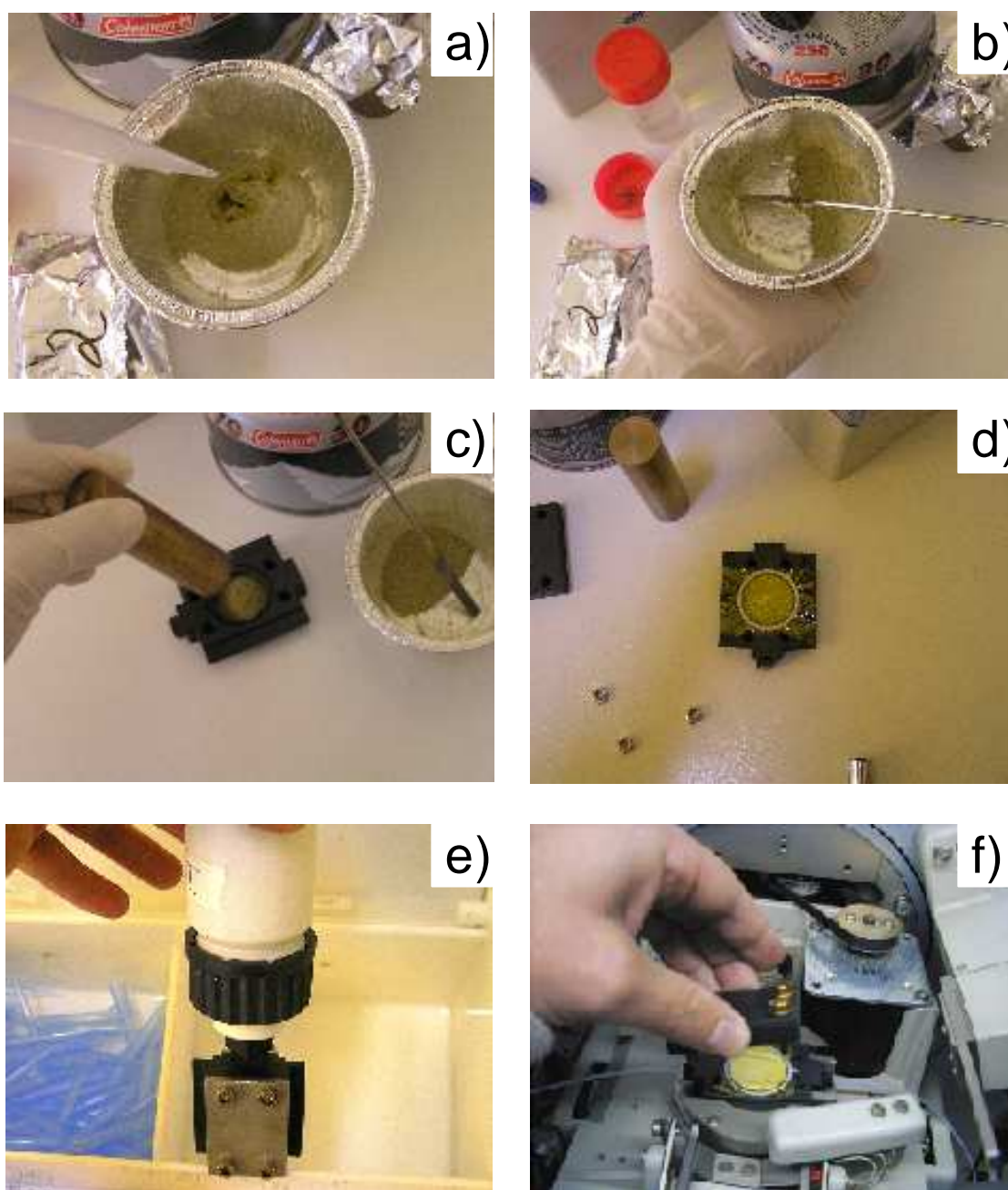
- O'Loughlin, E. J., P. Larese-Casanova, M. Scherer and R. Cook (2007). "Green rust formation from the bioreduction of α -FeOOH (Lepidocrocite): Comparison of several *Shewanella* species." *Geomicrobiology Journal* 24(3-4): 211-230.
- O'Reilly, S. E., Y. Furukawa and S. Newell (2006). "Dissolution and microbial Fe(III) reduction of nontronite (NAu-1)." *Chemical Geology* 235(1-2): 1-11.
- Obuekwe, C. O. and D. W. S. Westlake (1982). "Effect of reducible compounds (potential electron acceptors) on reduction of ferric iron by *Pseudomonas* species." *Microbios Letters* 19(74): 57-61.
- OECD (1999). Confidence in the evaluation of safety deep geological repositories - Its development and communication. N.E. Agency.
- OECD (2006). "Safety of Geological Disposal of High-level and Long-lived Radioactive Waste in France: An International Peer Review of the Dossier 2005 Argile Concerning Disposal in the Callovo-Oxfordian Formation." *OECD Papers* 6: 88-164.
- Olson, K. R. (1985). "Characterization of pore size distributions within soils by mercury intrusion and water-release methods." *Soil Science* 139(5): 400-404.
- Oscarson, D. W., H. B. Hume and J. W. Choi (1994). "Diffusive transport in compacted mixture of clay and crushed granite." *Radiochim. Acta* 65: 189-194.
- Payne, A. N. and T. J. DiChristina (2006). "A rapid mutant screening technique for detection of technetium [Tc(VII)] reduction-deficient mutants of *Shewanella oneidensis* MR-1." *FEMS Microbiology Letters* 259(2): 282-287.
- Pedersen, K. (2000). Microbial processes in radioactive waste disposal. TR-00-04. SKB. Stockholm: 93.
- Pedersen, K., M. Motamedi, O. Karnland and T. Sandén (2000). "Cultivability of microorganisms introduced into a compacted bentonite clay buffer under high-level radioactive waste repository conditions." *Engineering Geology* 58(2): 149-161.
- Perdrial, N. (2007). Nature et rôle des matières solides en suspension dans la dynamique du transfert des éléments polluants. Ecole et Observatoire des Sciences de la Terre UMR 7517. Strasbourg, Université Louis Pasteur. PhD: 284.
- Plançon, A. and V. A. Drits (1999). Programs for calculation of diffraction by oriented powders of two- and three component mixed layer clay minerals. CALCMIX.
- Postgate, J. R. (1976). Death in macrobes and microbes. In: The survival of vegetative microbes. T.R.G. Gray and J.R. Postgate. London, Cambridge University Press: 1-19.
- Prost, R. (1975). "Étude de l'hydratation des argiles : interactions eau-minérale et mécanisme de la rétention de l'eau." *Annales d'Agronomie* 26: 463-535.
- Pusch, R. (2001a). Experimental study of the effect of high porewater salinity on the physical properties of a natural smectitic clay. TR-01-07. SKB. Stockholm: 32.
- Pusch, R. (2001b). The microstructure of MX-80 clay with respect to its bulk physical properties under different environmental conditions. TR-01-08. SKB. Stockholm: 108.
- Pusch, R. (2006a). Chapter 6 Mechanical Properties of Clays and Clay Minerals. In: Developments in Clay Science. F. Bergaya, B.K.G. Theng and G. Lagaly, Elsevier. Volume 1: 247-260.
- Pusch, R. (2006b). Chapter 11.4 Clays and Nuclear Waste Management. In: Developments in Clay Science. F. Bergaya, B.K.G. Theng and G. Lagaly, Elsevier. Volume 1: 703-716.
- Pusch, R., J. Kasbohm, J. Pacovsky and Z. Cechova (2007). "Are all smectite clays suitable as "buffers"?" *Physics and Chemistry of the Earth, Parts A/B/C* 32(1-7): 116-122.
- Pusch, R. and R. Weston (2003). "Microstructural stability controls the hydraulic conductivity of smectitic buffer clay." *Applied Clay Science* 23(1-4): 35-41.
- Reynolds, R. C. (1980). Interstratified Clay Minerals. In: Crystal Structures of Clay Minerals and their X-ray Identification. G.W. Brindley and G. Brown. London, Mineralogical Society. 5: 249-304.
- Reynolds, R. C. (1985). NEWMOD a Computer Program for the calculation of One-Dimensional Diffraction Patterns of Mixed-Layered Clays. R.C. Reynolds. Hanover, USA.
- Rivkina, E. M., E. I. Friedmann, C. P. McKay and D. A. Gilichinsky (2000). "Metabolic activity of Permafrost Bacteria below the freezing point." *Applied and Environmental Microbiology* 66(8): 3230-3233.

- Roden, E. E., D. Sobolev, B. Glazer and G. W. Luther III (2004). "Potential for microscale bacterial Fe redox cycling at the aerobic-anaerobic interface." *Geomicrobiology Journal* 21(6): 379-391.
- Roden, E. E. and J. M. Zachara (1996). "Microbial reduction of crystalline iron(III) oxides: Influence of oxide surface area and potential for cell growth." *Environmental Science and Technology* 30(5): 1618-1628.
- Rogers, J. R. and P. C. Bennett (2004). "Mineral stimulation of subsurface microorganisms: Release of limiting nutrients from silicates." *Chemical Geology* 203(1-2): 91-108.
- Rogers, J. R., P. C. Bennett and W. J. Choi (1998). "Feldspars as a source of nutrients for microorganisms." *American Mineralogist* 83(11-12 PART 2): 1532-1540.
- Rosenberg, D. R. and P. A. Maurice (2003). "Siderophore adsorption to and dissolution of kaolinite at pH 3 to 7 and 22°C." *Geochimica et Cosmochimica Acta* 67(2): 223-229.
- Roszak, D. B. and R. R. Colwell (1987). "Survival Strategies of Bacteria in the Natural Environment." *Microbiological Reviews* 51(3): 365-379.
- Rotenberg, B., V. Marry, J.-F. Dufreche, N. Malikova, E. Giffaut and P. Turq (2007). "Modelling water and ion diffusion in clays: A multiscale approach." *Comptes Rendus Chimie* 10(10-11): 1108-1116.
- Rothfuchs, T., N. Jockwer and C. L. Zhang (2007). "Self-sealing barriers of clay/mineral mixtures - The SB project at the Mont Terri Rock Laboratory." *Physics and Chemistry of the Earth* 32(1-7): 108-115.
- Sarmento, M. R., J. C. Oliveira and R. B. Boulton (2000). "Selection of low swelling materials for protein adsorption from white wines." *International Journal of Food Science and Technology* 35(1): 41-47.
- Sato, T., T. Watanabe and R. Otsuka (1992). "Effects of layer charge, charge location, and energy change on expansion properties of dioctahedral smectites." *Clays & Clay Minerals* 40(1): 103-113.
- Sauzeat, E., T. F. Villiéras, M. François, M. Pelletier, O. Barrés, J. Yvon, D. Guillaume, J. Dubbessy, C. Pfeiffert, R. Ruck and M. Cathelineau (2001). Caractérisation minéralogique, cristallographique et texturale de l'argile MX-80. LEM-CREGU. France, ANDRA Technical Report.
- Schramm, L. L. and J. C. T. Kwak (1982). "Influence of exchangeable cation composition on the size and shape of montmorillonite particles in dilute suspension." *Clays & Clay Minerals* 30(1): 40-48.
- Shaw, D. J. (1992). Charged interfaces. In: Introduction of Colloid and Surface Chemistry Oxford, Butterworth-Heinemann: 174-189.
- Sposito, G. and R. Prost (1982). "Structure of water adsorbed on smectites." *Chemical Reviews* 82(6): 553-573.
- Sposito, G., N. T. Skipper, R. Sutton, S. H. Park, A. K. Soper and J. A. Greathouse (1999). "Surface geochemistry of the clay minerals." *Proceedings of the National Academy of Sciences of the United States of America* 96(7): 3358-3364.
- Stotzky, G. (1966a). "Influence of clay minerals on microorganisms. 3. Effect of particle size, cation exchange capacity, and surface area on bacteria." *Canadian Journal of Microbiology* 12(6): 1235-1246.
- Stotzky, G. (1966b). "Influence of clay minerals on microorganisms. II. Effect of various clay species, homoionic clays, and other particles on bacteria." *Canadian Journal of Microbiology* 12(4): 831-848.
- Stotzky, G. (1967). "Clay minerals and microbial ecology." *Transactions of the New York Academy of Sciences* 30(1): 11-21.
- Stotzky, G. and L. T. Rem (1966). "Influence of clay minerals on microorganisms. I. Montmorillonite and kaolinite on bacteria." *Canadian Journal of Microbiology* 12(3): 547-563.
- Stotzky, G. and L. T. Rem (1967). "Influence of clay minerals on microorganisms. IV. Montmorillonite and kaolinites on fungi." *Canadian Journal of Microbiology* 13(11): 1535-1550.
- Stroes-Gascoyne, S. and F. P. Sargent (1998). "The Canadian approach to microbial studies in nuclear waste management and disposal." *Journal of Contaminant Hydrology* 35(1-3): 175-190.

- Stroes-Gascoyne, S. and J. M. West (1994). Microbial issues to the Canadian concept for the disposal of nuclear fuel waste. Atomic Energy of Canada Limited, AECL (Report): 1-39.
- Stucki, J. W. (1988). Structural iron in smectites. In: Iron in soils and clay minerals. J.W. Goodman and B.A. Schwertmann. Dordrecht, D. Reidel Publishing Company: 625-675.
- Stucki, J. W. (2006). Chapter 8 Properties and Behaviour of Iron in Clay Minerals. In: Developments in Clay Science. F. Bergaya, B.K.G. Theng and G. Lagaly, Elsevier. Volume 1: 423-475.
- Stucki, J. W., P. Komadel and H. T. Wilkinson (1987). "Microbial reduction of structural iron(III) in smectites." *Soil Science Society of America Journal* 51(6): 1663-1665.
- Stucki, J. W. and J. E. Kostka (2006). "Microbial reduction of iron in smectite." *Comptes Rendus - Geoscience* 338(6-7): 468-475.
- Stucki, J. W., K. Lee, L. Zhang and R. A. Larson (2003). "Effects of iron oxidation state on the surface and structural properties of smectites." *Pure and Applied Chemistry* 74(11): 2145-2158.
- Stucki, J. W., J. Wu, H. Gan, P. Komadel and A. Banin (2000). "Effects of iron oxidation state and organic cations on dioctahedral smectite hydration." *Clays and Clay Minerals* 48(2): 290-298.
- Suzuki, S., S. Prayongphan, Y. Ichikawa and B. G. Chae (2005). "In situ observations of the swelling of bentonite aggregates in NaCl solution." *Applied Clay Science* 29(2): 89-98.
- Tamura, K., H. Yamada and H. Nakazawa (2000). "Stepwise hydration of high-quality synthetic smectite with various cations." *Clays and Clay Minerals* 48(3): 400-404.
- Tazaki, K. (2006). Chapter 9 Clays, Microorganisms, and Biomineralization. In: Developments in Clay Science. F. Bergaya, B.K.G. Theng and G. Lagaly, Elsevier. Volume 1: 477-497.
- Tchoubar, D. and N. Cohaut (2006). Chapter 12.5 Small-Angle Scattering Techniques. In: Developments in Clay Science. F. Bergaya, B.K.G. Theng and G. Lagaly, Elsevier. Volume 1: 879-907.
- Theng, B. K. G. and V. A. Orchard (1995). Interactions of clays with microorganisms and bacterial survival in soil: A physicochemical perspective. In: Environmental Impact of Soil Component Interactions. P.M. Huang, J. Berthelin, J.-M. Bollag, W.B. McGill and A.L. Page. Boca Raton, Lewis Publishers: 123-143.
- Todar, K. (2006). Textbook of Bacteriology, University of Wisconsin-Madison.
- Ueshima, M. and K. Tazaki (2001). "Possible role of microbial polysaccharides in nontronite formation." *Clays and Clay Minerals* 49(4): 292-299.
- Urrutia, M. M., M. A. Kemper, R. J. Doyle and T. J. Beveridge (1992). "The membrane-induced proton motive force influences the metal binding ability of *Bacillus subtilis* cell walls." *Appl. Environ. Microbiol.* 58: 3837-3844.
- Van Loosdrecht, M. C. M., J. Lyklema, W. Norde and A. J. B. Zehnder (1989). "Bacterial adhesion: A physicochemical approach." *Microbial Ecology* 17(1): 1-15.
- Van Loosdrecht, M. C. M., J. Lyklema, W. Norde and A. J. B. Zehnder (1990). "Influence of interfaces on microbial activity." *Microbiological Reviews* 54(1): 75-87.
- Vandevivere, P., S. A. Welch, W. J. Ullman and D. L. Kirchman (1994). "Enhanced dissolution of silicate minerals by bacteria at near-neutral pH." *Microbial Ecology* 27(3): 241-251.
- Velde, B. (1992). Introduction to clay minerals. London, Chapman & Hall.
- Venkateswaran, K., D. P. Moser, M. E. Dollhopf, D. P. Lies, D. A. Saffarini, B. J. MacGregor, D. B. Ringelberg, D. C. White, M. Nishijima, H. Sano, J. Burghardt, E. Stackebrandt and K. H. Nealson (1999). "Polyphasic taxonomy of the genus *Shewanella* and description of *Shewanella oneidensis* sp. nov." *International Journal of Systematic Bacteriology* 49(2): 705-724.
- Vervey, E. J. W. and J. T. G. Overbeek (1948). Theory of the Stability of Lyophobic Colloids: The interaction of Sol Particles Having an Electric Double Layer. New York, Elsevier.
- Villar, M. V. and A. Lloret (2007). "Dismantling of the first section of the FEBEX in situ test: THM laboratory tests on the bentonite blocks retrieved." *Physics and Chemistry of the Earth* 32(8-14): 716-729.
- Warr, L. and J. Berger (2007). "Hydration of bentonite in natural waters: Application of "confined volume" wet-cell X-ray diffractometry." *Physics and Chemistry of the Earth* 32(1-7): 247-258.
- Warr, L. N. and H. Hofmann (2003). "In situ monitoring of powder reactions in percolating solution by wet-cell X-ray diffraction techniques." *Journal of Applied Crystallography* 36(3 II): 948-949.

- Watanabe, T. and T. Sato (1988). "Expansion Characteristics of Montmorillonite and Saponite Under Various Relative Humidity Conditions." *Clay Science* 7(3): 129-138.
- Welch, S. A. and P. Vandevivere (1994). "Effect of microbial and other naturally occurring polymers on mineral dissolution." *Geomicrobiology Journal* 12(4): 227-238.
- Wersin, P. (2003). "Geochemical modelling of bentonite porewater in high-level waste repositories." *Journal of Contaminant Hydrology* 61(1-4): 405-422.
- Wersin, P., E. Curti and C. A. J. Appelo (2004). "Modelling bentonite-water interactions at high solid/liquid ratios: Swelling and diffuse double layer effects." *Applied Clay Science* 26(1-4 SPEC. ISS.): 249-257.
- Westlake, D. W. S., K. M. Semple and C. O. Obuekwe (1966). "Corrosion by ferric iron-reducing bacteria isolated from oil production systems."
- Willey, J., L. Sherwood and C. Woolverton (1996). *Microbiology*, McGraw-Hill.
- Wilson, J., G. Cressey, B. Cressey, J. Cuadros, K. V. Ragnarsdottir, D. Savage and M. Shibata (2006). "The effect of iron on montmorillonite stability. (II) Experimental investigation." *Geochimica et Cosmochimica Acta* 70(2): 323-336.
- Wilson, J., J. Cuadros and G. Cressey (2004). "An in situ time-resolved XRD-PSD investigation into Na-montmorillonite interlayer and particle rearrangement during dehydration." *Clays and Clay Minerals* 52(2): 180-191.
- Woese, C. R. (1987). "Bacterial evolution." *Microbiological Reviews* 51(2): 221-271.
- Woese, C. R. and G. E. Fox (1977). "Phylogenetic structure of the prokaryotic domain: The primary kingdoms." *Proceedings of the National Academy of Sciences of the United States of America* 74(11): 5088-5090.
- Wogelius, R. A. and D. J. Vaughan (2000). Analytical, experimental and computational methods in environmental mineralogy. In: *Environmental Mineralogy*. R.A. Wogelius and D.J. Vaughan. Budapest, Eötvös University Press: 7-87.
- Wu, J., C. B. Roth and P. F. Low (1988). "BIOLOGICAL REDUCTION OF STRUCTURAL IRON IN SODIUM-MONTMORILLONITE." *Soil Science Society of America Journal* 52(1): 295-296.
- Zachara, J. M., R. K. Kukkadapu, J. K. Fredrickson, Y. A. Gorby and S. C. Smith (2002). "Biomineralization of poorly crystalline Fe(III) oxides by dissimilatory metal reducing bacteria (DMRB)." *Geomicrobiology Journal* 19(2): 179-207.
- Zachara, J. M. and J. P. McKinley (1993). "Influence of hydrolysis on the sorption of metal cations by smectites: Importance of edge coordination reactions - Dedicated to Paul W. Schindler on his retirement." *Aquatic Sciences* 55(4): 250-261.

APPENDIX



Preparation of bacteria containing reaction-cell experiments. a) Bacteria containing solution is pipetted onto pre-dried smectite powder. b) Bacteria and smectite are mixed close to the flame of a Bunsen burner using a heat sterilized spatula. c) Powder is introduced into the reaction-cell and pressed down to enhance packing density. d) After adding some delaminated kaolinite as internal standard the reaction-cell is sealed by an X-ray transparent capton foil and fixed with an o-ring. e) In order to maintain constant reaction volume the reaction-cell is additionally closed by a pressure cap that is fixed by screws. Solution is provided from a Teflon© bottle situated on top of the reaction-cell. f) Only the bottle and the pressure cap are temporarily removed for XRD-measurements.

Procedure for biofilm and DNA colouration

In order to stain the cellulose in biofilms, about 40 μ l of the clay bacteria water suspension was introduced into 100 μ l calcofluor solution (1 μ g calcofluor fluorescent brightener 28ml⁻¹) and allowed to stand for 1 hour. During this time, the calcofluor was fixed to the polysaccharides of the biofilm (Ramaswamy et al. 1997) and, under the fluorescent light, the material appeared blue-green (wavelength of emission of calcofluor 780 nm and 800nm) and could be distinguished from DNA (bacteria) that was stained by ethidium bromide (EtBr). It absorbs light at two wavelengths: 370 nm and 530nm and it emits light at 622 nm leading to a reddish colour. In advance, an ethidium bromide solution was prepared as stock solution and diluted to a final concentration of 0.1 μ g/mg. 100 μ l of EtBr solution were then added to the sample and allowed to stand 15 min prior to microscopy study.

Figure 7.1a shows an example of MX80 observed under transmitted light. The particle in the upper right is presumably a montmorillonite grain. Elongated structures in the center are bacteria (size between 2 and 5 μ m). Under fluorescent light, the biofilms appear green due to the adsorption of calcofluor (wavelength of emission of calcofluor 780 nm and 800nm, fig.7.1b). It can be distinguishable from bacterial DNA stained by ethidium bromide (Fig. 7.1c) that emits light at 622 nm leading to a reddish colour. The bacteria cells that are visible in Fig 7.1 are not stained by the ethidium bromide, however this product is adsorbed together with calcofluor. Thus, it is likely that the smectite absorbs, at least partly, the products and the method is not fully adapted.

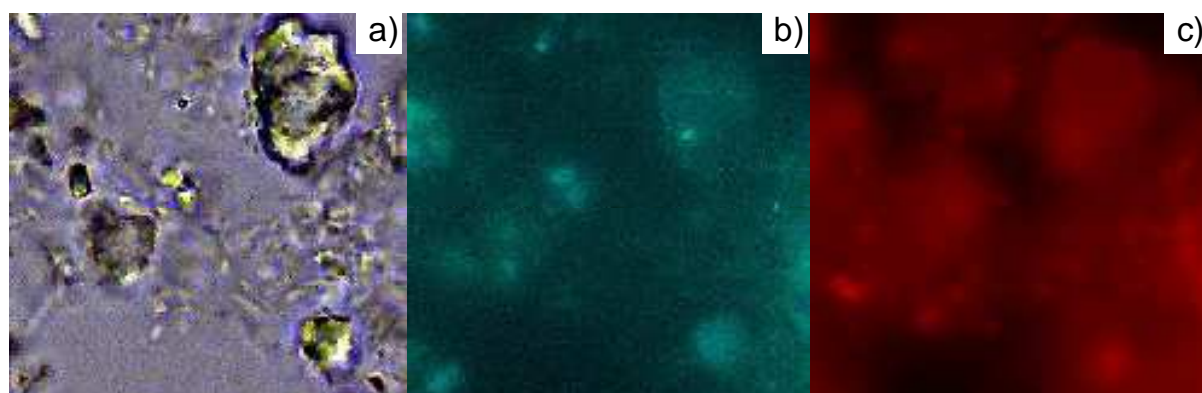


Fig. 7.1 a). Confocal microscope images of MX80 incubated with *S. putrefaciens* following the combined treatment with calcofluor and ethidium bromide. b) Under fluorescent light the calcofluor appears green (biofilms). c) Ethidium bromide appears red (DNA). Side length of the images correspond to 20 μ m.

Estimating the generation times of exponentially growing cultures

The generation time is a growth parameter that indicates the time a population needs to double in cfu. There is a direct relationship between initially present cells (N_0) and the number present after exponential growth (N), since one cell doubles to become two, those two double to become 4 and so on. The generation time is included in this relationship where n is the number of generations:

$$N = N_0 2^n$$

From knowledge of the initial and final cell numbers, it is possible to calculate the number of generations and, from there, the time (t/n). The generation time can be as well calculated directly from the slope of the line obtained in a semi-logarithmic plot of the exponential growth (Fig. 7.2):

$$\text{Slope} = 0.301/g$$

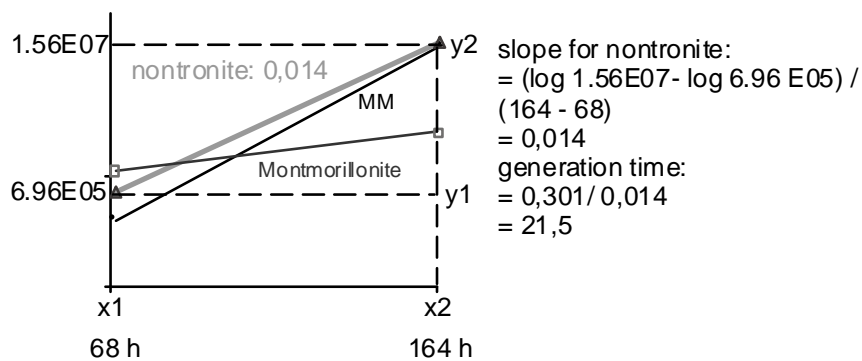


Fig. 7.2. Calculation of generation time based on the slope of exponential growth in a semilogarithmic graph. The plot shows the lines for nontronite (light grey), Minimal Medium (MM; black) and montmorillonite (dark grey). The slope is calculated by dividing Δy by Δx . It is then sufficient to divide the number 0,301 by the values for the slope to obtain the generation time (details see Madigan et al. 2003). The example calculation is done for nontronite.

Procedure for analyzing reaction-cell extracts

Between 0.2 -0.5 g of the sample were taken from the freshly opened reaction-cells. Then, a 20 fold amount of Millipore water was added (0.2g corresponds to 4ml of water, yielding a ratio of 50mg per ml for all samples). Precise amounts of sample material were determined by weighing previously weighed sample tubes after adding the sample. The samples were disaggregated in the ultra sonic bath twice for 15 minutes and allowed to stand for 24h. After repeated ultrasonic treatment, the samples were centrifuged (3500rpm for 15 minutes), filtrated by using a filter (0.22 μ m) and acidified by using concentrated HNO₃. The same procedure was applied for the HCl extraction where a 1N HCl was used as the leaching agent instead of water. As the samples were already acidified, further treatment with HNO₃ was no longer necessary.

Calculating the amount of interlayer water

The relative abundance of water layers obtained from CALCMIX-calculations were used to estimate the amount of interlayer water using data from isotherm absorption experiments of montmorillonites (Bérend et al., 1995; Cases et al., 1997). The nontronite values were estimated based on data of Jähnchen et al. (2006) and Milliken & Mustard (2007). An example calculation on SWy-2 is given for the following abundances: 58% 0-WL, 34% 1-WL and 8% 2-WL. The relative abundances of WL structures were multiplied with corresponding values for WL structures (see table 7.1):

$$(0.58 * 0) + (0.34 * 0.12) + (0.08 * 0.24) = 0 + 0.04 + 0.02 = 0.06 \text{ ml/g.}$$

	IBECO seal 80 (Na ⁺)	TIXOTON-TE (Ca ²⁺)	MX80 (Na ⁺ /Ca ²⁺)	SWy-2- Montmorillonite (Na ⁺)	Nontronite (NAu-1) (Ca ²⁺)
1-WL	0.12	0.11	0.09	0.12	0.12
2-WL	0.24	0.22	0.18	0.24	0.25
3-WL	0.36	0.33	0.27	0.36	0.37
4-WL	0.49	0.44	0.36	-	0.51

Table 7.1. Values used to calculate interlayer water (ml/g) as taken from water vapour adsorption isotherms (Bérend et al., 1995; Cases et al., 1997) for the homoionic montmorillonites and from (Sauzeat et al., 2001) for MX80. Values for nontronite were taken from (Jänchen et al., 2006; Milliken & Mustard, 2007). As values for 3 and 4-WL structures were not presented in the literature the data was interpolated based on values for 1 and 2-WLs.

Calculation of surface areas based on number of particles per stack

The number of layers per stack (N; the particle thickness) changes during hydration and, therefore, was adjusted in the CALCMIX-software calculations. In each experiment, the N value obtained for the initial and most dehydrated states was taken as a reference. In most of the samples, this was around 18 particles per stack and, although higher numbers were obtained in other studies, the lower values were taken to be consistent and, thus, assumed to correspond to the N value during the outgassing conditions of BET measurements. The decrease in layers per stack can be expressed as a relative increase in surface. The increase of the external surface was calculated based on the following relationships:

Change in number of surfaces (ΔN):

$$\Delta N = N_{\text{init}} / N * 2$$

N_{init} = Number of layers per stack at dry state

N = Number of layers per stack (CALCMIX)

Calculation of theoretical corresponding surface area (S_{calc}):

$$S_{\text{calc}} = \text{SSA}_{\text{BET}} / (\Delta N * 2)$$

SSA_{BET} = measured BET surface area

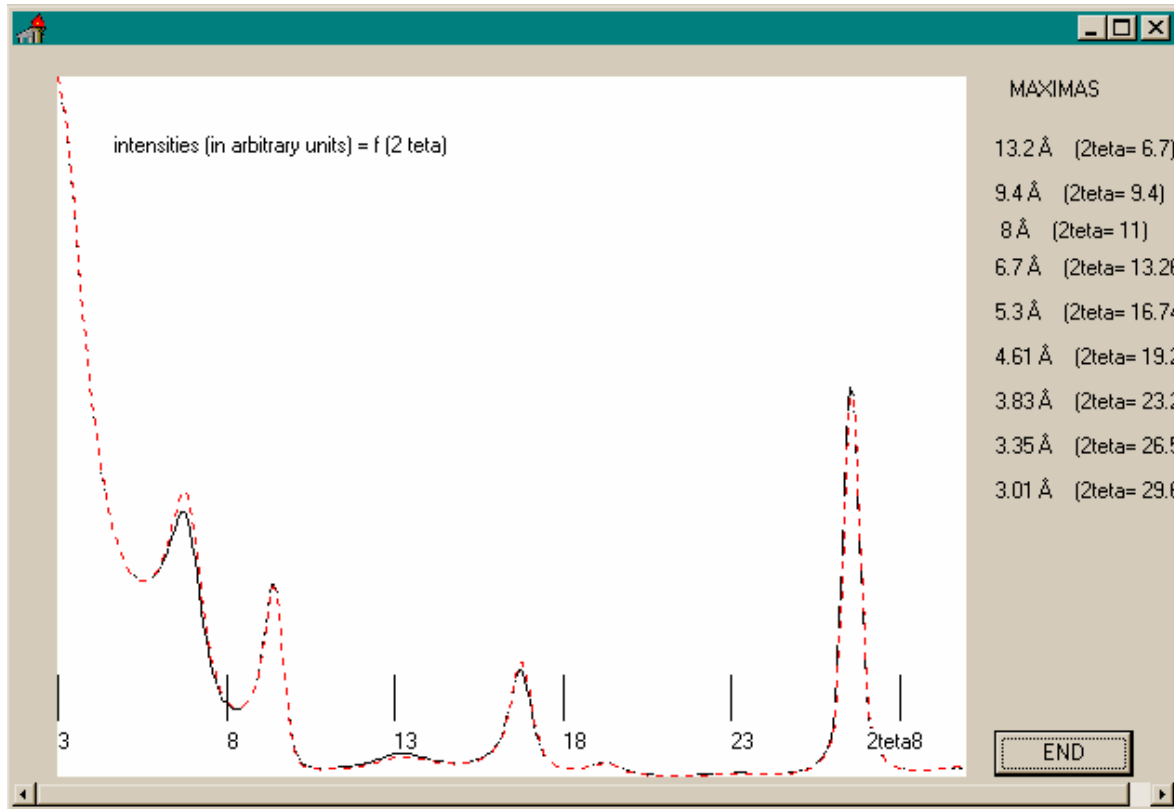
ΔN = Change in number of layers

The limitations of this method were obtained when calculating the maximal surface area for monolayer particles (table 7.2.). Here, smectites with divalent interlayer cations, theoretically, yield higher values than possible. This is basically due to the higher hydration energy of Ca that induces interlayer hydration at all relative pressures and, consequently, the BET surface area does include internal surfaces already at the “dry” state (Cases et al., 1997).

	IBECO	TIXOTON	MX80	Nontronite	SWy-2
Particles per stack initial (corresponding to BET)	18	18	19	15	18
BET - surface area [m ² /g]	55.33	103.01	30.03	83.98	27.64
Calculated maximal surface area [m ² /g]*	995.94	(1854)	570.6	(1259.7)	498.1

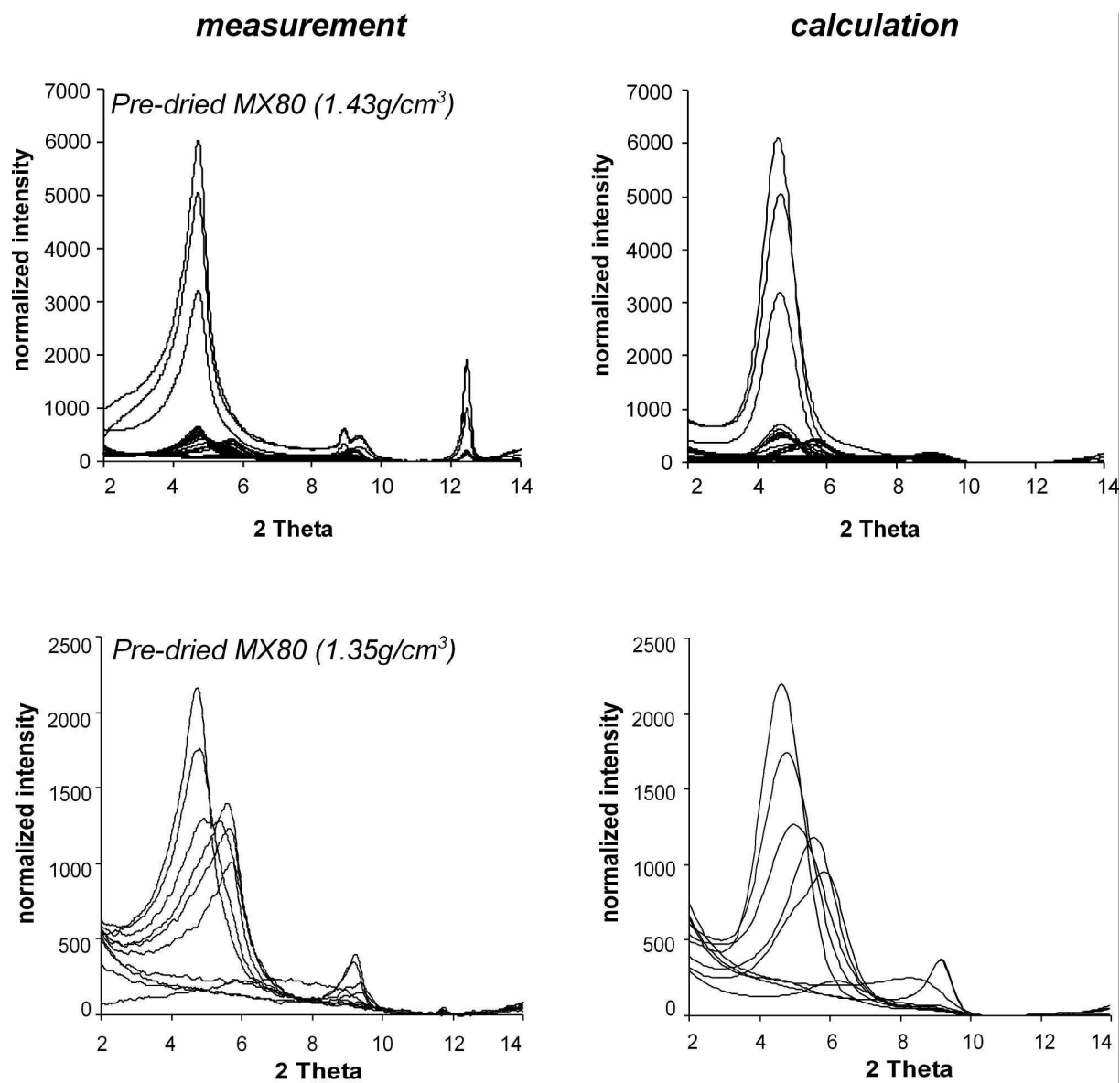
*Table 7.2. Theoretical surface area based on changes in layers per stack. * Assuming 1 layer per stack (monolayers). Values for materials with divalent interlayer cations (TIXOTON and nontronite) overestimate the theoretical surface area.*

CALCMIX

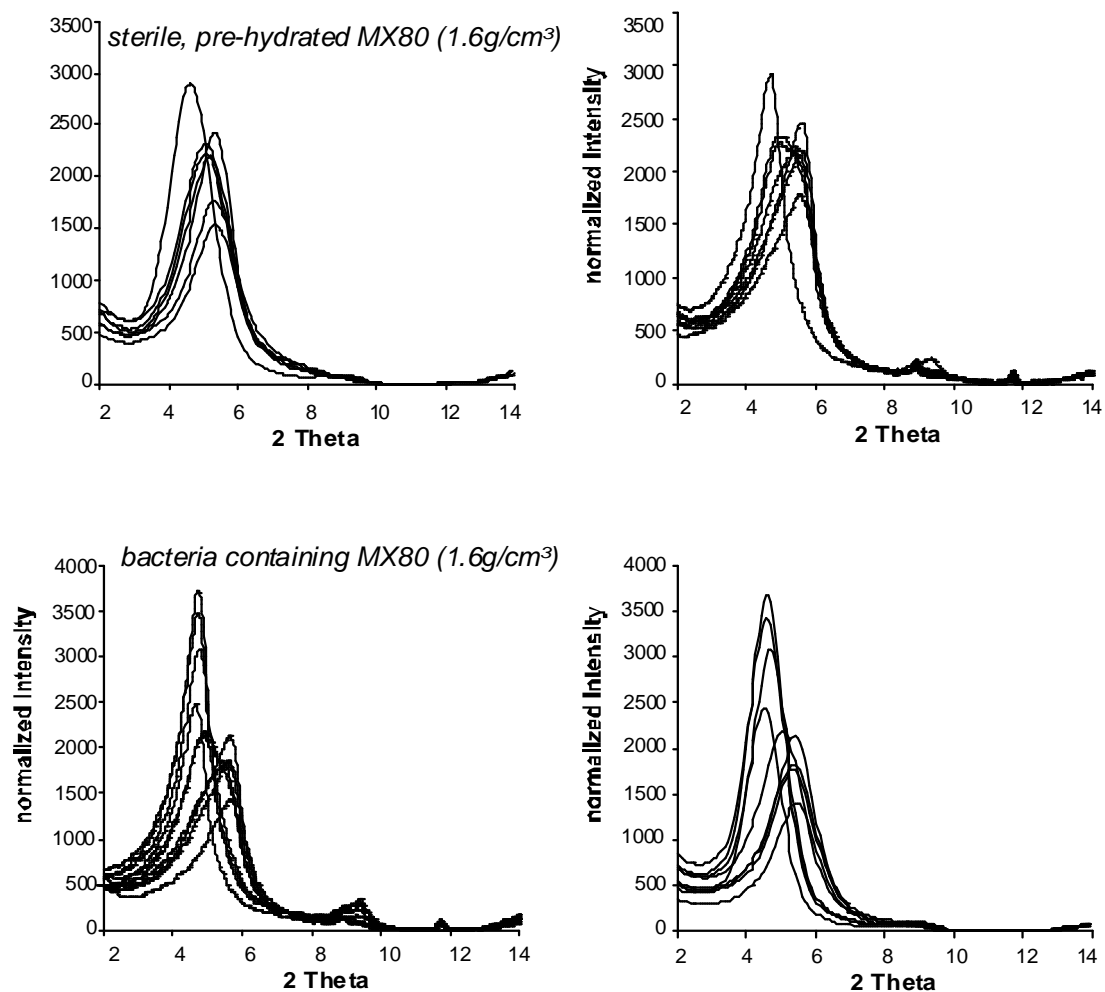


Example of the user interface of the CALCMIX results page after fitting a whole rock profile taken from the user manual (Plançon & Drits, 1999).

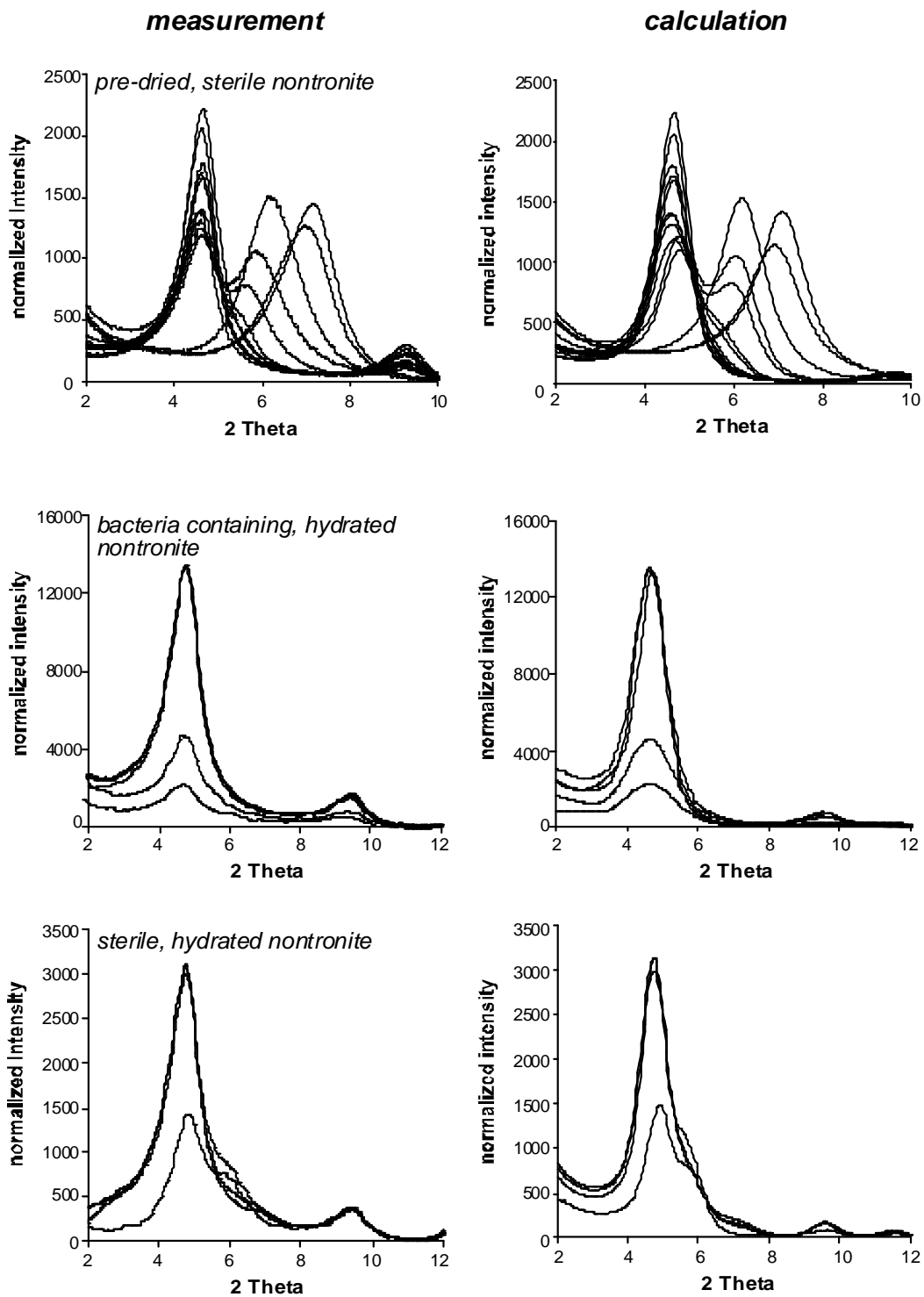
Comparison between the measured and manually fitted (calculated) patterns using CALCMIX:



Selected measured and calculated X-ray diffraction patterns from the confined volume reaction-cell experiments (Pre-dried MX80).

*measurement**calculation*

Selected measured and calculated X-ray diffraction patterns from the confined volume reaction-cell experiments (hydrated sterile and bacteria containing MX80).



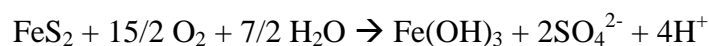
Selected measured and calculated X-ray diffraction patterns from the confined volume reaction-cell experiments (Pre-dried and hydrated, sterile and bacteria containing nontronite).

Biomineralisation

Biologically induced mineralization often occurs as a passive way, as a byproduct of the cells metabolic activity (Lowenstam, 1981) or due to the fact that they serve as nucleation sites (Ehrlich, 1996; , 1999; Kronhauser, 2007). The precipitation of amorphous silica was, for example, observed by TEM in biotic nontronite solution experiments and could be attributed to bacterially induced dissolution followed by precipitations. Furukawa and O'Reilly (2007) observed, in addition, the formation of Si globules which was interpreted to occur in combination with polymerization and stabilization by "biomolecules".

Another precipitate that was observed only in bacteria containing nontronite samples (XRD) was the hydrated iron phosphate vivianite ($\text{Fe}_3(\text{PO}_4)_2 \cdot 8\text{H}_2\text{O}$) that formed as a function of Fe(II) concentration and dissolved phosphate (Kronhauser, 2007). As this mineral was only detected at later stages of the experimentation and because its formation was described to be inhibited by viable *S. putrefaciens* cells (Jorand et al., 2000), it is likely that it precipitated after cell death by using phosphate, which was released during cell lyses. A similar process can be assumed for the precipitation of the sodium sulfate mirabilite ($\text{Na}_2\text{SO}_4 \cdot 10\text{H}_2\text{O}$) which was, as well, only visible in bacteria containing samples.

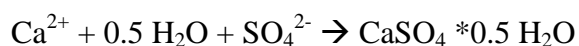
In case of both, the sterile and *S. putrefaciens* containing longterm MX80 experiments, the presence of "green rust", an iron carbonate with the generalized formula $\text{Fe}_6(\text{OH})_{12}(\text{CO}_3)$, was detected. Regarding its formation, the Fe might derive from pyrite, which makes up about 0.5% of the whole rock samples (Chapter 3). Because of this small amount, it could not be clearly detected in XRD patterns (Fig. 5.4.7) but it might have contributed to Fe oxide formation. Pyrite is oxidized in contact with the experimental solution pyrite according to the (simplified) reaction:



This reaction leads, besides a decrease in pH and the formation of sulphate and the precipitation of Fe(III)-hydroxides, which are then available to form the iron carbonate. The carbonate required for this formation might derive from the dissolved calcite according to the reaction:



This reaction buffers the pH to some degree and leads, at the same time, to a release of Ca^{2+} cations. It is possible that the calcium participates together with the sulfate (released from pyrite oxidation) to form the bassanite, frequently found both in bacteria containing and bacteria free samples:



Precipitation of green rust is visible in both the bacteria containing and the sterile sample. In the latter, the X-ray diffraction reflection of this mineral is constantly changing in intensity, which indicates an alternating dissolution and precipitation reactions. The same effect is visible in the case of calcite, bassanite and rhodocrosite (MnCO_3). As rhodochrosite formation requires iron reduction in combination with an excess of HCO_3^- its presence and disappearance indicates fluctuations in both Eh and pH conditions (Kronhauser, 2007).

In the presence of bacteria, the system appears less susceptible to mineralogical fluctuations. This is visible with the continuous dissolution of calcite, the synchronous formation of lepidocrocite ($\gamma\text{-FeOOH}$) and in the stable reflection of green rust. O'Loughlin and co-workers (2007) stated that the formation of green rust occurs as a result of bacterially reduced lepidocrocite. Nevertheless, this could not be confirmed from the MX80 experiments, since both phases co-exist and the anaerobic conditions alone induce the formation of the rust phase. In contrast, it seems that the presence of bacteria leads to a stabilization of the redox conditions and a buffering of pH. However, direct measurements of these parameters in the reaction-cells are not possible yet.

